Stratigraphy, Provenance, and Syn-orogenic Evolution of the Gibbett Hill and Quidi Vidi Formations (Lower Signal Hill Group), Avalon Peninsula (Newfoundland)

By

Santiago Alberto SERNA ORTIZ

A dissertation submitted to the School of Graduate Studies of

In partial fulfillment of the requirements for the degree of

Master of Science

Department of Earth Sciences

MEMORIAL UNIVERSITY OF NEWFOUNDLAND

June 2023

St. John's, Newfoundland

Abstract

Sedimentologic and provenance studies of the syn-orogenic Ediacaran lower Signal Hill Group (Gibbett Hill and Quidi Vidi formations) in the Avalon Peninsula, Newfoundland, Canada, were conducted to test structural and depositional models related to late Ediacaran West Avalonian orogenesis. Two facies associations corresponding to delta front and delta plain environments were identified from five stratigraphic sections. The presence of an unconformity between these facies near the location of a previously proposed thrust-related paleo-high and changes in sedimentary patterns reflecting shoreline regression supports hypothetical syn-sedimentary uplift and reveals coeval base level fall. Framework petrography, detrital geochronology, and detrital heavy mineral analysis indicate sediment sourcing from hinterlands of West Avalonian igneous and metamorphic basement. Changes in provenance were noted between the delta front and delta plain facies coeval with regression of the Signal Hill delta that suggests coeval thrusting of volcanic cover sequences over previously exhumed plutonic sources and the exhumation of higher-grade metamorphic rocks in the hinterlands. Detrital zircon U-Pb maximum depositional ages of the delta front and delta plain facies yield 557 $\pm$ 9 Ma and 556 $\pm$ 22 Ma, respectively, constraining this episode of West Avalonian hinterland exhumation, wedge-top foreland basin deformation, and forced regression to ca. 556 Ma.

General Summary

The lower Signal Hill Group (Gibbett Hill and Quidi Vidi formations) of the Avalon Peninsula, Newfoundland, expose rocks deposited during late Ediacaran (ca. 560-540 Ma) Avalonian mountain building. Two facies associations suggesting shallow marine delta front and delta plain environments were identified from five stratigraphic sections. The presence of a disconformity between these facies near the location of a previously proposed uplift and changes in sedimentary patterns reflecting shoreline migration supports shoreline regression. Sandstone provenance indicates sediment sourcing from uplifted West Avalonian igneous and metamorphic basement. Changes in provenance coincide with the regression of the Signal Hill delta and indicate the uplift of volcanic cover sequences over already exhumed plutonic rocks and the exhumation of deeper metamorphic rocks in the hinterland behind the coast. Detrital zircon U-Pb maximum depositional ages of the delta front and delta plain facies yield 557 $\pm$ 9 Ma and 556 $\pm$ 22 Ma, respectively, indicating an age of ca. 556 Ma for uplift and shoreline regression.

Acknowledgments

First and foremost, I thank my supervisor Dr. David Lowe for allowing me to pursue this research and for believing in me. I also acknowledge his invaluable mentorship and support; with his helpful instructions and constant discussions, I was able to compose a document of this scientific level and contribute to the research of West Avalon geology. I also acknowledge my committee member Dr. Luke Beranek for reviewing this thesis. I must thank Memorial University's CREAIT network for its support during the data acquisition.

I would like to thank all the nice people I have met during these last two years that made this an even more enriching experience, including some of my close friends Caroline Gini, Daniel Perez, Gabrielle Ledesma, Luisa González, Arlin Fonseca, Angie Antolinez, and Andrea Mills.

Finally, I would like to show my gratitude to my family and friends who encouraged and supported me from a distance while I was studying in a foreign country.

Table of Contents

List of Tables

Chapter II

Chapter IV

List of Figures

Chapter I

Chapter II

Asymmetric ripple formsets of current ripples exposed near Area 8. C) Small-scale bidirectionally cross-laminated sandstone formsets with rounded crests (Wave ripples), exposed at Area 1. D) Small-scale unidirectionally cross-laminated sandstone formset (Current ripples), exposed at Area 7.

Fig. 2-2. A) Trough cross-laminated current ripples (F1b), exposed at Area 10 (see Appendix A for area locations). B). C) Climbing ripples (F1c) exposed at Area 10 and Area 8, respectively. D) Bed top showing asymmetric adhesion warts (F1d), exposed near Area 4.

Fig. 2-3. A) Trough cross-stratified sandstone formed by the migration and buildup of 3D dunes (F1e). B). Tabular cross-stratified sandstone representing the migration of 2D dunes (F1e). Outcrops A and B are exposed between Areas 4 and 5 (see Appendix A for area locations). C) Tabular cross-stratified sandstone (F1e) transitioning into low-angle planar laminated (F2a). D) Subaqueous migrating dunes (F1e) showing internal reactivation surfaces and mud drapes. Outcrops C and D are exposed at Area 10.

Fig. 2-4. A) Rib-and-furrow structures from truncated 3D dune sets (F1e). B) Sigmoidal cross-stratified sandstone formed by humpback dunes (F1f). Outcrops from A and B are exposed between Areas 4 and 5 (see Appendix A for area locations). Red arrows indicate paleoflow direction. White dashed lines outline laminae.

Fig. 2-5. A) Cryptic planar lamination (F2a) in structureless sandstone (F3a) exposed at Area 7 (see Appendix A for area locations). B). C) Structureless sandstone (F3a) transitioning into planar-laminated sandstone (F2a), outcrops B and C are exposed in Area

4 and 9, respectively. D). E) Normally and reversely graded sandstone laminae formed under hyperpycnal flows (F2b). Yellow triangles represent grain size trends. The red dashed line represents erosive contact.

Fig. 2-6. A) Structureless medium to coarse-grained sandstone bed recording sedimentation at the base of a concentrated density current (F3a) with sandstone dykes (F6b) at the top, exposed at Area 7 (see Appendix A for area locations). B) Structureless to normally graded sandstone laminae formed by waning turbiditic flows (F2b) interlaminated with mudstone and siltstone (F5a, F5b), exposed at Area 7. C) Normally graded bed, from intraformational breccia at the bottom to planar lamination (F2a) at the top, recording sedimentation under a waning concentrated density current, exposed at Area 8. D) Intraformational matrix-supported breccia (F4a), exposed near Area 4.

Fig. 2-7. A) Structureless sandstone deposited at the base of a concentrated density current (F3a) evolving into upper plane bed lamination (F2a) and climbing ripple stratification (F1c), exposed at Area 10 (see Appendix A for area locations). B) Normally graded sandstone bed deposited under a waning concentrated density flow (F4a), defined by structureless, medium-grained sandstone evolving vertically into fine-grained sandstone interlaminated with mudstone, exposed in Area 7. C). Structureless sandstone from concentrated density currents (F3a) transitioning into upper plane lamination (F2a) and dune cross-stratified sandstone (F1e), exposed near Area 8. D). Structureless sandstone bed recording concentrated density current sedimentation (F3a) evolving into climbing ripples (F1c), exposed near Area 8. Yellow triangle indicates grain size trend.

Fig. 2-8. A) and B) Up-right to steeply inclined folded strata (F6a) enclosed by undeformed strata exposed at Area 10 (see Appendix A for area locations). C) Sandstone dykes (F6b) cutting siltstone-dominated layers in folded strata exposed at Area 10. Yellow solid lines outline folded strata; red solid lines define the limits of the sandstone dykes. The red arrow points towards the paleo flow direction.

Fig. 2-9. A) Convolute-laminated strata formed by localized liquefaction processes (F6b). B) and C) Sandstone dykes formed by liquefaction leading to fluidization and dewatering (F6b). D) Dish-and-pillar structures (F6b) recording liquefaction and dewatering processes. E) Convolute-laminated strata related to selective liquefaction (F6b). F) Small sandstone dykes through mudstone. Pictures A to E correspond to outcrops at Area 10; Picture F corresponds to rocks exposed at Area 7 (see Appendix A for area locations).

Fig. 2-10. A) Amalgamated tabular bed sets from FA1a, recording proximal mouth bar sedimentation defined by alternating dune cross-stratified and waning concentrated density flow deposits, exposed near Area 5. B) Stacked upward coarsening and thickening bed sets of FA1b, interpreted as prograding mouth bars, exposed at Area 6. C) Tabular heterolithic bed sets (FA1b) recording terminal/fringe mouth bar sedimentation, exposed at Area 8. Yellow triangles define upward coarsening and thickening trends. Yellow line defines the measured log. See Appendix A for area locations.

Fig. 2-11. Channel element (FA1a) cutting into tabular heterolithic strata (FA1b), interpreted as a feeder channel cutting into a distal/fringe mouth bar deposit, exposed near Area 6 (see Appendix A for area locations). The dashed yellow line represents erosional contact; the red arrow indicates paleoflow direction.

Fig. 2-12. A) Oblique-oriented photomosaic of the medial part of the delta front facies outcropping near Area 6 (see Appendix A for area locations). B) Bedding diagram showing terminal distributary channels (yellow) cutting amalgamated lobate to tabular sandstone beds representing proximal mouth bars interbedded with tabular heterolithic strata. Abbreviations: LA-lateral accretion; DA-downstream accretion; SSD-soft-sediment deformed interval; the red arrow indicates paleo flow direction.

Fig. 2-13. A). B). C) Tabular heterolithic bed sets from FA2 interpreted as marine flood plain or interdistributary bay deposits interbedded with crevasse splays (CS). Yellow triangles define the grain-size trend; yellow lines define the upper and lower boundary of the beds. Outcrops A and C are exposed in Area 10, outcrop B is exposed in Area 7 (see Appendix A for area locations).

Fig. 2-14. A) Dip parallel-oriented photomosaic of lower delta plain facies outcropping near Area 9 (see Appendix A for area locations). B) Bedding diagram showing amalgamated distributary channel deposits (white) interbedded with interdistributary bay deposits (red) and lobate sandstone beds formed by crevasse splays (white). Abbreviations: UA-upstream accretion; CS-crevasse splay; DC-distributary channels; IB-inter distributary bay deposits; red arrows indicate paleoflow direction.

Chapter III

Fig. 3-1. Correlation panel of detailed stratigraphic logs from measured sections with their corresponding architectural elements distribution (pie charts) and composite facies

association paleoflow rose diagrams (see Fig. 1-2B for section locations). Features used for correlations were: (1) the first appearance of amalgamated tabular sandstone bed sets (FA1a); (2) the first appearance of red beds corresponding to the lithostratigraphic boundary between the Gibbet Hill and the Quidi Vidi formations defined by Williams and King (1976) and King (1990); (3) contact between FA1 and FA2 (see Fig. 3-2).

Fig. 3-2. A) Disconformity between upper delta plain and delta front facies in Section C, exposed near Area 5 (see Appendix A for area locations). B). Contact between lower delta plain and delta front facies in Section D, exposed near Area 7. C). Interpreted sharp contact between lower delta plain and delta front facies in Section E, exposed at Area 10. Abbreviations: TDC-terminal distributary channel; PMB-proximal mouth bar; DMB-distal mouth bar; IB-interdistributary bay; DC-distributary channel. Red arrows indicate paleoflow directions. In panel C, the paleoflow is coming out of the photogrammetric model. Yellow solid lines represent sharp contacts; yellow dashed lines represent erosive contacts; red solid line represents sharp contact; red dashed line represents erosive contact. Yellow triangles represent upward coarsening and thickening trends.

Chapter IV

Fig. 4-1. A). Delta front and delta plain sandstone petrography, sandstone modal Q-F-L diagram after Garzanti (2019), and discrimination and proportion of volcanic lithics. B). Tectonic discrimination diagram Qm-F-L after Dickinson and Suczek (1979). C) Photomicrographs of some lithic fragments present in the delta front and delta plain samples: 1-sandstone fragment; 2-siltstone fragments; 3-intermediate volcanic fragments;

4-felsic volcanic fragment; 5 and 6-psammitic schist fragments; yellow dashed lines define grain boundaries. The gray arrow indicates sandstone composition evolution trend.

Fig. 4-2. A) Transparent heavy mineral counts from the delta front and the delta plain facies. B) ZTR maturity index after Hubert (1962) and ATi, GZi, RZi provenance sensitive index values after Morton and Hallsworth (1994).

Fig. 4-3. Kernel distribution estimation (KDE) plots and age distribution (pie charts) of detrital U-Pb ages from delta front and delta plain samples (see Fig. 3-1 for samples location).

Fig. 4-4. Kernel distribution estimation plots (KDE) and age distribution (pie charts) of detrital U-Pb ages from the delta front and delta plain. The delta front KDE plot resulted from the grouped delta front samples.

Chapter IV

Fig. 5-1. Wetherill and weighted average age diagrams of concordant zircon grains used for maximum depositional age calculations based on the youngest grain cluster at 2σ method of Dickinson and Gehrels (2009).

Fig. 5-2. Schematic diagram showing the depositional environment and their syn-orogenic response during the Avalon orogeny recorded in the GHF, QVF, and the correlative Ferryland Head Formation.

List of Appendices

Co-authorship Statement

This thesis is presented in a traditional style and consists of six chapters. Chapter I presents the topic, the problem, the objective, describes the geological setting of the studied units and the location of the measured sections, and the methods used in this study. Chapter II describes and presents the interpretation of sedimentary facies and environments. Chapter III presents the facies associations, including distribution of the facies, stratal relationships, and their contacts. Chapter IV describes the sediment provenance, including sandstone petrography, heavy minerals, and detrital zircon U-Pb geochronology. Chapter V discusses the results and explores the significance of these based on the current geological information and models for West Avalonia. Chapter VI summarizes the main conclusions of this research project.

The conceptualization and development of this research are attributed to Dr. David Lowe. The author was responsible for all primary research activities, including stratigraphic section measuring, sample collection, sample preparation, and petrographic analysis. Heavy mineral separation was carried out by the author under the supervision of Matthew Crocker. The author conducted SEM-MLA analyses and backscatter SEM imaging under the supervision of Dylan Goudie. The author completed the U-Pb LA-ICPMS analyses and data reduction with the assistance of Dr. Markus Wälle. The primary editor of the manuscript is Dr. David Lowe.

Chapter I – Thesis Introduction

1.1 Introduction

Avalonia is a composite superterrane extending from the Appalachian orogen of northeastern North America into the Caledonian-Variscan mountain system in Europe and northwestern Africa (Fig. 1-1A). Its type area is in the Avalon Zone of Newfoundland, which, together with the related Avalonian rocks located to the southeast along the Eastern part of the Appalachian orogen, define the West Avalon Terrane (e.g., Willner et al., 2013; Murphy et al., 2019). Regional mapping, geochemical, petrological, and provenance data suggest that parts of West Avalonia underwent Ediacaran orogenesis and denudation prior to its rifting, drifting, and accretion to the eastern Laurentian margin during the early Paleozoic (Dunning et al., 1990; Nance et al., 2008; van Staal et al., 2021; Beranek et al., 2023). This Ediacaran orogenesis, also termed Avalonian orogeny (Hughes, 1970; van Staal et al., 2021), is characterized by enigmatic compressional deformation recorded in different parts of West Avalonia that may have resulted from either oblique arc-arc collision or ridge-trench collision and propagation of a San Andreas-style transform fault between 600 – 540 Ma (Murphy et al., 1999; van Staal et al., 2021). Although evidence for late Neoproterozoic deformation is not recognized everywhere across the West Avalon terrane, features thought to be related to the Avalonian orogeny in the Avalon Zone include transcurrent faulting, low-grade metamorphism, folding, and thrust faulting with up to several km of displacement (Papezik, 1974; Calon, 2001; van Staal et al., 2021). However, the lack of good age control of associated structures and strata, combined with subsequent strike-slip dissection of the West Avalon terrane, hamper reconstruction of the internal

configuration of this orogen, thus limiting the understanding of its Ediacaran tectonic evolution. Notably, many orogens are rarely completely preserved, and their reconstruction relies on the stratigraphy of associated syn-orogenic sedimentary basins (e.g., DeCelles, 2012). Such basins, including foreland and transpressional basins, are the immediate repository of orogen-derived sediments and thus are sensitive recorders of compressional deformation, recording cycles of hinterland uplift and erosion (Garzanti et al., 2007; Tye et al., 2021).

In this thesis, an assessment of structural and depositional models for the late Ediacaran Avalonian orogenesis is carried out by examining the stratigraphic record of coinciding syn-orogenic Ediacaran basin strata in its type area, the Avalon Peninsula of eastern Newfoundland (Fig. 1-1B; Fig. 1-2A). To this end, a combined approach of facies analysis, paleocurrent analysis, and provenance analysis was carried out on the deltaic late Ediacaran lower Signal Hill Group (Gibbett Hill and Quidi Vidi formations), which according to King (1990), records progradation related to basement exhumation in hinterlands to the north (based on current day orientations). The results of this research project corroborate the hypothesis of King (1990) and constrain the paleoenvironmental and stratal record of Ediacaran hinterland and intra-basin deformation and the maximum depositional age of the Signal Hill deltaic succession.

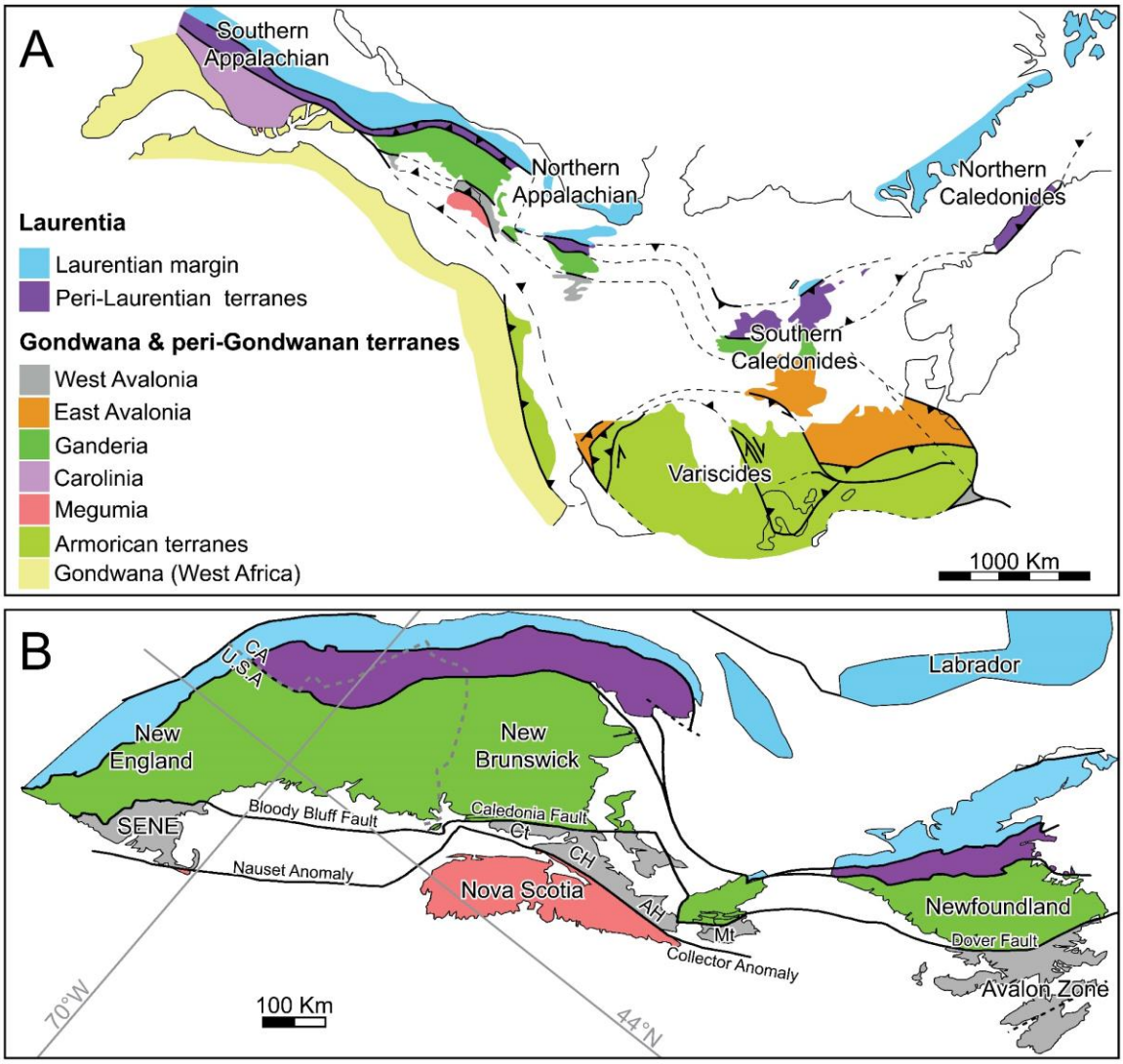

Fig. 1-1. (A) Paleogeographic reconstruction of the Appalachian-Caledonian-Variscan orogen before the opening of the Atlantic Ocean, modified from van Staal et al. (2021). (B) Current lithotectonic map of the northern Appalachian orogen modified from Hibbard et al. (2007). Abbreviations: Ct-Caledonia terrane; CH-Cobequid Highlands; AH-Antigonish Highlands; Mt-Mira terrane; CA-Canada; U.S.A-United States of America; SENE-Southeast New England.

1.2 Geological Setting

The geology of the Avalon Zone in eastern Newfoundland records the Neoproterozoic evolution of part of an exotic composite terrane known as Avalonia (Murphy and Nance, 1989; van Staal et al., 2021), which was most likely located at the periphery of West Gondwana during the Neoproterozoic (Dunning et al., 1990; Nance et al., 2008; Murphy et al., 2013). The Neoproterozoic history of West Avalonia, cropping out in the Eastern Appalachian orogeny, comprises several episodes of volcanic arc and marginal basin development (765-600 Ma) and diachronous termination of arc magmatism, an increase in clastic sedimentation, and localized shortening-related deformation between 600 and 540 Ma (Hughes, 1970; Murphy and Nance, 1989; Murphy et al., 2019; van Staal et al., 2021). In the eastern Avalon Zone of Newfoundland, the clastic strata deposited during this interval comprise up to 12 km of shallowing-upward submarine basin, slope, shelf, and fluvial facies of the Conception, St. John's, and Signal Hill groups (King, 1990), interpreted to record the progressive change from a marginal arc to a syn-orogenic foreland or strike-slip basin, coinciding with the shift in plate tectonic regime from active subduction to oblique arc-arc or ridge-trench collision (Murphy et al., 1999; Calon, 2001; Salas, 2004; Ichaso et al., 2007; van Staal et al., 2021). The syn-orogenic foreland or strike-slip basin strata comprise 2 km of fine-grained, pro-deltaic to shallow marine strata of the St. John's Group overlain by ~5 km thick shallow marine to fluvial strata of the Signal Hill Group (Fig. 1-3). Episodes of proximal syn-orogenic compressional deformation and syn-deformational sedimentation are evident from sections of the upper Signal Hill Group, specifically the Flatrock Cove Formation, exposed on the northeastern Avalon Peninsula,

where as much as 3.5 km of uplift and synchronous alluvial growth sedimentation occurred (Calon, 2001; Beranek et al., 2023). More subtle evidence of syn-orogenic deformation affecting the lower and middle units of the Signal Hill Group (Gibbett Hill and Quidi Vidi formations) on the eastern Avalon Peninsula include changes in isopach distributions and localized formation of an erosional unconformity between shallow marine and fluvial strata, that together are explained by differential uplift and erosion and interpreted to represent fault-induced changes in basin configuration (Rice, 1996; Stanley, 2009). In particular, local thinning of the lower shallow marine Gibbett Hill Formation (GHF) below the overlying alluvial Quidi Vidi Formation (QVF) between the Blackhead and Bay Bulls synclines (Fig. 1-2B) is interpreted to record blind thrusting and localized basin inversion between GHF and QVF sedimentation (Stanley, 2009).

The GHF, QVF, and the correlative Ferryland Head Formations comprise the lower units of the Signal Hill Group exposed along the eastern shoreline of the Avalon Peninsula (Williams and King, 1976). Here, the GHF is a succession of greenish gray-sandstone interbedded with siltstone that coarsens upwards to thick-bedded, massive sandstone and minor conglomerate, deposited in a shallow delta front to lower delta plain environment characterized by cyclic sandstone-siltstone sedimentation, minor shale deposition, and sheet flood deposits (King, 1990). The overlying QVF and its laterally equivalent Ferryland Head Formation consist of red sandstone interbedded with thin to medium-bedded siltstone, mudstone, and intraformational breccia. These strata have been interpreted to represent alluvial floodplain or a delta plain sedimentation with playa lakes transected by channels with subaqueous dunes, sheet floods, and crevasse splays (King, 1990; Salas, 2004).

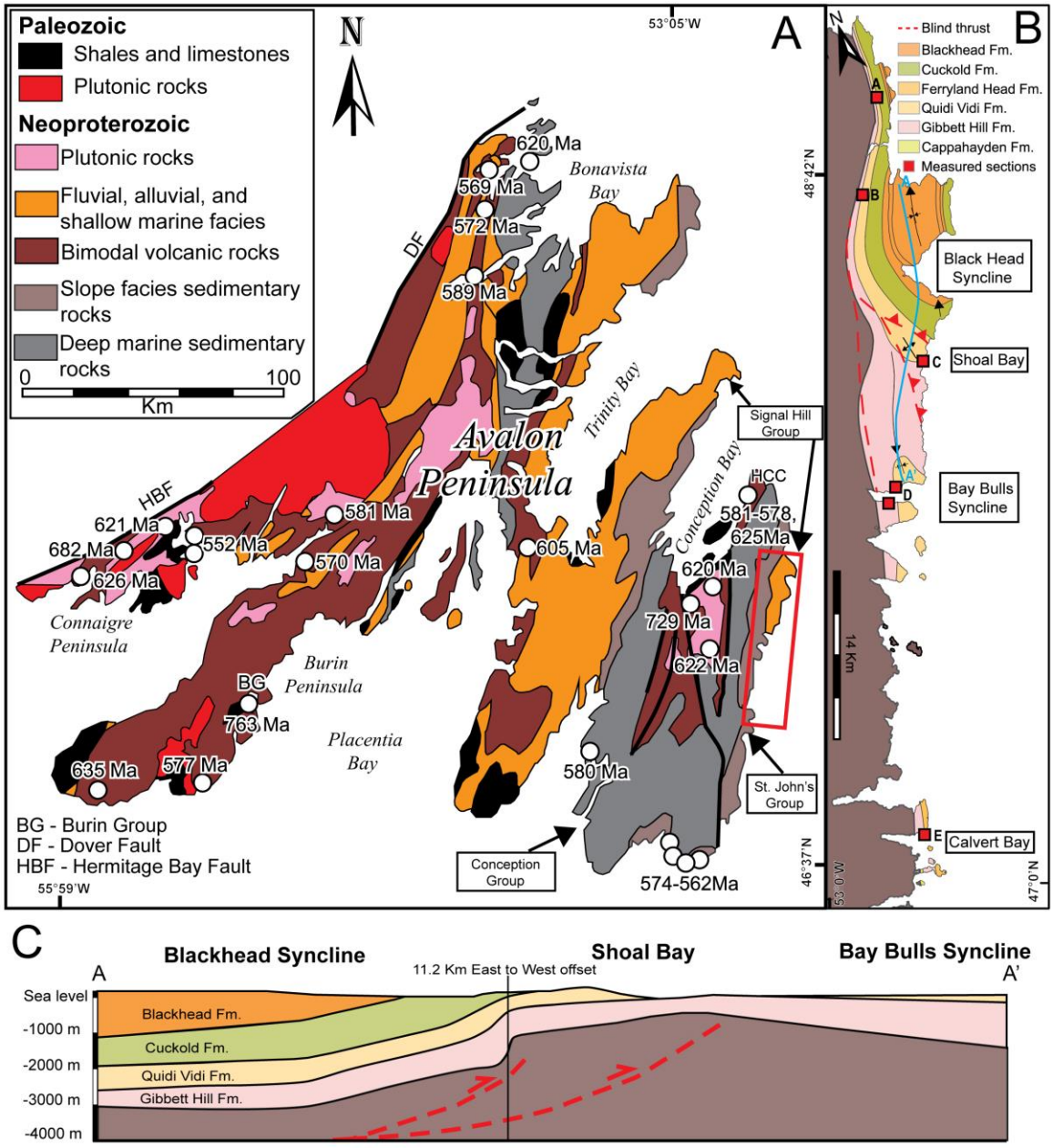

Fig. 1-2. (A) Simplified geological map of the Avalon Zone (Avalon Peninsula) modified from King (1990) and Mills et al. (2021). Quoted ages are zircon U-Pb crystallization and depositional ages of igneous and volcaniclastic rocks compiled from Israel (1998), Murphy et al. (2008), Canfield et al. (2020), Mills et al. (2021), and references therein. (B) Geological map of the east Avalon Peninsula with location of the measured sections. (C) Longitudinal cross-section modified from Stanley (2009).

Detrital zircon U-Pb geochronology of these units suggests sourcing from hinterlands dominated by local Ediacaran to Tonian igneous and volcanic basement with inherited Mesoproterozoic, Paleoproterozoic, and Archean zircons (Pollock et al., 2009, 2022; Beranek et al., 2023). In addition, detrital garnet, muscovite, and schist and quartzite clasts have been identified within the Signal Hill Group, suggesting a potential exhumed metamorphic basement in the northern hinterlands. Notably, such basement has yet to be identified in the Avalon Zone (Papezik, 1973; Gravenor, 1980; King, 1990; Beranek et al., 2023).

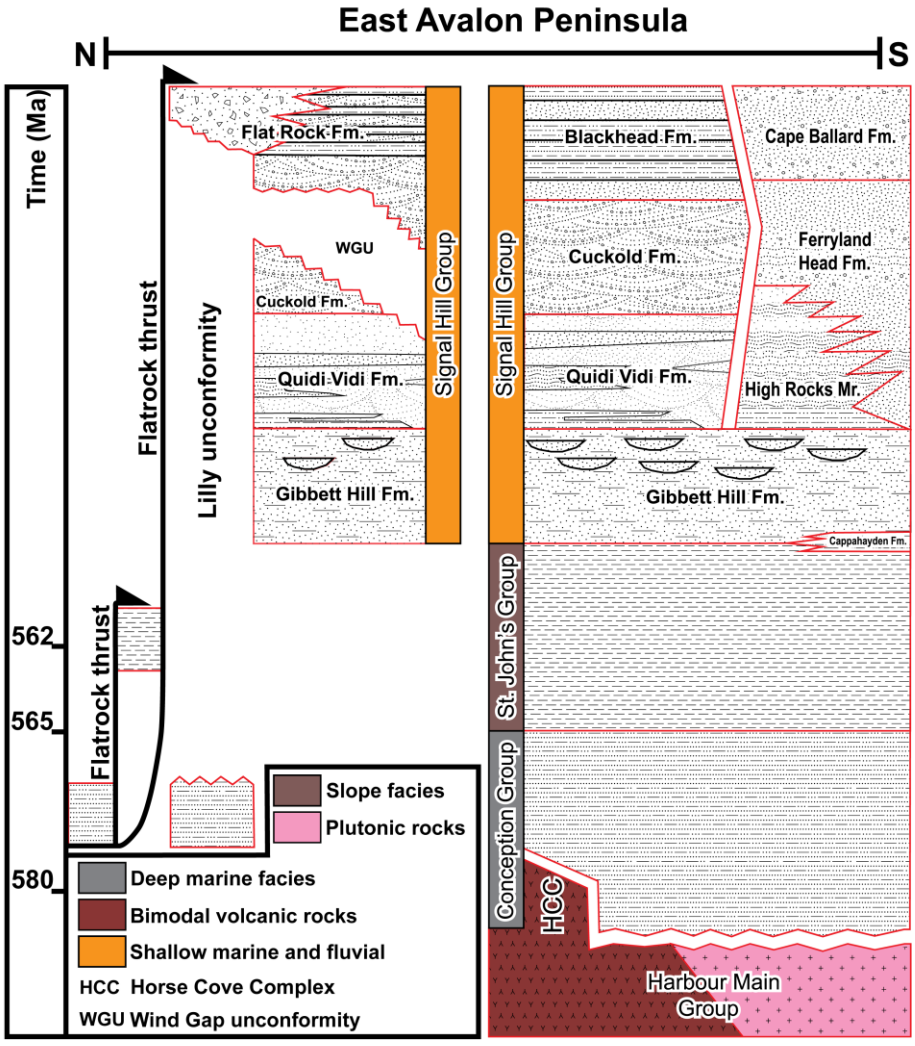

Fig. 1-3. Simplified lithostratigraphy of the East Avalon Peninsula modified from King (1988) and Pollock et al. (2009). Quoted dates are depositional ages of tuffaceous and sedimentary rocks compiled from Pu et al. (2016) and Canfield et al. (2020).

1.3 Methodology

1.3.1 Stratigraphy and sedimentology

Five stratigraphic sections of the Gibbett Hill and the Quidi Vidi formations were measured at a centimetric scale across the Avalon Peninsula, focusing on grain size, sedimentary structures, and contact relationships (Fig. 1-2B). Photogrammetric models and photomosaics of laterally continuous outcrops exposed along cliff faces allowed the identification of architectural elements within these units. A DJI Mavic 2 Pro was used to collect images, and the photogrammetric models were built using Pix4D software version 4.7.5. Photogrammetric models were visualized and interpreted in Leapfrog Geo software version 2021.2.5 and Virtual Reality Geological Studio software version 3.1. Paleocurrents were measured from dune and ripple cross-stratified sets and restored to horizontal via Stereonet software version 11 of Cardozo and Allmendinger (2013). Bed thickness was defined according to Ingram (1964). Bankfull channel depths were calculated following Leclair et al. (1997) and Bradley and Venditti (2017). Facies and facies associations were interpreted in terms of depositional processes and sedimentary environments, respectively, based on details of grain size, stratal geometry, and sedimentary structures (James and Dalrymple, 2010). Six sedimentary facies were described and interpreted, then grouped into two facies associations, discussed below.

1.3.2 Petrography

Sandstone petrography analyses on thin sections from 20 representative samples were carried out by point counting (200-300 points) following the Gazzi-Dickinson method (e.g., Ingersoll et al., 1985). The classification of the sandstone follows Garzanti (2019). The relationship between provenance and the tectonic environment of the sandstone was described by using the tectonic discrimination diagram of Dickinson and Suczek (1979). Metamorphic lithics were subdivided based on the composition of the protoliths into three groups: pelites, psammites, and metabasite; for each group, five metamorphic ranges were defined according to the increasing degree of recrystallization and progressive development of cleavage and schistosity following the method of Garzanti and Vezzoli (2003). The results of the sandstone petrography counts are in the supplementary material (Appendix F).

1.3.3 Heavy mineral analysis

Four sandstone samples (two from the GHF and two from the QVF) were selected for heavy mineral analysis. The samples were crushed, dry-sieved, and wet-sieved to a 63-250 μm fraction. The separation of minerals with a density above 2.89 g/cm^3 was accomplished using the separatory funnel technique through bromoform (Mange and Maurer, 1992). Representative aliquots of each sample were selected using an automatic rotatory micro riffler, mounted on epoxy pucks, and polished to expose the crystal cores. Heavy mineral identification was carried out using an Automated Scanning Electron Microscope equipped with Mineral Liberation Analysis (MLA) software version 3.14 at

the Micro Analysis Facility, Memorial University of Newfoundland. During the MLA analysis, the voltage was set to 25 kV; the beam current was 12nA, the spot size was between 7.3 to 7.5 µm, the working distance was 12 mm, and the X-ray acquisition time was 20ms. The Apatite-Tourmaline (ATi), Garnet-Zircon (GZi), and Rutile-Zircon (RZi) provenance-sensitive ratios of Morton and Hallsworth (1994) were then calculated to assess provenance variations. The results of heavy mineral counts are in the supplementary material (Appendix G).

1.3.4 Detrital zircon U-Pb geochronology

Detrital zircon crystals on the aforementioned four heavy mineral epoxy pucks were identified and backscatter-imaged using the FEI MLA 650 FEG scanning electron microscope at Memorial University of Newfoundland. The images were used to select homogeneous regions of the zircon grains for in-situ laser ablation. Complex internal zoning, cracks, and inclusions were avoided (see Appendix J). For each sample, 80 to 250 zircons were ablated with a GeoLas 193nm excimer laser ablation system coupled to a ThermoFinningan ELEMENT XR magnetic sector-inductively coupled plasma-mass spectrometer (ICP-MS). The analyses were performed using a 20 µm spot size, using a laser fluence of 4 J/cm^2, pulse rate of 5 Hz, and 200 pulses with a total analysis time of approximately 120s. Data reduction and U-Pb age calculations were done using the VizualAge data reduction scheme developed for Iolite (Paton et al., 2011; Petrus and Kamber, 2012). No common Pb correction was applied. U-Pb ages were calibrated using the 91500 and Plešovice zircon standards (Wiedenbeck et al., 1995; Sláma et al., 2008). Secondary reference materials 02123 and Temora2 were used to evaluate the instrument

drift (Black et al., 2004). Concordance values were calculated using the ratio of $^{206}Pb/^{238}U$ and $^{207}Pb/^{206}Pb$ ages; analyses with excessive discordance (>10% discordant, >5% reverse discordant) were excluded from plots and interpretations. The reported ages for grains younger and older than 1000 Ma are based on $^{206}Pb/^{238}U$ and $^{207}Pb/^{206}Pb$ ages, respectively (Appendix I). U-Pb ages are reported at 2σ uncertainty and presented in Kernel density estimate (KDE) plots made with IsoplotR of Vermeesch (2018). Maximum depositional ages (MDA) were calculated using the youngest grain cluster at 2σ of Dickinson and Gehrels (2009); for these calculations, ages younger than 562 Ma were used, as previous depositional ages calculated from ash layers within the underlying St. John's Group fall between 562 and 565 Ma (Canfield et al., 2020; Matthews et al., 2020). Quantitative statistical comparison between samples was performed using the cross-correlation coefficient of probability density plots (PDPs). These comparisons were conducted with the "DZstats" program of Saylor and Sundell (2016). Cross-correlation coefficient values close to 1 imply identical detrital zircon age distributions, whereas values closer to 0 suggest dissimilar zircon age distributions (Saylor and Sundell, 2016).

Chapter II – Facies and Depositional Environments

2.1 Lithofacies description and interpretation

Six sedimentary facies were recognized in the Signal Hill and the Quidi Vidi formations: cross-stratified sand stone (facies 1), planar-laminated sandstone (facies 2), structureless sandstone beds (facies 3), graded sandstone beds (facies 4), fine-grained siliciclastics (facies 5), and soft-sediment deformed siliciclastics (facies 6) (Table. 1). These were subdivided into subfacies to provide more detail on the near-bed depositional conditions.

2.1.1 F1: Cross-stratified sandstone

2.1.1.1 F1a: Bidirectional cross-laminated sandstone

Subfacies F1a comprises 2-3 cm thick bidirectional, occasionally unidirectional cross-laminated sets of moderately-sorted, very fine to medium-grained sandstone with, where observable, straight, rounded-crests and symmetric formsets 0.5 to 1.5 cm high (average 1 cm) and spacing of 2-8 cm, with an average spacing of 5 cm and length/height ratios (L/H) between 4 and 5.5 (Fig. 2-1.A, C).

2.1.1.2 F1a: Interpretation: Wave ripples

Bidirectional cross-laminated sandstone and symmetric formsets with L/H between 4 and 5.5 are interpreted as subaqueous wave ripples (Allen, 1982). Formsets with an average 5 cm length are classified as orbital ripples with a bottom orbital diameter of ~ 8 cm (Clifton, 1976). Based on the dominant grain size (low to medium sand) and the short wavelength (average 5 cm), short-period waves were likely required to keep sediment flow (Clifton and

Dingler, 1984). Therefore, these ripples were probably formed by short-period, short-wavelength wind waves in shallow water conditions.

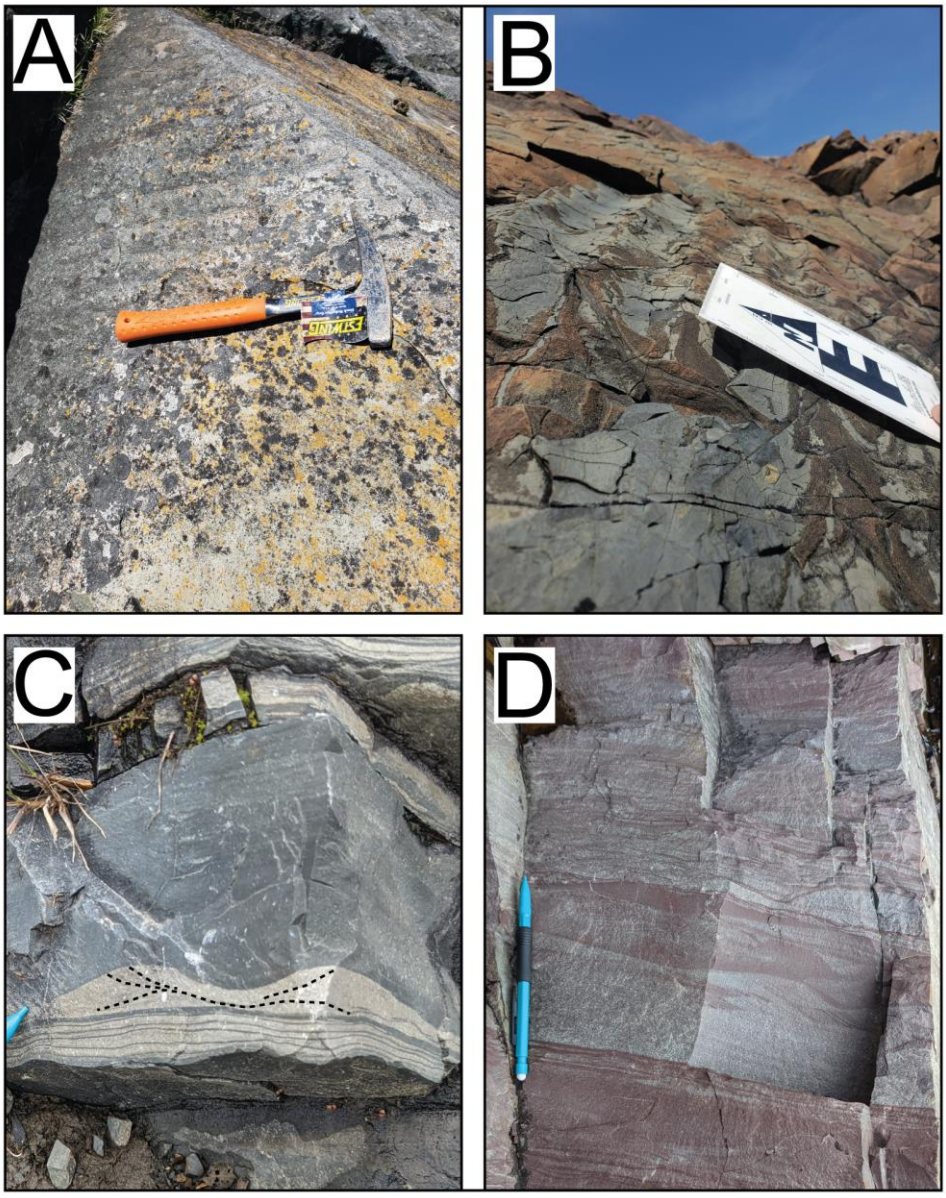

Fig. 2-1. Examples of cross-laminated sandstone subfacies F1a and F1b. A) Symmetric ripple formsets (wave ripples) exposed near Area 8 (see Appendix A for area locations). B) Asymmetric ripple formsets of current ripples exposed near Area 8. C) Small-scale bidirectionally cross-laminated sandstone formsets with rounded crests (Wave ripples), exposed at Area 1. D) Small-scale unidirectionally cross-laminated sandstone formset (Current ripples), exposed at Area 7.

Table. 1. Summary of lithofacies and subfacies in the Gibbett Hill, Quidi Vidi, and Ferryland head formations; Vf: very fine sand; F: fine sand; M: medium sand.

Facies `		Description	Grain size	Structures	Interpretation	Key references
F1: Cross-stratified and Cross-laminated sandstone	F1a	Bidirectional cross-laminated sandstone	Vf-M	2-3 cm thick bidirectional cross-laminated sets of moderately-sorted sandstone. Straight, rounded crests and symmetric formsets are 0.5 to 1.5 cm high (ave. 1 cm) with 2-8 cm spacing (ave. 5 cm; length/height ratios (L/H) range between 4 and 5.5).	Subaqueous wave ripples formed by short-period, short-wavelength wind waves in very shallow water conditions.	Allen, 1982; Clifton, 1976; Clifton and Dingler, 1984
	F1b	Unidirectional cross-laminated sandstone	Vf-M	1-3 cm thick, commonly high-angle (20°-40°) tangential cross-laminated sets of moderately-sorted sandstone. Trough cross-lamination exhibits incisional troughs of 1-2.5 cm deep. Local asymmetric formsets have sharp, mainly straight crests to moderately sinuous with 0.5-3 cm heights and 2-15 cm spacing (L/H ratios 4-5).	2D and 3D subaqueous current ripples built under unsteady and steady flow conditions, respectively.	Allen, 1982;
	F1c	Unidirectional, climbing cross-laminated sandstone	Vf-M	0.5-3 cm thick sets of unidirectionally cross-laminated, well-sorted sandstone. Cross-laminations are mainly tangential with stoss side dipping <15° and climbing angles >20°, but in some cases, they have erosive bases with climbing angles < 15°.	Subcritical to supercritical subaqueous climbing ripples formed under unsteady flow conditions with high sediment fallout rates.	Allen, 1971; Allen, 1982; Hunter, 1977
	F1d	Diffuse surface crenulations and bumps	F-M	Small domes to oval bumps (cm) wide and (cm) high. Local crescentic asymmetries on the domes.	Adhesion warts formed by wind-blown sand onto a wet (<80% water saturation) protuberance likely inherited from adhesion ripples.	Kocurek and Fielder, 1982; Olsen et al., 1989

Facies		Description	Grain size	Structures	Interpretation	Key references
F1: Cross-stratified and Cross-laminated sandstone	F1e	Cross-stratified sandstone	Vf-M	6-80 cm thick sets of moderately-sorted, cross-stratified sandstone. Tabular cross-strata are ~1-3 cm thick, normally graded to ungraded, with dominant tangential contacts between foresets. Through cross-stratification, exhibit 5-20 cm scour; associated bedding plane exposures show 80-90 cm wide rib-and-furrow structures.	2D and 3D subaqueous migrating dunes. High sediment fallout rates promote tangential contacts between individual cross-strata and bounding surfaces.	Ashley et al., 1990; Venditti et al., 2005; Leeder, 2011
	F1f	Sigmoidal cross-stratified sandstone	M	35 cm thick sets of moderately-sorted, sigmoidal cross-stratified sandstone. Cross-strata is defined by ~1-4 cm thick bed/laminae sandstone. Top sets are truncated and downdip-inclined (< 5°). Grading down-current into moderately inclined (20°-30°), long foresets and succeeded by inclined-laminated, short bottomsets that are tangential to the lower set boundary.	Subaqueous humpback dunes formed under critical to supercritical flow conditions.	Ashley et al., 1990; Chakraborty and Bose, 1992; Fielding, 2006; Saunderson and Lockett, 1983
F2: Planar-laminated sandstone	F2a	Massive to ungraded	Vf-M	0.2-0.5 cm thick, well-sorted sandstone laminae with sharp contacts. Laminations are horizontal or less commonly inclined at a low angle (<5°).	Subaqueous, unidirectional low-amplitude bed waves formed at supercritical Froude conditions (Fr > 1); Upper plane stage bed.	Best, 1992; Julien and Raslan, 1998
	F2b	Inverse to normally graded	Vf-M	0.2-0.5 cm thick, well-sorted, reverse to normally graded sandstone laminae with sharp to erosive contacts. Laminations are horizontal or less commonly inclined at low angles (<5°).	Reverse to normal grading motif represents waxing and waning turbidity flow conditions in hyperpycnal flows.	Kneller, 1995; Lamb and Mohrig, 2009; Mulder et al., 2001; Mulder et al., 2003; Zavala, 2020

Facies		Description	Grain size	Structures	Interpretation	Key references
F3: Structureless sandstone	F3a	Structureless sandstone beds	F-M	Thin to very thick-bedded, moderately to well-sorted sandstone beds with floating granules to pebbles, including mud rip-up clasts. These beds are sharp-based with local 1-15 cm deep scours into the underlying strata. Diffuse F2a is sporadically visible in some beds.	Deposition from high energy, concentrated density flows under high rates of sediment aggradation.	Arnott and Hand, 1989; Dasgupta, 2003; Leclair and Arnott, 2005; Lowe, 1982; Mulder and Alexander, 2001; Sumner et al., 2008
F4:Graded sandstone	F4a	Normally graded sandstone beds	F-M	Thin to very thick-bedded, moderately-sorted, normally graded sandstone beds with sharp to erosive contacts. Local intraformational matrix-supported, pebble-to-granule breccia occurs near the base of the bed, defining coarse-tail grading	Deposition from high energy, waning, concentrated density flows under high rates of sediment aggradation.	Arnott and Hand, 1989; Haughton et al., 2009; Mulder and Alexander, 2001; Parker, 1982
F5:Fine-grained siliciclastics	F5a	Parallel-laminated and thin-bedded	Mud-Silt	5mm-5cm laminated to thin-bedded siltstone and mudstone with sharp bases.	Low-energy deposition characterized by suspension fallout	Liang et al., 2016; Mulder and Alexander, 2001
	F5b	Structureless	Mud-Silt	5mm-3cm structureless laminae to thin-bedded mudstone to silty mudstone with sharp bases.	Fluid mud formed by rapid deposition of flocculated, high, near-bed, suspended-sediment concentration flows.	Ichaso and Dalrymple, 2009; McAnally et al., 2007; Trowbridge and Kineke, 1994
F6:Soft-sediment deformed siliciclastis	F6a	Folded strata	Mud-M	Meter-scale folded strata. Folds are moderately plunging and steeply inclined with rounded hinges. Folded strata are sporadically distributed, laterally restricted, and are commonly surrounded by undeformed strata. Internally, these folds depict cm-scale sand dikes cutting siltstone-dominated thin beds	Slump folds	Alsop and Marco, 2011; Owen and Moretti,2011; Waldronand Gagnon, 2011

Facies		Description	Grain size	Structures	Interpretation	Key references
F6:Soft-sediment deformed siliciclastis	F6b	Convolute strata	Mud-M	Convolute interlaminated to interbedded sandstone and siltstone/mudstone with abundant dish-and-pillars and sandstone dykes	Liquefaction and fluidization processes	Allen,1977 Lowe, 1975

2.1.1.3 F1b: Thin unidirectional cross-laminated sandstone sets

Subfacies F1b consists of thin (1-3 cm) sets of well-sorted, cross-laminated, very fine to medium-grained sandstone. High-angle (20°-40°) tangential cross-laminated sets are common. Trough cross-lamination exhibits incisional troughs of 1-2.5 cm deep (Fig. 2-2A). Where present, asymmetric formsets in plan view have sharp formset crests predominantly straight to moderately sinuous with 0.5-3 cm heights and spacing of 2-15 cm (L/H ratios 4-5; Fig. 2-1 B, D).

2.1.1.4 F1b: Interpretation: Subaqueous current ripples

The thinness of the sets, the unidirectional character of the cross-lamination, and the formset asymmetry suggest current ripple migration under low-energy unidirectional subaqueous currents (Allen, 1982). The high angle (20°-40°) tabular cross-laminated sandstone and sharp-crested straight to moderately sinuous formsets are interpreted as deposits of straight to moderately sinuous subaqueous 2D current ripples. Trough cross-laminated sets represent deposits of sinuous, linguoid-crested, 3D current ripples built under continuous flow conditions.

2.1.1.5 F1c: Unidirectional, climbing cross-laminated sandstone

Subfacies F1c is defined by (0.5-3 cm) thick climbing sets of unidirectionally cross-laminated, well-sorted, very fine to medium-grained sandstone. Cross-laminations are predominantly tangential with stoss side dipping <15°, lee side dipping (20°-40°), and set boundaries dipping >20° in the up-current direction. In some cases, sets have erosive bases and climb at angles < 15° (Fig. 2-2B-C).

2.1.1.6 F1c: Interpretation: Climbing ripples

The thinness and unidirectional character of the cross-laminations suggest ripple migration under unidirectional subaqueous currents (Allen, 1982). Ripple sets with climbing angles <15° and erosive bases are interpreted as subcritical climbing ripples; ripple sets with climbing angles > 20° and stoss side dipping < 15° are interpreted as supercritical climbing ripples (Allen, 1971; Hunter, 1977). The angle of climb is controlled by the sediment fallout rate and the bedload transport; rapid sediment fallout reduces or suppresses ripple erosion, promoting ripple preservation and upstream ripple climb over downstream ripples (Allen, 1971). Therefore, these ripples were likely formed under unsteady flow conditions with high sediment fallout rates, e.g., waning stages of sedimentation after rapid fluid deceleration.

2.1.1.7 F1d: Diffuse surface crenulations and bumps

Fine to medium-grained sandstone that forms small domes to oval bumps (1-3cm) wide and (0.6) high. Local asymmetry on the domes results in a crescentic form with short tails, and groups of such asymmetric domes exhibit consistent unidirectional orientations (Fig. 2-2D).

2.1.1.8 F1d: Interpretation: Asymmetric adhesion warts

The size and shape of F1d are consistent with bedforms termed adhesion warts, which are generated by wind-blown sand over a wet (<80 % water saturation) bed surface, and likely evolved from adhesion ripples formed under more water-saturated conditions (Kocurek and Fielder, 1982; Olsen et al., 1989).

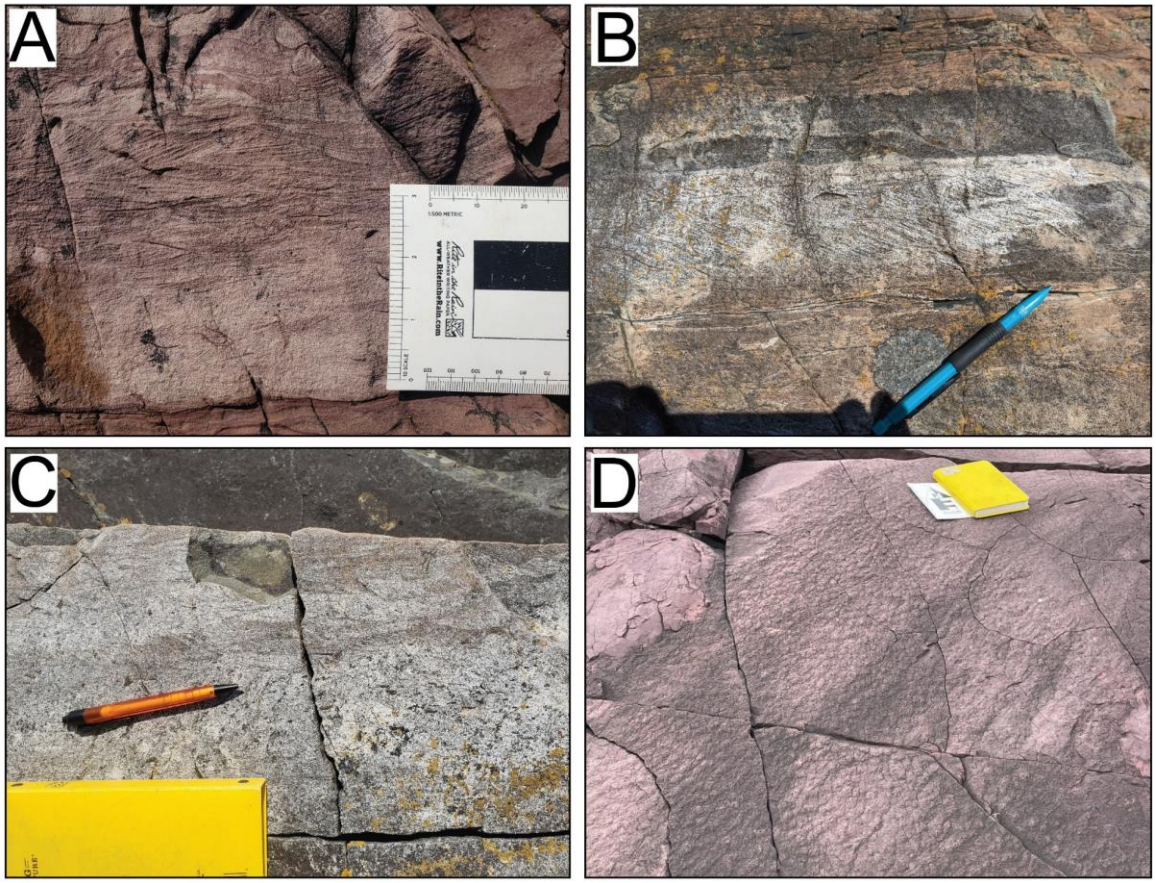

Fig. 2-2. A) Trough cross-laminated current ripples (F1b), exposed at Area 10 (see Appendix A for area locations). B). C) Climbing ripples (F1c) exposed at Area 10 and Area 8, respectively. D) Bed top showing asymmetric adhesion warts (F1d), exposed near Area 4.

2.1.1.9 F1e: Unidirectional, thick high-angle cross-stratified sandstone sets

Subfacies F1e consists of 6 to 80 cm thick sets of moderately sorted, cross-stratified, medium to coarse-grained sandstone. Tabular cross-strata are ~1-3 cm thick, normally graded to ungraded, with dominantly tangential contacts between foresets. Trough cross-stratified sets, where present, exhibit 5-20 cm of basal scour. Associated bedding plane exposures show 80-90 cm wide rib-and-furrow structures (Fig. 2-4A).

2.1.1.10 F1e: Interpretation: Subaqueous migrating Dunes

The unidirectional character, grain size, and thickness of the cross-stratified sets record the migration and buildup of subaqueous dunes (Ashley et al., 1990). Tabular cross-stratification represents 2D straight dunes, whereas trough cross-stratification record the migration of 3D dunes (Fig. 2-3). As with ripples, 2D dunes are unstable and transient bedforms that evolve into 3D linguoid dunes (Venditti et al., 2005). Tangential contacts between individual cross-strata and bounding surfaces are promoted by high sediment fallout rates in the dune lee and weak lee-side separation eddies (Leeder, 2011). The presence of 3D and 2D dunes with tangential contacts, therefore, suggests sedimentation under variable flow conditions with high sediment fallout rates.

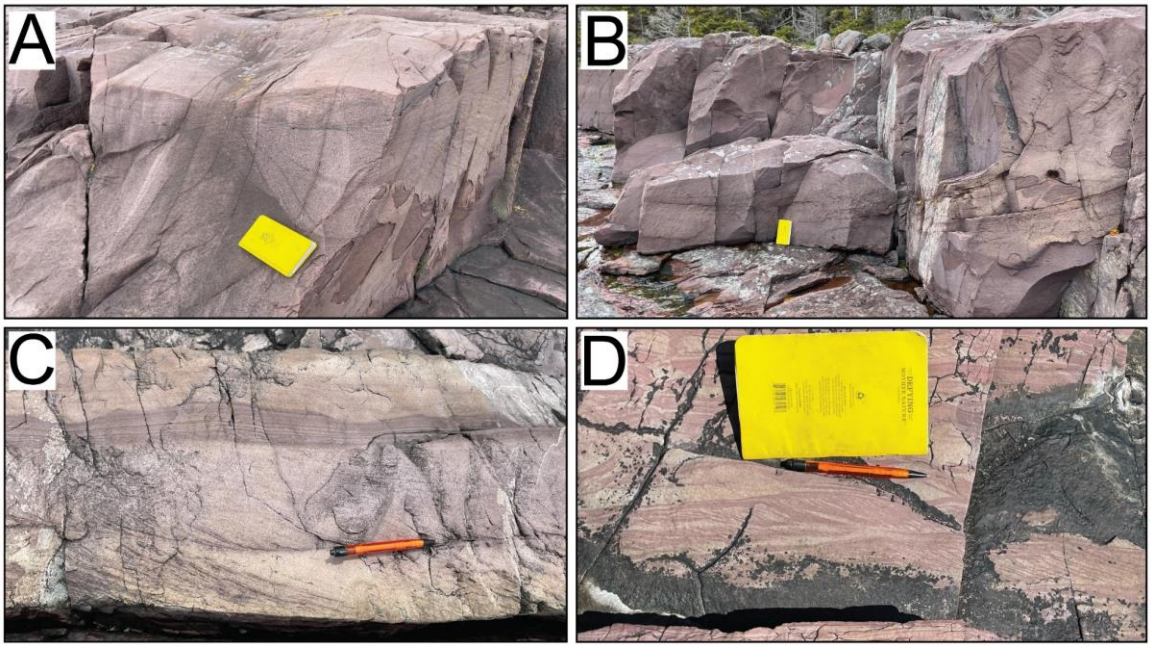

Fig. 2-3. A) Trough cross-stratified sandstone formed by the migration and buildup of 3D dunes (F1e). B). Tabular cross-stratified sandstone representing the migration of 2D dunes (F1e). Outcrops A and B are exposed between Areas 4 and 5 (see Appendix A for area locations). C) Tabular cross-stratified sandstone (F1e) transitioning into low-angle planar

laminated (F2a). D) Subaqueous migrating dunes (F1e) showing internal reactivation surfaces and mud drapes. Outcrops C and D are exposed at Area 10.

2.1.1.11 F1f: Unidirectional, sigmoidal cross-stratified sandstone sets

Subfacies F1f is represented by a rare cosets of 35 cm thick sets of well-sorted, sigmoidal cross-stratified sandstone. Cross-strata are defined by interlaminated thin (~1-4 cm) beds/laminae of medium-grained sandstone. Top sets are commonly truncated, but locally shallow, low angle downdip-inclined (< 5°) cross strata define them. Top sets grade down-current into moderately inclined (20°-30°) foresets, succeeded by inclined-laminated bottomsets that are tangential to the lower set boundary (Fig. 2-4B).

2.1.1.12 F1f: Interpretation: Subaqueous Humpback Dunes

The unidirectional character and thickness of the cross-stratification correspond to deposits of subaqueous dunes (Ashley et al., 1990). Flume experiments and field observations have identified sigmoidal cross-strata as transient bedforms between dune and upper-stage plane beds (Saunderson and Lockett, 1983; Chakraborty and Bose, 1992; Fielding, 2006). Furthermore, experimental observations suggest that sigmoidal cross-stratification with relatively longer foresets compared to the bottomsets is formed under low sediment fall-out rates over the dune lee side, forming “humpback dunes” (Chakraborty and Bose, 1992). The preservation of this transient bedform, its homogenous grain size, and the lateral and vertical transition from concave-up cross-stratification to sigmoidal cross-stratification and parallel to inclined lamination (Fig. 2-4B) suggest fluctuating flow conditions between dune and upper stage plane bed stability fields under net deposition.

Fig. 2-4. A) Rib-and-furrow structures from truncated 3D dune sets (F1e). B) Sigmoidal cross-stratified sandstone formed by humpback dunes (F1f). Outcrops from A and B are exposed between Areas 4 and 5 (see Appendix A for area locations). Red arrows indicate paleoflow direction. White dashed lines outline laminae.

2.1.2 F2: Planar-laminated sandstone

2.1.2.1 F2a: Massive to ungraded, planar-laminated sandstone

Subfacies F2a consists of 0.2-0.5 cm thick, well-sorted, very fine to medium-grained, ungraded sandstone laminae. Laminations are horizontal or less commonly inclined at a low angle (<5°); they are defined by subtle grain size and sorting changes with sharp to flat contacts (Fig. 2-5A-C).

2.1.2.2 F2a: Interpretation: Upper-stage plane bed stratification

F2a is interpreted as upper stage plane bed formed by unidirectional, low-amplitude bed waves at critical to supercritical Froude conditions (Fr ≥ 1) (Best, 1992; Julien and Raslan, 1998).

2.1.2.3 F2b: Inverse to normally graded, planar-laminated sandstones

Subfacies F2b is defined by 0.2-0.5 cm thick, well-sorted, very fine to medium-grained, reverse to normally graded sandstone laminae. Laminae are horizontal or less commonly inclined at low angles (<5°) with sharp to erosive basal contacts (Fig. 2-5D-E).

2.1.2.4 F2b: Interpretation: Deposition from hyperpycnal flows

Reverse-graded laminae (F2b) have been interpreted to represent waxing conditions in long-lived turbiditic flows (Kneller, 1995; Mulder et al., 2001). Inverse grading of beds or laminae is produced under these conditions, provided the flow velocity remains below the erosion threshold (Mulder et al., 2001). Whereas normally graded laminae represent rapid particle settling from decelerating, waning turbidity flows (Mulder and Alexander, 2001; Dasgupta, 2003). Therefore, the reverse to normal grading motif represents waxing and waning flow conditions, typical of deposits of quasi-steady turbiditic flows (e.g., hyperpycnal flows; Mulder et al., 2003; Lamb and Mohrig, 2009; Zavala, 2020).

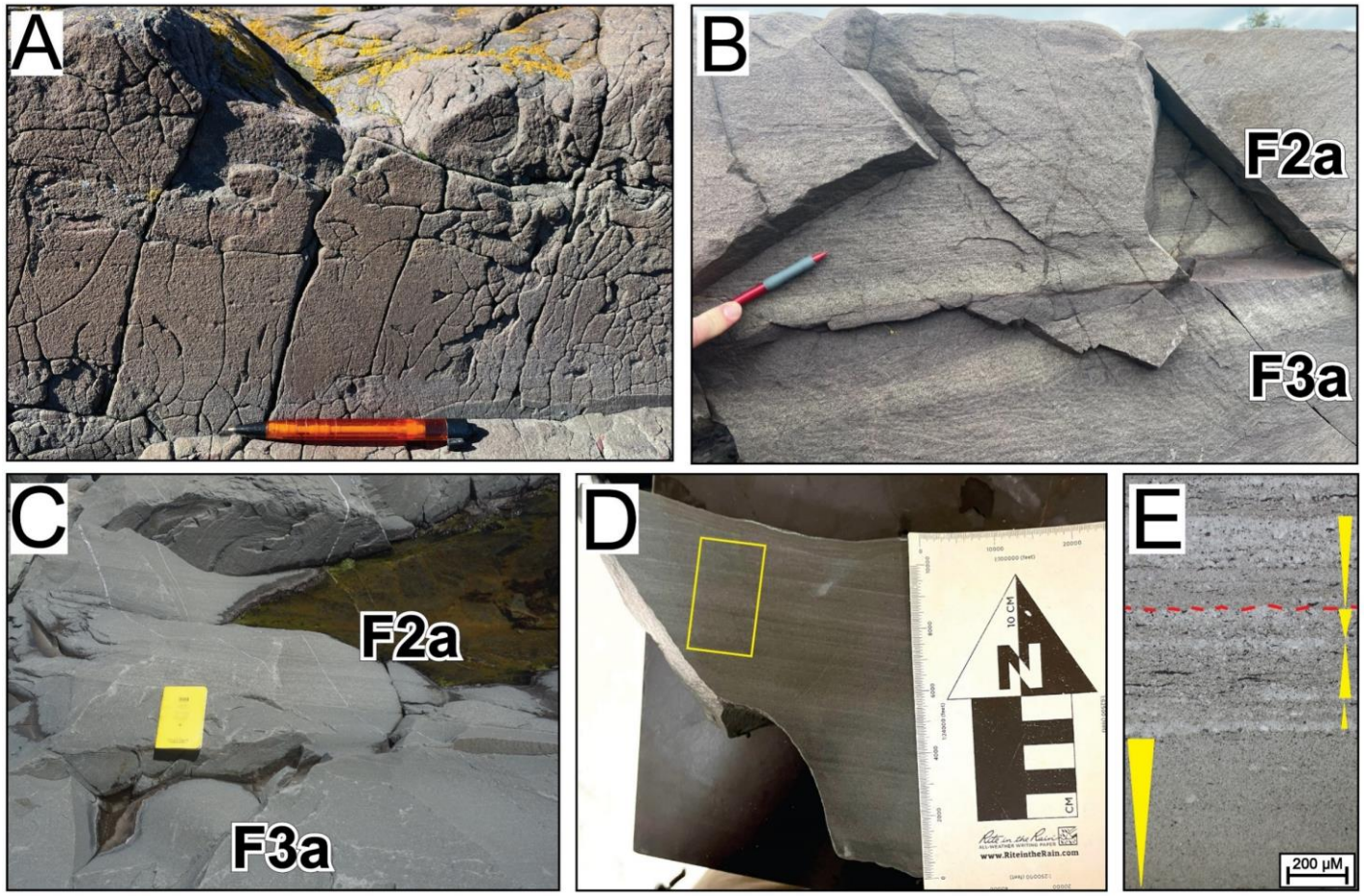

Fig. 2-5. A) Cryptic planar lamination (F2a) in structureless sandstone (F3a) exposed at Area 7 (see Appendix A for area locations). B). C) Structureless sandstone (F3a) transitioning into planar-laminated sandstone (F2a), outcrops B and C are exposed in Area 4 and 9, respectively. D). E) Normally and reversely graded sandstone laminae formed under hyperpycnal flows (F2b). Yellow triangles represent grain size trends. The red dashed line represents erosive contact.

2.1.3 F3: Structureless sandstone beds

2.1.3.1 F3a: Structureless sandstone beds

F3a consists of 0.1 m to 2 m thick, moderately to well-sorted, fine to medium-grained sandstone beds with floating granules to pebbles, including mud rip-up clasts. These beds are sharp-based with local 1-15 cm deep scours into underlying strata. Diffuse F2a lamination is sporadically visible in some beds (Fig. 2-5A-C; Fig. 2-6A).

2.1.3.2 F3a: Interpretation: Rapid deposition from concentrated density flows

The range in grain size, sharp-based to erosive nature of contacts, and lack of internal stratification suggest deposition from high energy, concentrated density flows. The general lack of stratification and the lack of any link to soft-sediment deformation, plus the occurrence of sporadic cryptic to diffuse planar lamination, indicate high rates of sediment aggradation and sediment concentration that generally precluded high-energy bedform generation (Arnott and Hand, 1989; Leclair and Arnott, 2005; Sumner et al., 2008). Furthermore, the presence of floating pebble-sized clasts and the absence of gradation imply frictional freezing and deposition without much water entrainment (Lowe, 1982; Postma et al., 1988; Mulder and Alexander, 2001; Dasgupta, 2003). Erosion at the base of concentrated density flows is common and can maintain flow momentum, even causing flow acceleration, resulting in long runout distances (Normark and Piper, 1991); this is consistent with the presence of centimetric scale scours into the underlying strata and mud-rip up clasts, suggest that the flow eroded and incorporated underlying cohesive strata.

2.1.4 F4: Graded Sandstone beds

2.1.4.1 F4a: Normally graded sandstone beds

F4a consists of 0.1 m thin to 1.5 m thick beds of moderately- to well-sorted, normally graded, fine- to medium-grained sandstone. Intraformational matrix-supported, pebble-to-granule sedimentary breccia occurs sporadically near the base of beds, defining coarse-tail grading (Fig. 2-6C-D). The beds are commonly sharp-based, with local erosion of 10-30 cm deep scours into the underlying strata. These beds commonly grade upwards into planar lamination (F2a), climbing ripples (F1c), and current ripples (F1b; Fig. 2-7).

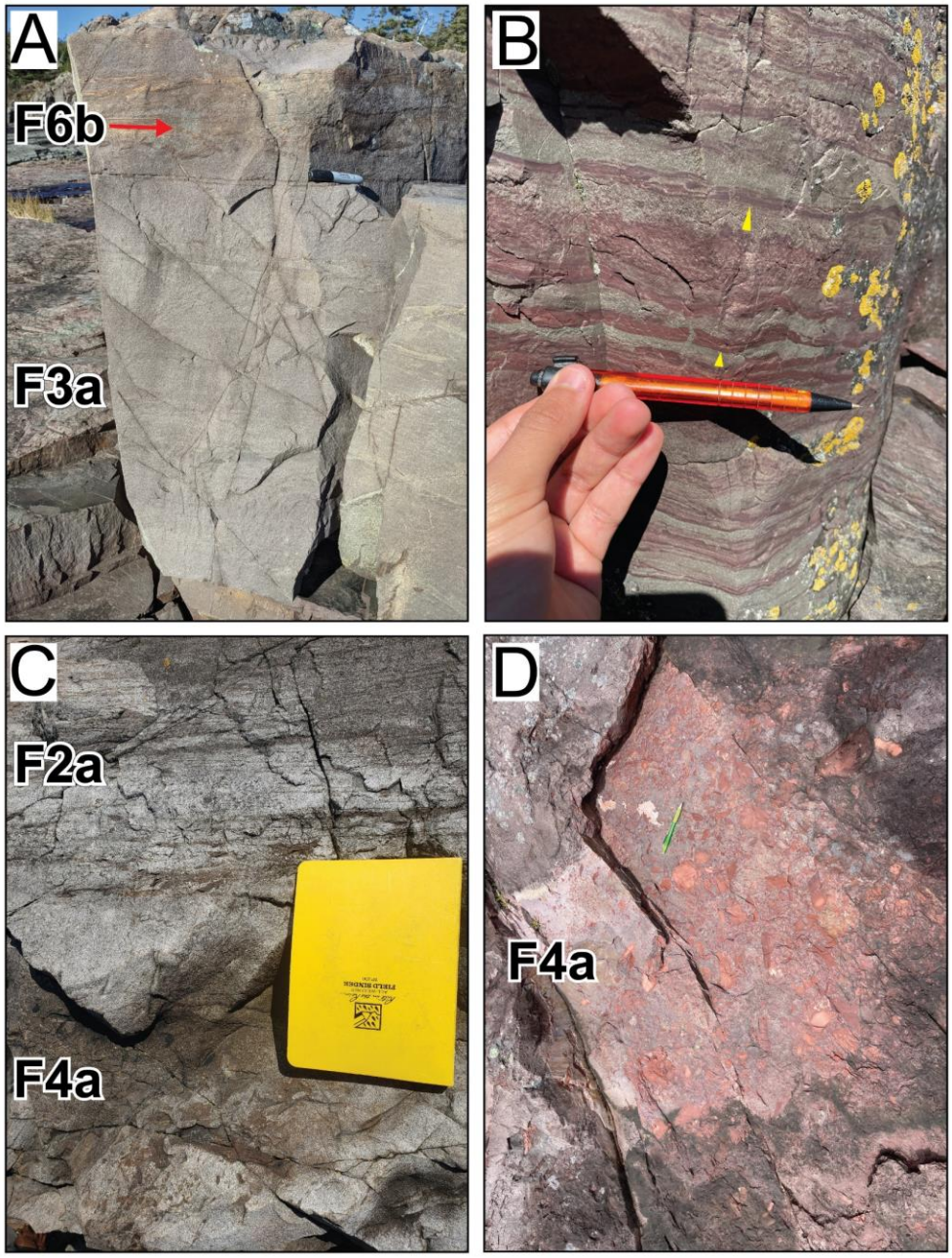

Fig. 2-6. A) Structureless medium to coarse-grained sandstone bed recording sedimentation at the base of a concentrated density current (F3a) with sandstone dykes (F6b) at the top, exposed at Area 7 (see Appendix A for area locations). B) Structureless to normally graded sandstone laminae formed by waning turbiditic flows (F2b) interlaminated with mudstone and siltstone (F5a, F5b), exposed at Area 7. C) Normally graded bed, from intraformational breccia at the bottom to planar lamination (F2a) at the top, recording sedimentation under a waning concentrated density current, exposed at Area 8. D) Intraformational matrix-supported breccia (F4a), exposed near Area 4.

2.1.4.2 F4a: Interpretation: Rapid deposition from waning concentrated density flows

The relatively homogeneous grain size, sharp to erosive basal contacts, lack of internal stratification, moderate sorting, and association with climbing ripples (F1c) suggests sedimentation from high energy, waning concentrated density flows (Haughton et al., 2009). The absence of stratification suggests that bedform generation was impeded, likely due to high rates of sediment aggradation and high sediment concentrations (Arnott and Hand, 1989; Sumner et al., 2008). Furthermore, the coarse tail grading implies particle rearrangement caused by the loss of cohesion and flow capacity due to progressive dilution and coinciding flow deceleration along the transport path (Parker, 1982; Mulder and Alexander, 2001). The deposition was followed by waning, lower concentration, but still aggradational flow conditions represented by an upward transition into planar lamination (Fa2) and climbing or current ripples (F1c, F1b) at the top of the bed.

2.1.5 F5: Fine-grained siliciclastic strata

2.1.5.1 F5a: Parallel-laminated and thin-bedded siltstone/mudstone

F5a is defined by finely parallel laminated, 5 mm to 5 cm thick, sharp-based laminae and thin beds of siltstone and mudstone. Internally, F5a strata are characterized by a fine parallel lamination defined by parallel-oriented clay particles and iron oxide ribbons. F5a is commonly interlaminated to interbedded with F1b, F1c, and F2b, defining a heterolithic bedding (Fig. 2-6B; Fig. 2-7B).

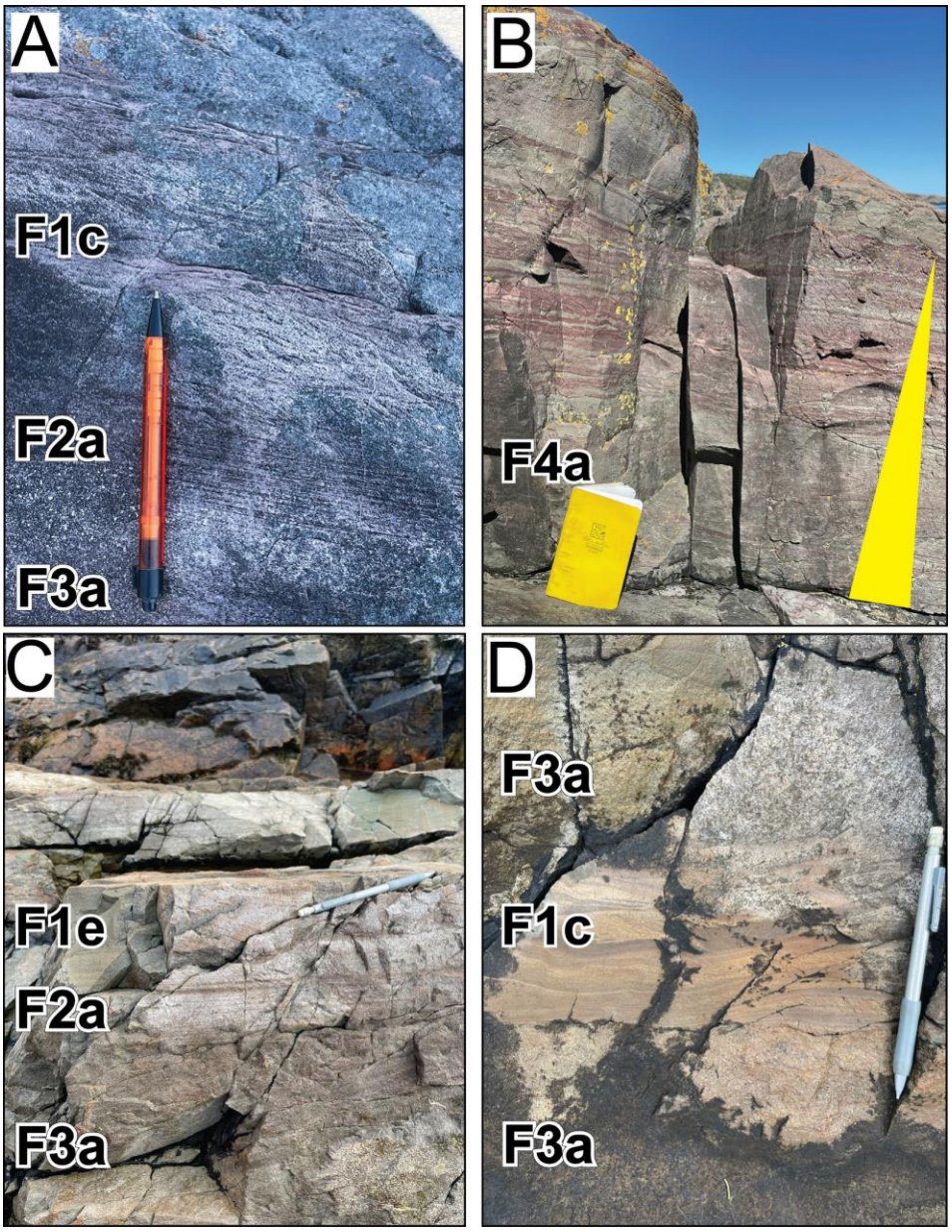

Fig. 2-7. A) Structureless sandstone deposited at the base of a concentrated density current (F3a) evolving into upper plane bed lamination (F2a) and climbing ripple stratification (F1c), exposed at Area 10 (see Appendix A for area locations). B) Normally graded sandstone bed deposited under a waning concentrated density flow (F4a), defined by structureless, medium-grained sandstone evolving vertically into fine-grained sandstone interlaminated with mudstone, exposed in Area 7. C). Structureless sandstone from concentrated density currents (F3a) transitioning into upper plane lamination (F2a) and dune cross-stratified sandstone (F1e), exposed near Area 8. D). Structureless sandstone bed recording concentrated density current sedimentation (F3a) evolving into climbing ripples (F1c), exposed near Area 8. Yellow triangle indicates grain size trend.

2.1.5.2 F5a: Interpretation: Slow sediment settling after rapid fluid deceleration

F5a represents periods of low-energy deposition. The close association with subfacies F1b, F1c, and F2b suggests fluctuating flow conditions between waning turbidity flows and quiet periods that allowed suspension fallout (Mulder and Alexander, 2001; Liang et al., 2016).

2.1.5.3 F5b: Structureless mudstone/siltstone

Subfacies F5b consists of 5 mm to 3 cm thick, structureless laminae and thin-beds of mudstone to silty mudstone with sharp basal contacts. Internally, F5b contrast with F5a in that it has no preferred particle orientation. F5b is usually interbedded/laminated with ripple subfacies F1a, F1b, F1c, waning and waxing turbiditic strata of F2b, and F5a (Fig. 2-6B).

2.1.5.4 F5b: Interpretation: Fluid Mud

The grain size, the thickness, and the homogeneous structureless aspect of subfacies F5b suggest rapid sedimentation of flocculated mud, forming high concentration, near-bed, suspended-sediment layers likely remobilized by high-energy currents as fluid mud flows (Trowbridge and Kineke, 1994; Ichaso and Dalrymple, 2009). The presence of sharp contacts with the underlying strata could represent the migration of the fluid mud likely triggered by the overriding shear flow or down-slope displacement as sediment gravity flow (McAnally et al., 2007; Ichaso and Dalrymple, 2009).

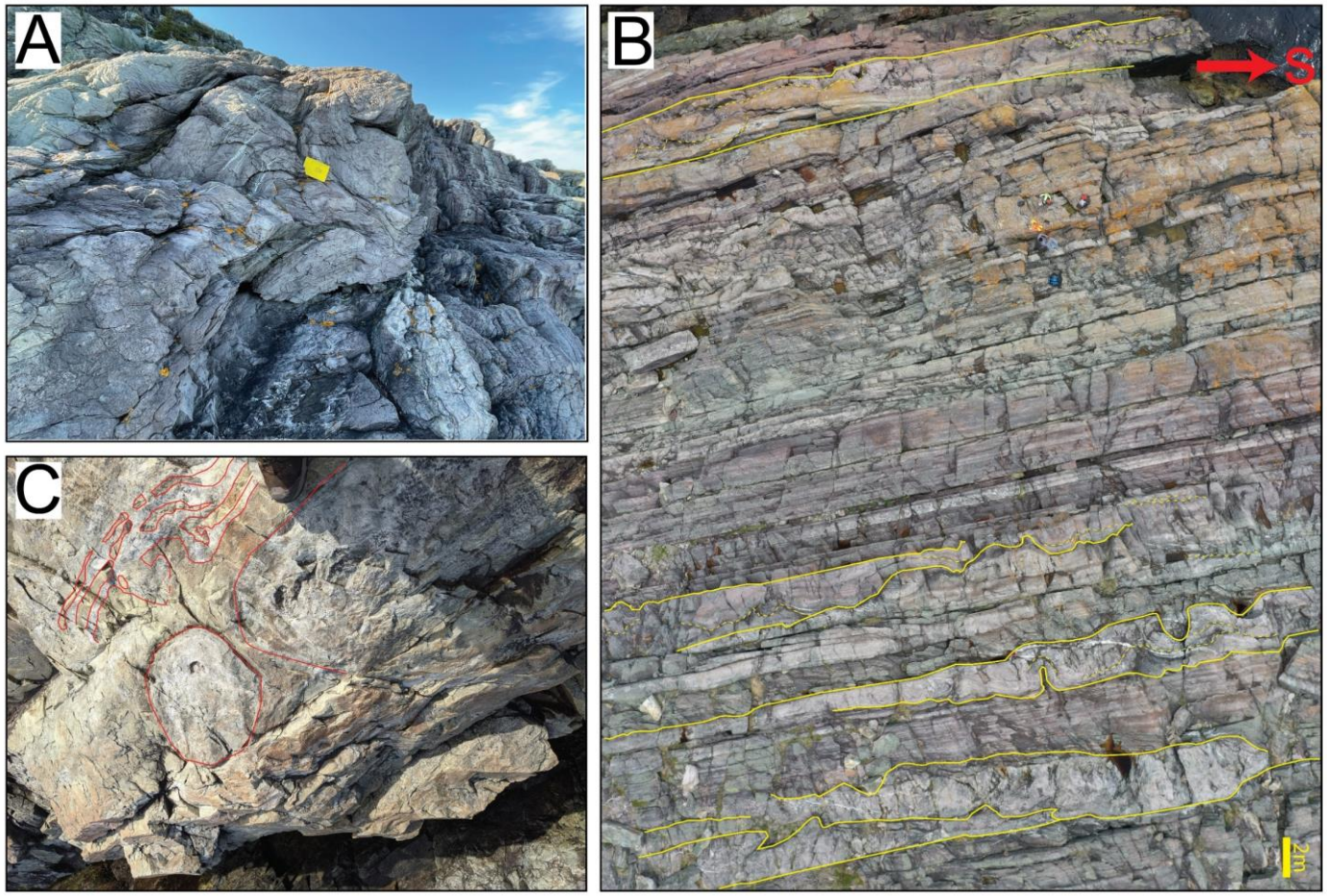

Fig. 2-8. A) and B) Up-right to steeply inclined folded strata (F6a) enclosed by undeformed strata exposed at Area 10 (see Appendix A for area locations). C) Sandstone dykes (F6b) cutting siltstone-dominated layers in folded strata exposed at Area 10. Yellow solid lines outline folded strata; red solid lines define the limits of the sandstone dykes. The red arrow points towards the paleo flow direction.

2.1.6 F6: Soft-sediment deformation

2.1.6.1 F6a: Folded strata

F6a comprises strata-bound, sharply to erosively based, laterally discontinuous, 1-4 m thick beds of meter-scale folding of all of the previously described facies. Folds are moderately plunging and steeply inclined (Fleuty, 1964), with rounded hinges and vergence toward the NW and the SE. Folded strata are sporadically distributed, laterally restricted, and are commonly surrounded by undeformed strata (Fig. 2-8A-B). Internally, these strata are cut by cm-scale sand dikes cutting siltstone-dominated thin beds (Fig. 2-8C).

2.1.6.2 F6a: Interpretation: Slump folds

The presence of sand dykes cutting siltstone-dominated beds within the folded strata suggests synchronous folding and liquefaction-fluidization, common in unconsolidated sediments (Owen and Moretti, 2011; Waldron and Gagnon, 2011). Furthermore, the isolated folded layers interbedded with undeformed strata represent alternating episodes of deformation of unconsolidated sediments. Therefore, these folds are interpreted as slump folds (Alsop and Marco, 2011). Upright to steeply inclined soft-sediment folding could represent initial slumping stages, characterized by coaxial-dominated vertical forces driven by seismically induced horizontal shortening or dewatering after rapid sediment deposition (Alsop and Marco, 2011; Waldron and Gagnon, 2011).

2.1.6.3 F6b: convolute interstratified sandstone, siltstone, and mudstone

Subfacies F6b is defined by localized convolute deformation of interlaminated to interbedded sandstone (F1a, F1b, F1c, F2a, F2b, F3a) and siltstone/mudstone (F5a, F5b) with abundant dish-and-pillars and vertical sandstone dykes (Fig. 2-9A-F). Pillars are perpendicular to the bedding and have sharp edges and are less than 3 cm in width with heights between 3-7 cm. Pillars divide 8 to 10 cm wide concave-upward interlaminated sandstone and siltstone. Sandstone dykes vary in length and width, reaching up to 18 cm in width and 30 cm in height; they are perpendicular to sub-perpendicular to the bedding.

2.1.6.4 F6b: Interpretation: Liquefied to fluidized interbedded/laminated sandstone and siltstone strata

Convolute lamination represents the deformation of the primary sedimentary fabric while the sediment was in a weakened state, caused by the temporal grain weight transfer to the pore fluid during an increment in pore-fluid pressure or the collapse of grain packing, e.g., liquefaction (Allen, 1977). Structures such as sandstone dikes and dish-and-pillars record the upward flow of liquefied sediments coinciding with the fluidization of overlying strata (Lowe, 1975).

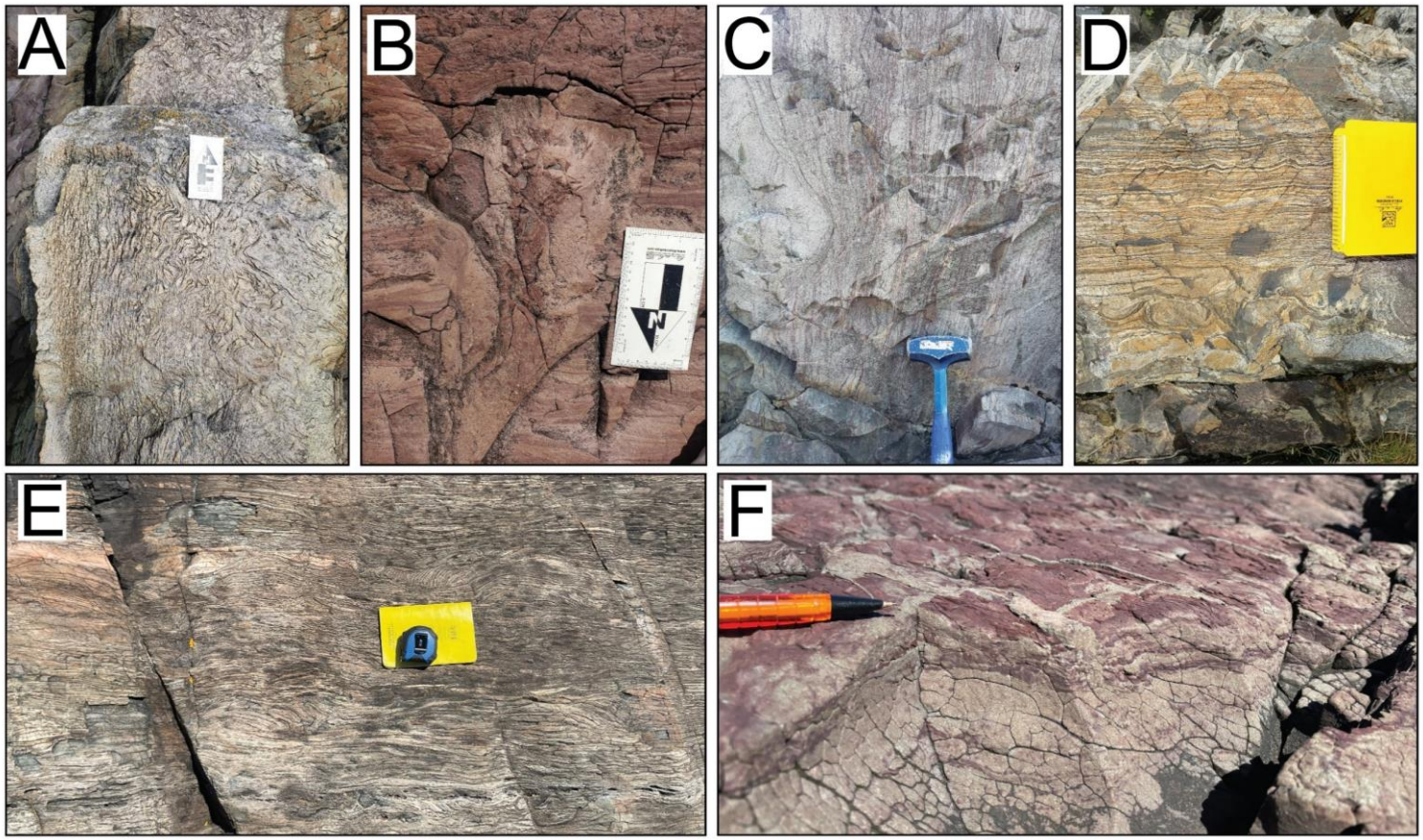

Fig. 2-9. A) Convolute-laminated strata formed by localized liquefaction processes (F6b). B) and C) Sandstone dykes formed by liquefaction leading to fluidization and dewatering (F6b). D) Dish-and-pillar structures (F6b) recording liquefaction and dewatering processes. E) Convolute-laminated strata related to selective liquefaction (F6b). F) Small sandstone dykes through mudstone. Pictures A to E correspond to outcrops at Area 10; Picture F corresponds to rocks exposed at Area 7 (see Appendix A for area locations).

2.2 Facies Associations (FA)

Two facies associations representing distinct deltaic depositional subenvironments (FA1, FA2) are recognized and correlated in strata of the GHF and QVF and equivalent Ferryland Head Formation based on bed-by-bed measurement of 5 outcrop sections and related facies and subfacies summarized in Table 1. Facies associations FA1 and FA2 were interpreted based on recurring grouping of facies and architectural elements between sections and the dominant flow process. Architectural elements identified include amalgamated tabular sandstone bed sets, amalgamated channel elements, tabular heterolithic bed sets, upward coarsening and thickening bed sets, and lobate sandstone beds. Additionally, it was found that facies associations are not constrained by the lithological boundaries. As a result, FA1 comprises the entire GHF and the lower part of the QVF strata, and FA2 makes up most, but not all of the remaining of the QVF and equivalent Ferryland Head Formation.

2.2.1 FA1: Amalgamated sandstone beds and upward coarsening and thickening bed sets

FA1 comprises intercalated units of sandstone and heterolithic mudstone-siltstone-sandstone strata, here defined as sub-associations FA1a and FA1b, respectively. FA1a comprises 2 to 80 m-thick sandstone-dominated intervals consisting of two architectural elements: amalgamated tabular bed sets (~ 51% of measured FA1 sections) and channel elements (~ 10%). The amalgamated tabular bed sets are laterally extensive (> 100 m), 5-10 m thick, and consist of alternating beds of 0.3 m to 2 m thick sustained and waning

concentrated density flow deposits (F3a, F4a) and rare 0.1 to 2 m thick dune cross-stratified or wave ripple-laminated sandstone beds (F1a, F1e) (Fig. 2-10A). Some of the waning concentrated density flow deposits depict structureless (F3a) to upper plane bed strata (F2a) that evolve upwards into subaqueous current ripples (F1b) or climbing ripples (F1c; Fig. 2-7C-D). Channel elements are 0.7-3 m thick, have erosive bases, and are composed of moderately sorted, fine to medium-grained, dune cross-stratified sandstone (F1e) with rare internal lateral-and downstream-accreting surfaces and mud clasts (Fig. 2-11; Fig. 2-12). Generally, FA1a channel elements scour into associated sandy sheet elements and into FA1b. Conversely, amalgamated tabular bed sets overly and laterally transition into FA1b.

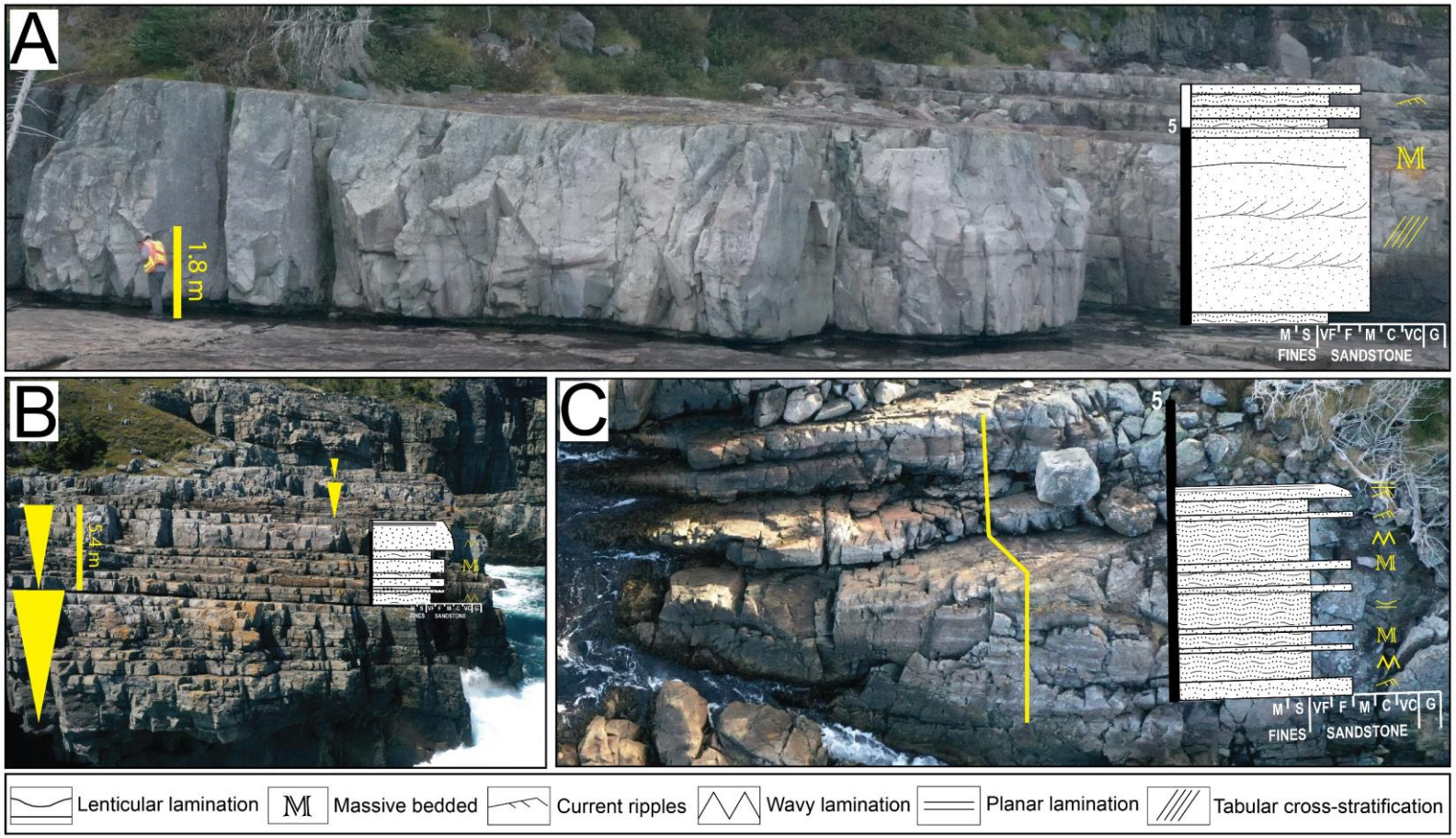

Fig. 2-10. A) Amalgamated tabular bed sets from FA1a, recording proximal mouth bar sedimentation defined by alternating dune cross-stratified and waning concentrated density flow deposits, exposed near Area 5. B) Stacked upward coarsening and thickening bed sets of FA1b, interpreted as prograding mouth bars, exposed at Area 6. C) Tabular heterolithic bed sets (FA1b) recording terminal/fringe mouth bar sedimentation, exposed at Area 8. Yellow triangles define upward coarsening and thickening trends. Yellow line defines the measured log. See Appendix A for area locations.

FA1b consists of 1 to 20 m-thick mudstone- and siltstone-dominated heterolithic intervals comprising two architectural elements: tabular heterolithic bed sets (~29%) and upward coarsening and thickening bed sets (~10%). Tabular heterolithic bed sets are 2-5 m thick and consist of 0.1-0.3 m thick beds of mudstone and siltstone deposited by suspension fallout (F5a) interlaminated with fine-grained hyperpycnites and ripple-laminated sandstone (F2b, F1a, F1b, F1c; Fig. 2-5D-E; Fig. 2-10C). The upward coarsening and thickening bed sets are 4-6 m thick and consist of heterolithic strata interstratified with 0.1-1.5 m thick, laterally persistent (> 100 m), tabular to lobate sandstone beds comprising sustained and waning concentrated density current deposits (F3a; F4a) (Fig. 2-10B), some of which show a vertical transition from supercritical to subcritical bedforms (F1b, F1c, F1e). Discrete centimeter- to meter-scale intervals of FA1b are affected by soft-sediment deformation characterized by convolute lamination and dish-and-pillars structures (F6b; Fig. 2-9 A, D).

Fig. 2-11. Channel element (FA1a) cutting into tabular heterolithic strata (FA1b), interpreted as a feeder channel cutting into a distal/fringe mouth bar deposit, exposed near Area 6 (see Appendix A for area locations). The dashed yellow line represents erosional contact; the red arrow indicates paleoflow direction.

2.2.2 FA1: Interpretation: Delta front

The combination of amalgamated tabular bed sets dominated by sediment gravity flow processes and lesser channel elements filled with dune cross-strata suggests a nearshore subaqueous terminal flow environment where unconfined high-energy and concentration of flows are widespread and fed by coeval channels. The presence of wave-ripple laminated beds, symmetric ripple marks, and the lack of hummocky cross-stratification suggest that FA1 was deposited above fair-weather wave base (James and Dalrymple, 2010). In the context of a deltaic sedimentary environment, the stratigraphic position of FA1 above the prodelta facies of the St John's Group (e.g., King, 1990) and evidence of shallow water sedimentation suggest that FA1 sedimentation took place in a river-dominated delta front environment (Bhattacharya, 2006). The dominance of sediment gravity flow processes within FA1a amalgamated tabular bed sets and FA1b lobate deposits, and in some cases, an upward transition from massive, through supercritical to subcritical bedforms and even mud in individual beds suggest deposition from waning high-energy hyperpycnal flows (Mulder et al., 2003; Sumner et al., 2008; Lamb and Mohrig, 2009; Zavala, 2020). In this context, the upward coarsening and thickening bed sets in FA1b that vertically transition into amalgamated tabular bet sets in FA1a are interpreted as prograding mouth bars formed by successive deposits of hyperpycnal flows derived from channel mouths (Bates, 1953; Fidolini and Ghinassi, 2016). The amalgamated tabular bed sets in FA1a are interpreted to represent proximal/axis mouth bars, whereas the upward coarsening and thickening bed sets and tabular heterolithic bed sets of FA1b, dominated by suspension fallout mudstone/siltstone and thin sandy hyperpycnite strata,

constitute medial to terminal/fringe mouth bars (Fidolini and Ghinassi, 2016; van Yperen et al., 2020). Soft-sediment deformation in these strata represent post-depositional liquefaction and fluidization triggered by accumulated normal stress due to the loading of rapidly deposited sediment (Owen and Moretti, 2011). Channel elements within FA1a that sometimes scour into FA1b are interpreted as the terminal distributary channels that fed mouth bars and splays (Olariu and Bhattacharya, 2006). Internal lateral and downstream accreting surfaces represent infilling by laterally- and downstream-accreting bars, respectively, and record variable sinuosity of channels (Bridge and Lunt, 2006; Olariu and Bhattacharya, 2006).

2.2.3 FA2: Tabular heterolithic strata and channelized cross-stratified sandstone

FA2 comprises mudstone- and siltstone-dominated heterolithic strata interbedded with sandstone, and consists of three architectural elements: tabular heterolithic bed sets (~ 46%), laterally and vertically amalgamated channel elements (~34 %), and lobate sandstone beds (20%). The tabular heterolithic bed sets are flaser to lenticular stratified, 0.2 to 10 m thick, and consist of 0.3 to 3 cm reddish, massive fluid mud strata (F5b) and planar- to wavy-laminated muddy siltstone (F5a) interstratified with 0.5 to 5 cm thin, very-fine to fine-grained, rippled-laminated sandstone (F1a, F1b) and waning turbidity flow sandstone strata (F2b) (Fig. 2-13). Laterally and vertically amalgamated channel elements have erosive bases with up to 1.5 m of incisional relief and rare internal downstream and upstream accretion surfaces.

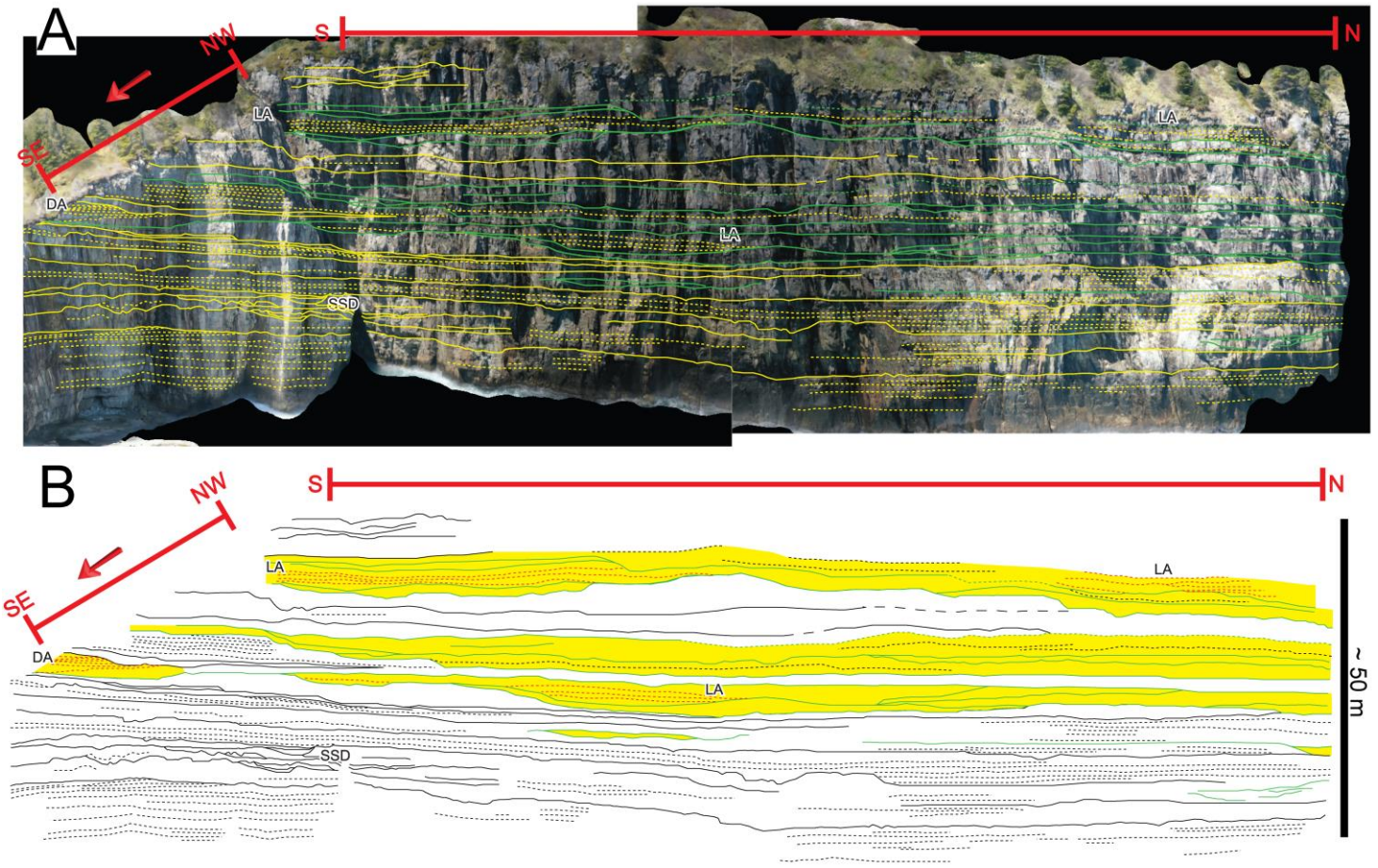

Fig. 2-12. A) Oblique-oriented photomosaic of the medial part of the delta front facies outcropping near Area 6 (see Appendix A for area locations). B) Bedding diagram showing terminal distributary channels (yellow) cutting amalgamated lobate to tabular sandstone beds representing proximal mouth bars interbedded with tabular heterolithic strata. Abbreviations: LA-lateral accretion; DA-downstream accretion; SSD-soft-sediment deformed interval; the red arrow indicates paleo flow direction.

Their combined thickness reaches up to 20 m and consists of 0.5 to 1.6 m thick, medium to coarse-grained trough and tabular dune cross-stratified beds with 0.15 to 0.9 m thick dune sets (F1e) and rare concentrated sediment gravity flow sandstone strata with abundant angular mud clasts (F4a) (Fig. 2-14; Appendix B-C). Rare upper plane bed stratification (F2a), asymmetric adhesion warts (F1d), and humpback dunes (F1f) occur at the top and within some of these beds. Lobate sandstone beds have sharp non-erosive to slightly erosive basal contacts and consist of medium-grained, structureless sandstone deposits of sustained and waning concentrated density currents (F3a, F4a) and rare tabular dune cross-stratified sandstone with mudstone drapes and internal reactivation surfaces (Fig 2-3D). These beds are laterally persistent > 20 m, reaching up to 1 m thick (Fig. 2-13C; Fig. 2-14). In addition, some of them show an internal transition from supercritical to subcritical bed forms, including structureless (F3a) to upper plane bed strata (F2a), followed by subaqueous current or climbing ripples (F1b, F1c). Generally, channel elements scour into the heterolithic bed sets, and lobate elements are interbedded with the heterolithic bed sets. Centimeter- to meter-scale intervals of heterolithic strata and channel elements are affected by soft-sediment deformation characterized by convolute lamination, dish-and-pillars structures, sand dykes, and rarer meter-scale up-right to steeply inclined slumped folds (F6a, F6b) (Fig. 2-8; Fig. 2-9)

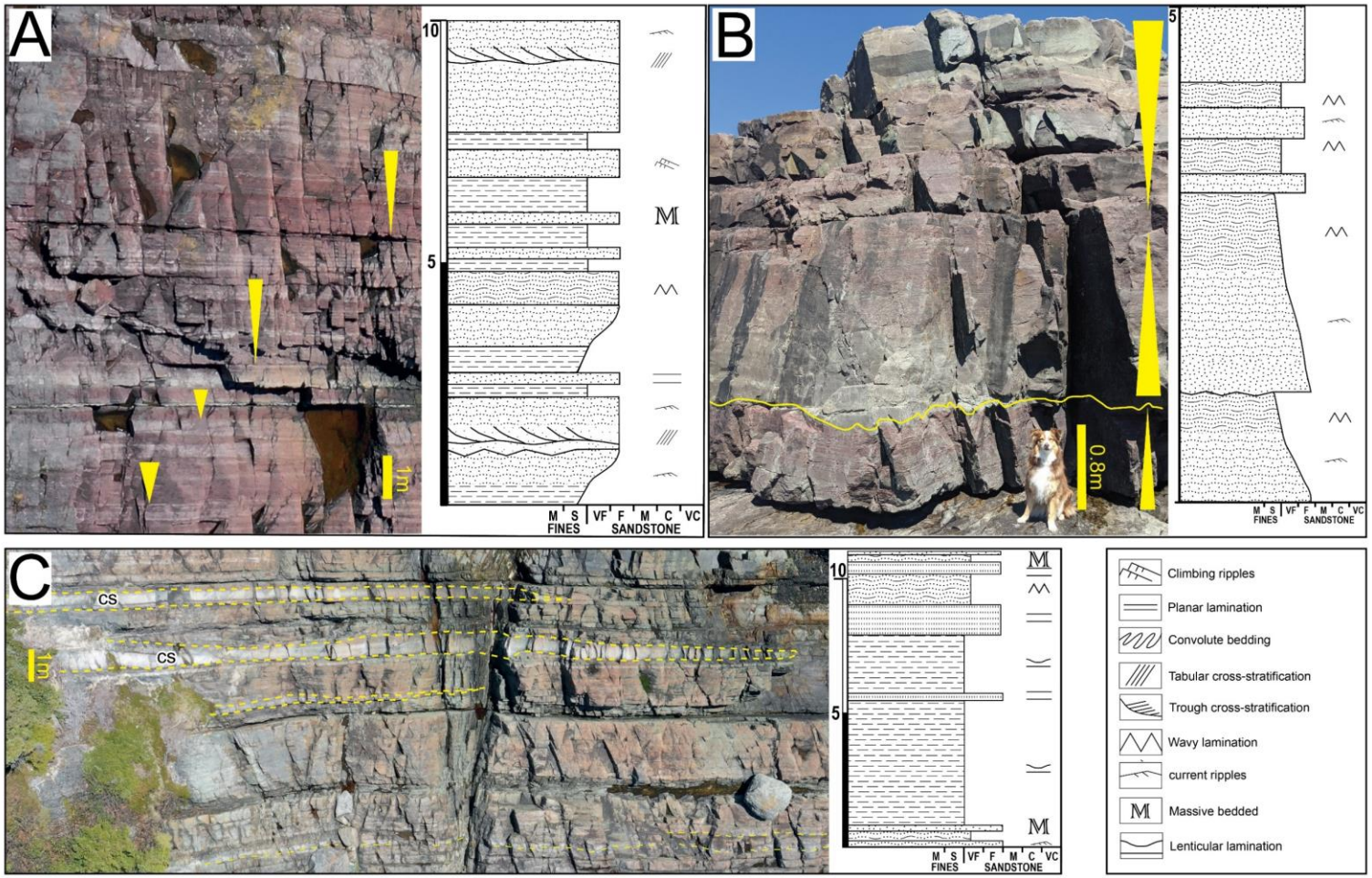

Fig. 2-13. A). B). C) Tabular heterolithic bed sets from FA2 interpreted as marine flood plain or interdistributary bay deposits interbedded with crevasse splays (CS). Yellow triangles define the grain-size trend; yellow lines define the upper and lower boundary of the beds. Outcrops A and C are exposed in Area 10, outcrop B is exposed in Area 7 (see Appendix A for area locations).

2.2.4 FA2: Interpretation: Lower to upper delta Plain

The dominance of flaser to lenticular stratified tabular heterolithic bed sets interstratified with lobe elements dominated by sediment gravity flow processes and cut by channel elements filled with dune cross-stratification suggest an ambient low-energy to periodic high-energy shallow water floodplain environment, with channels acting as distributive network cutting and feeding to interdistributary floodplains. The presence of mudstone drapes, fluid mud deposits, and flaser to lenticular bedding represents sedimentation in low-energy standing-water conditions, dominated by suspension fallout and rapid deposition of flocculated clay; common processes in brackish waters in tide-influenced and/or shallow marine environments (Longhitano et al., 2012; La Croix and Dashtgard, 2014; Gugliotta et al., 2016). The rare structureless sandstone, upper plane bed stratification, and humpback dunes within the channel elements record high-energy channelized bedload transport with high rates of sediment fallout that locally attained critical to supercritical flow conditions during episodes of high discharge or reduced water depths (Bristow, 1993; Hjellbakk, 1997; Fielding, 2006). In the context of a deltaic system, the stratigraphic position of FA2 over delta front strata (FA1) and below continental braided fluvial deposits of the Cuckold Formation (King, 1990), the dominant unidirectional paleoflow (Appendix D), and the evidence of marginal marine conditions suggest sedimentation in a subaqueous river-dominated, tide-influenced delta plain environment with sporadic subaerial exposure and episodic high-discharge events. In this context, the 0.2 to 10 m thick, tabular bed sets formed by heterolithic strata are then interpreted as shallow marine floodplain deposits or interdistributary bays (Elliott, 1974). Laterally and

vertically amalgamated channel elements consisting of dune cross-stratified sandstone and internal upstream and downstream accretion surfaces with a combined thickness between 4 – 20 m represent multi-storey deposits of low-sinuosity fluvial distributary channels, filled by deposits of upstream-and-downstream-migrating compound braided bars (Bridge and Lunt, 2006; Long, 2011; Miall, 2014)(Fig. 2-14; Appendix C). Single and multi-storey laterally amalgamated channel elements consisting of tabular cross-stratified sandstone and concentrated sediment flow deposits reaching up to 3 m thick of combined thickness are interpreted as crevasse channel fills (Gugliotta et al., 2015; Gulliford et al., 2017) (Appendix B). Lobate sandstone elements containing deposits of sustained and waning concentrated density currents, rare cross-stratified sandstone, and local upward transition from supercritical to subcritical bedforms are interpreted as crevasse-splay deposits (van Toorenenburg et al., 2016; Gulliford et al., 2017). Similar paleocurrent orientations between crevasse splays and crevasse channels further support a common link between these two elements (Appendix D). Soft-sediment deformation, including slump folds and dewatering structures, are interpreted to represent syn-sedimentary deformation and post-depositional liquefaction and fluidization possibly triggered by seismicity or the loading of rapidly deposited sediments (Alsop and Marco, 2011; Waldron and Gagnon, 2011).

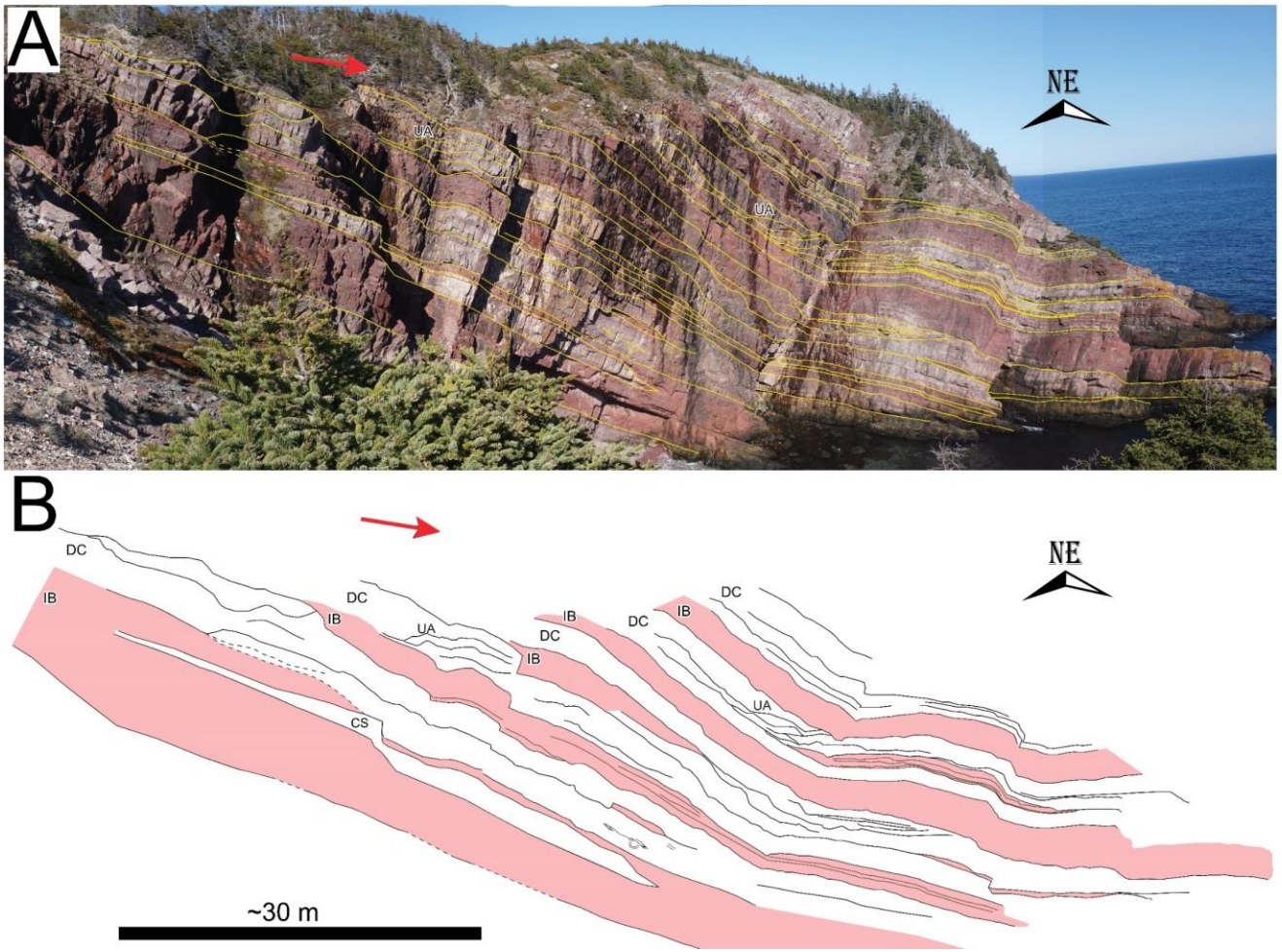

Fig. 2-14. A) Dip parallel-oriented photomosaic of lower delta plain facies outcropping near Area 9 (see Appendix A for area locations). B) Bedding diagram showing amalgamated distributary channel deposits (white) interbedded with interdistributary bay deposits (red) and lobate sandstone beds formed by crevasse splays (white). Abbreviations: UA-upstream accretion; CS-crevasse splay; DC-distributary channels; IB-inter distributary bay deposits; red arrows indicate paleoflow direction.

Chapter III - Stratigraphy, Contact relationships, and Distribution of facies

Figure 3-1 shows the correlation of the GHF and QVF facies associations using the change in color from grey to red as a datum. The first appearance of red beds has been previously defined as the lithostratigraphic boundary between the GHF and QVF by King (1990) and Williams and King (1976). This change in color does not coincide with facies changes, occurring in both delta front and delta plain facies, and it does not correspond with the changes in provenance either (see Chapter IV). This suggests that its origin is independent of changes in environments or regional basin processes, and therefore most likely correlates with a global or regional synchronous oxygenation event such as the Neoproterozoic oxygenation event (Och and Shields-Zhou, 2012), which makes it an appropriate datum for stratigraphic correlations.

The entire GHF and parts of the QVF north of the study area (Section A) comprise delta front facies consisting of proximal mouth bars, terminal distributary channels, and rare medial to distal mouth bars. Sections A and B highlight the characteristics of prograding proximal to distal delta front facies associated with an upward increase in the proportion of amalgamated proximal mouth bars and terminal distributary channels (FA1a) relative to medial to terminal/fringe mouth bars (FA1b), respectively (Fidolini and Ghinassi, 2016; van Yperen et al., 2020). Such distinctions permit the correlation of the outcropping intervals exposed in St. John's, Shoal Bay, Bay Bulls, and Calvert (Sections A, B, C, D, E; Fig. 1-2B). Overall, the distribution of delta front facies and its paleocurrent constraints (Fig. 3-1) suggests sedimentation of an SW-SE prograding river-dominated

delta front; however, the delta front facies do not entirely develop south of Section D, instead only distal mouth bars characterize the delta front facies in Section E. Such variation in the distribution of the delta front facies defines an overall proximal to distal southward thinning trend. The rest of the overlying QVF and equivalent Ferryland Head Formation and their paleocurrent constraints (Fig. 3-1) record SW-SE progradation of a delta plain consisting of low-sinuosity fluvial distributary channels and marine overbank deposits, including interdistributary bays, crevasse splays, and crevasse channels. In the southern part of the studied area (Section E), delta plain facies are dominated by overbank deposits and distributary channels with evidence of slump folding. Whereas to the north, Sections C and D show a higher occurrence of thick intervals of vertically stacked distributary channels and less abundant tide-influenced overbank deposits and slump folding. The north-to-south variation of delta plain facies defines a southward thickening wedge characterized by upper to lower delta plain transition.

The contact between the delta front and delta plain facies are conformable in sections D and E and unconformable in Section C (Fig. 3-2B-C). Conformable contacts between these facies are gradational in Section D and sharp in Section E; the sharp contact in Section E is characterized by a sharp boundary between distal mouth bars (delta front facies) and thick interdistributary bay deposits (lower delta plain facies). On the other hand, the unconformable contact in Section C is interpreted as a disconformity, underlain by medial delta front facies containing mouth bars and terminal distributary channels, and overlain by upper delta plain facies entirely consisting of deeply incised (~13 m), low aspect ratio (H/L = 0.11), amalgamated distributary channel deposits (Fig. 3-2A, Appendix C. C-D).

Representative fill of these channels, includes humpback dunes and 0.15 - 0.9 m thick dune sets, which imply a range of flow depths between 3 - 17.5 m. These flow depths differ from most channels in FA2 (1 - 11 m), which suggests a relative change in channel depth and wide towards Section C, resulting in funneling of discharge through relatively deeper and narrower channels (Lowe and Arnott, 2016). This, combined with an absence of interdistributary facies and an amalgamated architecture, indicates sedimentation on a low-accommodation floodplain, compared at least to other FA2 strata. These amalgamated high-discharge channels with the unconformity at its base and its correlation to a surface defining a sudden upward transition from distal delta front to delta plain (70 m at section E), represent an incisional knickpoint or valley, similar to those produced experimentally by van Heijst and Postma (2001).

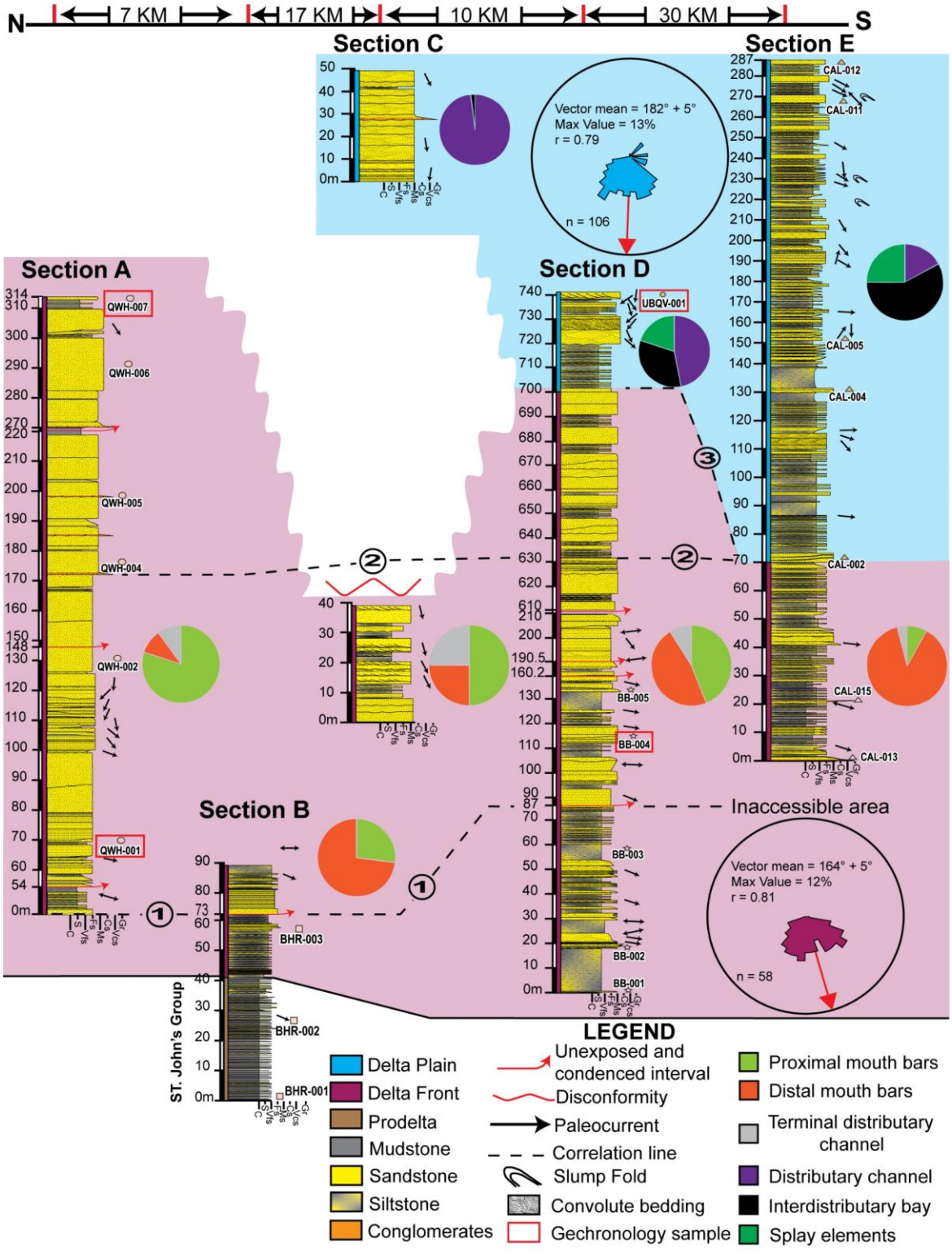
N
7 KM
17 KM
10 KM
30 KM
S
Section C
Section E
Section A
Section D
Section B
Inaccessible area
Vector mean = 182° + 5°
Max Value = 13%
r = 0.79
n = 106
Vector mean = 164° + 5°
Max Value = 12%
r = 0.81
n = 58
QWH-007
QWH-006
QWH-005
QWH-004
QWH-002
QWH-001
UBQV-001
BB-005
BB-004
BB-003
BB-002
BB-001
BHR-003
BHR-002
BHR-001
CAL-012
CAL-011
CAL-005
CAL-004
CAL-002
CAL-015
CAL-013
ST. John's Group
LEGEND
Delta Plain
Delta Front
Prodelta
Mudstone
Sandstone
Siltstone
Conglomerates
Unexposed and condenced interval
Disconformity
Paleocurrent
Correlation line
Slump Fold
Convolute bedding
Gechronology sample
Proximal mouth bars
Distal mouth bars
Terminal distributary channel
Distributary channel
Interdistributary bay
Splay elements

Fig. 3-1. Correlation panel of detailed stratigraphic logs from measured sections with corresponding architectural elements distribution (pie charts) and composite facies association paleoflow rose diagrams (see Fig. 1-2B for section locations). Features used for correlations were: (1) the first appearance of amalgamated tabular sandstone bed sets (FA1a); (2) the first appearance of red beds corresponding to the lithostratigraphic boundary between the Gibbet Hill and the Quidi Vidi formations defined by Williams and King (1976) and King (1990); (3) contact between FA1 and FA2 (see Fig. 3-2).

The along-strike variation in the nature of the delta front-delta plain contact, specifically the absence of a fully develop proximal delta front abruptly overlain by lower delta plain deposits toward the south (Section E), suggest sudden shoreline regression, causing the interruption of the delta front progradation and rapid delta plain progradation over delta front facies. Furthermore, the occurrence of incisional knickpoint or valley disconformably overlying medial delta front facies in Section C represents a localized change in accommodation towards a low accommodation setting, which resulted in the erosion of the upper delta front and lower delta plain facies. Notably, this localized change in accommodation appears to be constrained between the Blackhead and Bay Bulls synclines (Fig. 1-2B), the location where Stanley (2009) proposes localized uplift-related blind thrusting.

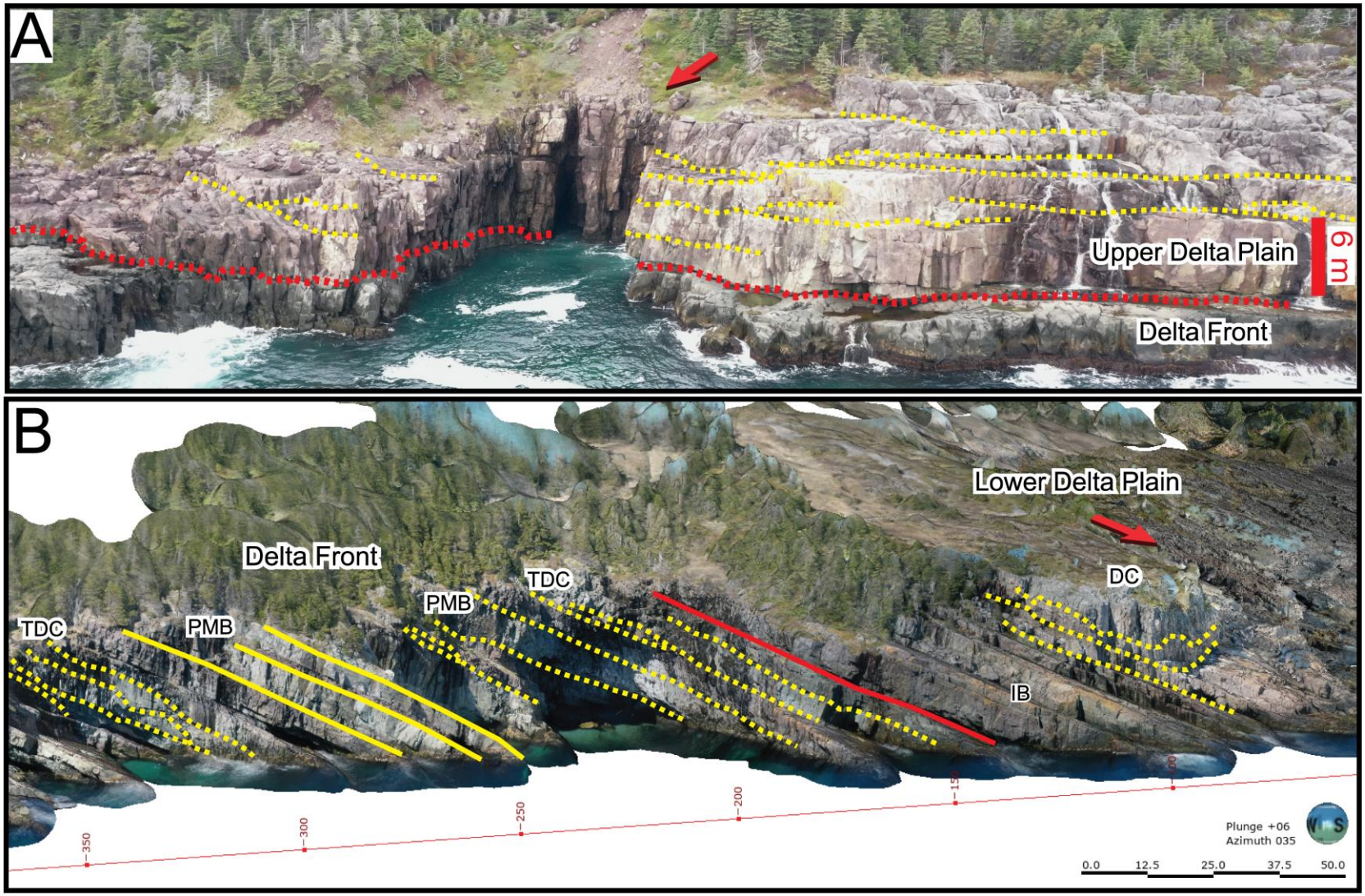
A
Upper Delta Plain
6 m
Delta Front
B
Lower Delta Plain
Delta Front
TDC
PMB
TDC
PMB
DC
IB
350
300
250
200
150
100
Plunge +06
Azimuth 035
0.0
12.5
25.0
37.5
50.0

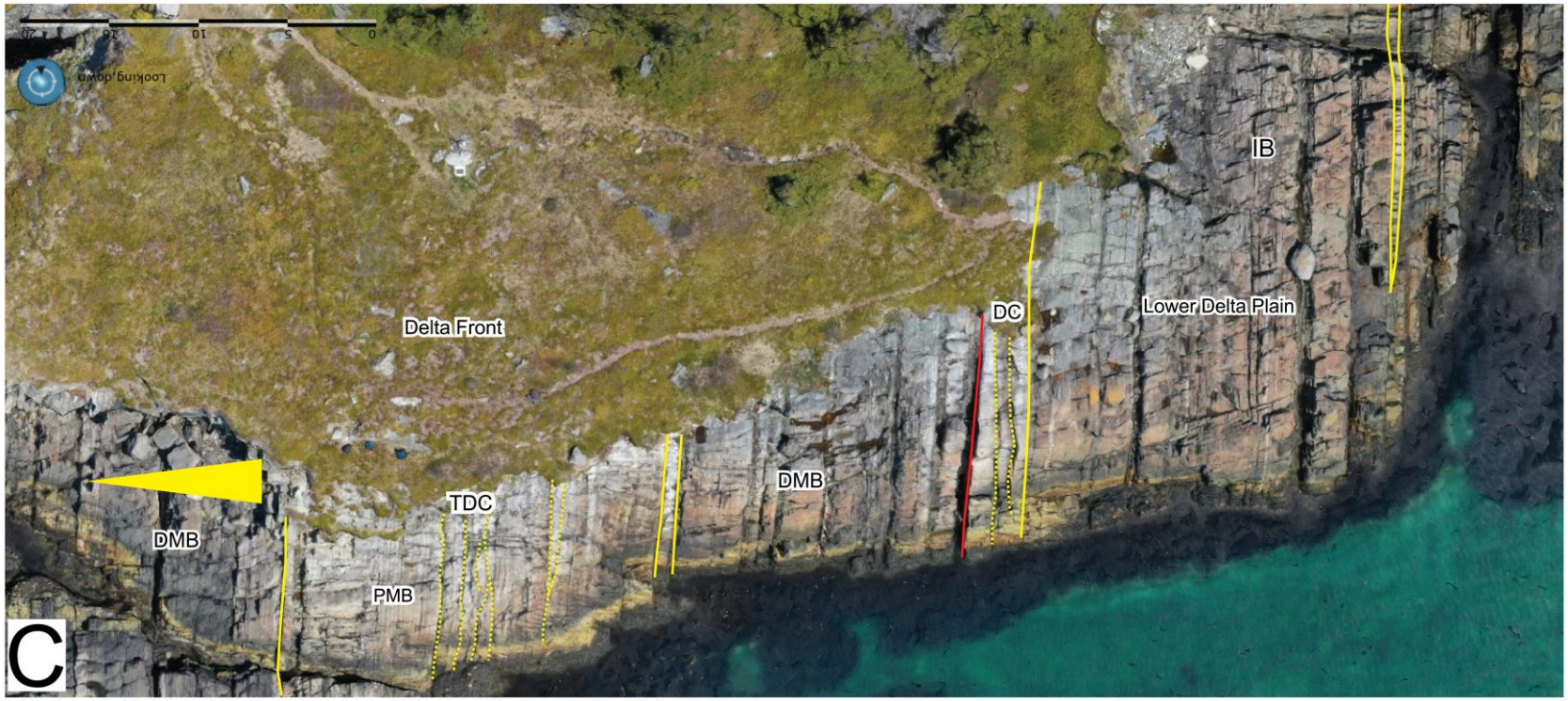

Fig. 3-2. A) Disconformity between upper delta plain and delta front facies in Section C, exposed near Area 5 (see Appendix A for area locations). B). Contact between lower delta plain and delta front facies in Section D, exposed near Area 7. C). Interpreted sharp contact between lower delta plain and delta front facies in Section E, exposed at Area 10. Abbreviations: TDC-terminal distributary channel; PMB-proximal mouth bar; DMB-distal mouth bar; IB-interdistributary bay; DC-distributary channel. Red arrows indicate paleoflow directions. In panel C, the paleoflow is coming out of the photogrammetric model. Yellow solid lines represent sharp contacts; yellow dashed lines represent erosive contacts; red solid line represents contact; red dashed line represents erosive contact. Yellow triangles represent upward coarsening and thickening trends.

Chapter IV - Sediment Provenance

4.1 Sandstone petrography

Sandstone samples from both delta front and delta plain facies are medium-grained and dominantly subrounded to well-sorted sandstone. The main framework constituents are plagioclase, polycrystalline and monocrystalline quartz, common volcanic and sedimentary lithic grains, and rare metamorphic grains. Volcanic grains are mostly of intermediate to felsic composition, and metamorphic grains include very low to low-grade psammites and pelites (Fig. 4-1A, C). Delta front samples plot between the quartz-feldspathic and quartzo-feldspatho-lithic fields in the QFL diagram and between the basement uplift and transitional arc fields in the tectonic discrimination diagram. Delta plain samples plot between the quartzo-litho-feldspathic and quartzo-feldspatho-lithic fields in the QFL diagram and on the transitional arc field in the tectonic discrimination diagram (Fig. 4-1A-B). The delta front sandstone composition represents the sourcing of mostly exhumed plutonic and volcanic rocks with minor and negligible contributions from sedimentary strata and low-grade metamorphic rocks, respectively. On the other hand, the sandstone composition of delta plain samples represents the sourcing from mainly volcanic and plutonic sources with a minor contribution of low-grade metamorphic rocks, which may indicate a shift from uplifted plutonic sources to comparatively more volcanic-rich sources between delta front and delta plain sedimentation.

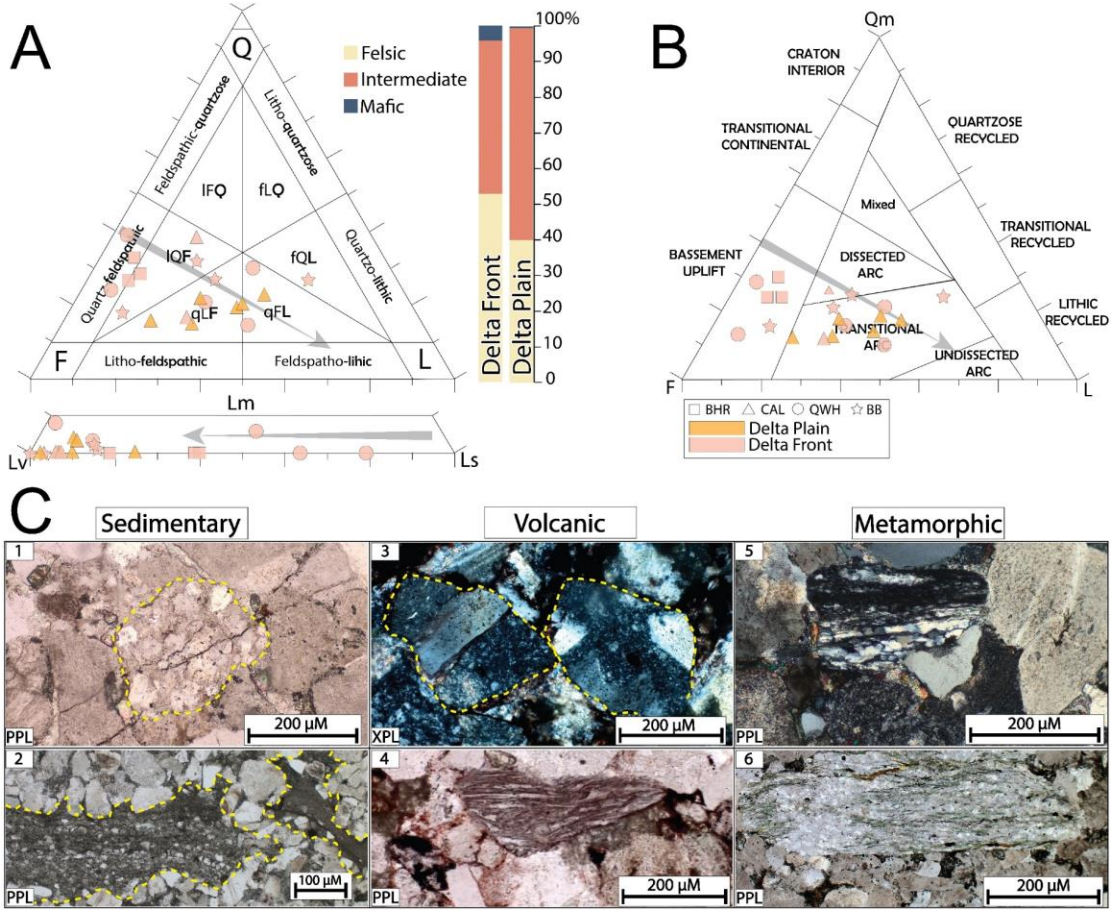

Fig. 4-1. A). Delta front and delta plain sandstone petrography, sandstone modal Q-F-L diagram after Garzanti (2019), and discrimination and proportion of volcanic lithics. B). Tectonic discrimination diagram Qm-F-L after Dickinson and Suczek (1979). C) Photomicrographs of some lithic fragments present in the delta front and delta plain samples: 1-sandstone fragment; 2-siltstone fragments; 3-intermediate volcanic fragments; 4-felsic volcanic fragment; 5 and 6-psammitic schist fragments; yellow dashed lines define grain boundaries. The gray arrow indicates sandstone composition evolution trend.

4.2 Detrital heavy minerals

Heavy minerals from the delta front and delta plain samples consist of abundant epidote and titanite; minor hornblende, garnet, zircon, rutile, and apatite; and trace ilmenite, monazite, allanite, thorite, Fe-spinel, and tourmaline (Appendix G). The relative proportions of heavy minerals between these samples show a 30% decrease in the epidote content from delta front to delta plain and a 7%, 4%, and 13% increment in the ilmenite, hornblende, and garnet content from the delta front to delta plain facies, respectively (Fig. 4-2A). The ZTR index for the delta front samples is 2.2%, whereas, for the delta plain, it is 8%. Provenance-sensitive heavy minerals index for the delta front and the delta plain depicts similar ATi (97% vs. 96%) values and dissimilar GZi (47% vs. 91%) and RZi values (40% vs. 21%) (Fig. 4-2B).

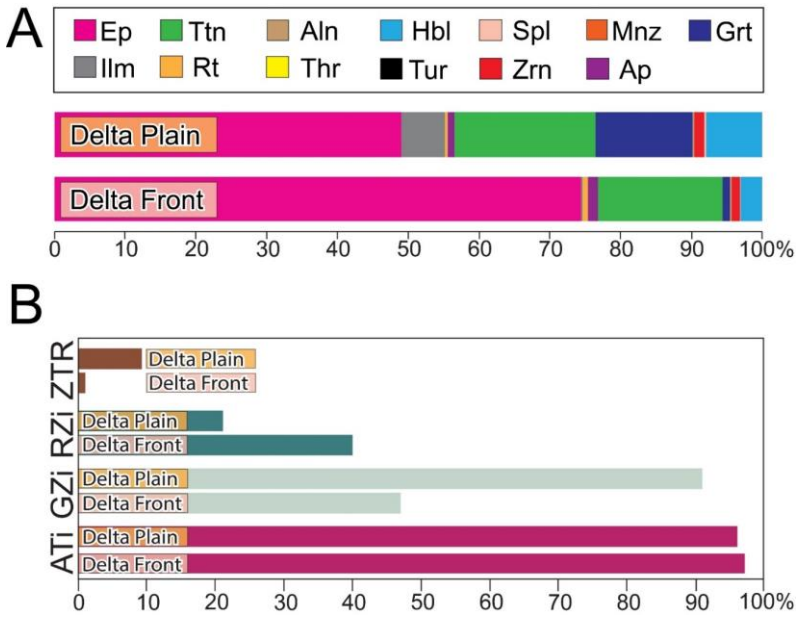

Fig. 4-2. A) Transparent heavy mineral counts from the delta front and the delta plain facies. B) ZTR maturity index after Hubert (1962) and ATi, GZi, RZi provenance sensitive index values after Morton and Hallsworth (1994).

The generally low ZTR index values for the delta front and the delta plain suggests sourcing from exhumed crystalline rocks instead of old sedimentary strata or heavily weathered cratonic sources (e.g., Hubert, 1962). Furthermore, high contents of epidote, titanite, hornblende, ilmenite, and apatite suggest both hydrothermally altered and unaltered mafic volcanic and intermediate plutonic sources (Garzanti and Andò, 2007). The occurrence of garnet, rutile, tourmaline, and Fe-spinel, suggests the presence of low to medium-grade metamorphic sources (Mange and Maurer, 1992; Garzanti and Andò, 2007;). The different GZi and RZi index values between the delta front and the delta plain, and the changes in the proportion of epidote, ilmenite, and hornblende, especially the increment in garnet in the delta plain sample, suggest an increment in the contribution of low to medium-grade metamorphic sources and may also represent the decrease in contribution from mafic volcanic and intermediate plutonic sources in the delta plain facies.

Table. 2. Cross-correlation Coefficient Matrix

	QWH-001	QWH-007	BB-004	UBQV-001
QWH-001	1	0.94	0.96	0.83
QWH-007	0.94	1	0.99	0.91
BB-004	0.96	0.99	1	0.91
UBQV-001	0.83	0.91	0.91	1

4.3 Intersample detrital zircon comparison

The KDE plots of detrital zircon ages from the delta front samples show relatively similar age peak distributions and abundances of Precambrian ages, which are different from the age peaks and abundance of Precambrian ages in the delta plain sample (Fig. 4-3). This suggests a low degree of difference in the detrital zircon age populations between

the delta front samples but a significant variation between the delta front and the delta plain samples. The cross-correlation coefficient matrix was used to quantify the degrees of difference (Table. 2). The delta front samples BB-004, QWH-001, and QWH-007 mutually yielded cross-correlation coefficient values higher than 0.94, suggesting a high degree of similarity of their detrital sources and indistinguishable detrital zircon distribution. On the other hand, the 0.83 to 0.91 cross-correlation coefficient values obtained between the delta front samples and the delta plain sample (UBQV-001) suggest that although there is a relatively high degree of similarity in the sources, certain differences between them and the detrital zircon distribution exist. Due to the indistinguishable detrital zircon age distribution of the delta front samples, they are grouped into a single representative sample, which will be treated as such from here onwards.

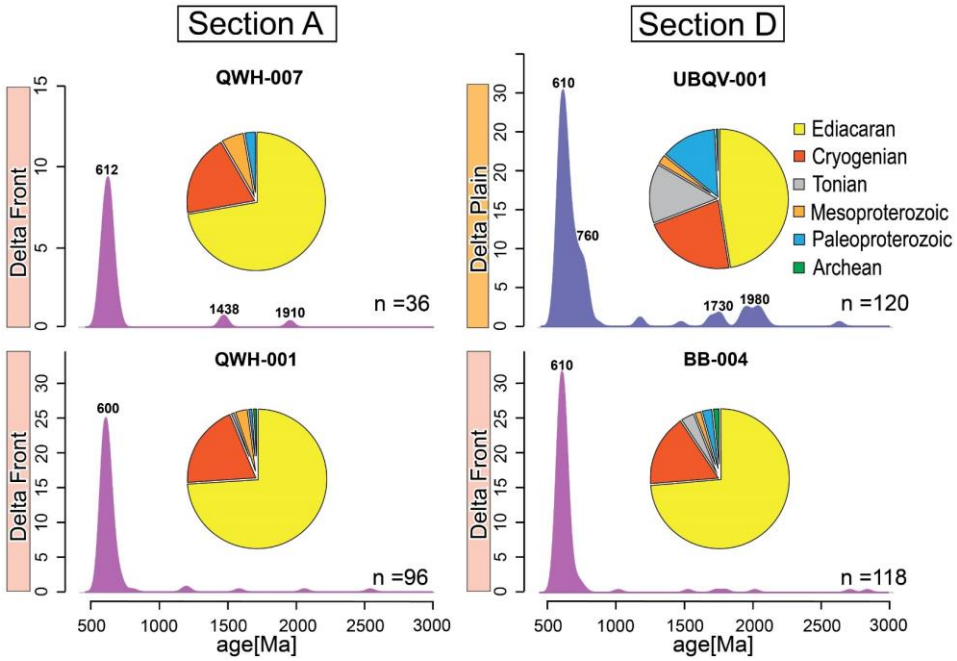

Fig. 4-3. Kernel distribution estimation (KDE) plots and age distribution (pie charts) of detrital U-Pb ages from delta front and delta plain samples (see Fig. 3-1 for samples location).

4.4 Detrital zircon geochronology

Detrital zircon ages from the delta front facies define a unimodal peak at ca. 605 Ma consisting mostly of Ediacaran (74%) and Cryogenian (18%) ages; the remaining 8% comprises Tonian, Mesoproterozoic, Paleoproterozoic, and Archean ages (Fig. 4-4). A sample from the overlying delta plain facies depicts a polymodal distribution with peaks at ca. 610 and 760 Ma comprising 47% Ediacaran ages spanning from 556 to 632 Ma, 22 % Cryogenian ages between 643 to 716 Ma, and 14% Tonian ages between 724 to 861 Ma. Subordinate peaks at ca. 1730 and 1980 include 17% Meso- and Paleoproterozoic ages between 1170 and 2097 Ma and a single Archean age of 2630 Ma (Fig. 4-4). Maximum depositional ages calculated using the youngest grain cluster at 2σ for the delta front and delta plain facies yield 557 ± 9 Ma and 556 ± 22 Ma, respectively (Fig. 5-1).

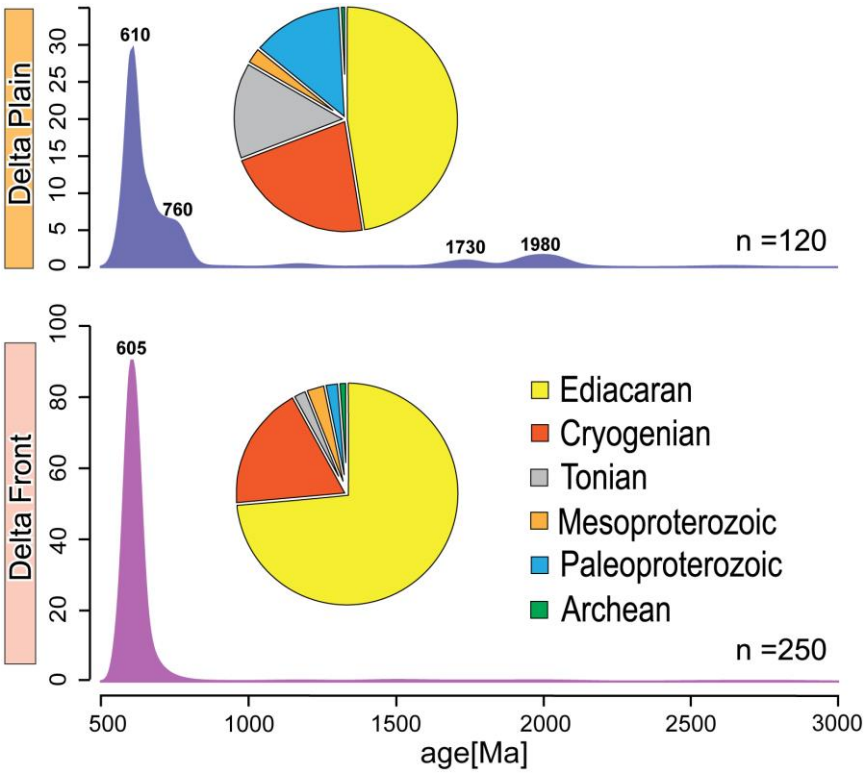

Fig. 4-4.

Kernel distribution estimation plots (KDE) and age distribution (pie charts) of detrital U-Pb ages from the delta front and delta plain. The delta front KDE plot resulted from the grouped delta front samples.

Chapter V - Discussion

5.1 Provenance Interpretations

The framework petrography and heavy mineral assemblages of the delta front and the delta plain facies suggest a mixed source area consisting of exhumed Ediacaran to Tonian intermediate plutonic, mafic to felsic volcanic, sedimentary, and low to medium-grade metamorphic rocks. The Ediacaran-Cryogenian detrital zircon ages within the delta front and the delta plain samples resemble those yielded by granitic and volcanic rocks from exposed igneous basement and bimodal volcanic cover sequences exposed throughout the Avalon Peninsula (Skipton et al., 2013; Mills et al., 2020; Pollock et al., 2022), including eroded post-560 Ma volcanic units similar to those exposed in the Connaigre Peninsula (O'Brien et al., 1995) (Fig. 1-2A). Tonian detrital zircon ages, however, have fewer outcropping sources within the Avalon Zone, but include the mafic-ultramafic Burin Group and rhyolitic Hawke Hills tuff, which represent the vestiges of a pre-composite Avalonia juvenile arc and the initial phase of composite West Avalonia magmatism (Israel, 1998; Murphy et al., 2008). Nevertheless, these rocks can only explain zircon ages between 724 and 764 Ma within the studied siliciclastic strata, as corresponding arc phases occurred between 765-750 Ma for the Burin Group and 739-727 Ma for the initial phase of the composite West Avalonia arc (Beranek et al., 2023). The remaining zircons with ages between 769-794 Ma within the studied Ediacaran strata have no known sources in the Avalon Zone. However, possible sources for these zircons might include eroded plutonic and volcanic cover sequences similar to the arc-rift-related intrusive and volcanic rocks outcropping in the correlative Cobequid Highlands (White et al., 2022).

Metamorphic rocks within the Avalon Zone are restricted to pre-625 Ma amphibolites, mylonitic paragneiss, metavolcanic, and metasedimentary rocks exposed in the Connaigre Peninsula (O'Brien et al., 1996). Although some of the metasedimentary grains found in the delta front and delta plain samples could have been derived from these rocks, the presence of garnets in the aforementioned metamorphic rocks has not been confirmed yet, making them incompatible sources to explain the garnets in my samples. Alternatively, metamorphic rocks containing garnets within correlative West Avalonian terranes, including the Mount Thom and the Gamble Brook formations in the Cobequid Highlands (White et al., 2022) and the subduction-related Hammondvale metamorphic suite in the Caledonia terrane (White et al., 2001) could be potential source candidates. White et al. (2022) reported MDA results for the metamorphic rocks in the Cobequid Highlands between ca. 776-1000 Ma and estimated the metamorphism of Mount Thom Formation between 800-770 Ma. Peaks of these ages do not occur in the delta front and delta plain samples, suggesting that sourcing from these or similar rocks was unlikely. On the other hand, age estimates for the Hammondvale metamorphic suite suggest metamorphism between 605-618 Ma and inherited zircons with Cryogenian, Tonian, and Meso-Paleo Proterozoic ages (White et al., 2001; Satkoski et al., 2010). Peaks of these ages occur in the delta front sample, and it is feasible to explain them by reworking rocks like the Hammondvale metamorphic suit, but this would require the exhumation and erosion of the accretionary subduction complex comprising the Hammondvale metamorphic rocks. van Staal et al. (2021) proposed a model involving a diachronous oblique collision between West Avalonia and Ganderia at ca. 575-550 Ma, in which the Hammondvale metamorphic rocks were exhumed and incorporated into the orogenic wedge that sourced the rocks under

investigation. If this model is correct, then the detrital garnets and some of the Cryogenian and older zircon grains in the delta plain sample could have been sourced from erosion of this exhumed accretionary subduction complex. However, van Staal et al. (2021) also proposed Ganderian sources to explain the metamorphic detritus in West Avalonia basins. The new sediment provenance results here presented are not able to refute the Ganderian source hypothesis. However, recent provenance studies of quartzite clasts in fluvial strata that overly these delta plain facies (see Appendix E) do not support Ganderian sources but rather some currently unexposed Avalonian sub-arc metamorphic basement rocks with Baltican affinity (Beranek et al., 2023). Detrital zircon ages from these clasts are between 1064-3220 Ma, which correlates well with the zircon grains ages between 1022 and 2843 from delta front and delta plain samples in this study. Although the exact composition and age of this Avalonian metamorphic basement are unknown, it could also have been the source of garnets in the delta front and delta plain samples.

The provenance change between the delta front and the delta plain is interpreted to reflect the reconfiguration of the hinterland sources defined by West Avalonia igneous-metamorphic basement. Exhumed Ediacaran-Cryogenian plutonic rocks and contemporaneous volcanic and sedimentary cover sequences and minor Cryogenian to older low-grade metamorphic rocks were replaced by dominantly Ediacaran to Tonian volcanic cover sequences and minor Cryogenian to older low to medium-grade metamorphic basement. These changes in provenance may indicate the thrusting of volcanic cover sequences over already exhumed plutonic sources and the exhumation of deeper/higher-grade metamorphic rocks in the hinterland area at ca. 556 Ma.

5.2 Depositional history and tectonic implications

The southward thinning trend of the delta front facies represents a basinward transition from a proximal to distal prograding delta front environment. The continuity of these facies and consistent SW-SE paleocurrents suggest sedimentation without intervening paleo topography. Furthermore, the statistical similarity in the detrital zircon distribution of the delta front samples implies that all parts of this delta front system were linked to the same source area, defined mostly by exhumed Ediacaran-Cryogenian plutonic rocks and contemporaneous volcanic and sedimentary cover sequences. These results support initial interpretations of continuous southward delta progradation mainly sourced by exhumed Avalonian arcs (King, 1990). Nevertheless, the abrupt to locally unconformable transition between the delta front and the delta plain suggests disruption of this deltaic system. The presence of upper delta plain facies characterized by incisional knickpoint or valley disconformably overlying medial delta front facies between the Blackhead and Bay Bulls synclines (Fig. 1-2B), the occurrence of slump folds within the delta plain facies, and the missing delta front facies further south, document intra-basin deformation and sudden shoreline regression. Previous structural and stratigraphic observations by Stanley (2009) proposed uplift-related blind thrusting post-dating the delta front and pre-dating the delta plain sedimentation to explain variations in the isopach distribution and differences in the fold axes orientation between the Blackhead and Bay Bulls synclines. Notably, Stanley (2009) inferred a topographic high between these two synclines. The absence of syn-sedimentary deformation of the delta front facies and the

localized unconformity separating delta front and delta plain strata, support the emergence of such local uplift that split the basin during the delta plain deposition.

The southward thickening trend of the delta plain facies and total absence of a proximal delta front to the south suggests that southward forced shoreline regression caused the delta plain to completely overstep the pre-existing delta front. Based on the provenance and stratigraphic evidence suggesting synchronous hinterland uplift and intra-basin thrusting, this sedimentary pattern is interpreted to reflect major tectonic-driven base level changes. Although the most convincing stratigraphic evidence of tectonic-related exhumation in the Avalon Zone is restricted to the younger Flatrock thrust and Lilly unconformity affecting the upper Signal Hill Group (Anderson et al., 1975; Calon, 2001; Beranek et al., 2023), paleogeographic reconstructions of the Ediacaran arc-platform transition in West Avalonia suggest transpressional deformation and coeval exhumation related to the Avalonian orogeny occurred between 575-550 Ma (e.g., Murphy and Nance, 1989; van Staal et al., 2021). The MDA results of the delta front and delta plain facies yielded 557 $\pm$ 9 Ma and 556 $\pm$ 22 Ma (Fig. 5-1), relating the hinterland, intra-basin deformation, and coeval base level change and forced regression to the Avalonian orogeny (Fig. 5-2).

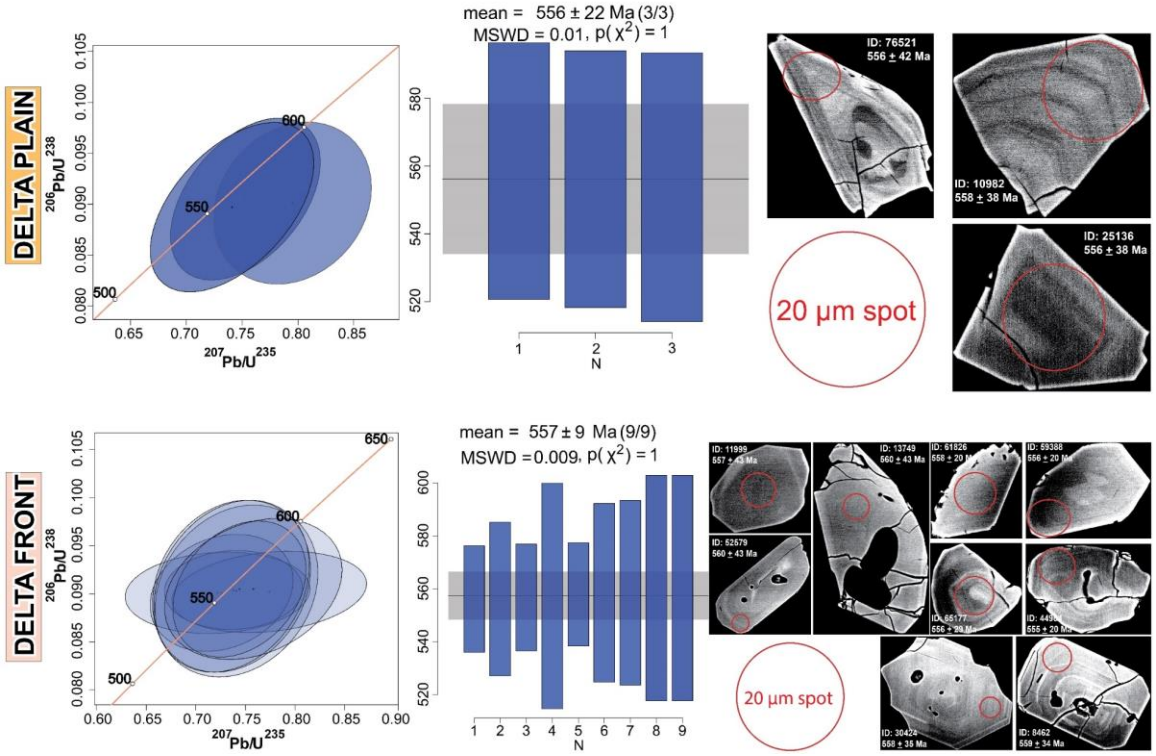

Fig. 5-1. Wetherill and weighted average age diagrams of concordant zircon grains used for maximum depositional age calculations based on the youngest grain cluster at 2σ method of Dickinson and Gehrels (2009).

Previous interpretations of the basin in which these shallow marine strata were deposited advocate for a pull-apart basin based on the evidence of coeval intracontinental extensional volcanism (Murphy et al., 1999; Salas, 2004). However, recent plate tectonic reconstructions challenge this hypothesis and place the rocks under investigation in a peripheral foreland basin (van Staal et al., 2021). By comparing the general characteristics of the Signal Hill Group against those of intracontinental pull-apart and foreland basins, important considerations on the type of basin these strata were deposited in can be achieved. The general stratigraphic features of intracontinental pull-apart basins include: (1) basal fining-upward sequences produced by rapid subsidence and progressive infilling; (2) rapid

lateral facies changes defined by fault adjacent conglomerates and breccias passing laterally into fine-grained facies; and (3) complex paleocurrents patterns related to changes in sources due to strike-slip displacements (Allen and Allen, 2013; Donaghy et al., 2021). In the Signal Hill Group, the lack of evidence of rapid subsidence or abrupt lateral variations of facies, the continuous southward paleocurrent directions over time, and the coarsening upward profile are not consistent with sedimentation in a pull-apart basin (King, 1990; Salas, 2004). Instead, the overall coarsening upward pattern, here associated with progressive hinterland exhumation, the development of local intra-basin unconformities and growth strata, and the textural and compositional immaturity of the sediments (Singh, 1969; King, 1990; Calon, 2001; Stanley, 2009; Peddle, 2017); resemble the formative features of wedge-top depozones in foreland basin systems (DeCelles and Giles, 1996). Therefore, it is suggested that the deltaic facies of the GBH and QDV may record the transition from a foredeep to a wedge-top basin in this part of West Avalonia rather than a pull-apart basin, as suggested by Salas (2004).

The two existing plate tectonic models surrounding the diachronous intra-arc extension and compressional deformation characterizing the Ediacaran arc to platform transition and the Avalonian orogeny in West Avalonia are: (a) dextral convergence with Ganderia and (b) dextral ridge-trench collision (ca. 575-550 Ma; Murphy et al., 1995; van Staal et al., 2021). Both models offer possible explanations for evidence of wedge-top sedimentation and blind thrust propagation outlined in this thesis for the lower Signal Hill Group. In the model of oblique collision with Ganderia (van Staal et al., 2021), the lower Signal Hill wedge top depocenter described here is envisaged to be part of the retro-wedge top of a peripheral

foreland basin system such as the New Guinean and Taiwan foreland basins (e.g., Pigram et al., 1989; Chiang et al., 2004; Lai et al., 2021). In this scenario, sediment sources were mainly from West Avalonia igneous-metamorphic basement (King, 1990; Beranek et al., 2023). On the other hand, in the ridge-trench collision model (Murphy et al., 1995), strike-slip faults along Avalonian arc segments and marginal basins could have generated fold and thrust belts at restraining bends with adjacent wedge-top-like depocenters, such as the current Transverse Ranges in the San Andreas Fault (e.g., Mueller and Suppe, 1997; Niemi et al., 2013) or the Anti-Lebanon in the Dead Sea (e.g., Gomez et al., 2007; Fedorik et al., 2022). This scenario could also explain the dominance of West Avalonian provenance. Therefore, based on the current sedimentologic and provenance data, it is concluded that either plate tectonic model could explain the development of a wedge-top depocenter in West Avalonia. Further sedimentologic, provenance, and geochronology data are needed from the Ediacaran basins of West Avalonia to test for possible sourcing from the Hammondvale accretionary subduction complex and to constrain the stratal evolution of the Signal Hill Group and coeval coarse clastic succession across Avalon Zone such as the Crown Hill Formation (Normore, 2010), providing insight into the configuration and evolution of basins throughout West Avalonia.

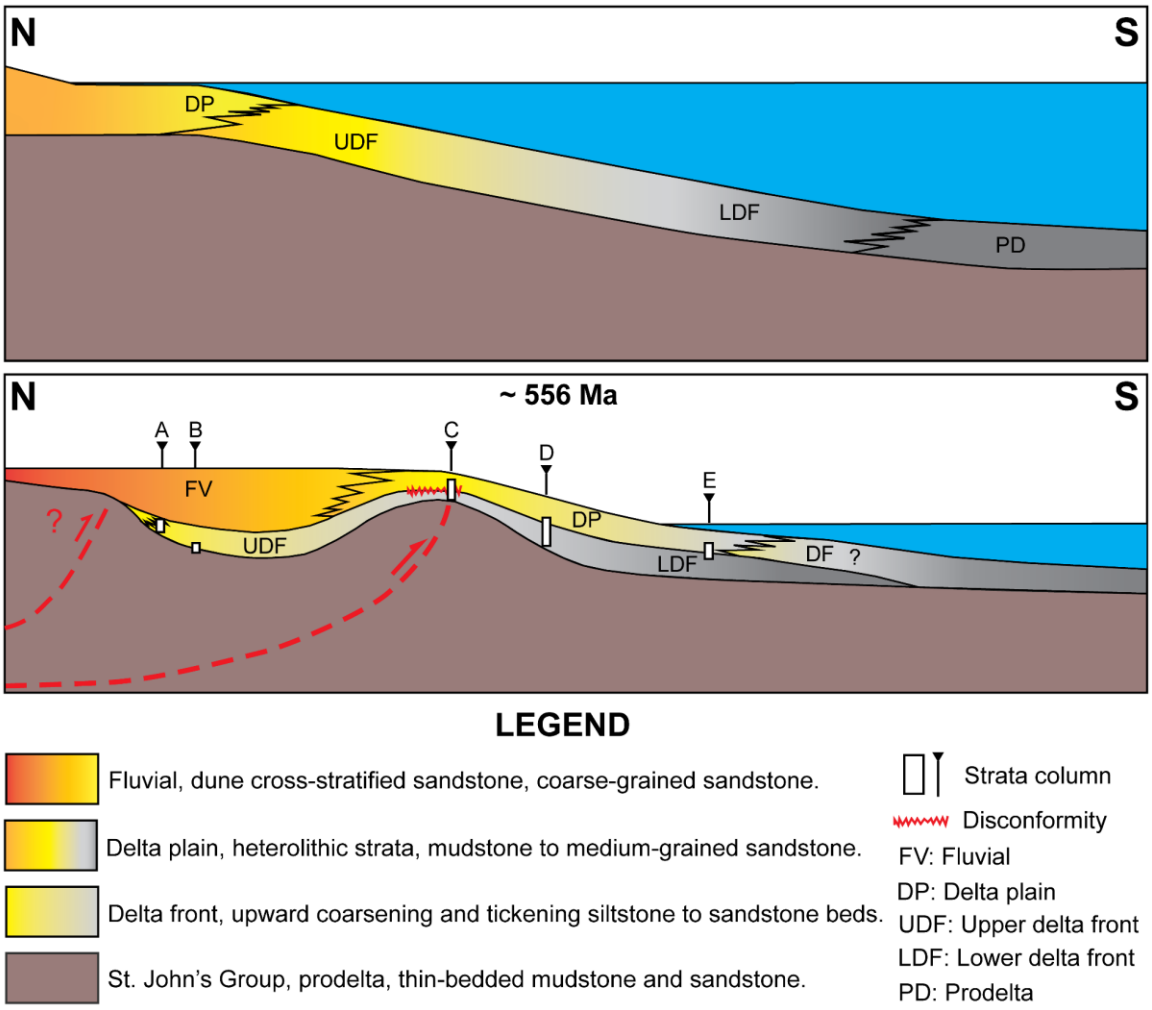

Fig. 5-2. Schematic diagram showing the depositional environment and their syn-orogenic response during the Avalon orogeny recorded in the GHF, QVF, and the correlative Ferryland Head Formations.

Chapter VI - Conclusions

Six sedimentary facies were identified and further subdivided into subfacies representing unique depositional processes recorded in the Gibbet Hill and the Quidi Vidi formations (and equivalent Ferryland Head Formation). These are:

Facies 1, consisting of very fine to medium-gained cross-stratified sandstone and cross-laminated sandstone, recording the development and evolution of different bedforms under specific flow conditions, including wave ripples, current ripples, climbing ripples, adhesion warts, subaqueous dunes, and subaqueous humpback dunes.

Facies 2, consisting of very fine to medium-grained planar laminated sandstone, recording the development of upper plane bed under critical flow conditions and hyperpycnites formed by waning and waxing conditions in hyperpycnal flows.

Facies 3 is defined by fine to medium-grained structureless sandstone beds formed by rapid deposition from high energy concentrated density flows with high rates of sediment aggradation.

Facies 4 consist of fine to medium-grained normally graded sandstone beds with local development of coarse-tail grading deposited from decelerating concentrated density flows.

Facies 5 consist of fine-grained siliciclastics including parallel-laminated, thin-bedded, and structureless mudstone and siltstone recording low-energy deposition characterized by suspension fallout and fluid mud deposited from flocculated, near-bed, suspended sediment concentrated flows.

Facies 6 consist of meter-scale folded and convolute strata recording syn-sedimentary slump folding and post-depositional liquefaction and fluidization processes.

Observations of the recurring groupings of facies and stratal geometry allowed the identification of two facies associations corresponding to shallow marine depositional environments recorded in the Gibbet Hill and the Quidi Vidi formations (and equivalent Ferryland Head Formation); these are:

Facies association 1 (FA1), consisting of amalgamated proximal/axis mouth bars, distal/fringe mouth bars, and terminal distributary channels recording nearshore terminal flow environments (delta front), where unconfined high-energy and concentrated flows fed by coeval channels are widespread.

Facies association 2 (FA2), consisting of interdistributary bay deposit interbedded with crevasse splay deposits, laterally amalgamated crevasse channel fills, and vertically and laterally amalgamated distributary channels deposits, defining a low-energy to periodic high-energy shallow water floodplain environment. Here, channels acted as a distributive network cutting into and feeding adjacent interdistributary flood plains located in a lower to upper delta plain environment.

Everywhere in the study area, FA1 is overlain by FA2, but the contact between the delta front and delta plain facies varies from north to south. The FA1-FA2 contacts are conformable in sections D and E in the south, but unconformable in Section C (Fig. 3-2B-C). Conformable contacts are gradational in Section D and sharp in Section E. Notably, the sharp contact in Section E is characterized by a sharp boundary between distal mouth bars

(distal delta front facies) and thick interdistributary bay deposits (lower delta plain facies), without an intervening proximal delta front succession. The unconformable contact in Section C is interpreted as a disconformity, underlain by medial delta front facies containing mouth bars and terminal distributary channels, and overlain by upper delta plain facies entirely consisting of deeply incised (~13 m), low aspect ratio (H/L = 0.11), amalgamated distributary channel deposits recording funneling of discharge through relatively deeper and narrower channels on a low-accommodation floodplain. These amalgamated high-discharge channels with the unconformity at its base and its correlation to a surface defining a sudden upward transition from distal delta front to delta plain (70 m at section E), represent an incisional knickpoint or valley, similar to those produced experimentally by van Heijst and Postma (2001). The occurrence of incisional knickpoint or valley in Section C coinciding with the location where Stanley (2009) placed a hypothetical blind thrust, and the absence of a fully developed proximal delta front basin-ward from this location (Section E) suggests coeval thrust-related uplift and sudden shoreline regression during the delta plain progradation.

Maximum depositional age estimates and sediment provenance for the delta front and delta plain facies yielded 557 $\pm$ 9 Ma and 556 $\pm$ 22 Ma, respectively, and suggest sourcing from West Avalonian igneous and metamorphic basement. The delta front facies record protracted erosion of the same source area throughout the delta front sedimentation, consisting mostly of exhumed Ediacaran-Cryogenian plutonic rocks and contemporaneous volcanic and sedimentary cover sequences and Cryogenian to older low-grade metamorphic sources. On the other hand, delta plain provenance data suggests sourcing

from Ediacaran to Tonian volcanic cover sequences and minor Cryogenian to older low to medium-grade metamorphic basement. These changes in provenance suggest the thrusting of volcanic cover sequences over already exhumed plutonic sources and the exhumation of deeper/higher-grade metamorphic rocks in the hinterland area during the Avalon orogeny at ca. 556 Ma.

Comparisons of the general characteristics of the Signal Hill group against those of intracontinental pull-apart and foreland basins allowed us to make considerations on the type of basin these strata were deposited. The overall coarsening upward pattern associated with progressive hinterland exhumation and development of local intra-basin unconformities, growth strata development, thinning towards the hinterlands, and the textural and compositional immaturity of the sediments (Singh, 1969; King, 1990; Calon, 2001; Stanley, 2009; Peddle, 2017) resemble the formative features of wedge-top depozones in foreland basin systems (DeCelles and Giles, 1996), which indicates that the deltaic facies of the GBH and QDV may record the transition from a foredeep to a wedge-top basin in this part of West Avalonia rather than a pull-apart basin as suggested by Salas (2004).

The two existing plate tectonic models surrounding the diachronous intra-arc extension and compressional deformation characterizing the Avalonian orogeny in West Avalonia are: (a) dextral convergence with Ganderia and (b) dextral ridge-trench collision (ca. 575-550 Ma; Murphy et al., 1995; van Staal et al., 2021). Both models offer possible explanations for evidence of wedge-top sedimentation and blind thrust propagation outlined in this study for the lower Signal Hill Group. In the model of oblique collision

with Ganderia (van Staal et al., 2021), the lower Signal Hill wedge top depocenter described here is envisaged to be part of the retro-wedge top of a peripheral foreland basin system. On the other hand, in the ridge-trench collision model (Murphy et al., 1995), strike-slip faults along Avalonian arc segments and marginal basins could have generated fold and thrust belts at restraining bends with adjacent wedge-top-like depocenters. Therefore, based on the current sedimentologic and provenance data, it is concluded that either plate tectonic model could explain the development of a wedge-top depocenter in West Avalonia.

Overall, the new sedimentological and geochronological observations of the Gibbet Hill and the Quidi Vidi formations (and equivalent Ferryland Head Formation) in the eastern part of the Avalon Zone support blind thrusting and forced regression in the lower Signal Hill Group coinciding with changes in provenance related to the exhumation of Cryogenian to older metamorphic basement of West Avalonia by ca. 556 Ma. These results strengthen the evidence for syn-deformational sedimentation during the Avalonian orogeny and suggest that the deltaic strata of the Signal Hill Group record the transition from foredeep to wedge-top depozones, which may represent the existence of a large foreland basin system or, instead, smaller localized wedge-top-like depocenters at restraining bends in regional strike-slip faults. More regional investigations of the Signal Hill Group and coeval strata, such as the Crown Hill Formation, are needed to determine the regional extent and significance of compressional basins in West Avalonia during the late Ediacaran.

Chapter VII - References

Allen. (1971). A theoretical and experimental study of climbing-ripple cross-lamination, with a field application to The Uppsala Esker. Geografiska Annaler, 53A, 157–187.

Allen. (1977). The possible mechanics of convolute lamination in graded sand beds. Journal of Geological Society, 134, 19–31.

Allen. (1982). Sedimentary structures, their character and physical basis. In Developments in Sedimentology (30A ed., Vol. 1). Elsevier.

Allen, P., and Allen, J. (2013). Basin Analysis: Principles and Application to Petroleum Play Assessment (3rd ed., p. 640). Wiley-Blackwell.

Alsop, G. I., and Marco, S. (2011). Soft-sediment deformation within seismogenic slumps of the Dead Sea Basin. Journal of Structural Geology, 33(4), 433–457. https://doi.org/10.1016/j.jsg.2011.02.003

Anderson, M. M., Bruckner, W. D., King, A. F., and Maher, J. B. (1975). The late Proterozoic "H. D. Lilly Unconformity" at Red Head, northeastern Avalon Peninsula, Newfoundland. American Journal of Science, 275(9), 1012–1027. https://doi.org/10.2475/ajs.275.9.1012

Arnott, R. W. C., and Hand, B. M. (1989). Bedforms, primary structures and grain fabric in the presence of suspended sediment rain. Journal of Sedimentary Petrology, 59(6), 1062–1069.

Ashley, G. M., Dalrymple, R. W., Flemming, B. W., and Harris, P. T. (1990). Classification of large-scale subaqueous bedforms: a new look at an old problem. Journal of Sedimentary Petrology, 60(1), 160–172.

Bates, C. C. (1953). Rational theory of delta formation. AAPG Bulletin, 37(9), 2119–2162.

Beranek, L. P., Hutter, A. D., Pearcey, S., James, C., Langor, V., Pike, C., Goudie, D., and Oldham, L. (2023). New evidence for the Baltican cratonic affinity and Tonian to Ediacaran tectonic evolution of West Avalonia in the Avalon Peninsula, Newfoundland, Canada. Precambrian Research, 390, 1–19. https://doi.org/10.1016/j.precamres.2023.107046

Best, J. I. M. (1992). The morphology and dynamics of low amplitude bedwaves upon upper stage plane beds and the preservation of planar laminae. Sedimentology, 39, 737–752.

Bhattacharya, J. (2006). Deltas. In H. W. Posamentier and R. G. Walker (Eds.), Facies Models Revisited (Vol. 84, pp. 237–292). SEPM (Society for Sedimentary Geology). https://doi.org/10.2110/pec.06.84

Black, L. P., Kamo, S. L., Allen, C. M., Davis, D. W., Aleinikoff, J. N., Valley, J. W., Mundil, R., Campbell, I. H., Korsch, R. J., Williams, I. S., and Foudoulis, C. (2004). Improved 206Pb/238U microprobe geochronology by the monitoring of a trace-element-related matrix effect; SHRIMP, ID-TIMS, ELA-ICP-MS and oxygen isotope documentation for a series of zircon standards. Chemical Geology, 205(1–2), 115–140. https://doi.org/10.1016/j.chemgeo.2004.01.003

Bradley, G.M. and Venditti, J.G. (2017). Re-evaluating dune scaling relations. Earth-Science Reviews, 165, 356 – 376.

Bridge, J., and Lunt, I. (2006). Depositional models of braided rivers. In G. Sambrook Smith, J. Best, C. Bristow, and G. Petts (Eds.), Braided Rivers: Process, Deposits, Ecology and Managements. International Association of Sedimentologists.

Bristow, C. S. (1993). Sedimentary structures exposed in bar tops in the Brahmaputra River, Bangladesh. Geological Society, 75, 277–289.

Calon, T. (2001). Late Precambrian sedimentation and related orogenesis of the Avalon Peninsula, eastern Avalon Zone, Newfoundland: Field Trip Guidebook. In GAC/MAC Annual Meeting.

Canfield, D. E., Knoll, A. H., Poulton, S. W., Narbonne, G. M., and Dunning, G. R. (2020). Carbon isotopes in clastic rocks and the Neoproterozoic carbon cycle. American Journal of Science, 320(2), 97–124. https://doi.org/10.2475/02.2020.01

Cardozo, N., and Allmendinger, R. W. (2013). Spherical projections with OSXStereonet. Computers and Geosciences, 51, 193–205.

Chakraborty, C., and Bose, P. K. (1992). Ripple/dune to upper stage plane bed transition: Some observations from the ancient record. Geological Journal, 27(4), 349–359. https://doi.org/10.1002/gj.3350270405

Chiang, C.-S., Yuw, H.-S., and Chouz, Y.-W. (2004). Characteristics of the wedge-top depozone of the southernTaiwan foreland basin system. Basin Research , 16, 65–78. https://doi.org/10.1111/j.1365-2117.2003.00222.x

Clifton, H. E. (1976). Wave-formed sedimentary structures; a conceptual model. In R. A. Davis and R. L. Ethington (Eds.), Beach and Nearshore Sedimentation (Vol. 24, pp. 126–148). Special Publication - Society of Economic Paleontologists and Mineralogists.

Clifton, H. E., and Dingler, J. R. (1984). Wave-formed structures and Paleoenvironmental Reconstruction. Marine Geology, 60, 165–198.

Dasgupta, P. (2003). Sediment gravity flow-the conceptual problems. Earth-Science Reviews, 62(3–4), 265–281. https://doi.org/10.1016/S0012-8252(02)00160-5

DeCelles, P. G. (2012). Foreland basin systems revisited: variations in response to tectonic settings. In C. Busby and A. Azor (Eds.), Tectonics of Sedimentary Basins: Recent Advances (1st ed., pp. 405–426). Blackwell Publishing Ltd. https://doi.org/10.1002/9781444347166.ch20

DeCelles, P. G., and Giles, K. A. (1996). Foreland basin systems. Basin Research, 8, 105–123. https://doi.org/10.1046/j.1365-2117.1996.01491.x

Dickinson, W. R., and Gehrels, G. E. (2009). Use of U-Pb ages of detrital zircons to infer maximum depositional ages of strata: A test against a Colorado Plateau Mesozoic database. In Earth and Planetary Science Letters (Vol. 288, Issues 1–2, pp. 115–125). https://doi.org/10.1016/j.epsl.2009.09.013

Dickinson, William. R., and Suczek, C. (1979). Plate tectonics and sandstone compositions . AAPG Bulletin, 63(12), 2164–2182.

Donaghy, E. E., Umhoefer, P. J., Eddy, M. P., Miller, R. B., and LaCasse, T. (2021). Stratigraphy, age, and provenance of the Eocene Chumstick basin, Washington Cascades; implications for paleogeography, regional tectonics, and development of strike-slip basins. Geological Society of America Bulletin, 133(11–12), 2418–2438. https://doi.org/10.1130/B35738.1

Dunning, G. R., O'Brien, S. J., Colman-Sadd, S. P., Blackwood, R. F., Dickson, W. L., O'Neill, P. P., and Krogh, T. E. (1990). Silurian Orogeny in the Newfoundland Appalachians. The Journal of Geology, 98(6), 895–913. https://doi.org/10.1086/629460

Elliott, T. (1974). Interdistributary bay sequences and their genesis. Sedimentology, 21, 611–622. https://doi.org/10.1111/j.1365-3091.1974.tb01793.x

Fedorik, J., Maesano, F. E., and Afifi, A. M. (2022). A validated geomechanical model for the strike-slip restraining bend in Lebanon. Scientific Reports, 12(1), 20071. https://doi.org/10.1038/s41598-022-24718-0

Fidolini, F., and Ghinassi, M. (2016). Friction- and inertia-dominated effluents in a lacustrine, river-dominated deltaic succession (Pliocene Upper Valdarno Basin, Italy). Journal of Sedimentary Research, 86(9), 1083–1101. https://doi.org/10.2110/jsr.2016.65

Fielding, C. R. (2006). Upper flow regime sheets, lenses and scour fills: Extending the range of architectural elements for fluvial sediment bodies. Sedimentary Geology, 190(1–4), 227–240. https://doi.org/10.1016/j.sedgeo.2006.05.009

Fleuty, M. J. (1964). The description of folds. Proceedings of the Geologists' Association, 75(4), 461–492. https://doi.org/10.1016/S0016-7878(64)80023-7

Garzanti, E. (2019). Petrographic classification of sand and sandstone. Earth-Science Reviews, 192, 545–563. https://doi.org/10.1016/j.earscirev.2018.12.014

Garzanti, E., and Andò, S. (2007). Heavy Mineral Concentration in Modern Sands: Implications for Provenance Interpretation. In M. Mange and D. Wright (Eds.), Heavy minerals in use (Vol. 58, pp. 517–545). Elsevier. https://doi.org/10.1016/S0070-4571(07)58020-9

Garzanti, E., Doglioni, C., Vezzoli, G., and Andò, S. (2007). Orogenic Belts and Orogenic Sediment Provenance. The Journal of Geology, 115(3), 315–334. https://doi.org/10.1086/512755

Garzanti, E., and Vezzoli, G. (2003). A classification of metamorphic grains in sands based on their composition and grade. Journal of Sedimentary Research, 73(5), 830–837. https://doi.org/10.1306/012203730830

Gomez, F., Nemer, T., Tabet, C., Khawlie, M., Meghraoui, M., and Barazangi, M. (2007). Strain partitioning of active transpression within the Lebanese restraining bend of the Dead Sea Fault (Lebanon and SW Syria). In W. D. Cunningham and P. Mann (Eds.), Tectonics of Strike-Slip Restraining and Releasing Bends (Vol. 290, Issue 1, pp. 285–303). The Geological Society of London. https://doi.org/10.1144/290.10

Gravenor, C. P. (1980). Heavy minerals and sedimentological studies on the glaciogenic late Precambrian Gaskiers Formation of Newfoundland. Canadian Journal of Earth Sciences, 17(10), 1331–1341. https://doi.org/10.1139/e80-140

Gugliotta, M., Flint, S. S., Hodgson, D. M., and Veiga, G. D. (2015). Stratigraphic record of river-dominated crevasse subdeltas with tidal influence (Lajas Formation, Argentina). Journal of Sedimentary Research, 85(3), 265–284. https://doi.org/10.2110/jsr.2015.19

Gugliotta, M., Flint, S. S., Hodgson, D. M., and Veiga, G. D. (2016). Recognition criteria, characteristics and implications of the fluvial to marine transition zone in ancient deltaic deposits (Lajas Formation, Argentina). Sedimentology, 63(7), 1971–2001. https://doi.org/10.1111/sed.12291

Gulliford, A. R., Flint, S. S., and Hodgson, D. M. (2017). Crevasse splay processes and deposits in an ancient distributive fluvial system: The lower Beaufort Group, South Africa. Sedimentary Geology, 358, 1–18. https://doi.org/10.1016/j.sedgeo.2017.06.005

Haughton, P., Davis, C., McCaffrey, W., and Barker, S. (2009). Hybrid sediment gravity flow deposits - Classification, origin and significance. Marine and Petroleum Geology, 26(10), 1900–1918. https://doi.org/10.1016/j.marpetgeo.2009.02.012

Hibbard, J. P., van Staal, C. R., and Miller, B. V. (2007). Links among Carolinia, Avalonia, and Ganderia in the Appalachian peri-Gondwanan realm. In J. W. Sears, T. A. Harms, and C. A. Evenchick (Eds.), Whence the Mountains? Inquiries into the Evolution of

Orogenic Systems: A Volume in Honor of Raymond A. Price (Vol. 433, Issue 14, pp. 291–311). Geological Society of America Special Paper. https://doi.org/10.1130/2007.2433(14)

Hjellbakk, A. (1997). Facies and fluvial architecture of a high-energy braided river: The Upper Proterozoic Seglodden Member, Varanger Peninsula, northern Norway. Sedimentary Geology, 114(1–4), 131–141. https://doi.org/10.1016/S0037-0738(97)00075-4

Hubert, J. F. (1962). A zircon-tourmaline-rutile maturity index and the interdependence of the composition of heavy minerals assemblages with the gross composition and texture of sandstones. Journal of Sedimentary Petrology, 32(3), 440–450.

Hughes, Charles. J. (1970). The late Precambrian Avalonian orogeny in Avalon, southeast Newfoundland. American Journal of Science, 269, 183–190.

Hunter, R. E. (1977). Terminology of cross-stratified sedimentary layers and climbing-ripple structures. Journal of Sedimentary Petrology, 47(2), 697–706.

Ichaso, A. A., and Dalrymple, R. W. (2009). Tide- and wave-generated fluid mud deposits in the Tilje Formation (Jurassic), offshore Norway. Geology, 37(6), 539–542. https://doi.org/10.1130/G25481A.1

Ichaso, A. A., Dalrymple, R. W., and Narbonne, G. M. (2007). Palaeoenvironmental and basin analysis of the late Neoproterozoic (Ediacaran) upper conception and St. John's groups, west Conception Bay, Newfoundland. Canadian Journal of Earth Sciences, 44(1), 25–41. https://doi.org/10.1139/E06-098

Ingersoll, R. V., Bullard, T. F., Ford, R. L., Grimm, J. P., Pickle, J. D., and Sares, S. W. (1985). The effect of grain size on detrital modes; a test of the Gazzi-Dickinson point-counting method; discussion and reply. Journal of Sedimentary Research, 55(4), 618–621. https://doi.org/10.1306/212f878d-2b24-11d7-8648000102c1865d

Ingram, R. L. (1964). Terminology for the thickness of stratification and parting units in sedimentary rocks. Geological Society of America Bulletin, 85, 937–938.

Israel, S. (1998). Geochronological, structural, and stratigraphic investigation of a Precambrian unconformity between the Harbour Main Group and Conception Group, east coast Holyrood Bay Avalon Peninsula, Newfoundland [Unpublished BSc honours thesis]. Memorial University of Newfoundland.

James, Noel. P., and Dalrymple, Robert. W. (Eds.). (2010). Facies models (GEOtext 6). Geological Association of Canada.

Julien, P. Y., and Raslan, Y. (1998). Upper-regime plane bed. Journal of Hydraulic Engineering, 124(11), 1085–1096.

King, A. F. (1988). Geology of the Avalon Peninsula, Newfoundland (parts of 1K, 1L, 1M, 1N and 2C). Newfoundland Department of Mines and Energy.

King, A. F. (1990). Geology of the St. John's area. Geological Survey Branch, Department of Mines and Energy, Goverment of Newfoundland and Labrador,Report 90-2, 93.

Kneller, B. (1995). Characterization of Deep Marine Clastic Systems. In A. J. Hartley and D. J. Prosser (Eds.), Characterization of Deep Marine Clastic Systems (Issue 94, pp. 31–49). Geological Society Special Publication.

Kocurek, G., and Fielder, G. (1982). Adhesion Structures. Journal of Sedimentary Petrology, 52(4), 1229–1241.

Kuang, H., Bai, H., Peng, N., Qi, K., Wang, Y., Chen, X., and Liu, Y. (2022). Temporal and spatial distribution of Precambrian red beds and their formation mechanisms. Geosystems and Geoenvironment, 1, 98. https://doi.org/10.1016/j.geogeo.2022.10

La Croix, A. D., and Dashtgard, S. E. (2014). Of sand and mud: Sedimentological criteria for identifying the turbidity maximum zone in a tidally influenced river. Sedimentology, 61(7), 1961–1981. https://doi.org/10.1111/sed.12126

Lai, L. S. H., Dorsey, R. J., Horng, C. S., Chi, W. R., Shea, K. S., and Yen, J. Y. (2021). Polygenetic mélange in the retrowedge foredeep of an active arc-continent collision, Coastal Range of eastern Taiwan. Sedimentary Geology, 418. https://doi.org/10.1016/j.sedgeo.2021.105901

Lamb, M. P., and Mohrig, D. (2009). Do hyperpycnal-flow deposits record river-flood dynamics? Geology, 37(12), 1067–1070. https://doi.org/10.1130/G30286A.1

Leclair, S. F., and Arnott, R. W. C. (2005). Parallel lamination formed by high-density turbidity currents. Journal of Sedimentary Research, 75(1), 1–5. https://doi.org/10.2110/jsr.2005.001

Leclair, S. F., Bridge, J. S., and Wang, F. (1997). Preservation of cross-strata due to migration of subaqueous dunes over aggrading and non-aggrading beds: comparison of experimental data with theory. Geoscience Canada, 24(1), 55 – 66.

Leeder, M. R. (2011). Sedimentology and Sedimentary Basins: From Turbulence To Tectonics (2nd ed.). Willet-Blackwell.

Liang, C., Jiang, Z., Cao, Y., Wu, M., Guo, L., and Zhang, C. (2016). Deep-water depositional mechanisms and significance for unconventional hydrocarbon exploration: A case study from the lower Silurian Longmaxi shale in the southeastern Sichuan Basin. AAPG Bulletin, 100(5), 773–794. https://doi.org/10.1306/02031615002

Long, D. G. F. (2011). Architecture and Depositional Style of Fluvial Systems before Land Plants: A Comparison of Precambrian, Early Paleozoic, and Modern River Deposits. In S. K. Davidson, S. Leleu, and C. P. North (Eds.), From River To Rock Record: The Preservation Of Fluvial Sediments And Their Subsequent Interpretation (Vol. 97, pp. 37–61). SEPM Special Publications.

Longhitano, S. G., Mellere, D., Steel, R. J., and Ainsworth, R. B. (2012). Tidal depositional systems in the rock record: A review and new insights. Sedimentary Geology, 279, 2–22. https://doi.org/10.1016/j.sedgeo.2012.03.024

Lowe, D.G. and Arnott, R.W.C. (2016). Composition and architecture of braided and sheetflood-dominated ephemeral fluvial strata in the Cambrian-Ordovician Potsdam Group: A case example of the morphodynamics of Early Phanerozoic fluvial systems and climate change. Journal of Sedimentary Research, 86, 587 – 612. https://doi.org/10.2110/jsr.2016.39

Lowe, D. R. (1975). Water escape structures in coarse-grained sediments. Sedimentology, 22, 157–204.

Lowe, D. R. (1982). Sediment Gravity Flows: II. Depositional models with special reference to the deposits of high-density turbidity currents. Journal of Sedimentary Petrology, 52(1), 0279–0297.

Mange, M. A., and Maurer, H. F. W. (1992). Heavy Minerals in Colour. In Heavy Minerals in Colour (1st ed.). Chapman and Hall. https://doi.org/10.1007/978-94-011-2308-2

Matthews, J. J., Liu, A. G., Yang, C., McIlroy, D., Levell, B., and Condon, D. J. (2020). A Chronostratigraphic Framework for the Rise of the Ediacaran Macrobiota: New Constraints from Mistaken Point Ecological Reserve, Newfoundland. Geological Society of America Bulletin, 133(3–4), 612–624. https://doi.org/10.1130/B35646.1

McAnally, W. H., Friedrichs, C., Hamilton, D., Hayter, E., Shrestha, P., Rodriguez, H., Sheremet, A., and Teeter, A. (2007). Management of Fluid Mud in Estuaries, Bays, and Lakes. I: Present State of Understanding on Character and Behavior ASCE Task Committee on Management of Fluid Mud. Journal of Hydraulic Engineering . https://doi.org/10.1061/ASCE0733-94292007133:19

Miall, A. (2014). Fluvial Depositional Systems. Springer International Publishing. https://doi.org/10.1007/978-3-319-00666-6

Mills, A. J., Dunning, G. R., and Sandeman, H. A. (2020). Lithogeochemical, isotopic, and U–Pb (zircon) age constraints on arc to rift magmatism, northwestern and central

Avalon Terrane, Newfoundland, Canada: implications for local lithostratigraphy. Canadian Journal of Earth Sciences, 23, 1–23. https://doi.org/10.1139/cjes-2019-0196

Morton, A. C., and Hallsworth, C. (1994). Identifying provenance-specific features of detrital heavy mineral assemblages in sandstones. Sedimentary Geology, 90, 241–256.

Mueller, K., and Suppe, J. (1997). Growth of Wheeler Ridge anticline, California: geomorphic evidence for fault-bend folding behaviour during earthquakes. Journal of Structural Geology, 19(3–4), 383–396.

Mulder, T., and Alexander, J. (2001). The physical character of subaqueous sedimentary density flow and their deposits. Sedimentology, 48(2), 269–299. https://doi.org/10.1046/j.1365-3091.2001.00360.x

Mulder, T., Migeon, S., Savoye, B., and Faugères, J. C. (2001). Inversely graded turbidite sequences in the deep Mediterranean: a record of deposits from flood-generated turbidity currents? Geo-Marine Letters, 21, 86–93. https://doi.org/10.1007/s003670100071

Mulder, T., Syvitski, J. P. M., Migeon, S., Faugères, J.-C., and Savoye, B. (2003). Marine hyperpycnal flows: initiation, behavior and related deposits. A review. Marine and Petroleum Geology, 20(6–8), 861–882. https://doi.org/10.1016/j.marpetgeo.2003.01.003

Murphy, J. B., Keppie, J. D., Dostal, J., and Nance, R. D. (1999). Neoproterozoic-early Paleozoic evolution of Avalonia. Geological Society of America Special Paper, 336, 253–266. https://doi.org/10.1130/0-8137-2336-1.253

Murphy, J. B., McCausland, P. J. A., O'Brien, S. J., Pisarevsky, S., and Hamilton, M. A. (2008). Age, geochemistry and Sm-Nd isotopic signature of the 0.76 Ga Burin Group: Compositional equivalent of Avalonian basement? Precambrian Research, 165(1–2), 37–48. https://doi.org/10.1016/j.precamres.2008.05.006

Murphy, J. B., and Nance, R. D. (1989). Model for the evolution of the Avalonian-Cadomian belt. Geology, 17(8), 735–738.

Murphy, J. B., Nance, R. D., Keppie, J. D., and Dostal, J. (2019). Role of Avalonia in the development of tectonic paradigms. Geological Society, London, Special Publications, 470(1), 265–287. https://doi.org/10.1144/SP470.12

Murphy, J. B., Pisarevsky, S., and Nance, R. D. (2013). Potential geodynamic relationships between the development of peripheral orogens along the northern margin of Gondwana and the amalgamation of West Gondwana. Mineralogy and Petrology, 107(5), 635–650. https://doi.org/10.1007/s00710-012-0207-9

Nance, R. D., Murphy, J. B., Strachan, R. A., Keppie, J. D., Gutiérrez-Alonso, G., Fernández-Suárez, J., Quesada, C., Linnemann, U., D'lemos, R., and Pisarevsky, S. A. (2008). Neoproterozoic-early Palaeozoic tectonostratigraphy and palaeogeography of the peri-Gondwanan terranes: Amazonian v. West African connections. In N. Ennih and J.-P. Liégeois (Eds.), The Boundaries of the West African Craton, Geological Society of London Special Publication (Vol. 297, pp. 345–383). https://doi.org/10.1144/SP297.17

Niemi, N. A., Buscher, J. T., Spotila, J. A., House, M. A., and Kelley, S. A. (2013). Insights from low-temperature thermochronometry into transpressional deformation and crustal exhumation along the San Andreas fault in the western Transverse Ranges, California. Tectonics, 32(6), 1602–1622. https://doi.org/10.1002/2013TC003377

Normark, W. R., and Piper, David. J. W. (1991). Initiation processes and flow evolution of turbidity currents: Implications for the depositional record. In From Shoreline to Abyss (46th ed.). SEPM Special Publication.

Normore, L. S. (2010). Geology of the Bonavista map area (NTS 2C/11), Newfoundland. Current Research, Newfoundland and Labrador Department of Natural Resources, Geological Survey, Report 10-1, 281–301.

O'Brien, S. J., O'Brien, B. H., Dunning, G. R., and Tucker, R. D. (1996). Late Neoproterozoic Avalonian and related peri-Gondwanan rocks of the Newfoundland Appalachians. Geological Society of America Special Paper, 304, 9–28. https://doi.org/10.1130/0-8137-2304-3.9

O'Brien, S. J., O'Driscoll, C. F., Greene, B. A., and Tucker, R. D. (1995). Pre-Carboniferous Geology of the Connaigre Peninsula and the adjacent coast of Fortune Bay, Southern Newfoundland. Current Research, Newfoundland Department of Natural Resources, Geological Survey, Report 95-1, 267–297.

Och, L. M., and Shields-Zhou, G. A. (2012). The Neoproterozoic oxygenation event: Environmental perturbations and biogeochemical cycling. Earth-Science Reviews, 110, 26–57. https://doi.org/10.1016/j.earscirev.2011.09.004

Olariu, C., and Bhattacharya, J. P. (2006). Terminal distributary channels and delta front architecture of river-dominated delta systems. Journal of Sedimentary Research, 76(2), 212–233. https://doi.org/10.2110/jsr.2006.026

Olsen, H., Due, P. H., and Clemmensen, L. B. (1989). Morphology and genesis of asymmetric adhesion warts-a new adhesion surface structure. Sedimentary Geology, 61, 277–285. https://doi.org/10.1016/0037-0738(89)90062-6

Owen, G., and Moretti, M. (2011). Identifying triggers for liquefaction-induced soft-sediment deformation in sands. Sedimentary Geology, 235(3–4), 141–147. https://doi.org/10.1016/j.sedgeo.2010.10.003

Papezik, V. S. (1973). Detrital garnet and muscovite in late Precambrian sandstone near St. John's, Newfoundland, and their significance. Canadian Journal of Earth Sciences, 10, 430–432. https://doi.org/10.1139/e73-162

Papezik, V. S. (1974). Prehnite-pumpellyite facies metamorphism of late Precambrian rocks of the Avalon Peninsula, Newfoundland. Canadian Mineralogist, 12, 463–468.

Parker, G. (1982). Conditions for the ignition of catastrophically erosive turbidity currents. Marine Geology, 46, 307–327.

Paton, C., Hellstrom, J., Paul, B., Woodhead, J., and Hergt, J. (2011). Iolite: Freeware for the visualisation and processing of mass spectrometric data. Journal of Analytical Atomic Spectrometry, 26(12), 2508–2518. https://doi.org/10.1039/c1ja10172b

Peddle, C. (2017). Structural analysis of the Country Pond Anticline and Bay Bulls Syncline pair, eastern Avalon Zone, Newfoundland (Issue March) [Unpublished BSc honours thesis]. Memorial University of Newfoundland.

Petrus, J. A., and Kamber, B. S. (2012). VizualAge: A Novel Approach to Laser Ablation ICP-MS U-Pb Geochronology Data Reduction. Geostandards and Geoanalytical Research, 36(3), 247–270. https://doi.org/10.1111/j.1751-908X.2012.00158.x

Pigram, C. J., Davies, P. J., Feary, D. A., and Symonds, P. A. (1989). Tectonic controls on carbonate platform evolution in southern Papua New Guinea: Passive margin to foreland basin. Geology, 17, 199–202.

Pollock, J. C., Barr, S. M., van Rooyen, D., and White, C. E. (2022). Insights from Lu-Hf zircon isotopic data on the crustal evolution of Avalonia and Ganderia in the northern Appalachian orogen. In Y. D. Kuiper, J. B. Murphy, R. D. Nance, R. A. Strachan, and M. D. Thompson (Eds.), New Developments in the Appalachian-Caledonian-Variscan Orogen (Special Paper, Vol. 554, pp. 173–207). Geological Society of America. https://doi.org/10.1130/2021.2554(08)

Pollock, J. C., Hibbard, J. P., and Sylvester, P. J. (2009). Early Ordovician rifting of Avalonia and birth of the Rheic Ocean: U-Pb detrital zircon constraints from Newfoundland. Journal of the Geological Society, 166(3), 501–515. https://doi.org/10.1144/0016-76492008-088

Postma, G., Nemec, W., and Kleinspehn, K. L. (1988). Large floating clasts in turbidites: a mechanism for their emplacement. Sedimentary Geology, 58, 47-61.

Pu, J. P., Bowring, S. A., Ramezani, J., Myrow, P., Raub, T. D., Landing, E., Mills, A., Hodgin, E., and Macdonald, F. A. (2016). Dodging snowballs: Geochronology of the Gaskiers glaciation and the first appearance of the Ediacaran biota. Geology, 44(11), 955–958. https://doi.org/10.1130/G38284.1

Rice, T. G. (1996). Structure of the Flat Rock thrust zone, Avalon Peninsula, Newfoundland Appalachians [Published BSc honours thesis]. Memorial University of Newfoundland.

Salas Rodrigo. A. (2004). Sedimentology and stratigraphy of the upper Neoproterozoic Ferryland Head Formation, eastern Avalon Peninsula, Newfoundland and Labrador with particular reference to the soft sediment deformation structures [Published MSc thesis]. Memorial University of Newfoundland.

Satkoski, A. M., Barr, S. D., and Samson, S. D. (2010). Provenance of late Neoproterozoic and Cambrian sediments in Avalonia: Constraints from detrital zircon ages and Sm-Nd isotopic compositions in southern New Brunswick, Canada. Journal of Geology, 118, 187–200. https://doi.org/10.1086/649818

Saunderson, H. C., and Lockett, F. P. J. (1983). Flume experiments on bedforms and structures at the dune-plane bed transition. In J. D. Collinson and J. Lewin (Eds.), Modern and Ancient Fluvial Systems (Vol. 6, pp. 49–58). Special Publications; The International Association of Sedimentologists.

Saylor, J. E., and Sundell, K. E. (2016). Quantifying comparison of large detrital geochronology data sets. Geosphere, 12(1), 203–220. https://doi.org/10.1130/GES01237.1

Singh, C. K. (1969). Petrology of the Signal Hill and Blackhead formations, Avalon Peninsula, Newfoundland. [Unpublished MSc thesis]. Memorial University of Newfoundland.

Skipton, D. R., Dunning, G. R., and Sparkes, G. W. (2013). Late Neoproterozoic arc-related magmatism in the Horse Cove Complex, eastern Avalon Zone, Newfoundland. Canadian Journal of Earth Sciences, 50(4), 462–482. https://doi.org/10.1139/cjes-2012-0090

Sláma, J., Košler, J., Condon, D. J., Crowley, J. L., Gerdes, A., Hanchar, J. M., Horstwood, M. S. A., Morris, G. A., Nasdala, L., Norberg, N., Schaltegger, U., Schoene, B., Tubrett, M. N., and Whitehouse, M. J. (2008). Plešovice zircon - A new natural reference material for U-Pb and Hf isotopic microanalysis. Chemical Geology, 249(1–2), 1–35. https://doi.org/10.1016/j.chemgeo.2007.11.005

Stanley, B. (2009). Structural analysis of the linkage between the Blackhead and Bay Bulls synclines, eastern Avalon Zone, Newfoundland [Unpublished BSc honours thesis]. Memorial University of Newfoundland.

Sumner, E. J., Amy, L. A., and Talling, P. J. (2008). Deposit structure and processes of sand deposition from decelerating sediment suspensions. Journal of Sedimentary Research, 78(8), 529–547. https://doi.org/10.2110/jsr.2008.062

Trowbridge, J. H., and Kineke, G. C. (1994). Structure and dynamics of fluid muds on the Amazon continental shelf. Journal of Geophysical Research, 99(C1), 865–874. https://doi.org/10.1029/93JC02860

Tye, A. R., Niemi, N. A., Safarov, R. T., Kadirov, F. A., and Babayev, G. R. (2021). Sedimentary response to a collision orogeny recorded in detrital zircon provenance of Greater Caucasus foreland basin sediments. Basin Research, 33(2), 933–967. https://doi.org/10.1111/bre.12499

van Heijst, M. W. I. M., Postma, G. (2001). Fluvial response to sea-level changes: a quantitative analogue, experimental approach. Basin Research, 13, 269–292.

van Staal, C. R., Barr, S. M., McCausland, P. J. A., Thompson, M. D., and White, C. E. (2021). Tonian–Ediacaran tectonomagmatic evolution of West Avalonia and its Ediacaran–early Cambrian interactions with Ganderia: an example of complex terrane transfer due to arc–arc collision? Geological Society, London, Special Publications, 503(1), 143–167. https://doi.org/10.1144/SP503-2020-23

van Toorenenburg, K. A., Donselaar, M. E., Noordijk, N. A., and Weltje, G. J. (2016). On the origin of crevasse-splay amalgamation in the Huesca fluvial fan (Ebro Basin, Spain): Implications for connectivity in low net-to-gross fluvial deposits. Sedimentary Geology, 343, 156–164. https://doi.org/10.1016/j.sedgeo.2016.08.008

van Yperen, A. E., Poyatos-Moré, M., Holbrook, J. M., and Midtkandal, I. (2020). Internal mouth-bar variability and preservation of subordinate coastal processes in low-accommodation proximal deltaic settings (Cretaceous Dakota Group, New Mexico,

USA). In Depositional Record (Vol. 6, Issue 2, pp. 431–458). https://doi.org/10.1002/dep2.100

Venditti, J. G., Church, M., and Bennett, S. J. (2005). On the transition between 2D and 3D dunes. Sedimentology, 52(6), 1343–1359. https://doi.org/10.1111/j.1365-3091.2005.00748.x

Vermeesch, P. (2018). IsoplotR: A free and open toolbox for geochronology. Geoscience Frontiers, 9(5), 1479–1493. https://doi.org/10.1016/j.gsf.2018.04.001

Waldron, J. W. F., and Gagnon, J. F. (2011). Recognizing soft-sediment structures in deformed rocks of orogens. Journal of Structural Geology, 33(3), 271–279. https://doi.org/10.1016/j.jsg.2010.06.015

White, C. E., Barr, S. M., Crowley, J. L., van Rooyen, D., and MacHattie, T. G. (2022). U-Pb zircon ages and Sm-Nd isotopic data from the Cobequid Highlands, Nova Scotia, Canada: New contributions to understanding the Neoproterozoic geologic history of Avalonia. In Y. D. Kuiper, J. B. Murphy, R. D. Nance, R. A. Strachan, and M. D. Thompson (Eds.), New Developments in the Appalachian-Caledonian-Variscan Orogen (Special Paper, Vol. 554, pp. 135–172). Geological Society of America Special Paper. https://doi.org/10.1130/2021.2554(07)

White, C. E., Barr, S. M., Jamieson, R. A., and Reynolds, P. H. (2001). Neoproterozoic high-pressure/low-temperature metamorphic rocks in the Avalon terrane, Southern New Brunswick, Canada. Journal of Metamorphic Geology, 19(5), 519–530. https://doi.org/10.1046/j.0263-4929.2001.00326.x

Wiedenbeck, M., Allé, P., Cordu, F., Griffin, W. L., Meier, M., Oberi, F., Quadt, A. V., Roddick, J. C., and Spiegel, W. (1995). Three natural zircon standards for U-Th-Pb, Lu-Hf, trace element, and REE analyses. Geostandards Newsletter, 19(1), 1–23. https://doi.org/10.1111/j.1751-908X.1995.tb00147.x

Williams, H., and King, A. F. (1976). Southern Avalon Peninsula, Newfoundland: Trepassey Map-Area (1K). In Paper 76-1A (pp. 179–182). Geological Survey of Canada.

Willner, A. P., Bar, S. M., Gerdes, A., Massonne, H. J., and White, C. E. (2013). Origin and evolution of Avalonia: Evidence from U-Pb and Lu-Hf isotopes in zircon from the Mira terrane, Canada, and the Stavelot-Venn Massif, Belgium. Journal of the Geological Society, 170(5), 769–784. https://doi.org/10.1144/jgs2012-152

Zavala, C. (2020). Hyperpycnal (over density) flows and deposits. Journal of Palaeogeography, 9(1), 17. https://doi.org/10.1186/s42501-020-00065-x

Appendix

Appendix A: Location map of the visited areas

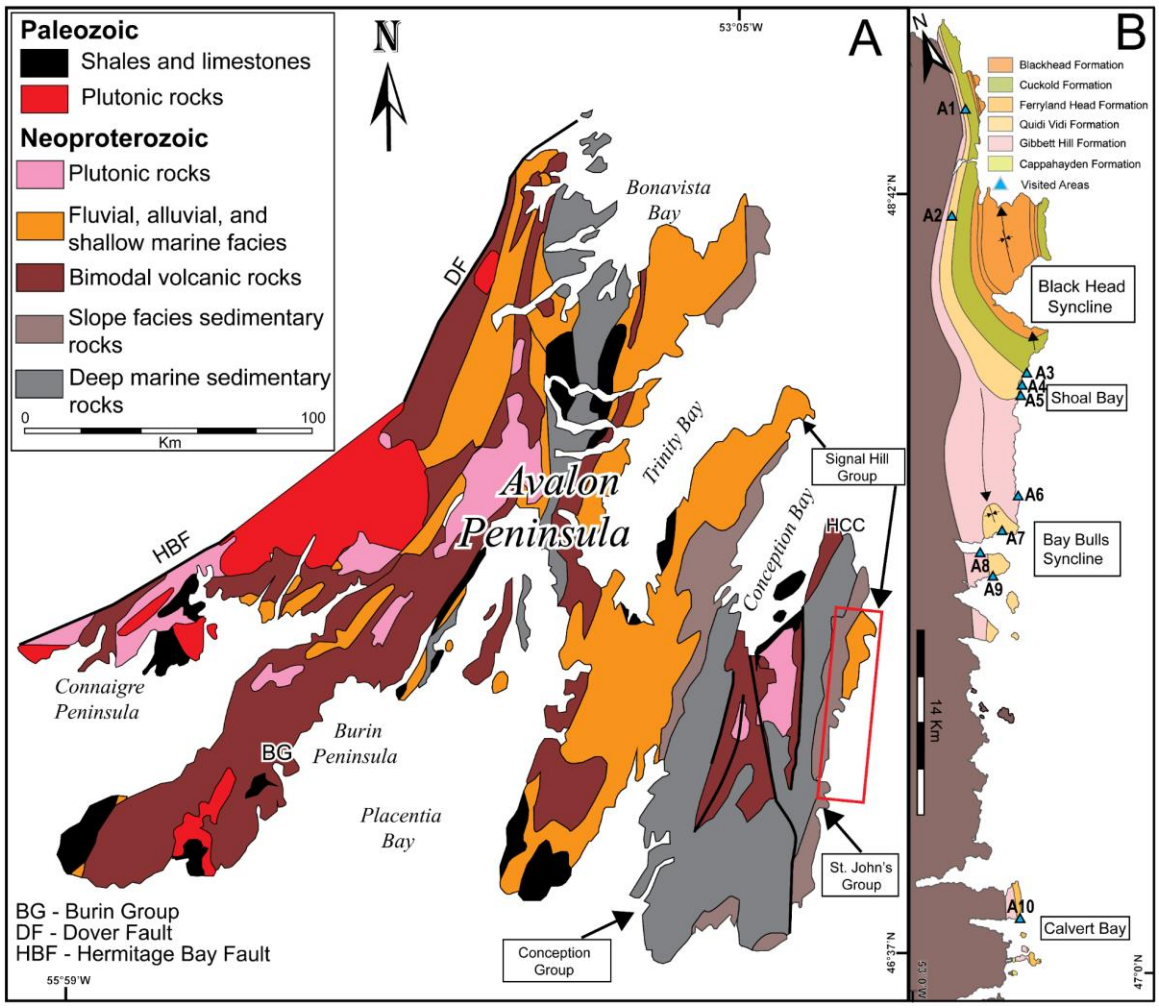

Appendix B: Crevasse channels

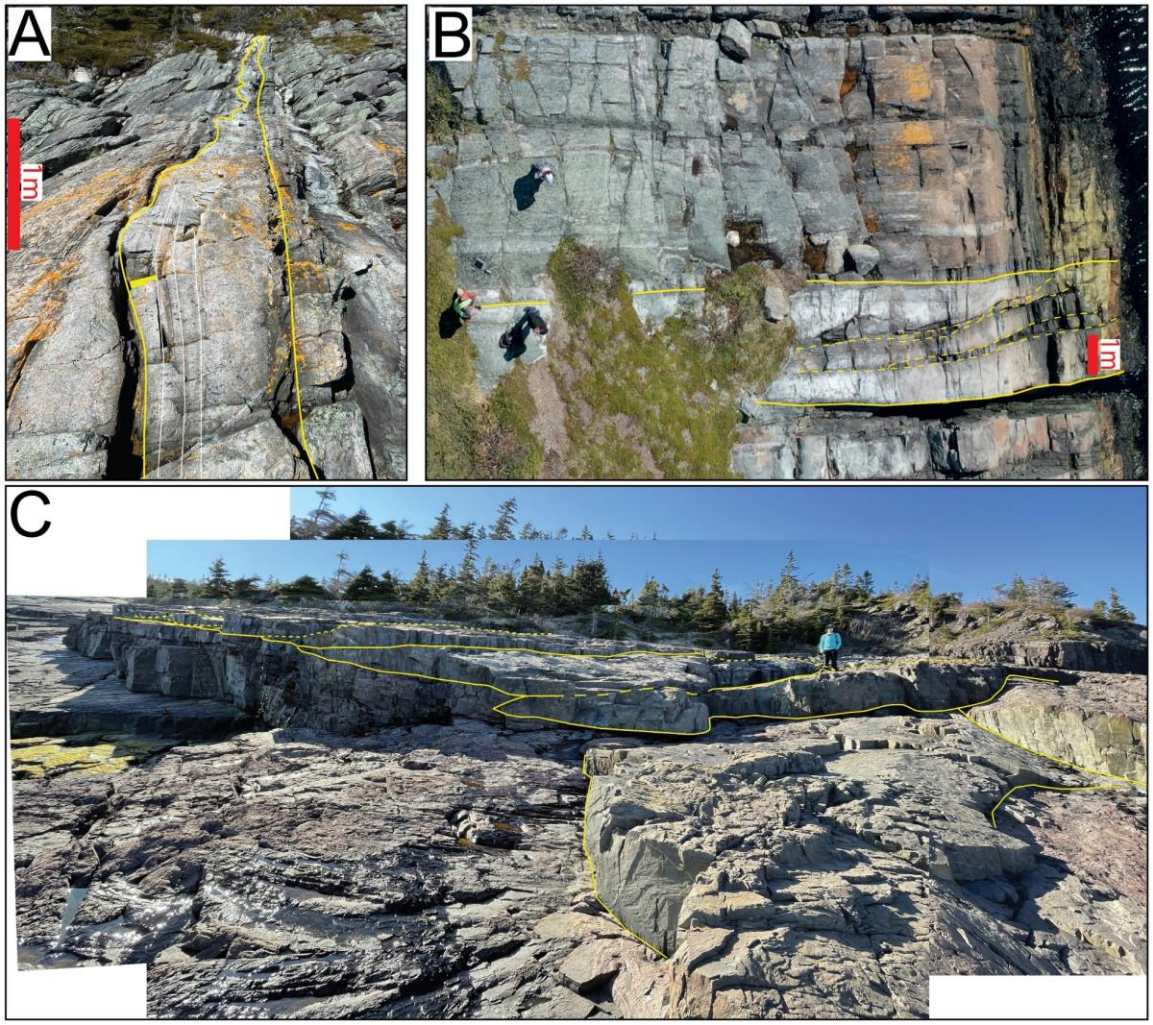

Appendix B. Lower delta plain crevasse channels (FA2). A) Single channel filled by concentrated sediment flow deposits, exposed in Area 10 (see Appendix A for area locations). B). Single channel fill showing internal lateral accretion features, exposed in Area 10. C). Laterally amalgamated multi-storey channel fills, exposed in Area 7. Yellow solid and dashed lines represent erosive contacts; the paleoflow is coming out in all the pictures; the person in picture C represents a scale of 1.60 m.

Appendix C: Distributary Channels

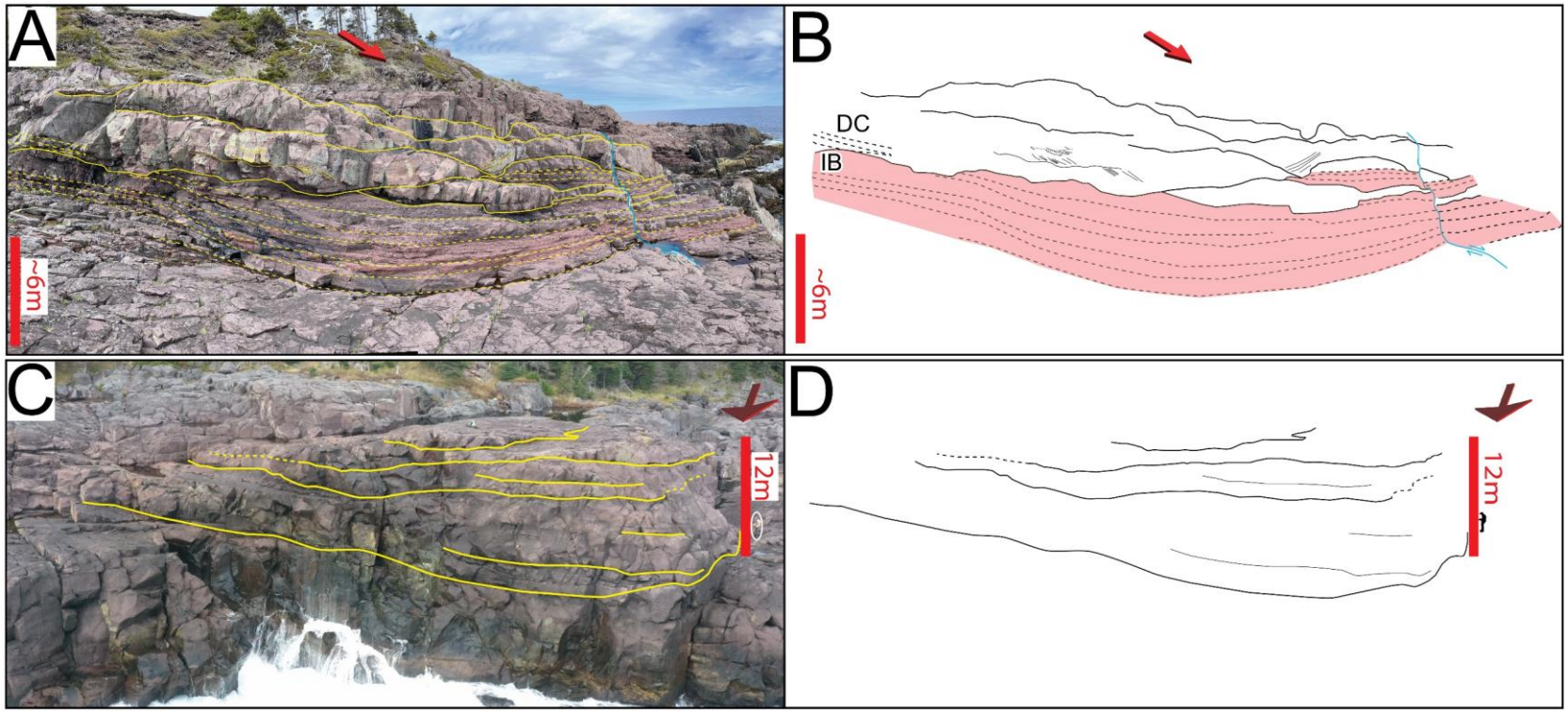

Appendix C. Upper delta plain distributary channels (FA2)**.** A). B) Bedding diagram showing laterally-amalgamated distributary channel deposits cutting interdistributary bay deposits (red), exposed near Area 4 (see Appendix A for area locations). C). D) Bedding diagram showing multi-storey, vertically-amalgamated distributary channel deposits, exposed at Area 5. Abbreviations: DC-distributary channel; IB-interdistributary bay. Red arrows indicate paleo flow directions. Yellow solid lines represent erosional contacts; yellow dashed lines represent bedding. The blue line represents a small normal fault.

Appendix D: Delta plain and delta front architectural elements paleo flow

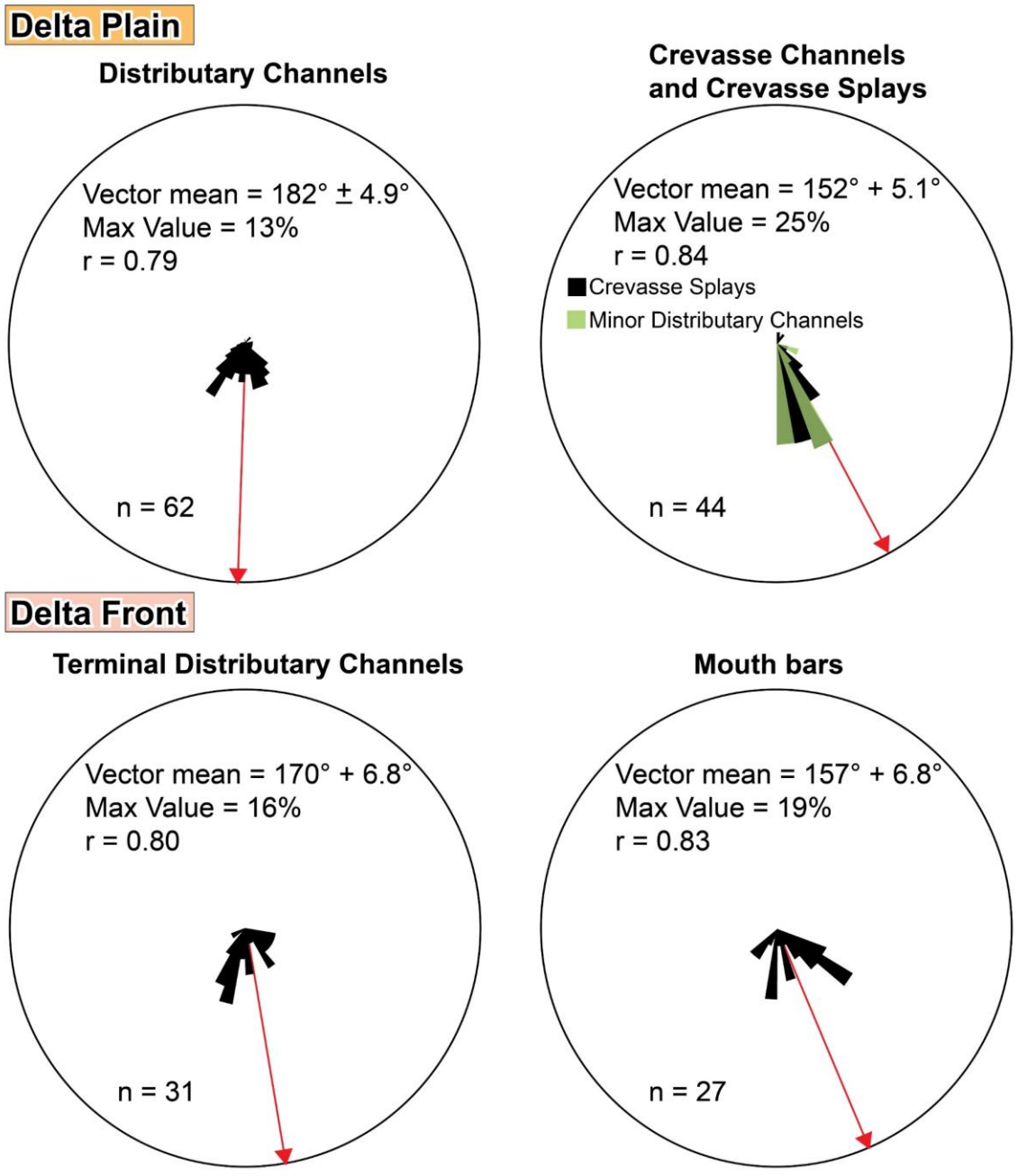

Appendix E: Gradational contact towards fluvial facies of the Cuckold Formation

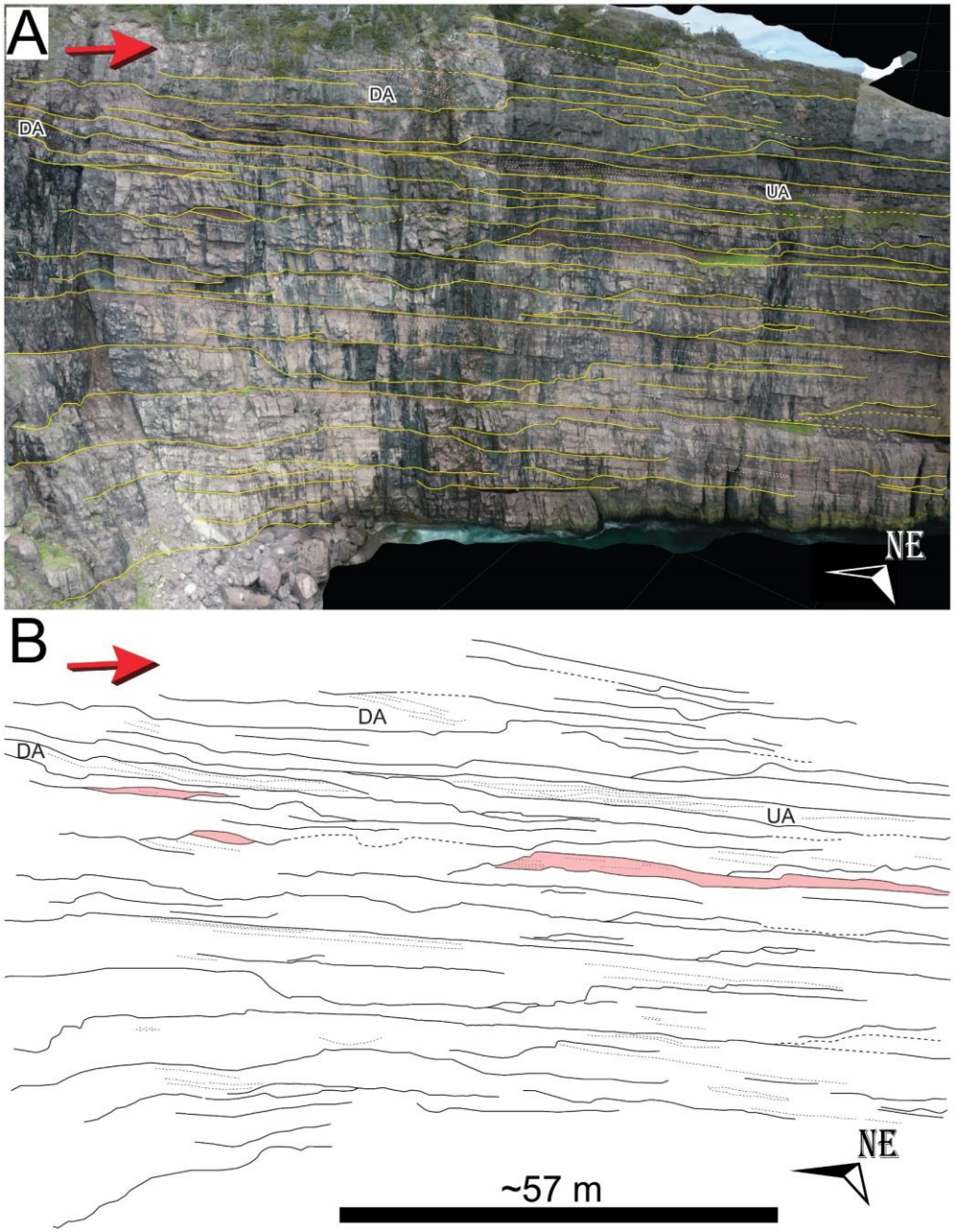

Appendix E. A) Oblique-oriented photogrammetric model of the upper delta plain to fluvial facies contact outcropping near Area 3 (see Appendix A for area locations). B). Bedding diagram showing vertically and laterally-amalgamated distributary channel deposits with preserved interdistributary bay deposits (red). Abbreviations: UA-upstream accretion; DA-downstream accretion; red arrows indicate paleoflow direction; yellow solid lines represent erosional contacts

Appendix F: Sandstone petrography counts

Sample ID		QWH-001	QWH-002	QWH-004	QWH-005	QWH-006	QWH-007	BHR-001	BHR-002	BHR-003	BB-001	BB-002	BB-004	BB-005	CAL-002	CAL-004	CAL-005	CAL-011	CAL-012	CAL-013	CAL-015
Quartz	Monocrystalline (QM)	49	32	26	42	58	33	64	35	50	36	54	45	54	36	27	25	11	34	24	46
	Polycrystalline (QP)	28	34	11	17	31	14	9	7	11	4	9	31	11	14	16	3	4	10	13	37
Feldspar		115	187	109	131	98	70	129	99	130	156	102	108	51	113	96	112	63	84	121	90
	Felsic	3	1	28	49	72	48	7	5	11	8	42	48	24	24	24	18	3	33	13	16
Volcanic clasts	Intermediate	0	2	20	19	25	26	3	3	10	20	15	4	75	28	58	43	16	43	45	22
	Mafic	0	1	3	3	2	5	1	0	0	1	2	4	5	0	0	2	0	0	0	2
	Mudstone	3	2	15	0	0	1	3	0	0	0	0	0	4	2	0	0	2	0	0	0
Sedimentary	Siltstone	0	0	29	4	0	1	4	5	5	1	4	0	1	0	1	0	0	1	0	0
	Sandstone	2	13	13	7	2	2	0	0	0	0	0	0	4	1	0	1	0	1	1	1
	Chert	0	0	0	0	0	5	0	0	0	0	7	0	8	13	5	0	0	5	3	2
	Lmp1	0	0	0	0	3	0	0	0	0	0	0	0	0	0	0	0	0	0	0	0
	Lmp2	0	0	2	0	0	0	0	0	0	0	0	0	0	0	0	0	0	0	0	0
Metapelite	Lmp3	0	0	0	0	0	0	0	0	0	0	0	0	0	0	0	0	0	0	0	0
	Lmp4	0	0	0	0	0	0	0	0	0	0	0	0	0	0	0	0	0	0	0	0
	Lmp5	0	0	0	0	0	0	0	0	0	0	0	0	0	0	0	0	0	0	0	0
	Lmf 1	0	0	2	0	2	1	0	0	0	0	0	0	1	0	0	0	0	0	0	0
	Lmf 2	0	0	1	2	0	1	0	0	0	0	0	0	1	0	0	0	0	0	0	0
Metapsammite	Lmf 3	0	0	2	1	4	1	0	0	0	0	1	0	2	0	0	0	0	4	0	0
	Lmf 4	0	0	0	0	0	0	0	0	0	0	0	0	0	0	0	0	0	0	0	0
	Lmf 5	0	0	0	0	0	0	0	0	0	0	0	0	0	0	0	0	0	0	0	0
	Lmb1	0	0	0	0	0	0	0	0	0	0	0	0	0	0	0	0	0	0	0	0
	Lmb2	0	0	0	0	0	0	0	0	0	0	0	0	0	0	0	0	0	0	0	0
Metabasite	Lmb3	0	0	0	0	0	0	0	0	0	0	0	0	0	0	0	0	0	0	0	0
	Lmb4	0	0	0	0	0	0	0	0	0	0	0	0	0	0	0	0	0	0	0	0
	Lmb5	0	0	0	0	0	0	0	0	0	0	0	0	0	0	0	0	0	0	0	0
	Epidote	4	1	11	25	23	6	7	4	10	7	14	8	4	0	1	4	2	32	1	2
	Zircon	1	2	0	0	0	0	3	0	1	1	0	0	0	0	0	0	0	0	1	0
	Rutile	0	0	1	0	0	0	0	0	0	0	0	0	0	0	0	0	0	0	0	0
Accessory	Titanite	1	1	2	0	0	0	1	0	0	1	0	0	0	0	0	0	0	0	0	1
Minerals	Muscovite	1	0	0	2	0	1	0	0	0	0	0	0	0	0	2	1	1	0	1	1
	Biotite	2	1	1	0	0	0	1	2	3	0	0	1	0	1	0	0	0	0	5	5
	Chlorite	3	6	3	1	0	0	3	2	12	1	3	0	1	7	4	1	0	3	8	9
	Opaque	5	8	3	14	0	1	1	3	4	4	0	1	0	5	2	4	1	1	2	2
	Carbonates	0	0	0	0	0	0	0	0	1	0	0	0	0	0	0	0	0	0	0	3
Matrix		30	9	12	0	0	0	14	50	4	16	0	38	13	12	16	43	27	0	15	19
Total counts		247	300	294	317	320	216	250	215	252	256	253	288	258	256	252	257	130	251	253	258
TOTAL (QFL)		200	272	261	275	297	208	220	154	217	226	236	240	240	231	227	204	99	215	220	216
Feldspar%		58%	69%	42%	48%	33%	34%	59%	64%	60%	69%	43%	45%	21%	49%	42%	55%	64%	39%	55%	42%
Q(Total)%		39%	24%	14%	21%	30%	23%	33%	27%	28%	18%	27%	32%	27%	22%	19%	14%	15%	20%	17%	38%
Lithics%		4%	7%	44%	31%	37%	44%	8%	8%	12%	13%	30%	23%	52%	29%	39%	31%	21%	40%	28%	20%
Total (QmFL)		172	238	250	258	266	194	211	147	206	222	227	209	229	217	211	201	95	205	207	179
Feldspar%		67%	79%	44%	51%	37%	36%	61%	67%	63%	70%	45%	52%	22%	52%	45%	56%	66%	41%	58%	50%
Qm(Total)%		28%	13%	10%	16%	22%	17%	30%	24%	24%	16%	24%	22%	24%	17%	13%	12%	12%	17%	12%	26%
Lithics%		5%	8%	46%	33%	41%	47%	9%	9%	13%	14%	31%	27%	54%	31%	42%	32%	22%	42%	30%	24%

Sample ID		QWH-001	QWH-002	QWH-004	QWH-005	QWH-006	QWH-007	BHR-001	BHR-002	BHR-003	BB-001	BB-002	BB-004	BB-005	CAL-002	CAL-004	CAL-005	CAL-011	CAL-012	CAL-013	CAL-015
Latitud (N)	*WGS 84*	47.59783	47.59802	47.59903	47.59906	47.59982	47.59975	47.54525	47.54559	47.54610	47.30229	47.30227	47.30146	47.30141	47.0481	47.0484	47.04841	47.04900	47.04953	47.04481	47.04809
Longitude (W)		52.67952	52.67854	52.67786	52.67746	52.67590	52.67559	52.71900	52.71821	52.71739	52.79905	52.79872	52.79670	52.79620	52.8617	52.861	52.86060	52.85901	52.85872	52.86266	52.86248

Appendix G: Transparent heavy mineral counts

Sample ID	QWH-001 (GC)	QWH-001 (Wt%)	QWH-007 (GC)	QWH-007 (Wt%)	BB-004 (GC)	BB-004 (Wt%)	UBQV-001 (GC)	UBQV-001 (Wt%)
Epidote	13932	58	62460	95	15150	46	13719	49
Zoisite	0	0	0	0	0	0	0	0
Ilmenite	5	0	201	0	40	0	1714	6
Rutile	731	3	17	0	223	1	104	0
Apatite	1425	6	64	0	235	1	279	1
Titanite	4634	19	2744	4	14288	43	5559	20
Monazite	14	0	0	0	16	0	0	0
Allanite	119	0	40	0	78	0	62	0
Thorite	0	0	0	0	2	0	0	0
Zircon	674	3	118	0	667	2	388	1
Fe-Mg Spinel	22	0	2	0	25	0	77	0
Hornblende	1640	7	352	1	1733	5	2197	8
Pyroxene	1	0	0	0	0	0	0	0
Tourmaline	45	0	0	0	3	0	11	0
Garnet	652	3	72	0	572	2	3835	14
Total	23894	100	66070	100	33032	100	27945	100

Appendix H: Paleoflow Data

Formation	*Facies*	*Measurement type*	*Azimuth*	*Latitud (N)*	*Longitud (W)*	*Location*
Gibbett Hill	Delta Front	Current Ripple	127	47.59793	52.67952	Area 1
Gibbett Hill	Delta Front	Dune	160	47.59793	52.67952	Area 1
Gibbett Hill	Delta Front	Current Ripple	147	47.59793	52.67952	Area 1
Gibbett Hill	Delta Front	Dune	175	47.59793	52.67952	Area 1
Gibbett Hill	Delta Front	Dune	192	47.59793	52.67952	Area 1
Gibbett Hill	Delta Front	Dune	194	47.59793	52.67952	Area 1
Gibbett Hill	Delta Front	Dune	206	47.59793	52.67952	Area 1
Gibbett Hill	Delta Front	Dune	178	47.59793	52.67952	Area 1
Gibbett Hill	Delta Front	Current Ripple	110	47.59793	52.67952	Area 1
Quidi Vidi	Delta Front	Current Ripple	159	47.59793	52.67952	Area 1
Gibbett Hill	Delta Front	Current Ripple	122	47.54559	52.71821	Area 2
Gibbett Hill	Delta Front	Current Ripple	119	47.54559	52.71821	Area 2
Quidi Vidi	Delta Plain	Dune	168	47.40984	52.69952	Area 3
Quidi Vidi	Delta Plain	Dune	138	47.40952	52.69984	Area 3-4
Quidi Vidi	Delta Plain	Dune	210	47.40952	52.69984	Area 3-4
Quidi Vidi	Delta Plain	Dune	220	47.40952	52.69984	Area 3-4
Quidi Vidi	Delta Plain	Rib and Furrow	232	47.40952	52.69984	Area 3-4
Quidi Vidi	Delta Plain	Dune	200	47.40944	52.70024	Area 3-4
Quidi Vidi	Delta Plain	Dune	204	47.40944	52.70024	Area 3-4
Quidi Vidi	Delta Plain	Dune	147	47.40719	52.70384	Area 3-4
Quidi Vidi	Delta Plain	Dune	140	47.40719	52.70384	Area 3-4
Quidi Vidi	Delta Plain	Dune	130	47.40719	52.70384	Area 3-4
Quidi Vidi	Delta Plain	Dune	185	47.40719	52.70384	Area 3-4
Quidi Vidi	Delta Plain	Dune	175	47.40719	52.70384	Area 3-4
Quidi Vidi	Delta Plain	Rib and Furrow	220	47.40643	52.7041	Area 3-4
Quidi Vidi	Delta Plain	Dune	155	47.40643	52.7041	Area 3-4
Quidi Vidi	Delta Plain	Dune	138	47.40643	52.7041	Area 3-4
Quidi Vidi	Delta Plain	Dune	210	47.40643	52.7041	Area 3-4
Quidi Vidi	Delta Plain	Dune	204	47.40643	52.7041	Area 3-4
Quidi Vidi	Delta Plain	Dune	210	47.40266	52.70435	Area 3-4
Quidi Vidi	Delta Plain	Dune	196	47.40266	52.70435	Area 3-4
Quidi Vidi	Delta Plain	Rib and Furrow	232	47.39716	52.70885	Area 3-4
Quidi Vidi	Delta Plain	Rib and Furrow	228	47.39716	52.70885	Area 3-4
Quidi Vidi	Delta Plain	Rib and Furrow	252	47.39716	52.70885	Area 3-4
Quidi Vidi	Delta Plain	Rib and Furrow	230	47.39716	52.70885	Area 3-4
Quidi Vidi	Delta Plain	Rib and Furrow	240	47.39716	52.70885	Area 3-4
Quidi Vidi	Delta Plain	Rib and Furrow	218	47.39716	52.70885	Area 3-4
Quidi Vidi	Delta Plain	Rib and Furrow	220	47.39716	52.70885	Area 3-4
Quidi Vidi	Delta Plain	Dune	180	47.39795	52.7085	Area 3-4
Quidi Vidi	Delta Plain	Dune	210	47.39795	52.7085	Area 3-4
Quidi Vidi	Delta Plain	Dune	180	47.39795	52.7085	Area 3-4
Quidi Vidi	Delta Plain	Dune	222	47.39795	52.7085	Area 3-4
Quidi Vidi	Delta Plain	Dune	210	47.39795	52.7085	Area 3-4
Quidi Vidi	Delta Plain	Dune	142	47.39392	52.71355	Area 4
Quidi Vidi	Delta Plain	Dune	210	47.39392	52.71355	Area 4-5
Quidi Vidi	Delta Plain	Dune	214	47.39392	52.71355	Area 4-5
Quidi Vidi	Delta Plain	Dune	190	47.39392	52.71355	Area 4-5
Quidi Vidi	Delta Plain	Dune	170	47.392168	52.71439	Area 5
Quidi Vidi	Delta Plain	Dune	160	47.392168	52.71439	Area 5
Gibbett Hill	Delta Front	Dune	188	47.38219	52.71552	Area 5-6
Gibbett Hill	Delta Front	Dune	220	47.38219	52.71552	Area 5-6
Gibbett Hill	Delta Front	Dune	210	47.38939	52.71808	Area 5-6
Gibbett Hill	Delta Front	Dune	200	47.38939	52.71808	Area 5-6
Gibbett Hill	Delta Front	Dune	150	47.38589	52.71614	Area 5-6
Gibbett Hill	Delta Front	Current Ripple	188	47.38219	52.71552	Area 5-6

Appendix H: Paleoflow Data (continued)

Gibbett Hill	Delta Front	Current Ripple	220	47.38219	52.71552	Area 5-6
Gibbett Hill	Delta Front	Current Ripple	150	47.37549	52.71883	Area 5-6
Gibbett Hill	Delta Front	Dune	132	47.37549	52.71883	Area 5-6
Gibbett Hill	Delta Front	Dune	160	47.37549	52.71883	Area 5-6
Gibbett Hill	Delta Front	Dune	190	47.366047	52.725937	Area 5-6
Gibbett Hill	Delta Front	Dune	180	47.366047	52.725937	Area 5-6
Gibbett Hill	Delta Front	Current Ripple	212	47.33015	52.73994	Area 6
Gibbett Hill	Delta Front	Current Ripple	210	47.33015	52.73994	Area 6
Gibbett Hill	Delta Front	Dune	192	47.32731	52.73952	Area 6-7
Gibbett Hill	Delta Front	Dune	204	47.32731	52.73952	Area 6-7
Gibbett Hill	Delta Front	Current Ripple	130	47.32454	52.74045	Area 6-7
Gibbett Hill	Delta Front	Current Ripple	142	47.32329	52.74253	Area 6-7
Gibbett Hill	Delta Front	Dune	204	47.32107	52.7442	Area 6-7
Gibbett Hill	Delta Front	Dune	180	47.31967	52.74521	Area 6-7
Gibbett Hill	Delta Front	Dune	212	47.31967	52.74521	Area 6-7
Gibbett Hill	Delta Front	Dune	200	47.31967	52.74521	Area 6-7
Gibbett Hill	Delta Front	Dune	230	47.31967	52.74521	Area 6-7
Gibbett Hill	Delta Front	Dune	241	47.31967	52.74521	Area 6-7
Gibbett Hill	Delta Front	Dune	192	47.30906	52.74917	Area 6-7
Quidi Vidi	Delta Plain	Dune	109	47.3129	52.7712	Area 7
Quidi Vidi	Delta Plain	Dune	137	47.3129	52.7712	Area 7
Quidi Vidi	Delta Plain	Dune	189	47.3129	52.7712	Area 7
Quidi Vidi	Delta Plain	Dune	200	47.3129	52.7712	Area 7
Quidi Vidi	Delta Plain	Dune	206	47.3129	52.7712	Area 7
Quidi Vidi	Delta Plain	Dune	184	47.3129	52.7712	Area 7
Quidi Vidi	Delta Plain	Dune	193	47.3129	52.7712	Area 7
Quidi Vidi	Delta Plain	Dune	155	47.3129	52.7712	Area 7
Quidi Vidi	Delta Plain	Dune	178	47.3129	52.7712	Area 7
Quidi Vidi	Delta Plain	Dune	153	47.3129	52.7712	Area 7
Quidi Vidi	Delta Plain	Current ripple	142	47.3129	52.7712	Area 7
Quidi Vidi	Delta Plain	Dune	103	47.3129	52.7712	Area 7
Quidi Vidi	Delta Plain	Dune	152	47.3129	52.7712	Area 7
Gibbett Hill	Delta Front	Dune	112	47.30198	52.79771	Area 8
Gibbett Hill	Delta Front	Dune	107	47.30198	52.79771	Area 8
Gibbett Hill	Delta Front	Dune	131	47.30198	52.79771	Area 8
Gibbett Hill	Delta Front	Dune	88	47.30198	52.79771	Area 8
Gibbett Hill	Delta Front	Dune	134	47.30198	52.79771	Area 8
Gibbett Hill	Delta Front	Dune	113	47.30198	52.79771	Area 8
Gibbett Hill	Delta Front	Dune	109	47.30198	52.79771	Area 8
Gibbett Hill	Delta Front	Dune	126	47.30198	52.79771	Area 8
Gibbett Hill	Delta Front	Dune	126	47.30198	52.79771	Area 8
Gibbett Hill	Delta Front	Dune	163	47.30198	52.79771	Area 8
Gibbett Hill	Delta Front	Current ripple	129	47.30198	52.79771	Area 8
Gibbett Hill	Delta Front	Dune	180	47.28384	52.78905	Area 9
Gibbett Hill	Delta Front	Dune	188	47.28384	52.78905	Area 9
Gibbett Hill	Delta Front	Dune	125	47.28384	52.78905	Area 9
Gibbett Hill	Delta Front	Dune	131	47.28384	52.78905	Area 9
Gibbett Hill	Delta Front	Dune	148	47.28384	52.78905	Area 9
Quidi Vidi	Delta Plain	Dune	85	47.28375	52.78845	Area 9
Quidi Vidi	Delta Plain	Dune	240	47.28375	52.78845	Area 9
Quidi Vidi	Delta Plain	Dune	190	47.28375	52.78845	Area 9
Quidi Vidi	Delta Plain	Dune	151	47.28382	52.78827	Area 9
Quidi Vidi	Delta Plain	Dune	161	47.28382	52.78827	Area 9
Quidi Vidi	Delta Plain	Current ripple	158	47.28382	52.78827	Area 9
Quidi Vidi	Delta Plain	Dune	160	47.28382	52.78827	Area 9
Quidi Vidi	Delta Plain	Dune	165	47.28382	52.78827	Area 9

Appendix H: Paleoflow Data (continued)

Quidi Vidi	Delta Plain	Dune	40	47.28411	52.78618	Area 9
Quidi Vidi	Delta Plain	Dune	171	47.28411	52.78618	Area 9
Quidi Vidi	Delta Plain	Dune	150	47.28411	52.78618	Area 9
Quidi Vidi	Delta Plain	Dune	165	47.28411	52.78618	Area 9
Quidi Vidi	Delta Plain	Current ripple	145	47.28411	52.78618	Area 9
Quidi Vidi	Delta Plain	Dune	110	47.28411	52.78618	Area 9
Quidi Vidi	Delta Plain	Dune	145	47.28411	52.78618	Area 9
Gibbett Hill	Delta Front	Dune	144	47.04807	52.8617	Area 10
Gibbett Hill	Delta Front	Dune	128	47.04841	52.86136	Area 10
Gibbett Hill	Delta Front	Dune	173	47.04841	52.86136	Area 10
Gibbett Hill	Delta Front	Current ripple	175	47.04844	52.86129	Area 10
Gibbett Hill	Delta Front	Dune	112	47.04844	52.86129	Area 10
Gibbett Hill	Delta Front	Dune	142	47.04844	52.86129	Area 10
Gibbett Hill	Delta Front	Climbing ripples	160	47.0485	52.86093	Area 10
Ferryland Head	Delta Plain	Current ripple	155	47.04843	52.86082	Area 10
Ferryland Head	Delta Plain	Current ripple	163	47.04843	52.86082	Area 10
Ferryland Head	Delta Plain	Current ripple	150	47.04837	52.86068	Area 10
Ferryland Head	Delta Plain	Climbing ripples	158	47.04837	52.86068	Area 10
Ferryland Head	Delta Plain	Dune	155	47.04842	52.86049	Area 10
Ferryland Head	Delta Plain	Climbing ripples	161	47.04842	52.86049	Area 10
Ferryland Head	Delta Plain	Dune	148	47.04842	52.86049	Area 10
Ferryland Head	Delta Plain	Dune	172	47.04842	52.86031	Area 10
Ferryland Head	Delta Plain	Climbing ripples	163	47.04839	52.86017	Area 10
Ferryland Head	Delta Plain	Climbing ripples	155	47.04839	52.86017	Area 10
Ferryland Head	Delta Plain	Dune	151	47.04839	52.86017	Area 10
Ferryland Head	Delta Plain	Climbing ripples	161	47.04839	52.86017	Area 10
Ferryland Head	Delta Plain	Dune	14	47.04839	52.86017	Area 10
Ferryland Head	Delta Plain	Dune	31	47.04846	52.86005	Area 10
Ferryland Head	Delta Plain	Climbing ripples	144	47.04846	52.86005	Area 10
Ferryland Head	Delta Plain	Current ripple	150	47.04846	52.86005	Area 10
Ferryland Head	Delta Plain	Current ripple	171	47.04845	52.85994	Area 10
Ferryland Head	Delta Plain	Dune	9	47.04845	52.85994	Area 10
Ferryland Head	Delta Plain	Dune	153	47.04851	52.85983	Area 10
Ferryland Head	Delta Plain	Dune	171	47.04851	52.85983	Area 10
Ferryland Head	Delta Plain	Current ripples	177	47.04851	52.85983	Area 10
Ferryland Head	Delta Plain	Current ripples	165	47.04855	52.85966	Area 10
Ferryland Head	Delta Plain	Current ripples	137	47.04855	52.85966	Area 10
Ferryland Head	Delta Plain	Dune	152	47.04855	52.85966	Area 10
Ferryland Head	Delta Plain	Current ripples	137	47.04877	52.85941	Area 10
Ferryland Head	Delta Plain	Current ripples	172	47.04877	52.85941	Area 10
Ferryland Head	Delta Plain	Current ripples	148	47.04877	52.85941	Area 10
Ferryland Head	Delta Plain	Current ripples	140	47.04877	52.85941	Area 10
Ferryland Head	Delta Plain	Current ripples	166	47.04879	52.85913	Area 10
Ferryland Head	Delta Plain	Current ripples	167	47.04903	52.85905	Area 10
Ferryland Head	Delta Plain	Current ripples	142	47.04903	52.85905	Area 10
Ferryland Head	Delta Plain	Dune	111	47.04903	52.85905	Area 10
Ferryland Head	Delta Plain	Current ripples	124	47.04922	52.85895	Area 10
Ferryland Head	Delta Plain	Current ripples	177	47.04922	52.85895	Area 10
Ferryland Head	Delta Plain	Current ripples	173	47.04933	52.85881	Area 10
Ferryland Head	Delta Plain	Current ripples	161	47.04933	52.85881	Area 10
Ferryland Head	Delta Plain	Current ripples	137	47.04933	52.85881	Area 10
Ferryland Head	Delta Plain	Current ripples	177	47.04949	52.85873	Area 10
Ferryland Head	Delta Plain	Current ripples	163	47.04949	52.85873	Area 10
Ferryland Head	Delta Plain	Dune	174	47.04819	52.86268	Area 10

Appendix I: U-Pb zircon data tables

Memorial University of Newfoundland

Gibbett Hill Formation; sample QWH-001; 47.59793°N , 52.67952°W WGS 84

Zircon U-Pb geochronology

				Isotopic ratios								Isotopic ages							
File name	Spot name	Approx. U (ppm)	Approx. Th (ppm)	$^{207}Pb/^{206}Pb$	± 2SE	$^{207}Pb/^{235}U$	± 2SE	$^{206}Pb/^{238}U$	± 2SE	Rho	$^{207}Pb/^{235}U$	± 2SE (Ma)	$^{206}Pb/^{238}U$	± 2SE (Ma)	$^{207}Pb/^{206}Pb$	± 2SE (Ma)	Conc. %	Best Age	± 2SE (Ma)
220223_010.FIN2	851	371	565	0.0611	0.0022	0.87	0.062	0.1039	0.0042	0.46344	632	34	637	25	643	77	99	637	25
220223_011.FIN2	1264	565	440	0.0793	0.0024	2.083	0.14	0.1935	0.0073	0.21735	1140	46	1140	39	1180	60	97	1180	60
220223_012.FIN2	2073	199.2	159.4	0.0613	0.0024	0.803	0.06	0.0948	0.0037	0.32399	596	34	583	22	650	84	90	583	22
220223_015.FIN2	2352	170.3	96.2	0.0606	0.0026	0.836	0.062	0.1004	0.0039	0.06061	613	35	616	23	625	93	99	616	23
220223_017.FIN2	2675	128.3	103.9	0.0615	0.0066	0.88	0.14	0.1064	0.0063	0.03257	643	77	651	37	657	230	99	651	37
220223_028.FIN2	6340 (Core)	404	340	0.0604	0.002	0.798	0.054	0.0968	0.0036	0.15749	593	30	596	21	618	71	96	596	21
220223_029.FIN2	6435	171	116.3	0.0609	0.0026	0.876	0.066	0.1036	0.0039	0.14964	632	35	635	23	636	92	100	635	23
220223_031.FIN2	7047	167	132	0.0612	0.0029	0.854	0.07	0.1006	0.0038	0.15921	620	39	618	22	646	102	96	618	22
220223_032.FIN2	7370	102.8	68.4	0.0603	0.0038	0.857	0.09	0.0992	0.0043	0.10158	613	46	609	25	614	136	99	609	25
220223_034.FIN2	7606	146.6	115.8	0.0627	0.0028	0.894	0.068	0.104	0.004	0.16524	645	37	637	24	698	95	91	637	24
220223_035.FIN2	8049	201	121	0.0655	0.0028	1.188	0.095	0.1315	0.0052	0.30278	781	43	796	30	790	90	101	796	30
220223_037.FIN2	8820	512	441	0.0606	0.0028	0.78	0.06	0.0955	0.004	0.10256	584	34	588	23	625	100	94	588	23
220223_046.FIN2	10075	237.9	203.9	0.0609	0.0024	0.798	0.057	0.0955	0.0035	0.05836	592	32	588	21	636	85	92	588	21
220223_047.FIN2	10098	224.8	211.5	0.0612	0.0024	0.854	0.062	0.102	0.0038	0.21228	622	33	626	22	646	84	97	626	22
220223_048.FIN2	10170	211	222	0.0595	0.0027	0.827	0.066	0.0984	0.0037	0.16456	606	35	605	22	585	98	103	605	22
220223_049.FIN2	10544	112.8	89.5	0.0605	0.0029	0.841	0.07	0.0988	0.0037	0.14304	611	38	607	21	622	103	98	607	21
220223_051.FIN2	10665	726	303	0.0614	0.002	0.96	0.065	0.1117	0.0043	0.46572	682	35	682	25	653	70	104	682	25
220223_053.FIN2	10742	210	193	0.0611	0.0022	0.875	0.063	0.1038	0.0039	0.12386	633	34	636	23	643	77	99	636	23
220223_054.FIN2	10784	191	136	0.0596	0.0025	0.875	0.066	0.1007	0.0037	0.09634	632	36	618	22	589	91	105	618	22
220223_072.FIN2	15395	318	258	0.0606	0.0045	0.838	0.079	0.0969	0.0044	0.08954	614	43	596	26	625	160	95	596	26
220223_073.FIN2	16645	681	306	0.0611	0.0019	0.89	0.061	0.1009	0.0038	0.18202	644	33	619	22	643	67	96	619	22
220223_083.FIN2	18280	146.4	38.87	0.0975	0.0033	3.65	0.28	0.254	0.0095	0.01002	1542	60	1458	49	1577	63	92	1577	63
220223_089.FIN2	20541	473	270	0.0606	0.002	0.787	0.054	0.09119	0.0033	0.23613	586	30	563	19	625	71	90	563	19
220223_093.FIN2	21615	225.5	192.8	0.0606	0.0038	0.76	0.068	0.0915	0.0037	0.14784	569	39	564	22	625	135	90	564	22
220223_100.FIN2	21706	67.5	47.9	0.0603	0.0042	0.887	0.093	0.1006	0.0042	0.01203	623	48	617	24	614	150	100	617	24
220223_104.FIN2	24094	182.7	70	0.0613	0.0035	0.864	0.08	0.1002	0.0042	0.21429	625	44	615	25	650	123	95	615	25
220223_106.FIN2	23427	191	165	0.0595	0.0024	0.839	0.064	0.0976	0.0036	0.2496	615	36	600	21	585	88	103	600	21
220223_111.FIN2	25772	124.6	133	0.0615	0.003	0.917	0.078	0.103	0.0039	0.03995	651	41	632	23	657	105	96	632	23
220223_119.FIN2	28006	211.2	74.1	0.0602	0.0025	0.826	0.06	0.0967	0.0036	0.07097	607	34	595	21	611	90	97	595	21
220223_123.FIN2	30583	149.7	92.1	0.0618	0.0028	0.944	0.073	0.1091	0.0042	0.15065	666	38	667	24	667	97	100	667	24
220223_124.FIN2	30836	264	140	0.0604	0.0025	0.838	0.062	0.1002	0.0039	0.29679	616	35	615	23	618	89	100	615	23
220223_128.FIN2	32536	396	168.4	0.127	0.0037	6.39	0.45	0.3577	0.013	0.22048	2026	62	1970	63	2057	51	96	2057	51
220223_129.FIN2	32985	350	156	0.0594	0.0025	0.784	0.062	0.0947	0.0036	0.05593	584	33	583	21	582	91	100	583	21
220223_140.FIN2	34255	178.6	148	0.0602	0.0031	0.773	0.065	0.0934	0.0036	0.01244	580	39	575	21	611	111	94	575	21
220223_143.FIN2	36020	143	65.1	0.1682	0.0051	11.79	0.99	0.4647	0.017	0.03533	2557	73	2458	77	2540	51	97	2540	51
220223_145.FIN2	36715 (Rim)	214.9	93.2	0.0597	0.0032	0.798	0.069	0.0955	0.0037	0.17169	593	41	588	22	593	116	99	588	22
220223_147.FIN2	38591	323	277	0.061	0.0023	0.796	0.058	0.0958	0.0035	0.08139	590	33	589	21	639	81	92	589	21
220223_148.FIN2	39229	448	259.9	0.0599	0.0025	0.824	0.062	0.0987	0.0037	0.14246	607	35	606	22	600	90	101	606	22
220223_149.FIN2	39511	393	218.5	0.0595	0.0022	0.803	0.056	0.0952	0.0035	0.14462	599	34	586	21	585	80	100	586	21
220223_159.FIN2	40009	662	473	0.0599	0.0024	0.757	0.055	0.0915	0.0033	0.26855	570	33	564	20	600	87	94	564	20
220223_160.FIN2	40319	149.2	172.7	0.0606	0.0036	0.804	0.072	0.096	0.0037	0.12362	595	41	591	22	625	128	95	591	22
220223_161.FIN2	40799	100.6	61.5	0.0602	0.0035	0.874	0.079	0.0952	0.0036	0.02857	623	41	586	21	611	126	96	586	21
220223_169.FIN2	41646	83.3	49.4	0.0602	0.0044	0.786	0.086	0.0934	0.0037	0.16236	574	46	576	22	611	158	94	576	22
220223_170.FIN2	41648	1100	446	0.06097	0.0019	0.776	0.051	0.0944	0.0034	0.27615	582	29	582	20	638	67	91	582	20
220223_173.FIN2	42051	119.2	93.4	0.0616	0.0035	0.815	0.072	0.0965	0.0037	0.07361	593	39	594	22	660	122	90	594	22
220223_175.FIN2	44466	79.9	67.5	0.0599	0.0034	0.845	0.082	0.0988	0.0039	0.00215	609	44	609	24	600	123	102	609	24
220223_177.FIN2	44904	271.9	265.6	0.0597	0.0037	0.722	0.075	0.0901	0.0034	0.09731	554	47	556	20	593	134	94	556	20
220223_178.FIN2	45491	268.6	230.7	0.0615	0.0024	0.797	0.059	0.0961	0.0037	0.20635	592	33	591	22	657	84	90	591	22
220223_180.FIN2	46690	412	370	0.0596	0.0027	0.826	0.067	0.0987	0.004	0.11017	607	37	607	23	589	98	103	607	23
220223_187.FIN2	47181	287	20.3	0.0622	0.004	0.982	0.24	0.1127	0.012	0.0984	689	81	688	64	681	137	101	688	64
220223_192.FIN2	49839	202.9	254	0.0607	0.0029	0.799	0.063	0.0956	0.004	0.23565	589	36	588	23	629	103	94	588	23
220223_193.FIN2	50020	477	414	0.0603	0.0022	0.779	0.055	0.0945	0.0038	0.28998	582	32	582	22	614	79	95	582	22
220223_194.FIN2	50710	78.8	15.3	0.0801	0.0034	2.15	0.26	0.1978	0.0086	0.2669	1165	72	1162	46	1199	84	97	1199	84
220223_195.FIN2	50724	692	188	0.0646	0.0024	0.996	0.069	0.1139	0.0045	0.37527	703	35	695	26	761	78	91	695	26
220223_196.FIN2	51011	179.9	79.9	0.0615	0.0025	0.857	0.061	0.1017	0.0041	0.01566	624	35	624	24	657	87	95	624	24
220223_198.FIN2	52054	513	294	0.0615	0.0021	0.858	0.061	0.1021	0.0039	0.17093	627	35	628	23	657	73	96	628	23
220223_211.FIN2	59388	151	187	0.0605	0.0031	0.774	0.079	0.0902	0.0034	0.20213	577	41	557	20	622	111	90	557	20
220223_224.FIN2	61826	188.4	167	0.0597	0.0025	0.738	0.056	0.0904	0.0033	0.04429	557	32	558	20	593	91	94	558	20
220223_227.FIN2	62910	202	81.6	0.0635	0.0027	0.973	0.077	0.1092	0.0041	0.01425	684	40	668	24	725	90	92	668	24
220223_228.FIN2	63111	687.8	305.7	0.0607	0.0021	0.777	0.054	0.0945	0.0034	0.14361	582	31	582	20	629	75	93	582	20
220223_230.FIN2	63435	255.7	181	0.061	0.0028	0.793	0.066	0.0945	0.0035	0.13468	586	38	582	20	639	99	91	582	20
220223_234.FIN2	63793 (Rim)	52.2	35.6	0.0628	0.0043	1.09	0.13	0.1085	0.0048	0.10712	711	60	663	28	701	146	95	663	28
220224_010.FIN2	65177	250.9	256	0.0597	0.002	0.726	0.058	0.0901	0.0049	0.21303	554	35	556	29	593	73	94	556	29
220224_014.FIN2	66248	268	136	0.0607	0.002	0.813	0.064	0.0981	0.0053	0.32313	604	35	603	31	629	71	96	603	31
220224_019.FIN2	67793 (Core)	170	180	0.0596	0.0029	0.727	0.072	0.0892	0.0058	0.28256	551	39	550	34	589	106	93	550	34
220224_030.FIN2	73951	125.7	90.4	0.0599	0.0028	0.804	0.07	0.0965	0.0057	0.35056	593	40	593	33	600	101	99	593	33
220224_032.FIN2	74199	168.2	211.2	0.0608	0.0026	0.862	0.074	0.1018	0.0057	0.35718	627	40	625	33	632	92	99	625	33
220224_033.FIN2	74598	49.2	39.8	0.0595	0.0038	0.771	0.075	0.0933	0.0054	0.12422	577	42	575	32	585	139	98	575	32
220224_036.FIN2	74931	40.8	33.9	0.061	0.0038	0.901	0.086	0.1045	0.006	0.18752	642	47	640	35	639	134	100	640	35
220224_047.FIN2	76841	298	172	0.0616	0.0028	0.913	0.078	0.1063	0.0061	0.26821	653	39	651	35	660	97	99	651	35
220224_049.FIN2	77770	74.3	54.8	0.0612	0.0033	0.808	0.071	0.0949	0.0052	0.15871	597	41	584	31	646	116	90	584	31
220224_050.FIN2	79149	124.6	99.1	0.0584	0.0031	0.742	0.13	0.0913	0.0069	0.23951	561	44	563	39	545	116	103	563	39
220224_053.FIN2	80956	405.6	407	0.0606	0.014	0.828	0.33	0.0985	0.0063	0.08101	611	91	605	36	625	498	97	605	36
220224_054.FIN2	81800	213	148.9	0.0604	0.0024	0.831	0.069	0.0979	0.0053	0.30826	610	38	602	31	618	86	97	602	31
220224_055.FIN2	82418	292	288	0.0605	0.0021	0.804	0.065	0.0943	0.0051	0.22477	597	36	581	30	622	75	93	581	30
220224_063.FIN2	84581	300.2	249	0.0617	0.0021	0.842	0.067	0.0972	0.0052	0.22792	619	38	598	31	664	73	90	598	31
220224_065.FIN2	84974	37	27.4	0.0639	0.0042	1.047	0.1	0.1176	0.0068	0.12555	715	53	716	39	738	139	97	716	39
220224_068.FIN2	85832	190.3	129.6	0.0608	0.0024	0.782	0.066	0.0922	0.0051	0.19613	585	38	568	30	632	85	90	568	30
220224_070.FIN2	86018	173.2	118.3	0.0596	0.0024	0.843	0.07	0.1007	0.0055	0.34839	619	37	619	32	589	87	105	619	32
220224_071.FIN2	86025	168	149	0.0601	0.0024	0.809	0.068	0.0967	0.0054	0.30625	597	38	595	31	607	86	98	595	31
220224_073.FIN2	86104	160	190.1	0.0615	0.0025	0.824	0.068	0.0962	0.0052	0.1894	608	39	592	31	657	87	90	592	31
220224_080.FIN2	84983	173	86.5	0.0585	0.0025	0.753	0.063	0.0911	0.0048	0.24528	564	37	562	29	549	93	102	562	29
220224_085.FIN2	87114	428	124.9	0.0658	0.0019	1.088	0.084	0.1176	0.0063	0.34203	746	41	717	36	800	61	90	717	36
220224_090.FIN2	89951	305	166	0.0607	0.0056	0.794	0.17	0.0935	0.006	0.55012	590	47	576	35	629	199	92	576	35
220224_091.FIN2	91878	132.9	88.4	0.06	0.0026	0.801	0.072	0.0954	0.0057	0.31944	591	40	587	34	604	94	97	587	34
220224_099.FIN2	95010	621	501	0.0614	0.0017	0.848	0.065	0.09885	0.0053	0.50292	622	36	608	31	653	59	93	608	31
220224_100.FIN2	95123	435	277	0.0601	0.0018	0.85	0.067	0.10071	0.0054	0.41478	624	37	619	32	607	65	102	619	32
220224_102.FIN2	95572	350	295	0.0627	0.0021	0.92	0.073	0.1049	0.0057	0.16757	660	39	643	33	698	71	92	643	33
220224_103.FIN2	96008	166.2	153.4	0.0611	0.0031	0.867	0.086	0.1022	0.0062	0.21927	629	44	627	36	643	109	98	627	36
220224_104.FIN2	96075	204.7	184.8	0.0594	0.0029	0.781	0.068	0.0946	0.0051	0.16118	582	39	583	30	582	106	100	583	30
220224_105.FIN2	96221	123.3	82.4	0.0599	0.0031	0.763	0.068	0.0915	0.005	0.22897	568	40	564	29	600	112	94	564	29
220224_106.FIN2	96590	277	145.4	0.0619	0.0024	0.86	0.07	0.0995	0.0054	0.19954	627	38	612	32	671	83	91	612	32
220224_108.FIN2	97185	316	202	0.0607	0.0026	0.815	0.081	0.0971	0.0057	0.43071	602	41	598	33	629	92	95	598	33
220224_109.FIN2	97354	190.2	186.3	0.0614	0.0022	0.917	0.075	0.1064	0.0059	0.50131	658	41	652	34	653	77	100	652	34
220224_117.FIN2	98112	302.8	169.5	0.0607	0.0022	0.883	0.075	0.1042	0.006	0.47032	640	40	641	35	629	78	102	641	35
220224_120.FIN2	99897	218	102.9	0.0615	0.0025	0.893	0.07	0.1052	0.0055	0.22359	644	39	645	32	657	87	98	645	32
Rejected analyses																			
220223_008.FIN2	1422	173.7	182.8	0.0577	0.0023	0.774	0.057	0.0945	0.0036	0.25429	580	33	582	21	518	88	112	582	21
220223_009.FIN2	679	60.9	50.1	0.0616	0.0033	0.81	0.071	0.0957	0.0038	0.15145	590	39	589	22	660	115	89	589	22
220223_013.FIN2	2323 (Core)	191	48.1	0.1079	0.0051	3.06	0.43	0.203	0.015	0.69655	1410	85	1188	77	1764	86	67	1764	86
220223_014.FIN2	2323 (Rim)	103.7	83	0.1555	0.0049	6.93	0.54	0.3168	0.013	0.23405	2072	67	1771	62	2407	54	74	2407	54
220223_016.FIN2	2603	133.8	146.1	0.0653	0.003	0.765	0.061	0.0878	0.0037	0.13223	569	35	542	22	784	97	69	542	22
220223_018.FIN2	3115	94.8	94.5	0.0686	0.0029	1.246	0.098	0.1267	0.0048	0.04249	810	45	769	28	887	87	87	769	28

Appendix I: U-Pb zircon data tables (continued)

220223_019.FIN2	3463	269	211	0.0573	0.0032	0.579	0.052	0.0683	0.0031	0.13688	462	33	426	19	503	123	85	426	19
220223_026.FIN2	6127	75.1	73	0.058	0.0032	0.788	0.071	0.0938	0.0036	0.18704	575	39	578	21	530	121	109	578	21
220223_027.FIN2	6340 (Rim)	185.5	115.5	0.0596	0.0022	0.865	0.061	0.1045	0.0038	0.01069	632	35	640	22	589	80	109	640	22
220223_030.FIN2	6675	438	238	0.0626	0.0022	0.776	0.054	0.0917	0.0035	0.28553	580	31	566	21	695	75	81	566	21
220223_033.FIN2	7519	376	364	0.0631	0.0023	0.843	0.06	0.0989	0.0039	0.12859	618	33	608	23	712	77	85	608	23
220223_036.FIN2	8355	401	95	0.0888	0.0034	2.013	0.16	0.1643	0.0081	0.46995	1108	54	984	43	1400	73	70	1400	73
220223_045.FIN2	9273	373	336	0.0647	0.0028	0.935	0.07	0.107	0.004	0.0128	667	36	655	24	765	91	86	655	24
220223_050.FIN2	10589	159.1	136.6	0.067	0.0027	0.956	0.073	0.1012	0.0038	0.06622	674	37	621	22	838	84	74	621	22
220223_052.FIN2	10698	218	131.1	0.0652	0.0033	0.815	0.065	0.0905	0.0035	0.03327	602	36	559	21	781	106	72	559	21
220223_056.FIN2	11319	57.2	36	0.0626	0.0047	0.897	0.1	0.0922	0.0038	0.02177	620	51	568	23	695	160	82	568	23
220223_063.FIN2	11999	150	164	0.266	0.025	4.18	0.56	0.1101	0.0057	0.6887	1650	130	673	33	3283	148	21	3283	148
220223_064.FIN2	12266	784	333	0.0648	0.0029	0.887	0.069	0.0944	0.0044	0.36769	641	37	581	26	768	94	76	581	26
220223_065.FIN2	12693	193.8	89.7	0.0583	0.0022	0.847	0.064	0.0996	0.0037	0.0913	615	34	612	21	541	83	113	612	21
220223_066.FIN2	13145	424.5	764	0.0621	0.0021	0.806	0.056	0.0894	0.0033	0.11794	600	33	552	20	678	72	81	552	20
220223_067.FIN2	13336	218	310	0.061	0.0029	0.731	0.058	0.081	0.0031	0.3413	552	34	502	19	639	102	79	502	19
220223_068.FIN2	13842	198	141	0.0616	0.0038	0.781	0.07	0.0921	0.0039	0.04884	586	42	568	23	660	132	86	568	23
220223_069.FIN2	13973	155.5	79.2	0.0664	0.0027	1.139	0.085	0.1146	0.0043	0.01987	766	41	699	25	819	85	85	699	25
220223_070.FIN2	14119	64.4	63.2	0.0614	0.0044	0.836	0.087	0.0904	0.004	0.17736	600	47	558	23	653	154	85	558	23
220223_071.FIN2	15344	2060	1480	0.06045	0.0018	0.5849	0.038	0.06723	0.0025	0.32446	468	26	419	15	620	64	68	419	15
220223_074.FIN2	17496	121.9	202	0.0724	0.0044	1.008	0.099	0.0895	0.0036	0.06805	697	50	552	21	997	123	55	552	21
220223_081.FIN2	17557	58.4	51.8	0.0632	0.0037	0.965	0.097	0.0963	0.0037	0.2956	670	48	592	22	715	124	83	592	22
220223_082.FIN2	17718	87.2	60.7	0.064	0.0053	0.98	0.12	0.0937	0.0044	0.15726	661	59	577	26	742	175	78	577	26
220223_084.FIN2	18434	603	342	0.0619	0.0021	0.832	0.057	0.0933	0.0034	0.12184	615	33	575	20	671	73	86	575	20
220223_085.FIN2	19587 (Core)	209	177	0.0657	0.0025	1.076	0.076	0.1132	0.0043	0.23136	737	38	691	25	797	80	87	691	25
220223_086.FIN2	19587 (Rim)	162	169	0.0657	0.0027	1.095	0.085	0.1121	0.0043	0.02644	740	40	685	25	797	86	86	685	25
220223_087.FIN2	19774	669	87.8	0.0619	0.0021	0.771	0.053	0.08769	0.0032	0.2192	577	30	542	19	671	73	81	542	19
220223_088.FIN2	20423	436	38.8	0.0648	0.0024	1.035	0.077	0.1083	0.0039	0.01567	720	40	663	23	768	78	86	663	23
220223_090.FIN2	20917	94.5	60.2	0.0584	0.0037	0.821	0.084	0.099	0.004	0.07053	607	51	608	23	545	138	112	608	23
220223_091.FIN2	20956	574	960	0.0628	0.0022	0.825	0.059	0.0919	0.0034	0.30994	607	32	567	20	701	75	81	567	20
220223_092.FIN2	21231	105.2	63.3	0.0578	0.0032	0.845	0.078	0.0931	0.0035	0.1458	608	41	574	20	522	121	110	574	20
220223_101.FIN2	22249	119	79.6	0.061	0.0044	0.772	0.081	0.0888	0.0037	0.15756	578	50	548	22	639	155	86	548	22
220223_102.FIN2	22453	197.8	185.3	0.0602	0.0033	0.761	0.072	0.084	0.0033	0.1423	566	40	520	19	611	118	85	520	19
220223_105.FIN2	23251	75.2	44.5	0.0689	0.0052	0.98	0.11	0.0957	0.0041	0.25582	672	53	589	24	896	156	66	589	24
220223_107.FIN2	24962	93.6	109.7	0.0636	0.004	0.868	0.083	0.0883	0.0034	0.08256	625	46	545	20	728	133	75	545	20
220223_108.FIN2	25297	92.1	86.2	0.058	0.0038	0.797	0.079	0.0949	0.0037	0.06285	585	44	584	22	530	144	110	584	22
220223_109.FIN2	25402	666	501	0.0671	0.0027	1.16	0.084	0.1232	0.0048	0.29343	784	42	749	28	841	84	89	749	28
220223_110.FIN2	25488	127.7	93.1	0.0577	0.003	0.821	0.074	0.0951	0.0036	0.07315	598	41	586	21	518	114	113	586	21
220223_118.FIN2	27369	90.3	76.1	0.0587	0.0047	0.848	0.096	0.0991	0.0041	0.19098	613	54	609	24	556	175	110	609	24
220223_120.FIN2	28740	672	41.1	0.119	0.0036	5.25	0.37	0.3082	0.013	0.52885	1867	63	1730	63	1941	54	89	1941	54
220223_121.FIN2	29298	112.4	81	0.15	0.016	2.09	0.31	0.0917	0.0041	0.46302	1071	99	565	24	2346	182	24	2346	182
220223_122.FIN2	29860	106	97.6	0.0691	0.0039	1.016	0.095	0.0968	0.0039	0.07487	684	42	595	23	902	116	66	595	23
220223_125.FIN2	31465	804	648	0.0683	0.0024	0.878	0.062	0.0922	0.0034	0.30716	640	34	568	20	878	73	65	568	20
220223_126.FIN2	31954 (Core)	196	150.9	0.0631	0.0034	0.788	0.065	0.0881	0.0035	0.23613	582	38	544	20	712	115	76	544	20
220223_127.FIN2	31954 (Rim)	352	273	0.0606	0.0024	0.769	0.058	0.0896	0.0034	0.05296	577	34	553	20	625	85	88	553	20
220223_130.FIN2	33125	97.3	66.6	0.062	0.0041	0.764	0.069	0.0871	0.0036	0.00401	569	40	538	21	674	141	80	538	21
220223_137.FIN2	33569	218.9	185.8	0.0627	0.0026	0.844	0.064	0.0933	0.0035	0.02423	617	35	575	21	698	88	82	575	21
220223_138.FIN2	33739	579	437	0.0631	0.0027	0.752	0.056	0.0869	0.0034	0.29505	567	33	537	20	712	91	75	537	20
220223_139.FIN2	34111	639	412	0.129	0.0037	5.87	0.39	0.3281	0.012	0.28295	1951	57	1828	60	2084	50	88	2084	50
220223_141.FIN2	35408	141.1	109.7	0.0626	0.0029	1.138	0.09	0.1279	0.0053	0.10489	759	43	777	31	695	99	112	777	31
220223_142.FIN2	35582	168	150	0.0618	0.0041	0.802	0.073	0.0914	0.004	0.21145	591	41	564	23	667	142	85	564	23
220223_144.FIN2	36715 (Core)	154.3	109.6	0.0589	0.0033	0.901	0.082	0.105	0.0041	0.05723	644	43	643	24	563	122	114	643	24
220223_146.FIN2	37170	55.8	33.6	0.0588	0.0057	0.88	0.13	0.0962	0.0043	0.07952	608	67	592	26	560	211	106	592	26
220223_156.FIN2	39548	217.9	131.6	0.0691	0.0032	1.068	0.087	0.1118	0.0043	0.20089	731	43	683	25	902	95	76	683	25
220223_157.FIN2	39792	290.8	246.3	0.0627	0.0032	0.869	0.078	0.0982	0.0037	0.14026	628	42	604	22	698	109	87	604	22
220223_158.FIN2	39900	57.3	39.6	0.0628	0.0048	0.91	0.13	0.1022	0.0042	0.0348	628	62	627	25	701	163	89	627	25
220223_162.FIN2	41328	180	208	0.0591	0.0028	0.849	0.072	0.1007	0.0039	0.10818	619	40	618	23	571	103	108	618	23
220223_171.FIN2	41785	145.9	105	0.062	0.0037	0.801	0.076	0.087	0.0033	0.05844	593	43	538	19	674	128	80	538	19
220223_172.FIN2	41884	205	174	0.0621	0.0041	0.765	0.072	0.0918	0.0036	0.11802	570	43	566	21	678	141	84	566	21
220223_174.FIN2	43651	3150	2420	0.0661	0.0021	0.754	0.05	0.08337	0.003	0.39394	570	29	516	18	810	66	64	516	18
220223_176.FIN2	44659	454.8	259	0.068	0.0028	0.927	0.072	0.0981	0.0038	0.45328	663	38	603	22	869	85	69	603	22
220223_179.FIN2	46352	108	102	0.072	0.0094	1.6	1.3	0.0925	0.0056	0.44624	648	65	570	33	986	266	58	570	33
220223_188.FIN2	47566	146.9	122.8	0.0629	0.0029	0.913	0.073	0.1027	0.0041	0.05269	652	38	630	24	705	98	89	630	24
220223_189.FIN2	48281	239	247	0.0606	0.0032	0.749	0.063	0.0904	0.0037	0.09146	562	35	558	22	625	114	89	558	22
220223_190.FIN2	49278	65.9	87	0.0848	0.017	1.25	0.49	0.0959	0.0052	0.39431	817	110	590	30	1311	389	45	590	30
220223_191.FIN2	49823	288	211	0.098	0.0036	1.417	0.1	0.1032	0.0041	0.32996	888	42	633	24	1586	69	40	1586	69
220223_197.FIN2	51734	70.9	105.8	0.0715	0.0051	0.949	0.1	0.0916	0.0037	0.10223	650	51	565	22	972	145	58	565	22
220223_205.FIN2	52323	803	96.3	0.0609	0.0043	0.758	0.086	0.0919	0.0035	0.17806	570	43	567	21	636	152	89	567	21
220223_206.FIN2	52471	114.1	47.3	0.0801	0.0041	0.938	0.079	0.0826	0.0038	0.07728	651	42	511	23	1199	101	43	511	23
220223_207.FIN2	54088	141.1	111	0.0587	0.0028	0.806	0.07	0.097	0.0037	0.17454	592	39	597	22	556	104	107	597	22
220223_208.FIN2	57545	507	194.2	0.0626	0.0066	0.872	0.1	0.099	0.0036	0.06757	633	45	609	21	695	225	88	609	21
220223_209.FIN2	57957	197	125	0.0882	0.0038	1.236	0.096	0.1038	0.0039	0.15077	804	44	636	23	1387	83	46	1387	83
220223_210.FIN2	59233	117	119.9	0.0627	0.0044	0.856	0.085	0.0904	0.0047	0.25022	609	46	558	28	698	149	80	558	28
220223_212.FIN2	59887	339	443	0.0648	0.0025	0.842	0.059	0.0945	0.0035	0.08949	616	34	582	20	768	81	76	582	20
220223_213.FIN2	60409	310	253	0.0626	0.005	0.826	0.089	0.0942	0.0049	0.12002	606	48	580	28	695	170	83	580	28
220223_214.FIN2	60456	475	287	0.0665	0.0024	1	0.069	0.1087	0.004	0.15545	699	35	665	23	822	75	81	665	23
220223_215.FIN2	60699	569	264	0.0623	0.0027	0.809	0.46	0.0943	0.013	0.0006	599	40	581	62	684	93	85	581	62
220223_216.FIN2	61029	307	206	0.0619	0.0053	0.746	8.04	0.0865	0.0093	0.01036	561	28	535	51	671	183	80	535	51
220223_223.FIN2	61489	773	875	0.0632	0.0027	0.858	1.28	0.1017	0.011	0.25752	631	21	624	45	715	91	87	624	45
220223_225.FIN2	62073	47.4	40.1	0.1128	0.0086	1.71	0.21	0.0984	0.0041	0.27872	950	76	605	24	1845	138	33	1845	138
220223_226.FIN2	62388	326	182	0.0707	0.012	0.945	0.22	0.096	0.0045	0.01724	667	72	591	26	949	347	62	591	26
220223_229.FIN2	63335	347	172	0.0669	0.063	0.813	460	0.0877	0.093	0.2398	605	310	542	410	835	1962	65	542	410
220223_231.FIN2	63455	85.6	91	0.083	0.0053	1.1	0.11	0.0846	0.0034	0.43081	709	48	523	20	1269	125	41	523	20
220223_232.FIN2	63497	370	322	0.0615	0.0023	0.742	0.053	0.0874	0.0033	0.15461	560	31	540	19	657	80	82	540	19
220223_235.FIN2	63856	56.1	52	0.0586	0.0041	0.88	0.084	0.0999	0.0039	0.06149	615	48	613	23	552	153	111	613	23
220224_007.FIN2	63856	225	108.6	0.0618	0.0021	0.804	0.064	0.09679	0.0052	0.32797	596	36	596	31	667	73	89	596	31
220224_008.FIN2	63885	142.3	126.7	0.0617	0.024	0.732	0.38	0.0887	0.006	0.614	553	110	548	35	664	833	83	548	35
220224_009.FIN2	64326	92.8	101	0.061	0.003	0.754	0.064	0.0917	0.0048	0.17446	565	37	565	29	639	106	88	565	29
220224_011.FIN2	65438	940	561	0.0618	0.002	0.756	0.061	0.0892	0.0048	0.57387	571	35	551	28	667	69	83	551	28
220224_012.FIN2	65778	111.2	65.2	0.0709	0.0096	0.84	0.14	0.0868	0.0059	0.21236	613	64	537	35	955	277	56	537	35
220224_013.FIN2	66122	1900	1450	0.1103	0.0099	1.284	0.58	0.0846	0.024	0.48092	833	99	523	100	1804	163	29	1804	163
220224_015.FIN2	66296	748	272.8	0.0654	0.059	0.918	71	0.1031	0.66	0.45112	660	430	633	900	787	1894	80	633	900
220224_016.FIN2	66418	243	163	0.0639	0.0034	0.847	0.089	0.0958	0.0059	0.18898	620	48	590	34	738	113	80	590	34
220224_018.FIN2	66419	66.1	43.1	0.0614	0.0033	0.792	0.071	0.0943	0.0053	0.14289	585	41	580	31	653	115	89	580	31
220224_020.FIN2	67793 (Rim)	44.8	35.1	0.0647	0.0043	0.837	0.086	0.0946	0.0061	0.10917	605	46	582	36	765	140	76	582	36
220224_027.FIN2	68264	318	460	0.0698	0.0032	0.795	0.07	0.0822	0.0046	0.46824	594	37	509	27	922	94	55	509	27
220224_028.FIN2	69109	117.9	67.4	0.0669	0.0032	0.759	0.065	0.082	0.0049	0.18089	566	37	508	29	835	100	61	508	29
220224_029.FIN2	73387	114.5	121	0.0637	0.0031	0.805	0.072	0.0904	0.0052	0.39325	593	40	558	31	732	103	76	558	31
220224_031.FIN2	74009	162	130.9	0.0714	0.0047	0.925	0.094	0.0937	0.0054	0.44547	659	49	577	32	969	134	60	577	32
220224_034.FIN2	74781	1194	4470	0.2993	0.014	1.783	0.14	0.0443	0.0033	0.78425	1036	58	279	20	3467	72	8	3467	72
220224_035.FIN2	74854	327	10.8	0.0779	0.0059	1.51	0.92	0.1415	0.043	0.70155	944	140	852	190	1144	151	74	852	190
220224_037.FIN2	75470	172.2	151.8	0.0749	0.0092	0.936	0.17	0.0888	0.0054	0.39796	665	60	548	32	1066	247	51	548	32
220224_038.FIN2	75517	92.1	75.1	0.065	0.0039	0.775	0.073	0.0863	0.0049	0.28082	579	40	533	29	774	126	69	533	29
220224_046.FIN2	76470	207.1	140.9	0.0915	0.0037	1.256	0.11	0.0981	0.0055	0.3995	820	47	603	32	1457	77	41	1457	77
220224_048.FIN2	77075	990	1050	0.0659	0.0018	0.985	0.077	0.106	0.006	0.70977	696	39	649	34	803	57	81	649	34
220224_051.FIN2	80260	235.6	127.8	0.0777	0.011	1.001	0.23	0.0915	0.0056	0.16815	700	76	564	33	1139	282	50	564	33
220224_052.FIN2	80524	362.8	146.7	0.0658	0.0025	0.819	0.073	0.0886	0.005	0.38678	605	39	547	30	800	80	68	547	30
220224_056.FIN2	84457	269.8	90.7	0.0606	0.0021	0.922	0.072	0.1079	0.0056	0.29784	661	40	660	33	625	75	106	660	33
220224_064.FIN2	84719	193.2	152.2	0.0744	0.014	0.925	0.28	0.0885	0.0055	0.23012	661	88	546	32	1052	379	52	546	32
220224_066.FIN2	85149	406	282	0.0673	0.0032	0.889	0.081	0.09374	0.0052	0.18254	642	39	578	30	847	99	68	578	30
220224_067.FIN2	85360	174.3	113.1	0.0624	0.0037	0.793	0.18	0.0907	0.014	0.21778	589	67	560	79	688	127	81	560	79
220224_069.FIN2	85844	50.7	33.8	0.0938	0.023	1.052	0.37	0.0799	0.0053	0.28004	711	100	495	31	1504	463	33	495	31
220224_072.FIN2	86099	93.3	45.3	0.0618	0.0037	0.788	0.073	0.0917	0.0052	0.40859	581	41	566	31	667	128	85	566	31

Appendix I: U-Pb zircon data tables (continued)

220224_081.FIN2	86301	264	172.8	0.0686	0.04	0.88	4.5	0.092	0.046	0.18675	636	260	567	220	887	1205	64	567	220
220224_082.FIN2	86436	299.8	283.8	0.0647	0.0024	0.959	0.087	0.106	0.0065	0.38793	680	44	650	37	765	78	85	650	37
220224_083.FIN2	86766	101.6	64.3	0.0615	0.0026	0.792	0.068	0.0914	0.0051	0.22837	587	38	563	30	657	91	86	563	30
220224_084.FIN2	86827	160.3	137.3	0.061	0.0027	0.79	0.069	0.0925	0.0052	0.14026	587	38	570	30	639	95	89	570	30
220224_086.FIN2	87362	147.6	135.6	0.0631	0.0032	0.825	0.078	0.0943	0.0052	0.15048	607	41	581	31	712	108	82	581	31
220224_087.FIN2	87747	252	322	0.0637	0.0043	0.883	0.1	0.0992	0.0057	0.27745	640	48	609	33	732	143	83	609	33
220224_088.FIN2	87871	142	121	0.0681	0.058	0.821	4.41	0.0873	0.039	0.40586	600	310	539	190	872	1764	62	539	190
220224_089.FIN2	88836	177.8	56.1	0.0857	0.0026	2.452	0.2	0.2025	0.011	0.29426	1255	55	1189	63	1331	59	89	1331	59
220224_092.FIN2	94086	294	302	0.0715	0.0062	1.034	0.13	0.1033	0.0057	0.095	711	51	634	33	972	177	65	634	33
220224_101.FIN2	95220	85.1	53.7	0.0645	0.0038	0.745	0.071	0.0809	0.0047	0.15731	556	42	501	28	758	124	66	501	28
220224_107.FIN2	96718	113.9	71.5	0.0782	0.0043	1.022	0.093	0.094	0.0052	0.20115	708	48	579	31	1152	109	50	579	31
220224_110.FIN2	97449	21.7	19.9	0.0596	0.0056	0.856	0.1	0.1032	0.0067	0.22718	600	57	632	39	589	204	107	632	39
220224_118.FIN2	98781	50	55.3	0.0577	0.0038	0.793	0.079	0.1004	0.0059	0.22102	581	44	616	35	518	145	119	616	35
220224_119.FIN2	98861	48.1	31.9	0.0771	0.012	1.15	7.7	0.1061	0.11	0.38564	753	91	649	130	1124	310	58	649	130
220224_121.FIN2	100949	70.3	42.8	0.0865	0.01	1.108	0.16	0.0907	0.0055	0.04227	735	63	562	32	1349	223	42	562	32

Memorial University of Newfoundland

Quidi Vidi Formation; samples QWH-007 and QWH-007B; 47.59975°N , 52.67559°W WGS 84

Zircon U-Pb geochronology

				Isotopic ratios							Isotopic ages								
File name	Spot name	Approx. U (ppm)	Approx. Th (ppm)	$^{207}Pb/^{206}Pb$	± 2SE	$^{207}Pb/^{235}U$	± 2SE	$^{206}Pb/^{238}U$	± 2SE	Rho	$^{207}Pb/^{235}U$	± 2SE (Ma)	$^{206}Pb/^{238}U$	± 2SE (Ma)	$^{207}Pb/^{206}Pb$	± 2SE (Ma)	Conc. %	Best Age	± 2SE (Ma)
220224_134.FIN2	1390 (Rim)	376	215.5	0.0609	0.0023	0.821	0.074	0.0989	0.0058	0.29775	606	38	608	34	636	81	96	608	34
220224_135.FIN2	1390 (Core)	171	87.9	0.0602	0.0093	0.824	0.16	0.1011	0.0056	0.26044	605	65	621	33	611	334	102	621	33
220224_137.FIN2	4367	101.3	62	0.0597	0.0031	0.8	0.071	0.0982	0.0054	0.27581	588	40	604	32	593	113	102	604	32
220224_138.FIN2	5034	149.1	196.1	0.1194	0.0034	5.81	0.48	0.3604	0.021	0.63539	1942	69	1983	96	1947	51	102	1947	51
220224_144.FIN2	8790	222	108.6	0.0601	0.0024	0.801	0.067	0.0993	0.0056	0.28421	593	37	610	33	607	86	100	610	33
220224_145.FIN2	12880	28.9	29.2	0.0611	0.006	0.842	0.1	0.1023	0.0061	0.14215	595	56	627	37	643	211	98	627	37
220224_146.FIN2	14544	203.4	221	0.0638	0.0025	0.96	0.081	0.1123	0.0062	0.36749	681	41	686	36	735	83	93	686	36
220224_155.FIN2	20203	82.8	58.4	0.0619	0.0032	0.884	0.078	0.107	0.0061	0.26853	634	42	655	36	671	111	98	655	36
220224_158.FIN2	26504 (Core)	278.1	178.9	0.0606	0.0022	0.819	0.067	0.1014	0.0056	0.13408	607	38	622	32	625	78	100	622	32
220224_161.FIN2	27334	102.5	66.5	0.0599	0.0043	0.821	0.094	0.1028	0.0062	0.04574	599	49	631	36	600	155	105	631	36
220224_164.FIN2	29307	132.3	96.6	0.0604	0.0025	0.842	0.07	0.1051	0.0058	0.34338	619	39	644	34	618	89	104	644	34
220224_176.FIN2	37085	223	134.1	0.0598	0.0023	0.799	0.065	0.0999	0.0054	0.32285	594	37	614	31	596	83	103	614	31
220224_177.FIN2	37886	110.9	106.8	0.06	0.0031	0.769	0.069	0.0947	0.0052	0.27799	572	39	583	31	604	112	97	583	31
220224_182.FIN2	51603	289	166.1	0.0602	0.0023	0.793	0.064	0.0985	0.0054	0.21975	591	37	606	31	611	83	99	606	31
220224_192.FIN2	58817 (Core)	338	37.4	0.0923	0.0025	3.159	0.24	0.2521	0.014	0.49544	1446	61	1449	70	1474	51	98	1474	51
220224_193.FIN2	58817 (Rim)	142.8	65.9	0.0911	0.0029	3.035	0.25	0.2442	0.014	0.41386	1411	62	1408	71	1449	61	97	1449	61
220224_194.FIN2	61580	383	231.4	0.0613	0.0021	0.838	0.069	0.0995	0.0057	0.51814	614	39	611	33	650	74	94	611	33
220224_195.FIN2	65420	87.3	87.6	0.0631	0.034	0.9	0.78	0.1042	0.0091	0.34374	645	180	638	52	712	1145	90	638	52
220224_197.FIN2	66896	166	116.1	0.0618	0.0029	0.872	0.074	0.1036	0.0057	0.00766	633	40	636	33	667	100	95	636	33
220224_199.FIN2	70274	291	288	0.061	0.0022	0.819	0.066	0.0982	0.0053	0.17792	605	37	603	31	639	78	94	603	31
220224_205.FIN2	68169	550	279	0.0603	0.002	0.841	0.068	0.1005	0.0055	0.385	617	37	617	32	614	72	100	617	32
220228_007.FIN2	7302	94.1	49.9	0.0635	0.0031	0.964	0.084	0.1115	0.0089	0.26705	677	43	681	52	725	104	94	681	52
220228_009.FIN2	11999	98.8	80	0.0605	0.0031	0.741	0.066	0.0903	0.0072	0.20991	558	38	557	43	622	111	90	557	43
220228_010.FIN2	13749	119.9	48.03	0.0596	0.003	0.736	0.064	0.0908	0.0072	0.19824	556	38	560	43	589	109	95	560	43
220228_014.FIN2	22138	440	181.9	0.06	0.0022	0.753	0.061	0.09208	0.0073	0.31044	568	36	568	43	604	79	94	568	43
220228_015.FIN2	22368	257.3	166.3	0.0601	0.0027	0.747	0.063	0.0922	0.0073	0.22083	566	38	568	43	607	97	94	568	43
220228_016.FIN2	26712	441	371	0.0608	0.0024	0.771	0.065	0.0945	0.0075	0.51695	582	37	582	44	632	85	92	582	44
220228_017.FIN2	28585	339	305	0.0612	0.0024	0.855	0.071	0.1028	0.0082	0.37346	627	39	631	48	646	84	98	631	48
220228_019.FIN2	29778	92.4	44.1	0.0589	0.0029	0.746	0.066	0.0935	0.0075	0.26655	561	38	576	44	563	107	102	576	44
220228_028.FIN2	36521	200	117.9	0.0607	0.0025	0.836	0.07	0.1005	0.008	0.22045	613	38	617	47	629	89	98	617	47
220228_029.FIN2	37549	183.1	122.6	0.06	0.0025	0.84	0.07	0.1022	0.0081	0.2717	618	40	627	47	604	90	104	627	47
220228_030.FIN2	38928	175.1	106.2	0.0628	0.0029	0.94	0.081	0.1108	0.0088	0.33149	671	41	677	51	701	98	97	677	51
220228_034.FIN2	44183	104.8	81.1	0.0609	0.0029	0.836	0.074	0.1004	0.0081	0.48674	616	44	616	48	636	102	97	616	48
220228_035.FIN2	52579	150	140.2	0.0594	0.0026	0.736	0.063	0.0908	0.0072	0.24123	557	36	560	43	582	95	96	560	43
220228_036.FIN2	52854	618	275	0.0601	0.0023	0.743	0.061	0.0915	0.0073	0.37018	565	37	564	43	607	83	93	564	43
220228_038.FIN2	61602	437	196.6	0.0602	0.0024	0.791	0.066	0.0965	0.0077	0.54607	589	37	594	45	611	86	97	594	45
Rejected analyses																			
220224_136.FIN2	4215	107.8	109.8	0.0634	0.0035	0.796	0.068	0.0937	0.005	0.09827	586	40	577	30	722	117	80	577	30
220224_140.FIN2	5693	174	77.4	0.0882	0.017	1.122	0.37	0.0932	0.0075	0.18644	750	110	574	43	1387	370	41	574	43
220224_141.FIN2	5869	164	127	0.0675	0.0046	0.823	0.077	0.0916	0.0052	0.27858	597	39	565	31	853	142	66	565	31
220224_142.FIN2	7091	364	224	0.0604	0.0022	0.731	0.071	0.0896	0.0058	0.29435	558	38	553	34	618	79	89	553	34
220224_143.FIN2	8418	109.1	66.4	0.0893	0.0064	1.38	0.15	0.1121	0.0063	0.41768	849	62	686	37	1411	137	49	1411	137
220224_147.FIN2	17333	165.4	172.3	0.0614	0.0056	0.784	0.11	0.0947	0.0055	0.32031	583	48	583	32	653	196	89	583	32
220224_156.FIN2	26157	191	159.8	0.0638	0.007	0.818	0.12	0.0964	0.0055	0.00951	600	53	593	32	735	232	81	593	32
220224_159.FIN2	26504 (Rim)	238	139.7	0.063	0.0025	0.853	0.069	0.1016	0.0055	0.26434	623	38	624	32	708	84	88	624	32
220224_160.FIN2	26955	209.6	87.6	0.0637	0.0029	0.851	0.074	0.1011	0.006	0.14387	620	41	621	35	732	96	85	621	35
220224_162.FIN2	29203	320.8	674	0.0585	0.0023	0.749	0.065	0.0964	0.0055	0.22701	565	37	593	32	549	86	108	593	32
220224_163.FIN2	29510	109.3	164.2	0.156	0.011	2.06	0.19	0.1	0.0059	0.03645	1096	69	614	34	2413	120	25	2413	120
220224_165.FIN2	29686	34.8	94.1	0.124	0.012	1.34	0.15	0.0841	0.0056	0.32076	851	62	520	33	2015	172	26	2015	172
220224_166.FIN2	33972	125.3	104.8	0.0596	0.0026	0.865	0.073	0.1084	0.006	0.2169	629	39	663	35	589	95	113	663	35
220224_167.FIN2	34329	175.5	109.2	0.0627	0.0042	0.826	0.097	0.0992	0.0058	0.40122	610	46	609	34	698	143	87	609	34
220224_174.FIN2	35346	2051	1580	0.0692	0.002	0.627	0.052	0.0677	0.0043	0.74001	496	32	422	26	905	60	47	422	26
220224_175.FIN2	36707	177.7	99.8	0.0636	0.0052	0.871	0.11	0.1022	0.0057	0.03098	631	48	627	34	728	173	86	627	34
220224_178.FIN2	45079	388	320	0.0622	0.0022	0.802	0.066	0.0967	0.0055	0.22402	595	37	595	32	681	76	87	595	32
220224_179.FIN2	48994	86.4	79.1	0.0736	0.0041	0.9	0.082	0.0917	0.0053	0.13866	642	44	565	31	1031	113	55	565	31
220224_180.FIN2	51169	231.2	103.9	0.0631	0.0025	0.827	0.068	0.0977	0.0053	0.23239	608	37	601	31	712	84	84	601	31
220224_181.FIN2	51749	2150	837	0.0814	0.04	0.705	3.44	0.0648	0.037	0.23671	540	260	405	190	1231	964	33	405	190
220224_183.FIN2	53986	238	171.7	0.0624	0.0027	0.836	0.072	0.0992	0.0055	0.17622	612	39	610	32	688	92	89	610	32
220224_184.FIN2	57833	79	141	0.0758	0.0089	0.936	0.13	0.0905	0.0055	0.19579	653	60	558	32	1090	235	51	558	32
220224_185.FIN2	58139	281.5	230	0.0633	0.0048	0.828	0.096	0.0982	0.0061	0.00259	608	58	604	35	718	161	84	604	35
220224_196.FIN2	66859	58.5	68.4	0.0634	0.0048	0.87	0.09	0.1026	0.0061	0.11538	629	51	629	35	722	161	87	629	35
220224_198.FIN2	58919	126	95	0.0724	0.032	0.999	2.3	0.0995	0.021	0.28964	695	190	611	100	997	898	61	611	100
220224_200.FIN2	71350	199	157.1	0.0643	0.0029	0.854	0.073	0.0971	0.0054	0.17847	624	42	597	31	752	95	79	597	31
220224_201.FIN2	72734	125.8	93.7	0.0673	0.004	1.001	0.091	0.1095	0.0061	0.16282	701	48	669	35	847	124	79	669	35
220224_202.FIN2	74653	85.6	38.9	0.0725	0.0053	0.862	0.091	0.0872	0.0051	0.28941	613	50	539	30	1000	148	54	539	30
220224_203.FIN2	76344	166.3	127.4	0.065	0.0033	0.868	0.079	0.097	0.0054	0.10108	627	42	597	32	774	107	77	597	32
220224_204.FIN2	82351	169.1	109.6	0.062	0.003	0.82	0.074	0.0971	0.0055	0.50969	604	40	597	32	674	103	89	597	32
220228_008.FIN2	7433	306	230.3	0.0699	0.0033	0.824	0.073	0.08559	0.0068	0.35641	607	40	529	40	925	97	57	529	40
220228_011.FIN2	18127	284	233	0.0605	0.0027	0.729	0.063	0.0892	0.0072	0.47547	556	39	551	43	622	96	89	551	43
220228_012.FIN2	18424	130.7	78.8	0.0619	0.0039	0.783	0.075	0.0939	0.0076	0.0887	581	43	579	45	671	135	86	579	45
220228_013.FIN2	20214	394.8	264.8	0.0644	0.0027	0.948	0.079	0.1094	0.0088	0.3275	676	41	669	51	755	88	89	669	51
220228_018.FIN2	29744	185.5	84.3	0.0608	0.003	0.746	0.066	0.0909	0.0073	0.26347	562	39	561	43	632	106	89	561	43
220228_026.FIN2	32530	137.3	80.8	0.0627	0.0036	0.694	0.063	0.0807	0.0064	0.04694	531	38	500	38	698	122	72	500	38
220228_027.FIN2	33223	153.3	134.5	0.0683	0.0032	0.841	0.072	0.0901	0.0072	0.08724	615	40	556	42	878	97	63	556	42
220228_031.FIN2	39379	475	486	0.0619	0.0022	0.755	0.061	0.08942	0.0071	0.3146	571	36	552	42	671	76	82	552	42
220228_033.FIN2	41441	75.2	33.4	0.0652	0.0043	0.88	0.088	0.0983	0.0081	0.27405	635	46	604	47	781	139	77	604	47
220228_037.FIN2	56057	471	215	0.0606	0.0022	0.743	0.061	0.0894	0.0071	0.43725	562	36	552	42	625	78	88	552	42
220228_039.FIN2	63390	24.1	8.54	0.079	0.008	0.935	0.11	0.0908	0.0076	0.18686	651	59	559	45	1172	200	48	559	45

Appendix I: U-Pb zircon data tables (continued)

Memorial University of Newfoundland

Gibbett Hill Formation; sample BB-004; 47.30146°N , 52.7967°W WGS 84

Zircon U-Pb geochronology

File name	Spot name	Approx. U (ppm)	Approx. Th (ppm)	Isotopic ratios $^{207}Pb/^{206}Pb$	± 2SE	$^{207}Pb/^{235}U$	± 2SE	$^{206}Pb/^{238}U$	± 2SE	Rho	Isotopic ages $^{207}Pb/^{235}U$ (Ma)	± 2SE	$^{206}Pb/^{238}U$ (Ma)	± 2SE	$^{207}Pb/^{206}Pb$ (Ma)	± 2SE	Conc. %	Best Age	± 2SE (Ma)
220302_007.FIN2	265	136.8	76.7	0.0634	0.0039	0.916	0.067	0.1066	0.0067	0.24367	655	36	653	39	722	131	90	653	39
220302_009.FIN2	628	254	201	0.0608	0.0036	0.851	0.064	0.1033	0.0067	0.21995	626	34	634	39	632	128	100	634	39
220302_010.FIN2	1490	85.8	59.6	0.0613	0.0041	0.888	0.071	0.1073	0.0069	0.27388	639	38	657	40	650	144	101	657	40
220302_012.FIN2	3676	188.7	141.7	0.0621	0.0073	0.882	0.11	0.1042	0.0065	0.00437	640	50	639	38	678	251	94	639	38
220302_014.FIN2	4359	150	121.1	0.0612	0.0036	0.908	0.066	0.109	0.007	0.25251	651	36	667	40	646	126	103	667	40
220302_019.FIN2	5332	257	76.3	0.2021	0.01	15.16	0.98	0.5511	0.034	0.68645	2823	64	2828	140	2843	81	99	2843	81
220302_026.FIN2	5483	55.6	64.9	0.1104	0.0063	4.8	0.35	0.317	0.02	0.56534	1774	61	1773	99	1806	104	98	1806	104
220302_027.FIN2	5489	203.2	214	0.0596	0.0036	0.814	0.072	0.0986	0.0079	0.3911	600	38	606	45	589	131	103	606	45
220302_028.FIN2	5890	284	358	0.06	0.0034	0.806	0.056	0.0979	0.006	0.39717	597	32	602	36	604	123	100	602	36
220302_029.FIN2	6131	68.8	48	0.0601	0.0042	0.866	0.069	0.1042	0.0067	0.08815	629	40	639	39	607	151	105	639	39
220302_030.FIN2	6214	263	124.7	0.0599	0.0033	0.851	0.06	0.1032	0.0065	0.35478	625	34	633	38	600	119	105	633	38
220302_031.FIN2	6248	217.3	126.7	0.0607	0.0036	0.823	0.059	0.098	0.0061	0.20849	606	33	602	36	629	128	96	602	36
220302_033.FIN2	6924	150	96.9	0.0604	0.0036	0.817	0.06	0.098	0.0061	0.29451	602	35	602	36	618	129	97	602	36
220302_037.FIN2	8462	240.2	131.3	0.0589	0.0034	0.744	0.054	0.0905	0.0057	0.28655	562	31	559	34	563	126	99	559	34
220302_044.FIN2	8463	180.7	165.7	0.0619	0.0037	0.865	0.062	0.0996	0.0063	0.11803	629	34	612	37	671	128	91	612	37
220302_046.FIN2	9037	182.3	139.2	0.0597	0.0038	0.79	0.058	0.0943	0.006	0.01584	587	33	581	35	593	138	98	581	35
220302_047.FIN2	9062	148.6	62.7	0.059	0.0037	0.792	0.059	0.0951	0.006	0.24817	589	35	586	36	567	137	103	586	36
220302_050.FIN2	10463	134	96.7	0.0606	0.0038	0.886	0.067	0.1036	0.0066	0.24099	638	36	635	39	625	135	102	635	39
220302_052.FIN2	11360	239	139.8	0.0608	0.0037	0.861	0.059	0.0984	0.006	0.21814	630	32	605	36	632	131	96	605	36
220302_064.FIN2	14522	109.1	76	0.0609	0.0039	0.881	0.067	0.1018	0.0064	0.1777	640	36	625	38	636	138	98	625	38
220302_071.FIN2	16136	81.9	51.5	0.0603	0.0043	0.854	0.067	0.1014	0.0066	0.15718	622	38	622	38	614	154	101	622	38
220302_072.FIN2	16176	391.5	73.5	0.1869	0.0092	12.84	0.86	0.491	0.032	0.7007	2666	64	2574	140	2715	81	95	2715	81
220302_074.FIN2	16677	180.2	195	0.06	0.0037	0.785	0.059	0.0939	0.0059	0.15884	585	34	579	35	604	133	96	579	35
220302_076.FIN2	16259	309.3	138.3	0.0602	0.0034	0.788	0.055	0.0947	0.0059	0.01292	588	33	583	35	611	122	95	583	35
220302_085.FIN2	17778	236.2	29.4	0.0733	0.004	1.682	0.13	0.1682	0.012	0.19043	998	47	1002	64	1022	110	98	1022	110
220302_086.FIN2	17946	153	78.2	0.0661	0.004	1.073	0.076	0.1192	0.0073	0.22688	736	39	726	42	810	127	90	726	42
220302_089.FIN2	19017	216	119	0.0626	0.0039	0.902	0.072	0.1054	0.0068	0.49798	645	38	645	39	695	133	93	645	39
220302_090.FIN2	20894	269	223.1	0.0609	0.0047	0.827	0.081	0.099	0.0079	0.20286	608	42	608	45	636	166	96	608	45
220302_091.FIN2	21019	324	131.5	0.0612	0.0033	0.86	0.059	0.1028	0.0065	0.32519	628	33	631	38	646	116	98	631	38
220302_092.FIN2	21251	303	188	0.0611	0.0034	0.837	0.058	0.0998	0.0063	0.22915	615	32	613	37	643	120	95	613	37
220302_094.FIN2	17763	1005	478	0.06122	0.0031	0.806	0.054	0.09562	0.006	0.51592	600	29	589	35	647	109	91	589	35
220302_095.FIN2	21627	190	97.7	0.0634	0.006	0.947	0.17	0.1091	0.0089	0.29632	672	53	668	50	722	201	93	668	50
220302_103.FIN2	21884	249	170	0.0607	0.0037	0.797	0.058	0.0946	0.006	0.20463	594	33	583	35	629	131	93	583	35
220302_104.FIN2	21947	367	161	0.0617	0.0034	0.887	0.062	0.1044	0.0065	0.25042	642	33	640	38	664	118	96	640	38
220302_109.FIN2	22998	330.3	228	0.0589	0.0033	0.765	0.055	0.0933	0.0059	0.23655	574	30	575	35	563	122	102	575	35
220302_112.FIN2	24188	68.7	52.6	0.0601	0.0047	0.852	0.077	0.1005	0.0065	0.14922	611	42	617	38	607	169	102	617	38
220302_113.FIN2	24265	208.1	118.2	0.0629	0.0037	0.938	0.064	0.1069	0.0065	0.14046	672	35	654	38	705	125	93	654	38
220302_121.FIN2	25248	154.9	134.7	0.0609	0.0038	0.858	0.065	0.101	0.0065	0.32717	623	36	620	38	636	134	98	620	38
220302_122.FIN2	25632	257.1	187.6	0.0611	0.0035	0.836	0.06	0.0976	0.0062	0.37795	615	33	600	36	643	123	93	600	36
220302_123.FIN2	25639	637	710	0.0645	0.0034	1.015	0.069	0.1123	0.0071	0.54194	708	35	686	41	758	111	90	686	41
220302_124.FIN2	25664	454	205	0.0604	0.0033	0.819	0.057	0.097	0.0061	0.40559	605	32	596	36	618	118	97	596	36
220302_126.FIN2	27075	233.6	166.7	0.0602	0.0034	0.88	0.063	0.1039	0.0066	0.4416	639	35	637	38	611	122	104	637	38
220302_127.FIN2	27624	111	58.8	0.0608	0.0038	0.858	0.065	0.1014	0.0064	0.19118	626	35	622	38	632	135	98	622	38
220302_131.FIN2	28406	66.5	32.11	0.0629	0.0043	0.981	0.078	0.1125	0.0072	0.16533	688	39	687	42	705	145	97	687	42
220302_138.FIN2	30424	245	280.5	0.0604	0.0047	0.758	0.072	0.0905	0.0059	0.27171	569	39	558	35	618	168	90	558	35
220302_140.FIN2	30470	158.1	141.8	0.0606	0.0092	0.8	0.22	0.0956	0.0064	0.24082	592	31	588	37	625	327	94	588	37
220302_141.FIN2	30554	168.1	132.7	0.0593	0.0038	0.748	0.057	0.0922	0.006	0.32069	563	34	568	35	578	139	98	568	35
220302_144.FIN2	31631	332	191	0.0616	0.0033	0.882	0.061	0.1032	0.0066	0.49085	641	34	633	38	660	115	96	633	38
220302_146.FIN2	32484	130.2	59.1	0.0604	0.0037	0.832	0.061	0.0997	0.0064	0.23149	612	33	612	37	618	132	99	612	37
220302_148.FIN2	33189	159.5	96.1	0.0614	0.0037	0.874	0.066	0.1026	0.0067	0.21611	633	36	629	39	653	129	96	629	39
220302_149.FIN2	33457	94.5	57.9	0.0616	0.0043	0.829	0.066	0.097	0.0062	0.16268	607	37	597	36	660	150	90	597	36
220302_159.FIN2	35074	217.2	140.5	0.0615	0.0034	0.917	0.059	0.1083	0.0065	0.02106	657	33	663	38	657	119	101	663	38
220302_161.FIN2	35857	169.4	162.3	0.0618	0.0037	0.867	0.063	0.1027	0.0065	0.24652	628	34	630	38	667	128	94	630	38
220302_162.FIN2	35913	376	153.4	0.0603	0.0033	0.814	0.057	0.0986	0.0062	0.20829	602	32	606	37	614	118	99	606	37
220302_164.FIN2	36816	135.7	89.8	0.0591	0.0038	0.751	0.057	0.0945	0.0059	0.18818	568	33	582	35	571	140	102	582	35
220302_166.FIN2	37003	114.5	96.6	0.0617	0.004	0.81	0.062	0.097	0.0061	0.1551	596	35	597	36	664	139	90	597	36
220302_182.FIN2	40040	634	425	0.061	0.0034	0.813	0.059	0.0975	0.0062	0.55966	603	32	601	36	639	120	94	601	36
220302_185.FIN2	41346	110.6	61	0.0606	0.0039	0.827	0.064	0.0986	0.0065	0.34613	604	36	606	38	625	139	97	606	38
220302_192.FIN2	41661	306	180.7	0.06	0.0034	0.807	0.057	0.096	0.0061	0.3161	597	32	591	36	604	123	98	591	36
220302_193.FIN2	41951	120.3	72.1	0.0616	0.0039	0.826	0.063	0.0963	0.0062	0.22891	607	36	592	36	660	136	90	592	36
220302_194.FIN2	42032	82.7	79	0.0599	0.0043	0.846	0.07	0.1018	0.0067	0.2152	619	38	625	39	600	155	104	625	39
220302_195.FIN2	42065	161.2	78.2	0.0593	0.0038	0.782	0.059	0.0952	0.0062	0.31051	581	34	586	36	578	139	101	586	36
220302_196.FIN2	42243	225	155.7	0.0608	0.0035	0.862	0.061	0.1008	0.0064	0.35992	627	33	619	38	632	124	98	619	38
220302_197.FIN2	42465	207.6	183	0.0614	0.0044	0.863	0.088	0.0991	0.007	0.31364	626	41	609	40	653	154	93	609	40
220302_198.FIN2	42517	120.3	77.4	0.0626	0.004	0.914	0.07	0.1059	0.0068	0.32906	659	36	649	40	695	136	93	649	40
220302_201.FIN2	43227	188.8	89.8	0.0603	0.0036	0.846	0.063	0.1003	0.0065	0.29436	620	35	617	38	614	129	100	617	38
220302_213.FIN2	46866	35.3	24.9	0.0599	0.0066	0.786	0.088	0.0923	0.0062	0.10086	565	49	569	38	600	239	95	569	38
220302_215.FIN2	47591	248	105.8	0.0601	0.0034	0.776	0.056	0.0914	0.0057	0.32554	580	32	564	34	607	122	93	564	34
220302_216.FIN2	47894	157.3	104.8	0.0599	0.0036	0.833	0.062	0.099	0.0063	0.27714	612	35	609	37	600	130	101	609	37
220302_217.FIN2	47915	179	120.6	0.0608	0.0041	0.804	0.069	0.093	0.0061	0.37391	594	36	573	36	632	145	91	573	36
220302_219.FIN2	48193	283	171.9	0.0613	0.0036	0.834	0.06	0.09667	0.0061	0.14395	612	33	595	36	650	126	92	595	36
220302_221.FIN2	49239	202	111.7	0.0614	0.0038	0.839	0.062	0.0979	0.0061	0.26399	615	34	602	36	653	133	92	602	36
220302_229.FIN2	49458	109.2	94.7	0.0621	0.0041	0.866	0.067	0.1027	0.0065	0.23473	628	37	630	38	678	141	93	630	38
220302_234.FIN2	50420	435	401	0.0624	0.0033	0.884	0.062	0.1053	0.0068	0.30381	642	34	645	40	688	113	94	645	40
220302_246.FIN2	53067	438	68.7	0.0596	0.0032	0.793	0.053	0.09819	0.0062	0.23726	591	30	604	36	589	116	103	604	36
220302_247.FIN2	53237	411	236	0.0608	0.0033	0.861	0.059	0.1046	0.0065	0.27612	628	32	641	38	632	117	101	641	38
220302_248.FIN2	53298	218.7	137.7	0.0592	0.0035	0.767	0.055	0.0959	0.006	0.15909	575	31	590	35	574	129	103	590	35
220302_250.FIN2	53418	217.6	61.5	0.06	0.0034	0.843	0.06	0.1035	0.0065	0.2232	617	33	635	38	604	123	105	635	38
220302_253.FIN2	53475	484	349	0.0624	0.0034	0.866	0.063	0.1026	0.0069	0.29163	631	33	631	40	688	116	92	631	40
220302_255.FIN2	53914	70.2	59.2	0.061	0.0046	0.818	0.071	0.0984	0.0065	0.08113	595	39	605	38	639	162	95	605	38
220302_256.FIN2	53925	370	242	0.0608	0.0033	0.801	0.055	0.0973	0.0062	0.30257	597	32	599	36	632	117	95	599	36
220302_266.FIN2	54843	243	153.9	0.06	0.0034	0.833	0.059	0.0995	0.0063	0.17364	612	33	612	37	604	123	101	612	37
220302_268.FIN2	55154	530	219	0.0602	0.0039	0.86	0.075	0.103	0.0084	0.33394	628	38	632	38	611	140	103	632	38
220302_269.FIN2	56620	502	518	0.0597	0.0033	0.772	0.056	0.0934	0.0061	0.16737	579	32	575	36	593	120	97	575	36
220302_270.FIN2	57736	178.5	129.3	0.0606	0.0035	0.866	0.062	0.1032	0.0065	0.34506	631	35	633	38	625	125	101	633	38
220302_273.FIN2	58698	89.3	64.6	0.0597	0.0043	0.812	0.067	0.0981	0.0063	0.15334	597	37	603	37	593	156	102	603	37
220302_275.FIN2	59309	189.5	24.9	0.059	0.0036	0.798	0.06	0.0959	0.0062	0.3606	592	35	590	36	567	133	104	590	36
220302_284.FIN2	60108	282	112.6	0.0595	0.0034	0.838	0.059	0.1	0.0063	0.27339	615	32	614	37	585	124	105	614	37
220302_286.FIN2	60259	272	165.3	0.0599	0.0034	0.837	0.059	0.0999	0.0063	0.33407	614	33	615	37	600	123	102	615	37
220302_287.FIN2	60497	22.9	14	0.0632	0.0066	1.054	0.12	0.1178	0.0082	0.23714	698	62	716	47	715	222	100	716	47
220302_289.FIN2	60746	453	275	0.0591	0.0034	0.804	0.07	0.0964	0.0068	0.50039	596	32	593	39	571	125	104	593	39
220302_291.FIN2	60804	308	179	0.059	0.0033	0.771	0.055	0.0933	0.0059	0.44965	581	31	575	35	567	122	101	575	35
220302_292.FIN2	61160	172.4	147.4	0.0607	0.0036	0.869	0.066	0.1018	0.0066	0.38254	631	34	626	39	629	128	100	626	39
220302_303.FIN2	61765	277	153.1	0.0614	0.0036	0.838	0.061	0.0968	0.0062	0.28356	614	34	595	37	653	126	91	595	37
220302_304.FIN2	61878	289	120.2	0.0591	0.0039	0.8	0.063	0.0963	0.0064	0.50795	597	34	592	37	571	144	104	592	37
220302_305.FIN2	62326	310	65.7	0.0952	0.0048	3.673	0.25	0.274	0.017	0.53148	1562	54	1560	88	1532	95	102	1532	95
220302_309.FIN2	63617	276	164	0.0596	0.004	0.79	0.067	0.0955	0.0062	0.38385	590	36	588	36	589	146	100	588	36
220302_318.FIN2	66211	83.4	52.4	0.0608	0.0041	0.9	0.067	0.1072	0.0069	0.30559	645	39	656	40	632	145	104	656	40
220302_319.FIN2	67073	257.8	213.2	0.0606	0.0035	0.821	0.058	0.0977	0.0061	0.20869	605	33	601	36	625	125	96	601	36
220302_320.FIN2	67134	659	670	0.0634	0.0033	1.075	0.07	0.1225	0.0076	0.39699	740	36	745	44	722	110	103	745	44
220302_321.FIN2	67381	166	101.4	0.0602	0.0036	0.825	0.059	0.0986	0.0062	0.2048	606	33	606	37	611	129	99	606	37
220302_322.FIN2	67484	258.6	226.5	0.06	0.0035	0.835	0.06	0.1005	0.0064	0.22163	613	33	617	37	604	126	102	617	37
220302_323.FIN2	67641	147.9	135.3	0.1244	0.0063	6.66	0.45	0.3914	0.025	0.64703	2070	61	2128	110	2020	90	105	2020	90
220302_326.FIN2	68280	293	185	0.0615	0.0036	0.846	0.06	0.1006	0.0064	0.16752	619	33	618	37	657	126	94	618	37
220302_328.FIN2	70031	1485	965	0.0611	0.0032	0.799	0.056	0.0959	0.0061	0.36028	596	31	590	36	643	113	92	590	36

Appendix I: U-Pb zircon data tables (continued)

220303_014.FIN2	72197	114.1	74.8	0.0604	0.0022	0.795	0.066	0.0991	0.007	0.23803	591	38	609	41	618	79	99	609	41
220303_015.FIN2	72309	158.7	104.4	0.063	0.0018	0.875	0.07	0.1044	0.0074	0.27234	636	39	640	43	708	61	90	640	43
220303_017.FIN2	72593	122.8	88.3	0.0611	0.003	0.815	0.07	0.0982	0.0068	0.22576	599	39	603	40	643	106	94	603	40
220303_025.FIN2	73493	262	81.8	0.0606	0.0018	0.888	0.072	0.1026	0.0072	0.38599	642	39	630	42	625	64	101	630	42
220303_026.FIN2	73644	204	113	0.0625	0.0023	0.898	0.075	0.1009	0.0071	0.23925	646	40	620	43	691	78	90	620	43
220303_031.FIN2	74208	470	350	0.0595	0.0015	0.78	0.064	0.0919	0.0065	0.3017	583	36	566	41	585	55	97	566	41
220303_033.FIN2	74490	187.4	134	0.061	0.0024	0.867	0.074	0.1015	0.0072	0.13073	630	41	623	42	639	85	98	623	42
220303_046.FIN2	79719	115.3	100.6	0.063	0.0022	1.007	0.084	0.1194	0.0085	0.28784	702	43	727	49	708	74	103	727	49
220303_047.FIN2	81896	388	195	0.1063	0.0026	4.27	0.36	0.2972	0.023	0.63538	1679	69	1679	110	1737	45	97	1737	45
220303_048.FIN2	82572	813	714	0.0609	0.001	0.801	0.063	0.0982	0.007	0.47437	598	35	604	41	636	35	95	604	41
220303_049.FIN2	82689	486	321.6	0.0619	0.0012	0.835	0.066	0.10081	0.0071	0.35284	615	36	619	42	671	41	92	619	42
220303_050.FIN2	84709	407	215.8	0.0611	0.0015	0.834	0.066	0.1017	0.0073	0.53873	613	37	624	43	643	53	97	624	43
220303_052.FIN2	86168	180.5	100.6	0.0649	0.0017	1.111	0.089	0.1276	0.0092	0.44972	756	45	774	51	771	55	100	774	51
Rejected analyses																			
220302_008.FIN2	343	163	87	0.0704	0.0044	0.876	0.066	0.0921	0.0058	0.05876	637	37	568	34	940	128	60	568	34
220302_011.FIN2	2847	73.1	72.5	0.101	0.015	1.47	0.31	0.1009	0.0081	0.62403	856	96	619	49	1643	276	38	1643	276
220302_013.FIN2	4085	408	185	0.064	0.0052	0.799	0.083	0.0926	0.007	0.08223	597	41	571	40	742	172	77	571	40
220302_015.FIN2	4436	49.5	46	0.0591	0.0048	0.805	0.072	0.101	0.0066	0.01098	585	41	620	38	571	177	109	620	38
220302_016.FIN2	4716	135.8	89.7	0.0691	0.0044	0.889	0.069	0.0949	0.0061	0.07527	641	37	584	36	902	131	65	584	36
220302_017.FIN2	4720	240	160	0.062	0.0033	0.746	0.047	0.084	0.005	0.39687	563	30	520	30	674	114	77	520	30
220302_018.FIN2	4915	288	228	0.0613	0.0037	0.755	0.057	0.0899	0.0057	0.14555	567	33	555	33	650	130	85	555	33
220302_032.FIN2	6419	191.8	94.4	0.0678	0.0038	0.963	0.08	0.1021	0.0079	0.35499	681	39	627	45	862	116	73	627	45
220302_034.FIN2	7800	128	106.9	0.0699	0.025	0.954	1.72	0.0982	0.026	0.37115	675	190	603	130	925	735	65	603	130
220302_035.FIN2	7996	387	335	0.0631	0.0037	0.782	0.052	0.0893	0.0053	0.14215	584	31	551	32	712	125	77	551	32
220302_036.FIN2	8427	236	215.9	0.1022	0.0062	1.286	0.091	0.0894	0.0055	0.36422	815	42	552	33	1664	112	33	1664	112
220302_045.FIN2	8657	161.3	77.5	0.0634	0.004	0.851	0.063	0.0958	0.0061	0.1474	625	34	589	36	722	134	82	589	36
220302_048.FIN2	9110	673	399	0.0629	0.0038	0.83	0.069	0.093	0.0063	0.19481	612	34	573	34	705	129	81	573	34
220302_049.FIN2	10391	218	119.3	0.0935	0.0059	1.244	0.093	0.0943	0.0059	0.19176	812	43	581	35	1498	119	39	1498	119
220302_051.FIN2	11245	418	322	0.0627	0.004	0.754	0.052	0.0847	0.0055	0.64329	568	32	524	33	698	136	75	524	33
220302_053.FIN2	12095	191	67	0.0609	0.0037	0.8	0.06	0.0922	0.0058	0.28402	592	33	568	34	636	131	89	568	34
220302_054.FIN2	13019	31.2	26.9	0.065	0.0064	0.802	0.085	0.0875	0.0058	0.26227	572	51	540	34	774	207	70	540	34
220302_055.FIN2	14199	204.4	110.4	0.0573	0.0035	0.742	0.055	0.0906	0.0057	0.30543	560	32	559	34	503	134	111	559	34
220302_065.FIN2	14722	90	53.2	0.0663	0.0056	0.916	0.099	0.0988	0.0069	0.17309	652	58	607	40	816	177	74	607	40
220302_066.FIN2	14959	26.1	22.3	0.0831	0.0095	1.05	0.12	0.0901	0.006	0.03911	670	59	555	35	1272	223	44	555	35
220302_067.FIN2	15383	163.7	430	0.0624	0.0038	0.877	0.065	0.0991	0.0063	0.26081	634	36	609	37	688	130	89	609	37
220302_068.FIN2	15595	836	292	0.067	0.054	0.863	14	0.0924	0.13	0.48532	628	360	570	460	838	1679	68	570	460
220302_069.FIN2	15704	277.7	15.85	0.066	0.0036	1.058	0.078	0.1149	0.0079	0.36438	730	37	701	45	806	114	87	701	45
220302_073.FIN2	16324	102.2	51.6	0.0668	0.0056	1.012	0.086	0.1088	0.0071	0.16043	707	46	666	41	832	175	80	666	41
220302_075.FIN2	17151	165	122	0.068	0.0054	0.97	0.091	0.1026	0.0072	0.07101	685	44	629	41	869	165	72	629	41
220302_083.FIN2	17285	605	286	0.073	0.0046	0.981	0.078	0.09801	0.0062	0.2925	691	37	603	36	1014	128	59	603	36
220302_087.FIN2	18224	316	288	0.0663	0.0038	0.887	0.064	0.0977	0.0062	0.30109	641	34	601	36	816	120	74	601	36
220302_088.FIN2	18694	97	71	0.0749	0.012	0.987	0.31	0.0986	0.009	0.42954	698	86	608	51	1066	322	57	608	51
220302_093.FIN2	21623	125.7	154	0.0629	0.0038	0.823	0.06	0.0957	0.0061	0.16884	604	34	589	36	705	129	84	589	36
220302_102.FIN2	21854	121.3	65.5	0.0581	0.0037	0.834	0.066	0.1036	0.0066	0.2694	610	36	635	38	534	139	119	635	38
220302_105.FIN2	22063	643	578	0.0603	0.0033	0.717	0.047	0.0851	0.0052	0.55767	546	29	526	31	614	118	86	526	31
220302_106.FIN2	22167	194	137.1	0.075	0.0046	0.945	0.072	0.0905	0.0057	0.45578	676	40	558	34	1069	123	52	558	34
220302_107.FIN2	22226	246.8	201.3	0.0728	0.0049	1.038	0.084	0.1014	0.0063	0.35811	715	40	622	37	1008	137	62	622	37
220302_108.FIN2	22662	304	115.4	0.0767	0.026	0.985	0.7	0.092	0.01	0.1045	691	130	568	59	1113	677	51	568	59
220302_110.FIN2	23554	355	190.4	0.0591	0.0034	0.827	0.055	0.1005	0.0061	0.25744	612	32	617	36	571	125	108	617	36
220302_111.FIN2	23650	73.5	35.1	0.0559	0.0039	0.778	0.065	0.0987	0.0064	0.09042	574	37	606	38	448	155	135	606	38
220302_120.FIN2	24875	249	83.4	0.0621	0.0041	0.852	0.067	0.0976	0.0062	0.50953	626	37	600	36	678	141	89	600	36
220302_125.FIN2	26082	320	284.4	0.0677	0.0095	0.877	0.2	0.0922	0.0073	0.10011	636	66	569	42	859	291	66	569	42
220302_128.FIN2	27717	136	138.7	0.0704	0.058	0.924	7.94	0.0933	0.068	0.1681	660	320	575	300	940	1689	61	575	300
220302_129.FIN2	27934	58.4	62.2	0.1676	0.012	3.01	0.26	0.1292	0.0084	0.50573	1394	85	783	48	2534	120	31	2534	120
220302_130.FIN2	28138	57	19.5	0.081	0.012	1.11	0.15	0.1003	0.0069	0.04024	737	60	616	40	1221	291	50	616	40
220302_139.FIN2	30425	142.8	64.6	0.0651	0.0064	0.859	0.15	0.0954	0.011	0.40888	622	69	587	59	778	207	75	587	59
220302_142.FIN2	30960	269	143.9	0.0636	0.0052	0.858	0.081	0.0981	0.0065	0.47185	625	39	603	38	728	173	83	603	38
220302_143.FIN2	31120	349	222	0.0801	0.0054	0.943	0.14	0.0846	0.0079	0.3788	670	50	523	45	1199	133	44	523	45
220302_145.FIN2	31747	205.5	114.9	0.0639	0.0039	0.861	0.063	0.0975	0.0062	0.19591	626	34	600	36	738	129	81	600	36
220302_147.FIN2	33145	906	834	0.1141	0.0062	0.958	0.12	0.061	0.011	0.28756	681	46	382	56	1866	98	20	1866	98
220302_156.FIN2	33980	356	214	0.0663	0.0053	0.87	0.17	0.0969	0.01	0.17392	632	56	596	57	816	167	73	596	57
220302_157.FIN2	34444	173.5	114.6	0.0946	0.025	1.227	0.93	0.095	0.014	0.13573	794	140	585	73	1520	498	38	1520	498
220302_158.FIN2	35018	84.1	37.7	0.063	0.0044	0.844	0.068	0.098	0.0062	0.28066	615	37	603	36	708	149	85	603	36
220302_160.FIN2	35204	114.6	83.1	0.0733	0.0045	0.885	0.067	0.0886	0.0059	0.16458	636	36	547	35	1022	124	53	547	35
220302_163.FIN2	36431	158.5	155.5	0.0589	0.0036	0.81	0.059	0.1013	0.0064	0.05063	598	33	622	37	563	133	110	622	37
220302_165.FIN2	36996	318	128.7	0.0727	0.0048	0.942	0.073	0.0959	0.006	0.13691	670	37	590	36	1006	134	59	590	36
220302_167.FIN2	37186	208.1	91.6	0.0584	0.0034	0.807	0.059	0.1012	0.0064	0.31918	597	33	621	38	545	127	114	621	38
220302_174.FIN2	37359	210	195	0.0617	0.0036	0.76	0.055	0.0905	0.0056	0.05183	571	31	558	33	664	125	84	558	33
220302_175.FIN2	37375	246	159.6	0.0638	0.0038	0.909	0.066	0.1043	0.0066	0.24382	653	34	639	38	735	126	87	639	38
220302_176.FIN2	37929	148.9	160	0.0625	0.0043	0.796	0.064	0.0934	0.006	0.32776	592	36	576	37	691	147	83	576	37
220302_177.FIN2	38103	284.2	140.1	0.0584	0.0051	0.774	0.13	0.0973	0.013	0.22464	580	55	598	69	545	191	110	598	69
220302_178.FIN2	38270	37.1	50.1	0.0601	0.0055	0.891	0.093	0.1078	0.0072	0.21101	630	51	659	42	607	198	109	659	42
220302_179.FIN2	39108	949	715	0.1921	0.011	1.663	0.11	0.0635	0.0041	0.56216	991	42	397	25	2760	94	14	2760	94
220302_180.FIN2	39508	49.5	25	0.0569	0.0061	0.794	0.088	0.1029	0.0067	0.00088	588	49	631	39	488	237	129	631	39
220302_181.FIN2	39890	103.4	67.2	0.0655	0.0044	0.984	0.077	0.1106	0.007	0.44836	690	40	676	41	790	141	86	676	41
220302_183.FIN2	40290	265	146.5	0.0587	0.0035	0.775	0.056	0.0959	0.0061	0.32309	581	32	590	36	556	130	106	590	36
220302_184.FIN2	40671	256	163	0.0589	0.0034	0.834	0.061	0.1025	0.0066	0.46484	612	33	629	39	563	126	112	629	39
220302_199.FIN2	42715	122.8	92.2	0.0589	0.0036	0.818	0.062	0.0986	0.0064	0.00064	601	35	606	37	563	133	108	606	37
220302_200.FIN2	42936	159.5	90.7	0.0602	0.0037	0.929	0.07	0.1098	0.0071	0.29704	664	38	673	41	611	133	110	673	41
220302_202.FIN2	43834	173.7	82	0.0576	0.0034	0.806	0.058	0.0989	0.0062	0.05996	597	33	608	37	515	130	118	608	37
220302_203.FIN2	44082	353	449	0.0603	0.0034	0.9	0.063	0.1061	0.0067	0.2753	651	33	650	39	614	122	106	650	39
220302_210.FIN2	44191	231	138	0.0665	0.0042	0.953	0.074	0.1013	0.0065	0.37043	677	38	622	38	822	132	76	622	38
220302_211.FIN2	44719	155	126	0.0637	0.004	0.859	0.066	0.0949	0.0061	0.23861	624	36	584	36	732	133	80	584	36
220302_212.FIN2	45669	86.9	50	0.1142	0.0086	1.512	0.14	0.0924	0.0059	0.26209	921	51	570	35	1867	136	31	1867	136
220302_214.FIN2	47065	184.8	212	0.0606	0.0037	0.759	0.058	0.0887	0.0057	0.36613	569	33	547	34	625	132	88	547	34
220302_218.FIN2	48040	163.5	119.2	0.0736	0.0044	0.934	0.068	0.0894	0.0058	0.31107	669	36	552	34	1031	121	54	552	34
220302_220.FIN2	49071	321	188	0.0989	0.0071	1.069	0.086	0.0772	0.0049	0.25703	731	42	479	29	1603	134	30	1603	134
220302_228.FIN2	49246	68.5	45.6	0.0683	0.005	0.897	0.073	0.0952	0.0061	0.26762	637	40	586	36	878	152	67	586	36
220302_230.FIN2	49594	201	116.4	0.0627	0.0088	0.837	0.2	0.0995	0.0094	0.2819	613	78	611	53	698	299	88	611	53
220302_231.FIN2	49767	231.3	244.7	0.0639	0.0038	0.753	0.054	0.0861	0.0054	0.36003	566	32	533	32	738	126	72	533	32
220302_232.FIN2	49800	383	255	0.0674	0.0063	0.686	0.23	0.0709	0.014	0.48415	528	74	441	74	850	194	52	441	74
220302_233.FIN2	50216	287.8	185.6	0.0675	0.005	0.906	0.12	0.0989	0.01	0.25654	652	48	608	50	853	154	71	608	50
220302_235.FIN2	51907	163.5	149	0.0596	0.0035	0.841	0.061	0.1035	0.0066	0.32177	617	35	635	38	589	127	108	635	38
220302_236.FIN2	52530	396	256	0.0594	0.0033	0.814	0.057	0.1007	0.0064	0.13687	602	32	619	37	582	121	106	619	37
220302_237.FIN2	52631	340	224.7	0.064	0.014	0.857	0.71	0.0998	0.012	0.38725	631	90	613	54	742	463	83	613	54
220302_238.FIN2	52831	154.9	68.9	0.065	0.0063	0.947	0.098	0.1085	0.0068	0.22332	669	47	664	39	774	204	86	664	39
220302_239.FIN2	52956	278	112.1	0.0597	0.0034	0.822	0.06	0.1021	0.0066	0.24625	608	33	627	39	593	123	106	627	39
220302_249.FIN2	53299	557.8	360	0.0654	0.0035	0.78	0.054	0.0885	0.0056	0.23842	584	30	547	33	787	112	69	547	33
220302_251.FIN2	53454	51.2	31.5	0.0588	0.005	0.787	0.074	0.0992	0.0064	0.03812	577	43	609	38	560	185	109	609	38
220302_252.FIN2	53458	427	151.5	0.0629	0.0084	0.876	0.26	0.1027	0.0097	0.17061	637	76	630	54	705	284	89	630	54
220302_254.FIN2	53642	35	26.77	0.0582	0.0047	0.86	0.076	0.1085	0.0069	0.17394	610	43	664	40	537	177	124	664	40
220302_257.FIN2	54353	442	313	0.1649	0.0083	2.377	0.15	0.1058	0.0066	0.19726	1229	49	649	38	2507	85	26	2507	85
220302_264.FIN2	54384	470	615	0.0633	0.0034	0.864	0.058	0.0992	0.0062	0.40329	632	32	609	36	718	114	85	609	36
220302_271.FIN2	57855	45.7	43.1	0.0619	0.0059	0.827	0.086	0.0968	0.0063	0.06893	591	47	595	37	671	204	89	595	37
220302_272.FIN2	57950	104.7	60.4	0.0626	0.0042	0.852	0.066	0.0984	0.0065	0.22511	622	37	605	38	695	143	87	605	38
220302_274.FIN2	58815	273	125.7	0.0647	0.0038	0.832	0.061	0.0923	0.0059	0.35652	612	34	569	35	765	124	74	569	35
220302_282.FIN2	59353	85.3	78.6	0.0631	0.0043	0.845	0.068	0.0965	0.0062	0.18071	613	38	594	36	712	145	83	594	36
220302_283.FIN2	59478	94.8	60.9	0.0617	0.0038	1.017	0.076	0.1161	0.0075	0.19041	704	38	707	43	664	132	107	707	43
220302_285.FIN2	60178	158	127	0.0665	0.0057	0.937	0.095	0.1014	0.007	0.15237	671	43	622	41	822	179	76	622	41
220302_288.FIN2	60706	190	173	0.0719	0.0046	0.923	0.074	0.0907	0.0059	0.35126	659	39	559	35	983	130	57	559	35
220302_290.FIN2	60774	141.5	108.3	0.0641	0.0041	0.831	0.064	0.0927	0.0061	0.34578	606	36	571	36	745	135	77	571	36

Appendix I: U-Pb zircon data tables (continued)

220302_293.FIN2	61382	229	122	0.0704	0.0068	0.939	0.16	0.094	0.0074	0.42636	667	54	579	42	940	198	62	579	42
220302_300.FIN2	61593	280	136.4	0.0704	0.0055	1.054	0.16	0.1058	0.01	0.54725	726	57	648	57	940	160	69	648	57
220302_301.FIN2	61612	93.3	59	0.073	0.0056	0.898	0.076	0.0877	0.0062	0.1339	639	43	541	37	1014	155	53	541	37
220302_302.FIN2	61731	179	91.7	0.0588	0.0035	0.825	0.062	0.0993	0.0064	0.26654	607	35	610	38	560	130	109	610	38
220302_306.FIN2	62397	213.9	129.3	0.0626	0.0037	0.746	0.055	0.085	0.0056	0.45753	562	32	526	33	695	126	76	526	33
220302_307.FIN2	62452	265	297	0.0588	0.0033	0.846	0.061	0.1015	0.0065	0.36547	619	33	623	38	560	122	111	623	38
220302_308.FIN2	62596	38.1	16.7	0.0564	0.0045	0.767	0.071	0.0967	0.0065	0.22913	567	41	595	38	468	177	127	595	38
220302_310.FIN2	64066	193	179	0.0599	0.0034	0.873	0.062	0.1043	0.0065	0.27019	635	33	639	38	600	123	107	639	38
220302_311.FIN2	65197	273	189	0.0707	0.0043	0.859	0.063	0.0878	0.0057	0.29734	625	33	543	33	949	124	57	543	33
220302_324.FIN2	67751	393	248	0.0645	0.0037	0.86	0.062	0.0967	0.0061	0.22765	626	33	595	36	758	121	78	595	36
220302_325.FIN2	68164	31.11	28.23	0.0635	0.0059	0.817	0.082	0.0959	0.0065	0.13666	586	48	590	38	725	197	81	590	38
220302_327.FIN2	69984	186	144	0.0688	0.0073	0.938	0.14	0.1	0.0067	0.41041	673	53	614	39	893	219	69	614	39
220302_329.FIN2	70131	198	134.7	0.0632	0.0044	0.883	0.068	0.1035	0.0066	0.03889	640	37	634	39	715	148	89	634	39
220303_007.FIN2	70578	100.1	59.3	0.058	0.0024	0.834	0.073	0.1124	0.008	0.13554	609	40	686	46	530	91	130	686	46
220303_008.FIN2	70647	502.6	261	0.0657	0.0016	0.831	0.065	0.0998	0.0071	0.0237	614	37	613	42	797	51	77	613	42
220303_009.FIN2	71103	202	140.9	0.122	0.0013	6.41	0.47	0.4053	0.027	0.61694	2031	70	2193	130	1986	19	110	1986	19
220303_010.FIN2	71409	237	98.1	0.094	0.021	1.26	0.54	0.1023	0.0092	0.30914	801	120	628	52	1508	422	42	1508	422
220303_011.FIN2	71732	93.6	61.5	0.0669	0.0044	0.955	0.093	0.1103	0.0078	0.24178	672	48	674	44	835	137	81	674	44
220303_012.FIN2	71981	571	216	0.0611	0.032	0.9	2.09	0.1137	0.028	0.52144	650	220	694	140	643	1126	108	694	140
220303_013.FIN2	72026	151.4	148.5	0.0595	0.002	0.858	0.072	0.1101	0.0078	0.24155	627	38	673	45	585	73	115	673	45
220303_016.FIN2	72325	94.4	69.4	0.0637	0.0023	0.865	0.079	0.1028	0.0079	0.40547	632	42	630	46	732	76	86	630	46
220303_018.FIN2	72596	303	154	0.0617	0.0026	0.749	0.074	0.0897	0.007	0.36482	565	38	553	41	664	90	83	553	41
220303_027.FIN2	73877	200	158	0.0677	0.003	0.852	0.072	0.087	0.0061	0.04467	619	39	538	36	859	92	63	538	36
220303_028.FIN2	74005	55.3	33	0.0713	0.0054	0.824	0.089	0.0801	0.0066	0.15982	604	50	497	39	966	155	51	497	39
220303_029.FIN2	74155	577	329	0.0595	0.0013	0.876	0.07	0.1026	0.0071	0.33555	637	37	629	42	585	47	107	629	42
220303_030.FIN2	74195	587	88.3	0.0722	0.012	1.199	0.42	0.1143	0.011	0.20725	797	96	698	58	992	338	70	698	58
220303_032.FIN2	74425	161	128	0.0962	0.014	1.21	0.28	0.0898	0.0082	0.07127	785	83	554	47	1552	273	36	1552	273
220303_034.FIN2	74505	136.5	70.8	0.0582	0.0023	0.804	0.069	0.0966	0.0068	0.31798	596	38	594	40	537	86	111	594	40
220303_035.FIN2	75063	237	178	0.0664	0.0067	0.849	0.12	0.0889	0.0071	0.14375	628	70	549	42	819	211	67	549	42
220303_036.FIN2	75805	169	80.9	0.0719	0.0082	0.901	0.2	0.0896	0.0076	0.06608	648	76	553	44	983	232	56	553	44
220303_043.FIN2	75811	109.8	84.8	0.0625	0.0028	0.828	0.073	0.0989	0.0072	0.28958	606	40	608	42	691	96	88	608	42
220303_044.FIN2	76669	295	99.9	0.0618	0.044	0.577	2.68	0.0796	0.034	0.61149	459	250	494	170	667	1524	74	494	170
220303_045.FIN2	78851	126.8	83	0.0592	0.0024	0.812	0.067	0.1026	0.0072	0.01553	600	40	630	42	574	88	110	630	42
220303_051.FIN2	85341	329	214	0.0616	0.03	0.563	3.17	0.0779	0.048	0.69227	454	260	483	200	660	1044	73	483	200

Appendix I: U-Pb zircon data tables (continued)

Memorial University of Newfoundland

Quidi Vidi Formation; sample UBQV-001; 47.3129°N , 52.7712°W WGS 84

Zircon U-Pb geochronology

				Isotopic ratios							Isotopic ages							
File name	Spot name	Approx. U (ppm)	Approx. Th (ppm)	$^{207}Pb/^{206}Pb$	± 2SE	$^{207}Pb/^{235}U$	± 2SE	$^{206}Pb/^{238}U$	± 2SE	Rho	$^{207}Pb/^{235}U$	± 2SE (Ma)	$^{206}Pb/^{238}U$	± 2SE (Ma)	$^{207}Pb/^{206}Pb$	± 2SE (Ma)	Conc. %	Best Age	± 2SE (Ma)
220225_008.FIN2	835	114.4	80.9	0.0616	0.0027	0.918	0.068	0.107	0.0076	0.25588	655	36	655	44	660	94	99	655	44
220225_015.FIN2	10982	278	195	0.0602	0.0023	0.753	0.054	0.0905	0.0064	0.45527	569	30	558	38	611	83	91	558	38
220225_016.FIN2	12124	112.2	59.2	0.0603	0.0026	0.817	0.06	0.0988	0.007	0.24154	603	34	607	41	614	93	99	607	41
220225_018.FIN2	14690	85.5	59.1	0.1082	0.0039	4.56	0.32	0.3104	0.022	0.55856	1738	57	1741	110	1769	66	98	1769	66
220225_028.FIN2	20280	86.9	78.8	0.0588	0.0028	0.776	0.061	0.0951	0.0068	0.34651	576	34	586	40	560	104	105	586	40
220225_029.FIN2	20640	123.6	122.4	0.0605	0.0032	0.798	0.065	0.0967	0.0069	0.24211	591	36	595	41	622	114	96	595	41
220225_030.FIN2	21241	167.5	83.7	0.0616	0.0026	0.812	0.058	0.0971	0.0069	0.13899	602	33	597	41	660	90	90	597	41
220225_032.FIN2	24467	47	23.8	0.0655	0.0043	1.104	0.1	0.1217	0.0088	0.15522	736	45	742	52	790	138	94	742	52
220225_033.FIN2	25136	212.6	134	0.0587	0.0025	0.795	0.057	0.0901	0.0064	0.18903	592	32	556	38	556	93	100	556	38
220225_035.FIN2	27839	189.8	79.3	0.0619	0.0029	0.838	0.063	0.0994	0.0071	0.28501	614	35	611	41	671	100	91	611	41
220225_036.FIN2	29305	61.7	19.7	0.0638	0.0037	0.933	0.076	0.1083	0.0077	0.0247	664	43	664	46	735	123	90	664	46
220225_047.FIN2	40739	1636	788	0.06883	0.0021	1.335	0.091	0.1429	0.01	0.71858	860	39	861	57	894	63	96	861	57
220225_049.FIN2	43052	934	506	0.0639	0.0021	0.963	0.068	0.1112	0.008	0.70706	683	35	680	46	738	70	92	680	46
220225_050.FIN2	43275	310	84.5	0.1243	0.0039	5.71	0.4	0.3371	0.024	0.1	1930	60	1871	120	2019	56	93	2019	56
220225_052.FIN2	45038	783	1012	0.06331	0.002	0.969	0.065	0.1123	0.0079	0.45538	686	33	686	46	719	67	95	686	46
220225_053.FIN2	47449	245	248	0.0625	0.0026	0.856	0.062	0.1012	0.0072	0.12429	626	34	622	42	691	89	90	622	42
220225_054.FIN2	47517	151.8	146.4	0.0609	0.0025	0.812	0.059	0.0982	0.0069	0.28077	601	32	603	41	636	88	95	603	41
220225_055.FIN2	52885	181.6	80.3	0.0595	0.0028	0.804	0.063	0.1001	0.0077	0.56592	603	37	614	45	585	102	105	614	45
220225_056.FIN2	55171	498	298	0.0612	0.0023	0.807	0.056	0.0979	0.0071	0.52059	598	31	602	41	646	81	93	602	41
220225_057.FIN2	58309	145.1	62.9	0.0635	0.0032	0.905	0.071	0.106	0.0076	0.22964	650	38	649	44	725	107	90	649	44
220225_064.FIN2	58776	132.8	126.2	0.0623	0.0027	0.844	0.061	0.101	0.0071	0.20443	620	35	620	42	684	93	91	620	42
220225_067.FIN2	64787	161.7	96.8	0.0618	0.0025	0.812	0.059	0.0971	0.0068	0.35223	600	33	597	40	667	87	90	597	40
220225_071.FIN2	76521	261	136.8	0.0601	0.0028	0.741	0.059	0.0897	0.0067	0.51749	559	34	556	42	607	101	92	556	42
220225_072.FIN2	78638	214.8	81.1	0.0618	0.0025	0.945	0.068	0.1123	0.008	0.39371	673	36	686	46	667	87	103	686	46
220225_073.FIN2	79434	521	229	0.0606	0.0022	0.833	0.059	0.0923	0.0066	0.53577	613	32	569	39	625	78	91	569	39
220225_075.FIN2	83979	182.1	113.3	0.0665	0.0026	1.129	0.08	0.1257	0.0088	0.24647	763	39	763	51	822	82	93	763	51
220225_083.FIN2	85513	130.2	48.9	0.0659	0.0032	1.075	0.083	0.1217	0.0087	0.39652	738	42	740	50	803	102	92	740	50
220225_087.FIN2	92784	129.5	86.8	0.0608	0.0033	0.766	0.062	0.0934	0.0067	0.17468	572	36	575	39	632	117	91	575	39
220225_088.FIN2	93612	234	186	0.0625	0.0028	0.895	0.067	0.105	0.0075	0.29506	648	37	643	43	691	96	93	643	43
220225_089.FIN2	93981	270	136.6	0.0641	0.0023	1.006	0.07	0.1152	0.0081	0.31566	704	36	703	47	745	76	94	703	47
220225_090.FIN2	97660	51.4	35.96	0.1775	0.0063	10.92	0.78	0.4547	0.033	0.63023	2509	67	2413	140	2630	59	92	2630	59
220225_091.FIN2	98876	138.2	79.5	0.0607	0.0027	0.789	0.059	0.0953	0.0067	0.24929	585	34	588	39	629	96	93	588	39
220225_092.FIN2	54301	847	617	0.0633	0.0022	1.007	0.072	0.1162	0.0085	0.66744	706	36	708	49	718	74	99	708	49
220225_101.FIN2	85912	96.2	74.5	0.0608	0.0029	0.863	0.065	0.1031	0.0073	0.16976	627	34	632	42	632	103	100	632	42
220225_102.FIN2	318	78	83.7	0.0627	0.0034	0.953	0.076	0.1101	0.0079	0.21446	668	40	673	46	698	116	96	673	46
220225_104.FIN2	1097	73.1	36.9	0.0612	0.0035	0.814	0.067	0.096	0.0069	0.20296	594	37	591	41	646	123	91	591	41
220225_105.FIN2	1112	127.6	163.4	0.0611	0.0027	0.894	0.066	0.1066	0.0076	0.20839	648	37	653	44	643	95	102	653	44
220225_106.FIN2	1289	324	137.5	0.0617	0.0025	0.846	0.061	0.0989	0.0071	0.44578	621	33	608	41	664	87	92	608	41
220225_107.FIN2	2716	724	78.7	0.1171	0.0039	5.53	0.39	0.3453	0.026	0.69509	1913	70	1910	120	1912	60	100	1912	60
220225_108.FIN2	3133	59.8	64.6	0.1193	0.0053	5.55	0.43	0.3355	0.025	0.58498	1896	68	1863	120	1946	79	96	1946	79
220225_109.FIN2	3247	175	86	0.0585	0.0033	0.745	0.06	0.0917	0.0066	0.01955	562	35	565	39	549	123	103	565	39
220225_118.FIN2	3430	121.4	85.8	0.0616	0.0033	0.875	0.071	0.1014	0.0072	0.24913	633	37	622	42	660	115	94	622	42
220225_126.FIN2	7103	194.9	106.2	0.0664	0.0027	1.195	0.088	0.127	0.0091	0.3807	794	40	770	52	819	85	94	770	52
220225_129.FIN2	10769	73.8	46.8	0.0609	0.0047	0.835	0.077	0.0975	0.0071	0.03802	604	44	600	42	636	166	94	600	42
220225_139.FIN2	11408	150.9	53.2	0.0791	0.0033	2.31	0.17	0.2058	0.015	0.29362	1211	51	1206	78	1175	83	103	1175	83
220225_140.FIN2	11717	158.7	80.8	0.06	0.0033	0.794	0.064	0.0934	0.0067	0.21999	592	35	576	40	604	119	95	576	40
220225_142.FIN2	12524	91.3	139	0.0619	0.0035	0.918	0.076	0.1034	0.0074	0.23608	652	40	634	43	671	121	95	634	43
220225_146.FIN2	10771	232.9	129.9	0.0613	0.0023	0.949	0.066	0.1098	0.0078	0.33359	675	34	671	45	650	81	103	671	45
220225_147.FIN2	13955	21.34	15	0.1067	0.0055	4.83	0.38	0.3166	0.024	0.35714	1764	69	1768	110	1744	94	101	1744	94
220225_148.FIN2	13981	359	285	0.0592	0.0023	0.797	0.056	0.0952	0.0067	0.26304	595	31	586	39	574	84	102	586	39
220225_155.FIN2	14467	174	106.5	0.0607	0.0027	0.869	0.065	0.1003	0.0071	0.28717	630	35	616	42	629	96	98	616	42
220225_157.FIN2	16138	105.4	78	0.0617	0.0034	0.858	0.07	0.0977	0.0071	0.21475	626	39	601	41	664	118	91	601	41
220225_158.FIN2	16783	285	132	0.0607	0.0027	0.827	0.061	0.0969	0.007	0.2091	609	34	596	41	629	96	95	596	41
220225_160.FIN2	19285	941	3.35	0.1183	0.0035	5.274	0.35	0.3161	0.022	0.69602	1869	54	1770	110	1931	53	92	1931	53
220225_161.FIN2	19698	386	174.8	0.0607	0.0023	0.785	0.056	0.0918	0.0065	0.48137	588	33	566	38	629	82	90	566	38
220225_162.FIN2	19825	124.5	19.85	0.0655	0.0029	1.084	0.079	0.1169	0.0083	0.23621	739	39	712	48	790	93	90	712	48
220225_163.FIN2	20326	77.9	34.6	0.0596	0.0036	0.812	0.07	0.0961	0.007	0.24232	591	39	591	41	589	131	100	591	41
220225_164.FIN2	20368	56.4	83.8	0.0611	0.0045	0.85	0.083	0.0952	0.007	0.28609	609	46	586	41	643	158	91	586	41
220225_176.FIN2	22181	209	250	0.0623	0.0027	0.906	0.068	0.1006	0.0074	0.46095	648	37	620	45	684	93	91	620	45
220225_180.FIN2	24569	327	12.3	0.0645	0.0022	1.086	0.074	0.119	0.0084	0.38093	744	36	724	48	758	72	96	724	48
220225_182.FIN2	25413	258	152	0.06	0.0024	0.846	0.061	0.1004	0.0071	0.29486	618	33	617	41	604	87	102	617	41
220225_183.FIN2	25973	141.2	61.1	0.1257	0.0043	6.48	0.45	0.3621	0.026	0.48643	2039	60	1991	120	2039	60	98	2039	60
220225_184.FIN2	26298	204.9	104.4	0.0628	0.0025	0.957	0.069	0.1081	0.0076	0.34501	678	36	662	45	701	85	94	662	45
220225_192.FIN2	26738	70.6	35.7	0.0615	0.0049	0.942	0.095	0.1079	0.0079	0.10598	659	49	660	46	657	171	100	660	46
220225_193.FIN2	26801	130	50	0.0649	0.0029	1.166	0.086	0.1292	0.0092	0.28637	779	42	783	52	771	94	102	783	52
220225_197.FIN2	27343	45.3	26.95	0.0642	0.0043	1.013	0.089	0.1131	0.0081	0.06587	691	45	690	47	748	142	92	690	47
220225_199.FIN2	27871	116.3	76.1	0.0609	0.0029	0.839	0.065	0.0991	0.0071	0.12603	615	34	609	41	636	102	96	609	41
220225_201.FIN2	28489	393	77.6	0.1234	0.004	6.26	0.43	0.3665	0.026	0.63525	2013	63	2012	120	2006	58	100	2006	58
220225_202.FIN2	28549	108.1	51	0.0608	0.0031	0.888	0.07	0.1049	0.0074	0.42352	640	39	643	43	632	110	102	643	43
220225_211.FIN2	31441	103.3	67.7	0.0597	0.0035	0.839	0.069	0.1007	0.0075	0.25314	617	37	618	44	593	127	104	618	44
220225_217.FIN2	35703	256.4	128	0.0643	0.0029	1.042	0.078	0.1175	0.0084	0.15951	721	39	716	49	752	95	95	716	49
220225_228.FIN2	42613	135.1	75.1	0.0644	0.0032	1.069	0.081	0.1208	0.0086	0.14071	732	40	735	50	755	105	97	735	50
220225_230.FIN2	43004	173.1	118.9	0.0612	0.0027	0.855	0.064	0.1014	0.0072	0.2465	623	35	622	42	646	95	96	622	42
220225_231.FIN2	43033	219	360	0.0607	0.0027	0.816	0.06	0.0982	0.007	0.28004	601	33	603	41	629	96	96	603	41
220225_234.FIN2	43517	389	38.1	0.0654	0.0023	1.133	0.078	0.1258	0.0088	0.29714	768	38	764	51	787	74	97	764	51
220225_236.FIN2	43640	135.5	64.4	0.0635	0.0029	1.025	0.078	0.1167	0.0082	0.34145	710	39	711	47	725	97	98	711	47
220225_238.FIN2	43750	238	194	0.1201	0.0038	5.89	0.4	0.3551	0.025	0.59582	1962	53	1957	120	1958	56	100	1958	56
220225_239.FIN2	44174	263	113	0.0602	0.0028	0.775	0.058	0.094	0.0067	0.24021	578	34	579	39	611	101	95	579	39
220225_240.FIN2	44328	49.6	27.6	0.1036	0.005	4.41	0.35	0.3021	0.022	0.3667	1698	65	1700	110	1690	89	101	1690	89
220225_247.FIN2	44400	1014	580	0.0653	0.0021	1.132	0.077	0.1257	0.0088	0.51147	767	37	763	51	784	68	97	763	51
220225_248.FIN2	45328	156	108	0.0652	0.0028	1.168	0.086	0.1298	0.0092	0.39269	780	41	787	52	781	90	101	787	52
220225_249.FIN2	46822	597	1170	0.0605	0.0024	0.77	0.055	0.093	0.0066	0.33535	578	31	573	39	622	86	92	573	39
220225_250.FIN2	47621	681	168	0.1268	0.0036	6.556	0.43	0.3756	0.026	0.69603	2052	58	2055	120	2054	50	100	2054	50
220225_251.FIN2	47741	82	105.5	0.0667	0.0034	1.151	0.09	0.1268	0.009	0.21626	767	43	769	52	828	106	93	769	52
220225_252.FIN2	48803	108.3	106.5	0.0638	0.0033	1.019	0.079	0.1154	0.0082	0.2021	703	40	703	48	735	110	96	703	48
220225_254.FIN2	51424	158.3	115.3	0.0618	0.0029	0.864	0.066	0.102	0.0075	0.35128	627	37	627	45	667	100	94	627	45
220225_257.FIN2	58986	122.4	61.9	0.0659	0.003	1.104	0.083	0.1217	0.0086	0.24079	749	41	740	49	803	95	92	740	49
220225_265.FIN2	60109	259	180	0.0616	0.0024	0.923	0.068	0.1084	0.0077	0.37844	660	36	663	45	660	84	100	663	45
220225_269.FIN2	61183	230	254	0.0607	0.0026	0.814	0.059	0.0988	0.007	0.30494	605	36	607	41	629	92	97	607	41
220225_270.FIN2	61284	125.9	48.7	0.1209	0.0049	5.66	0.43	0.3406	0.025	0.59852	1914	68	1887	120	1970	72	96	1970	72
220225_272.FIN2	61981	228.4	182.7	0.059	0.0025	0.784	0.058	0.0972	0.0069	0.27313	583	33	598	40	567	92	105	598	40
220225_273.FIN2	62381	189.2	145.8	0.0601	0.0026	0.813	0.06	0.099	0.007	0.17187	604	34	608	41	607	94	100	608	41
220225_274.FIN2	62409	300	181.7	0.0613	0.0025	0.843	0.061	0.101	0.0072	0.33909	616	34	620	42	650	88	95	620	42
220225_276.FIN2	62626	1052	1118	0.0612	0.002	0.826	0.057	0.0994	0.007	0.46414	610	31	611	41	646	70	94	611	41
220225_283.FIN2	62780	353	118.4	0.1034	0.0035	3.843	0.27	0.2731	0.019	0.62333	1601	55	1555	99	1686	62	92	1686	62
220225_284.FIN2	63203	767	510	0.0655	0.0022	1.141	0.078	0.1283	0.0091	0.45229	772	37	778	52	790	70	98	778	52
220225_286.FIN2	63496	148.2	172.3	0.0609	0.0027	0.852	0.064	0.1021	0.0073	0.39436	621	35	626	42	636	95	99	626	42
220225_287.FIN2	63601	327	144	0.06	0.003	0.792	0.061	0.0969	0.0068	0.13704	592	30	596	40	604	108	99	596	40
220225_290.FIN2	65310	975	679	0.0607	0.002	0.81	0.055	0.0981	0.0069	0.37993	602	30	603	40	629	71	96	603	40
220225_291.FIN2	65788	313	155	0.06	0.0026	0.768	0.056	0.0935	0.0066	0.11065	578	31	576	39	604	94	95	576	39
220225_292.FIN2	71910	114	54.7	0.0624	0.0037	0.889	0.075	0.1054	0.0078	0.30508	641	41	645	46	688	127	94	645	46
220225_293.FIN2	72267	120.9	86.4	0.0638	0.0034	0.979	0.08	0.1132	0.0085	0.29376	686	41	690	49	735	113	94	690	49
220225_301.FIN2	78717	714	325	0.0618	0.0021	0.863	0.059	0.1027	0.0072	0.47884	630	32	631	43	667	73	95	631	43
220225_304.FIN2	81856	125.2	73.6	0.0629	0.0031	0.906	0.07	0.1063	0.0076	0.2604	650	39	651	44	705	105	92	651	44
220225_305.FIN2	82577	70.6	38.1	0.0623	0.004	0.892	0.078	0.1068	0.0077	0.13071	636	42	654	45	684	137	96	654	45

Appendix I: U-Pb zircon data tables (continued)

220225_306.FIN2	82780	217	123.2	0.0651	0.0046	1.065	0.098	0.1208	0.0087	0.13224	738	52	735	50	778	149	95	735	50
220225_309.FIN2	83317	223	93.3	0.0644	0.0025	1.155	0.083	0.1312	0.0093	0.38813	774	39	794	53	755	82	105	794	53
220225_310.FIN2	83537	64.5	29.2	0.0789	0.0036	2.047	0.15	0.1905	0.014	0.26594	1119	52	1123	73	1170	90	96	1170	90
220225_319.FIN2	85369	472	281	0.1073	0.0044	4.51	0.34	0.3086	0.023	0.61156	1728	64	1733	110	1754	75	99	1754	75
220225_320.FIN2	85985	224.9	120.8	0.0669	0.0027	1.148	0.083	0.1269	0.009	0.2963	774	38	770	51	835	84	92	770	51
220225_323.FIN2	86933	233	181	0.0616	0.0034	0.796	0.064	0.0965	0.0069	0.27677	590	36	594	41	660	118	90	594	41
220225_325.FIN2	88976	409	316	0.061	0.0024	0.826	0.059	0.0998	0.0071	0.20137	610	33	613	41	639	85	96	613	41
220225_327.FIN2	90537	209	126.4	0.0616	0.0037	0.854	0.081	0.1	0.0088	0.5834	606	43	611	51	660	129	93	611	51
220225_329.FIN2	92563	173.6	138.8	0.0604	0.0026	0.821	0.061	0.0997	0.0071	0.42366	602	34	613	41	618	93	99	613	41
220225_330.FIN2	92664	274	126.3	0.0612	0.0027	0.79	0.059	0.0953	0.0068	0.30965	587	34	587	40	646	95	91	587	40
220225_337.FIN2	93024	464	54.5	0.1267	0.004	6.21	0.42	0.3626	0.026	0.52906	2006	62	1998	130	2053	56	97	2053	56
220225_339.FIN2	93052	135.6	75.7	0.0616	0.0029	0.899	0.067	0.1064	0.0075	0.07831	646	36	653	45	660	101	99	653	45
220225_340.FIN2	93605	141.3	123	0.0617	0.0035	0.81	0.066	0.0976	0.0069	0.22561	600	38	600	41	664	122	90	600	41
220225_341.FIN2	95691	338	287	0.1299	0.0044	6.68	0.47	0.379	0.027	0.61896	2066	61	2070	130	2097	60	99	2097	60
220225_346.FIN2	98888	746	179	0.0922	0.0029	3.085	0.21	0.2472	0.017	0.61089	1429	50	1424	90	1472	60	97	1472	60
Rejected analyses																			
220225_009.FIN2	1074	164.9	79.4	0.06	0.0029	0.671	0.052	0.0815	0.0058	0.27814	518	32	505	35	604	105	84	505	35
220225_010.FIN2	1847	234	31.6	0.0719	0.0035	1.167	0.095	0.1194	0.0089	0.4629	786	47	726	51	983	99	74	726	51
220225_011.FIN2	3178	50	24.41	0.0741	0.0041	1.114	0.091	0.1096	0.0078	0.22905	749	44	670	45	1044	112	64	670	45
220225_012.FIN2	6744	97.2	69.7	0.0778	0.0046	0.966	0.082	0.0887	0.0064	0.07308	679	42	547	38	1142	118	48	547	38
220225_013.FIN2	9147	177	139	0.0644	0.0038	0.837	0.07	0.0947	0.007	0.31689	614	39	583	41	755	125	77	583	41
220225_014.FIN2	9822	742	459	0.0614	0.0032	0.645	0.055	0.0699	0.0063	0.68645	504	34	435	38	653	112	67	435	38
220225_017.FIN2	13005	152.6	115	0.1459	0.0062	1.627	0.12	0.0814	0.0057	0.23753	976	45	504	34	2298	73	22	2298	73
220225_021.FIN2	18037	174	103	0.1252	0.0053	5.16	0.38	0.2975	0.022	0.45855	1847	62	1677	110	2032	75	83	2032	75
220225_031.FIN2	22768	409	415	0.0596	0.0023	0.662	0.047	0.081	0.0057	0.4095	514	29	502	34	589	84	85	502	34
220225_034.FIN2	25731	36.7	15.85	0.0602	0.0049	0.969	0.096	0.1193	0.0086	0.01984	668	49	726	49	611	176	119	726	49
220225_038.FIN2	33193	310	120.7	0.0599	0.003	0.708	0.061	0.0863	0.0068	0.63006	543	38	533	40	600	108	89	533	40
220225_039.FIN2	37568	152	129	0.0986	0.0048	1.225	0.096	0.0907	0.0065	0.12696	804	43	559	38	1598	91	35	1598	91
220225_046.FIN2	40263	237.9	273	0.0749	0.0038	0.829	0.065	0.0805	0.0058	0.10713	608	35	499	35	1066	102	47	499	35
220225_048.FIN2	42704	275	290	0.0992	0.01	1.44	0.19	0.1064	0.0076	0.6082	876	71	651	44	1609	188	40	1609	188
220225_051.FIN2	44418	99.6	86.8	0.0638	0.0031	0.923	0.071	0.1067	0.0075	0.23732	656	38	653	44	735	103	89	653	44
220225_065.FIN2	61776	194	59.1	0.0642	0.0025	0.932	0.066	0.1086	0.0077	0.36065	667	35	665	45	748	82	89	665	45
220225_066.FIN2	63128	431	258	0.0632	0.0023	0.795	0.055	0.093	0.0065	0.30641	592	31	573	39	715	77	80	573	39
220225_068.FIN2	65227	64.5	41.3	0.0656	0.0068	0.856	0.1	0.0973	0.0075	0.13413	615	53	598	44	794	217	75	598	44
220225_069.FIN2	69608	508	189.3	0.0609	0.002	0.744	0.051	0.0905	0.0063	0.43249	563	30	558	38	636	71	88	558	38
220225_070.FIN2	75468	95.5	76.5	0.0608	0.004	0.737	0.066	0.0902	0.0069	0.35205	553	38	556	41	632	142	88	556	41
220225_074.FIN2	80841	131	97.2	0.0744	0.0036	0.84	0.065	0.0836	0.006	0.32673	614	35	518	35	1052	97	49	518	35
220225_082.FIN2	85414	184	153	0.0638	0.0033	0.837	0.069	0.0971	0.007	0.47773	613	38	597	41	735	110	81	597	41
220225_084.FIN2	91257	42.6	35.9	0.119	0.0064	3.31	0.32	0.201	0.019	0.75902	1473	80	1177	100	1941	96	61	1941	96
220225_085.FIN2	91583	411	623	0.0642	0.0038	0.777	0.064	0.0887	0.0074	0.49081	585	35	547	43	748	125	73	547	43
220225_086.FIN2	92407	352	352	0.0636	0.0025	0.808	0.058	0.0937	0.0066	0.44416	599	33	577	39	728	83	79	577	39
220225_093.FIN2	69335	75.6	46.8	0.0589	0.0033	0.811	0.069	0.099	0.0071	0.315	592	38	608	42	563	122	108	608	42
220225_100.FIN2	75220	165	81.5	0.0908	0.0066	1.18	0.12	0.0941	0.0071	0.36994	771	50	579	42	1442	139	40	1442	139
220225_103.FIN2	1049	266.1	87	0.0869	0.0033	2.014	0.14	0.1674	0.012	0.50722	1118	48	997	67	1358	73	73	1358	73
220225_110.FIN2	3271	110.2	104	0.0601	0.0027	0.88	0.065	0.1057	0.0075	0.23098	637	36	647	44	607	97	107	647	44
220225_111.FIN2	3278	51.6	24.2	0.0599	0.0039	0.897	0.081	0.1061	0.0078	0.32366	632	43	649	45	600	141	108	649	45
220225_119.FIN2	4751	353	224	0.0624	0.0024	0.75	0.054	0.0863	0.0061	0.45155	567	30	534	36	688	82	78	534	36
220225_120.FIN2	4990	76.2	38.8	0.103	0.0069	1.349	0.12	0.093	0.0067	0.04981	848	50	573	40	1679	124	34	1679	124
220225_121.FIN2	5054	154	75	0.0851	0.0069	1.35	0.2	0.1049	0.0087	0.88734	836	73	642	49	1318	157	49	642	49
220225_122.FIN2	5177	81.3	93.6	0.0629	0.0035	0.84	0.069	0.0941	0.0067	0.29146	611	37	581	41	705	118	82	581	41
220225_123.FIN2	5461	109.4	63.6	0.0623	0.0031	0.801	0.062	0.0916	0.0065	0.18358	592	35	565	38	684	106	83	565	38
220225_124.FIN2	5120	56.4	23	0.0913	0.0095	1.12	0.13	0.0876	0.0071	0.24445	748	61	541	42	1453	198	37	541	42
220225_125.FIN2	6483	174	96.1	0.0579	0.0038	0.731	0.063	0.0899	0.0065	0.15866	552	37	555	39	526	144	106	555	39
220225_127.FIN2	7720	196.3	106.5	0.1749	0.0077	9.37	0.77	0.377	0.031	0.69192	2383	64	2058	140	2605	73	79	2605	73
220225_128.FIN2	9375	178.6	101.8	0.0634	0.0029	0.851	0.065	0.0952	0.0068	0.43105	621	36	586	40	722	97	81	586	40
220225_137.FIN2	10851	189	182	0.0638	0.0032	1.251	0.1	0.1363	0.0098	0.49232	822	43	823	55	735	106	112	823	55
220225_138.FIN2	11039	1710	2650	0.06174	0.0019	0.824	0.055	0.0939	0.0066	0.3921	610	31	579	39	665	66	87	579	39
220225_141.FIN2	12499	79.5	30.2	0.0794	0.0053	1.165	0.1	0.103	0.0076	0.27519	772	49	632	45	1182	132	53	632	45
220225_143.FIN2	12838	78.3	74.1	0.07	0.0037	1.092	0.088	0.1095	0.0079	0.28562	747	44	670	46	928	109	72	670	46
220225_144.FIN2	13422	115.7	89.6	0.0596	0.0034	0.873	0.072	0.1026	0.0073	0.17571	630	39	629	43	589	124	107	629	43
220225_145.FIN2	13720	397	151.6	0.0629	0.0026	0.87	0.063	0.0972	0.0068	0.17484	633	34	598	40	705	88	85	598	40
220225_156.FIN2	15171	208.8	171.6	0.0587	0.0024	0.809	0.058	0.0967	0.0068	0.25189	598	33	595	40	556	89	107	595	40
220225_159.FIN2	17811	473	319	0.0573	0.0022	0.748	0.054	0.0915	0.0066	0.39809	568	31	564	39	503	85	112	564	39
220225_165.FIN2	20763	122.3	120.7	0.061	0.0031	0.801	0.063	0.0925	0.0067	0.30478	593	36	570	40	639	109	89	570	40
220225_166.FIN2	21974	428	19.7	0.106	0.0053	3.37	0.31	0.226	0.021	0.7391	1486	77	1321	120	1732	92	76	1732	92
220225_173.FIN2	21989	247	94.6	0.064	0.003	0.837	0.067	0.0923	0.007	0.58517	611	37	568	41	742	99	77	568	41
220225_174.FIN2	22015	124.8	168	0.0682	0.0062	0.796	0.084	0.0834	0.007	0.22	591	50	516	42	875	188	59	516	42
220225_175.FIN2	22156	220	198	0.0636	0.003	0.838	0.063	0.0939	0.0069	0.46135	612	35	578	41	728	100	79	578	41
220225_177.FIN2	22288	112.5	80.3	0.0586	0.0031	0.815	0.067	0.0963	0.0069	0.25453	596	37	592	40	552	115	107	592	40
220225_178.FIN2	23684	251.6	32.91	0.0759	0.0037	1.395	0.11	0.131	0.0094	0.24343	883	44	793	54	1092	98	73	793	54
220225_179.FIN2	24483	219	161	0.0704	0.0045	0.856	0.076	0.0873	0.0062	0.27203	620	41	539	37	940	131	57	539	37
220225_181.FIN2	24906	59.5	14.9	0.093	0.005	2.2	0.18	0.1652	0.012	0.42637	1169	58	985	68	1488	102	66	1488	102
220225_191.FIN2	26615	954	53.4	0.0761	0.0024	1.586	0.11	0.1486	0.011	0.66215	963	43	893	59	1098	63	81	893	59
220225_194.FIN2	26878	541	521	0.0711	0.0027	1.034	0.072	0.1036	0.0073	0.19692	718	36	635	42	960	78	66	635	42
220225_196.FIN2	26986	322	224	0.0569	0.0028	0.761	0.064	0.0929	0.0068	0.58359	572	37	572	40	488	109	117	572	40
220225_198.FIN2	27371	254	211	0.0697	0.0033	0.908	0.074	0.0912	0.0065	0.49248	646	38	562	38	920	97	61	562	38
220225_200.FIN2	28452	190	105	0.068	0.0049	0.827	0.077	0.0872	0.0064	0.28932	606	43	538	38	869	149	62	538	38
220225_203.FIN2	29811	214	149	0.0622	0.003	0.764	0.06	0.0877	0.0062	0.30684	569	34	542	37	681	103	80	542	37
220225_210.FIN2	30171	191.4	151.5	0.0609	0.0028	0.759	0.056	0.0904	0.0064	0.18518	569	32	558	38	636	99	88	558	38
220225_212.FIN2	31668	770	41.4	0.1623	0.0059	6.02	0.44	0.2662	0.02	0.50767	1972	63	1520	100	2480	61	61	2480	61
220225_213.FIN2	31683	236	85.8	0.1075	0.0038	3.67	0.26	0.2441	0.018	0.60231	1563	58	1405	93	1757	65	80	1757	65
220225_214.FIN2	32897	488	40	0.072	0.0037	1.317	0.11	0.1316	0.0099	0.5481	844	48	796	56	986	105	81	796	56
220225_215.FIN2	34771	504	270	0.0707	0.0027	0.925	0.067	0.0931	0.0068	0.51064	661	35	576	42	949	78	61	576	42
220225_216.FIN2	35265	156	75.5	0.072	0.0049	1.037	0.1	0.1027	0.0076	0.53099	710	50	630	44	986	139	64	630	44
220225_218.FIN2	35790	421	476	0.0648	0.0024	0.834	0.059	0.0928	0.0066	0.5231	613	32	572	39	768	78	74	572	39
220225_219.FIN2	36460	196	111	0.0709	0.0056	0.976	0.1	0.0971	0.0072	0.20025	687	52	597	42	955	162	63	597	42
220225_220.FIN2	38783	637	522	0.0593	0.0021	0.827	0.058	0.0996	0.0072	0.57749	609	32	612	42	578	77	106	612	42
220225_221.FIN2	42593	428	390	0.0601	0.0026	0.65	0.048	0.0698	0.005	0.43091	506	30	435	30	607	94	72	435	30
220225_229.FIN2	42746	149.8	111.8	0.0609	0.0026	1.084	0.079	0.1271	0.009	0.21134	739	39	771	51	636	92	121	771	51
220225_233.FIN2	43364	99	3.5	0.0778	0.0084	0.926	0.1	0.0812	0.0066	0.07611	663	50	503	39	1142	215	44	503	39
220225_235.FIN2	43616	27.7	16.7	0.0712	0.0062	1.129	0.12	0.1179	0.0091	0.16682	735	60	717	52	963	178	74	717	52
220225_237.FIN2	43689	1597	963	0.0616	0.0021	0.766	0.053	0.0902	0.0064	0.46274	576	30	557	38	660	73	84	557	38
220225_253.FIN2	49731	102.3	50.5	0.0642	0.004	0.896	0.078	0.1019	0.0074	0.27776	635	41	625	43	748	132	84	625	43
220225_255.FIN2	52612	195	116.7	0.0618	0.003	0.723	0.057	0.0843	0.0061	0.40911	547	34	521	36	667	104	78	521	36
220225_256.FIN2	57240	120.9	78.9	0.0655	0.0037	0.859	0.071	0.0952	0.007	0.24794	619	39	586	41	790	119	74	586	41
220225_258.FIN2	59783	153.1	150.1	0.0623	0.0029	0.828	0.063	0.0974	0.0069	0.1937	608	35	599	40	684	99	88	599	40
220225_266.FIN2	60326	139.9	88.8	0.1025	0.0073	1.48	0.14	0.105	0.0075	0.3928	903	58	643	44	1670	132	39	1670	132
220225_267.FIN2	60481	83.4	85.3	0.1	0.012	1.28	0.19	0.0935	0.0073	0.45192	797	80	576	43	1624	223	35	1624	223
220225_268.FIN2	60644	137.2	41.8	0.1262	0.0041	6.94	0.47	0.4014	0.028	0.47166	2099	60	2177	130	2046	57	106	2046	57
220225_271.FIN2	61760	534	409	0.0707	0.003	0.849	0.062	0.0876	0.0062	0.39835	624	35	541	37	949	87	57	541	37
220225_275.FIN2	62617	231	145.5	0.0744	0.0038	0.927	0.073	0.0917	0.0066	0.25719	661	38	567	41	1052	103	54	567	41
220225_285.FIN2	63384	136.2	64.1	0.0583	0.003	0.757	0.059	0.0953	0.0068	0.24021	568	35	588	41	541	113	109	588	41
220225_289.FIN2	64313	194.5	134.7	0.0612	0.0027	0.777	0.057	0.0937	0.0066	0.03031	581	33	577	39	646	95	89	577	39
220225_294.FIN2	76810	88.8	57.8	0.0628	0.0041	0.795	0.069	0.0939	0.0068	0.11712	583	40	578	40	701	139	82	578	40
220225_302.FIN2	79230	142	36	0.1225	0.0041	6.61	0.48	0.394	0.03	0.6945	2053	67	2136	130	1993	60	107	1993	60
220225_303.FIN2	80738	350	163	0.0644	0.0031	1.178	0.093	0.1351	0.0097	0.49656	786	43	817	55	755	102	108	817	55
220225_307.FIN2	82879	383	199	0.0654	0.0029	0.914	0.07	0.1028	0.0074	0.38764	655	37	630	43	787	93	80	630	43
220225_308.FIN2	83107	473	403	0.0616	0.0024	0.79	0.057	0.095	0.0067	0.3589	589	33	585	40	660	84	89	585	40
220225_311.FIN2	83562	56.7	55.2	0.0974	0.0096	1.28	0.15	0.0985	0.0074	0.11194	800	65	605	43	1575	185	38	1575	185
220225_312.FIN2	84429	1395	425	0.0635	0.0021	0.776	0.055	0.0904	0.0065	0.73666	583	33	558	38	725	70	77	558	38
220225_321.FIN2	86104	312	225	0.06	0.0024	0.859	0.062	0.1066	0.0076	0.39093	627	34	652	44	604	87	108	652	44

Appendix I: U-Pb zircon data tables (continued)

220225_322.FIN2	86272	133.4	63	0.0644	0.0033	0.82	0.064	0.094	0.0067	0.24072	600	36	579	39	755	108	77	579	39
220225_324.FIN2	88038	189	123	0.0804	0.0065	0.883	0.087	0.0838	0.0062	0.3634	630	44	518	37	1207	159	43	518	37
220225_326.FIN2	89902	72.4	50.1	0.12	0.017	1.42	0.21	0.0863	0.007	0.01708	872	87	533	42	1956	253	27	1956	253
220225_328.FIN2	92300	244	150	0.0669	0.0029	0.928	0.067	0.1023	0.0072	0.16413	661	35	628	42	835	90	75	628	42
220225_342.FIN2	95760	88.9	109.3	0.0857	0.0063	1.035	0.097	0.0889	0.0065	0.0575	708	49	551	37	1331	142	41	551	37
220225_343.FIN2	96909	472	395	0.0717	0.0027	0.914	0.065	0.0934	0.0066	0.38865	657	35	576	39	977	77	59	576	39
220225_344.FIN2	97418	354	30.8	0.11	0.013	1.9	0.25	0.1264	0.0093	0.04125	1066	83	767	53	1799	215	43	1799	215
220225_345.FIN2	98777	153.8	37.2	0.0682	0.0041	0.814	0.07	0.0876	0.0062	0.35432	595	39	541	37	875	124	62	541	37

Appendix J: Backscatter images of concordant zircon grains

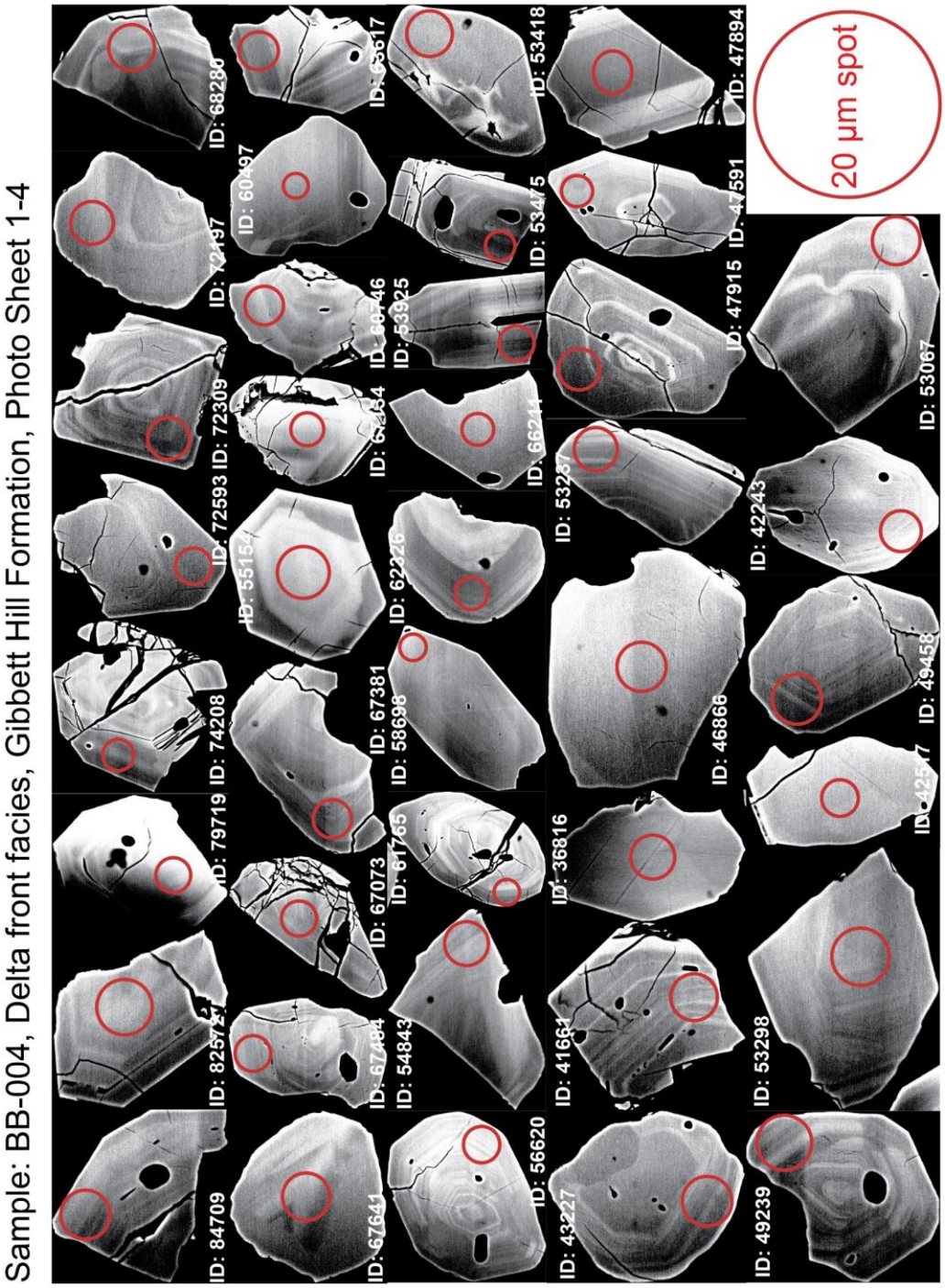

Appendix J: Backscatter images of concordant zircon grains (continued)

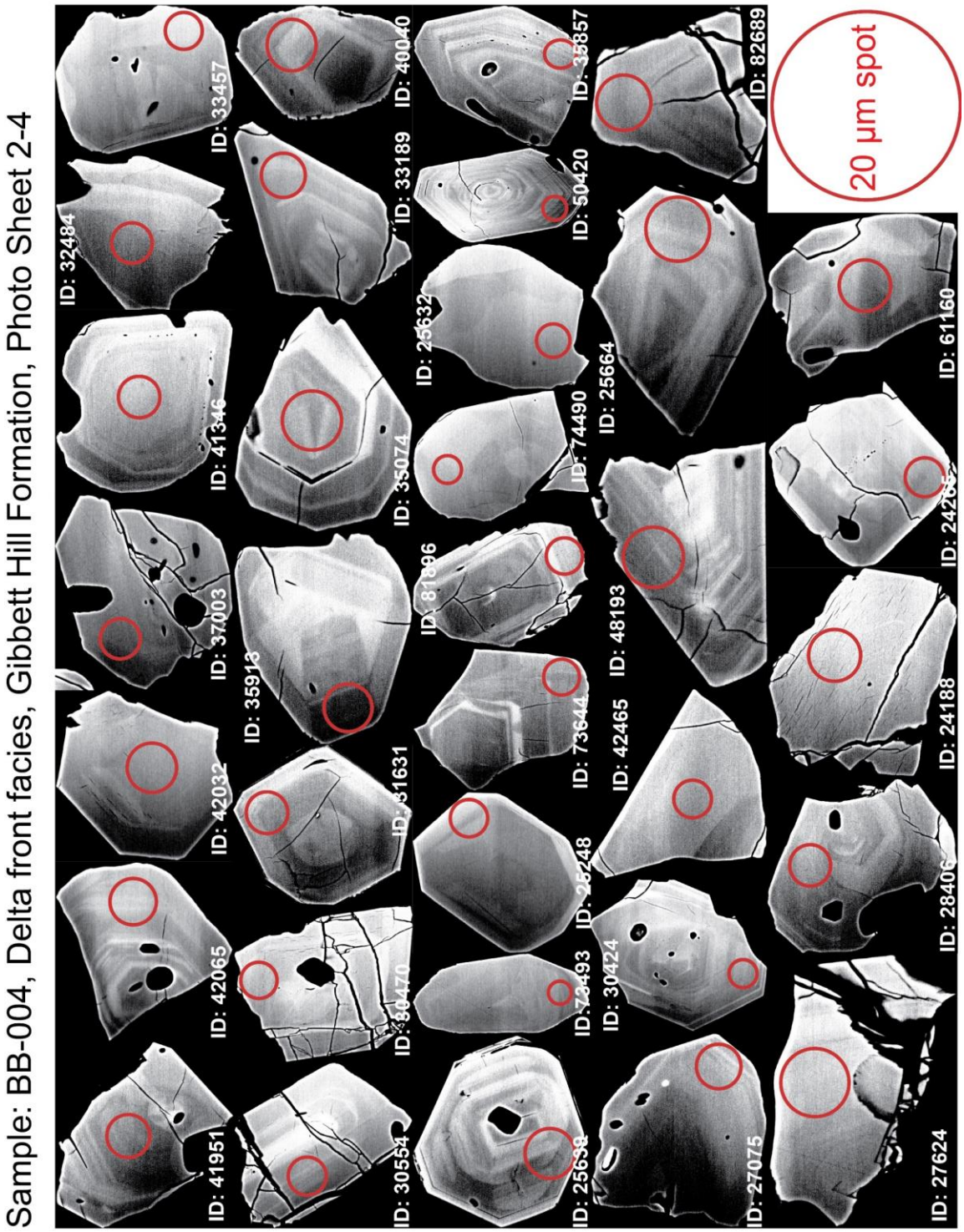

Appendix J: Backscatter images of concordant zircon grains (continued)

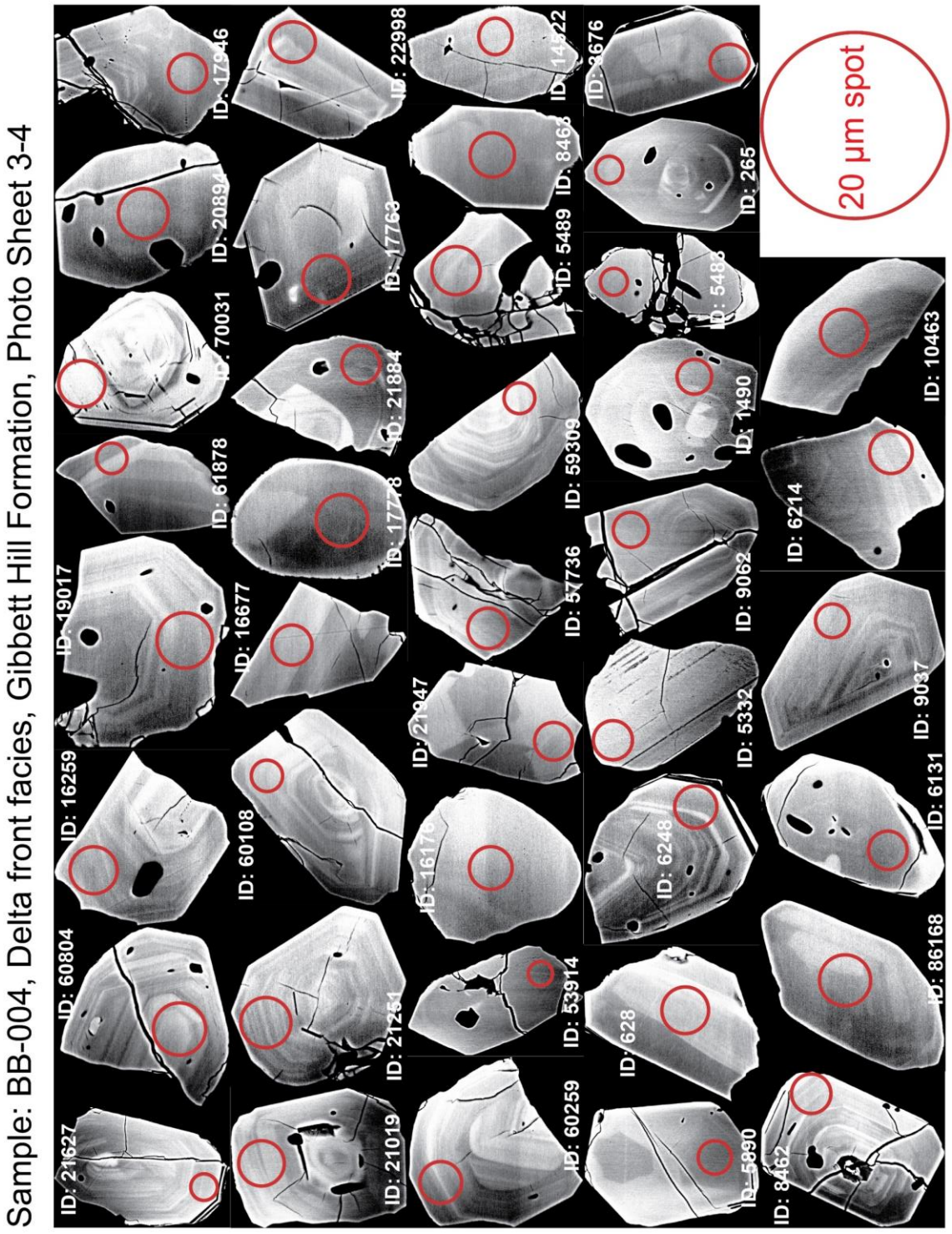

Appendix J: Backscatter images of concordant zircon grains (continued)

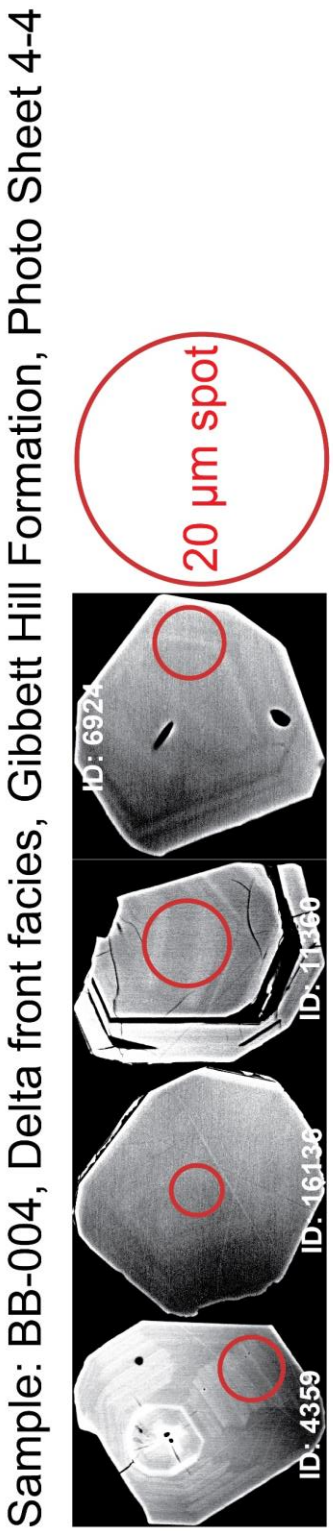

Appendix J: Backscatter images of concordant zircon grains (continued)

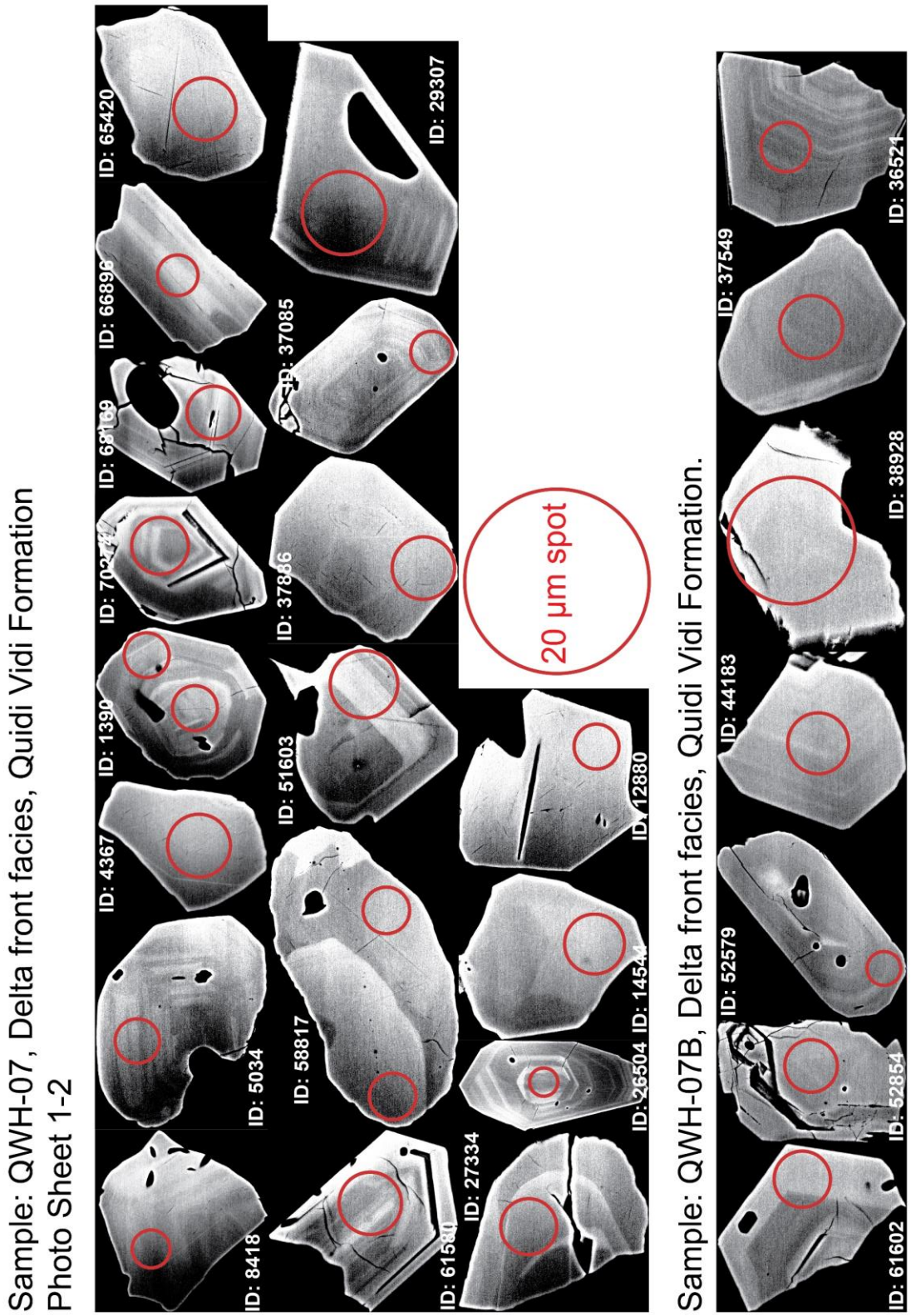

Appendix J: Backscatter images of concordant zircon grains (continued)

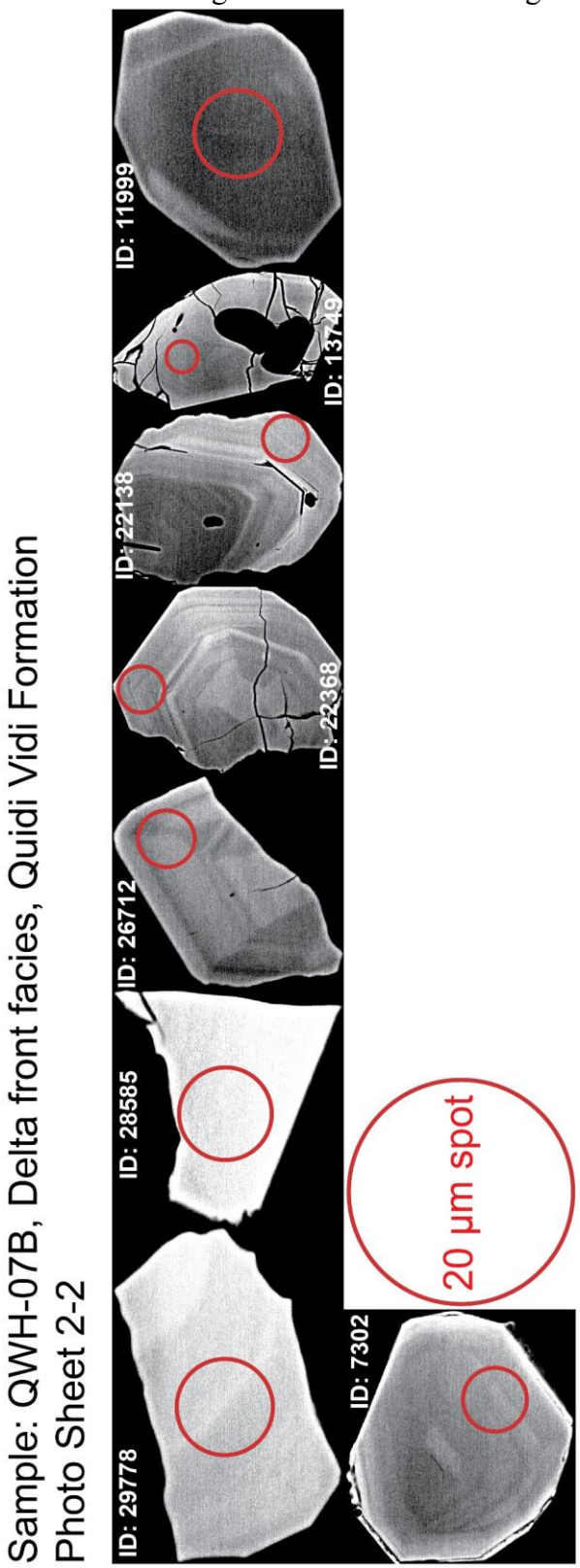

Appendix J: Backscatter images of concordant zircon grains (continued)

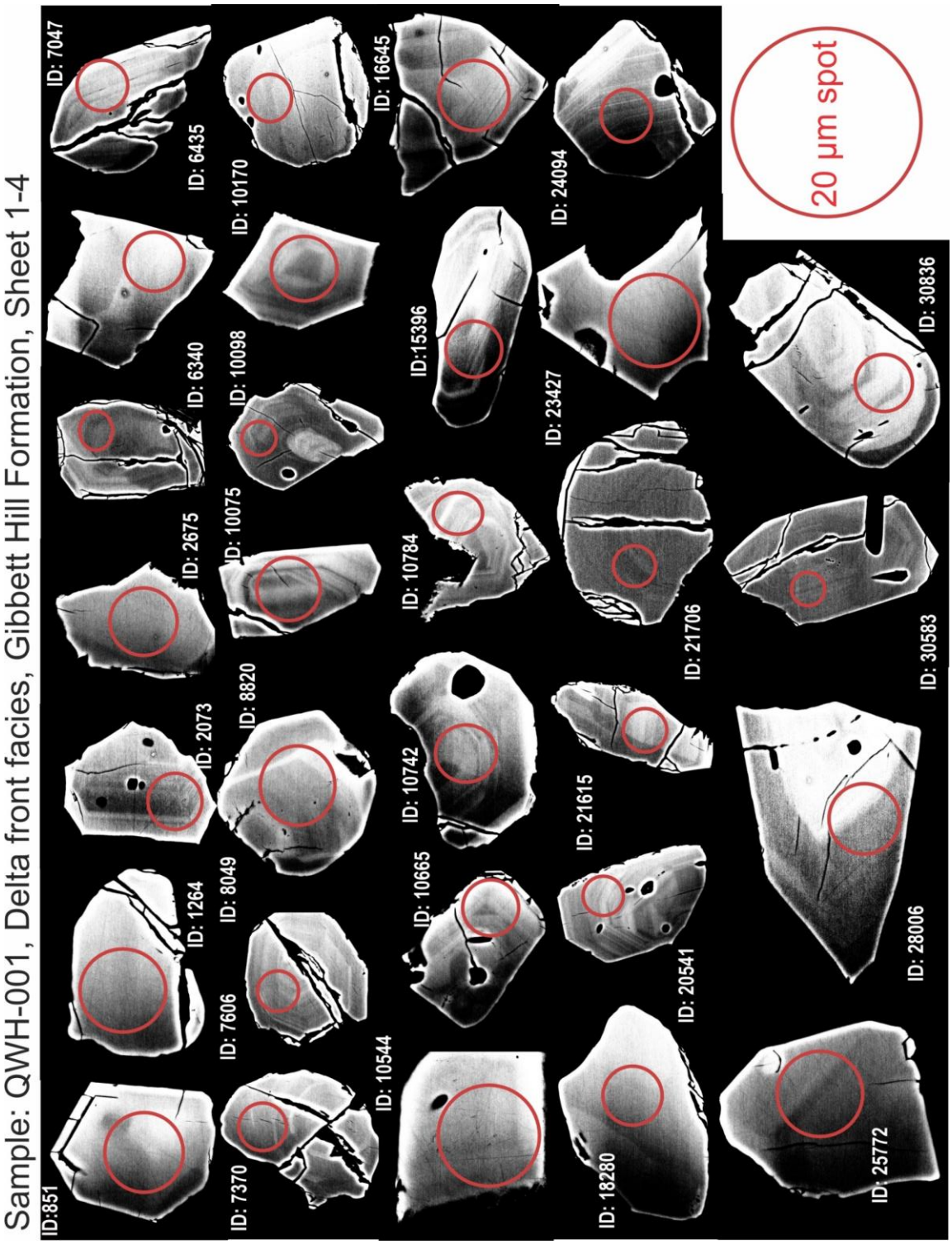

Appendix J: Backscatter images of concordant zircon grains (continued)

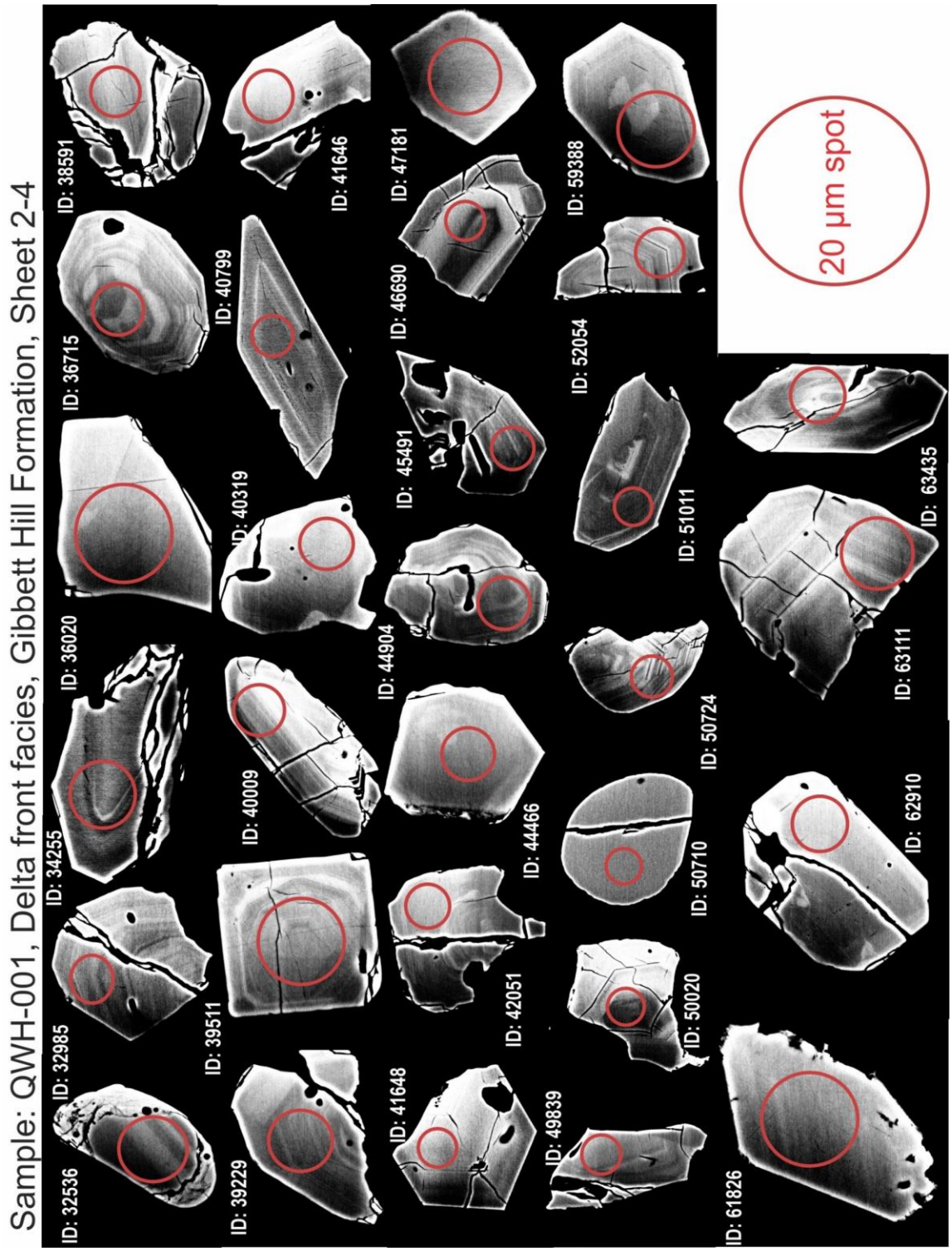

Appendix J: Backscatter images of concordant zircon grains (continued)

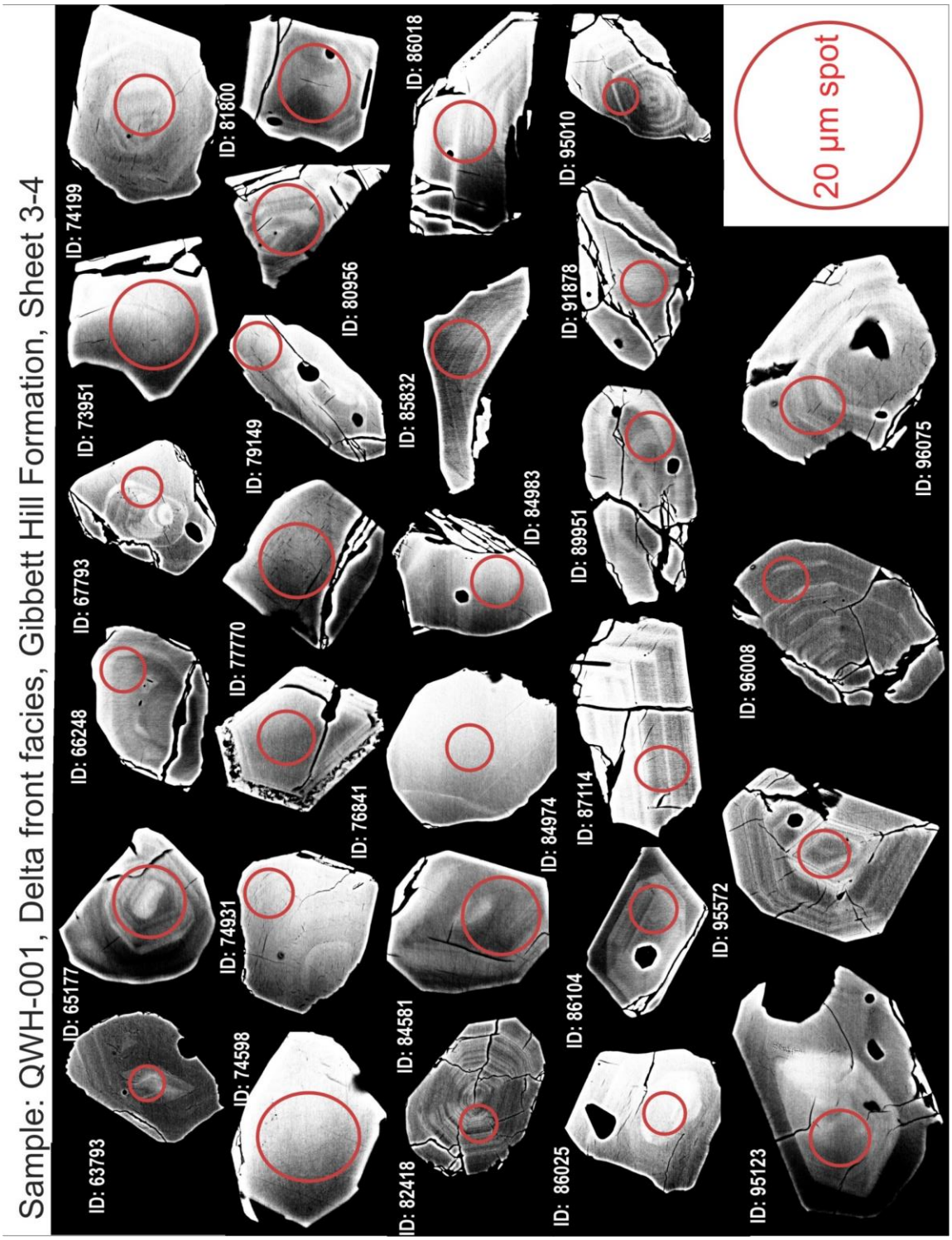

Appendix J: Backscatter images of concordant zircon grains (continued)

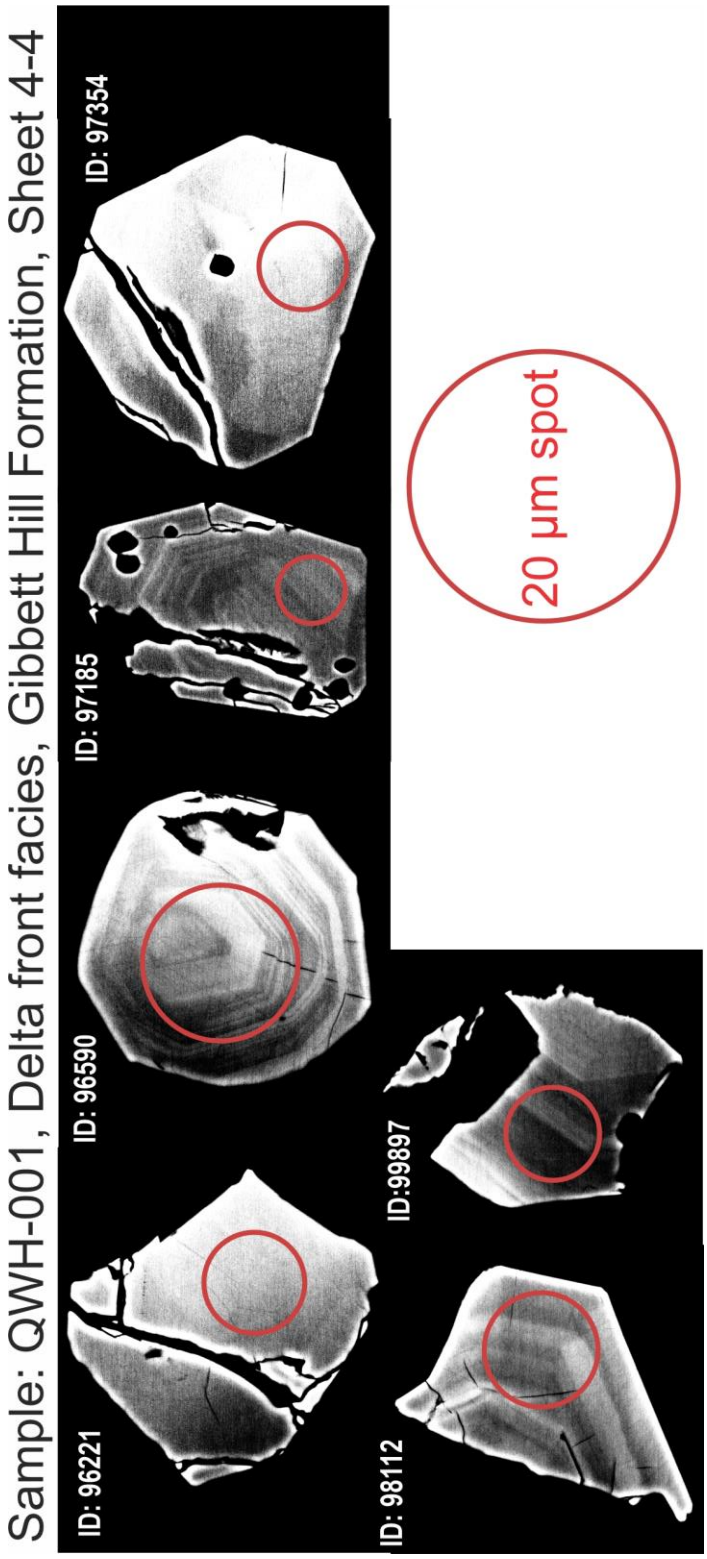

Appendix J: Backscatter images of concordant zircon grains (continued)

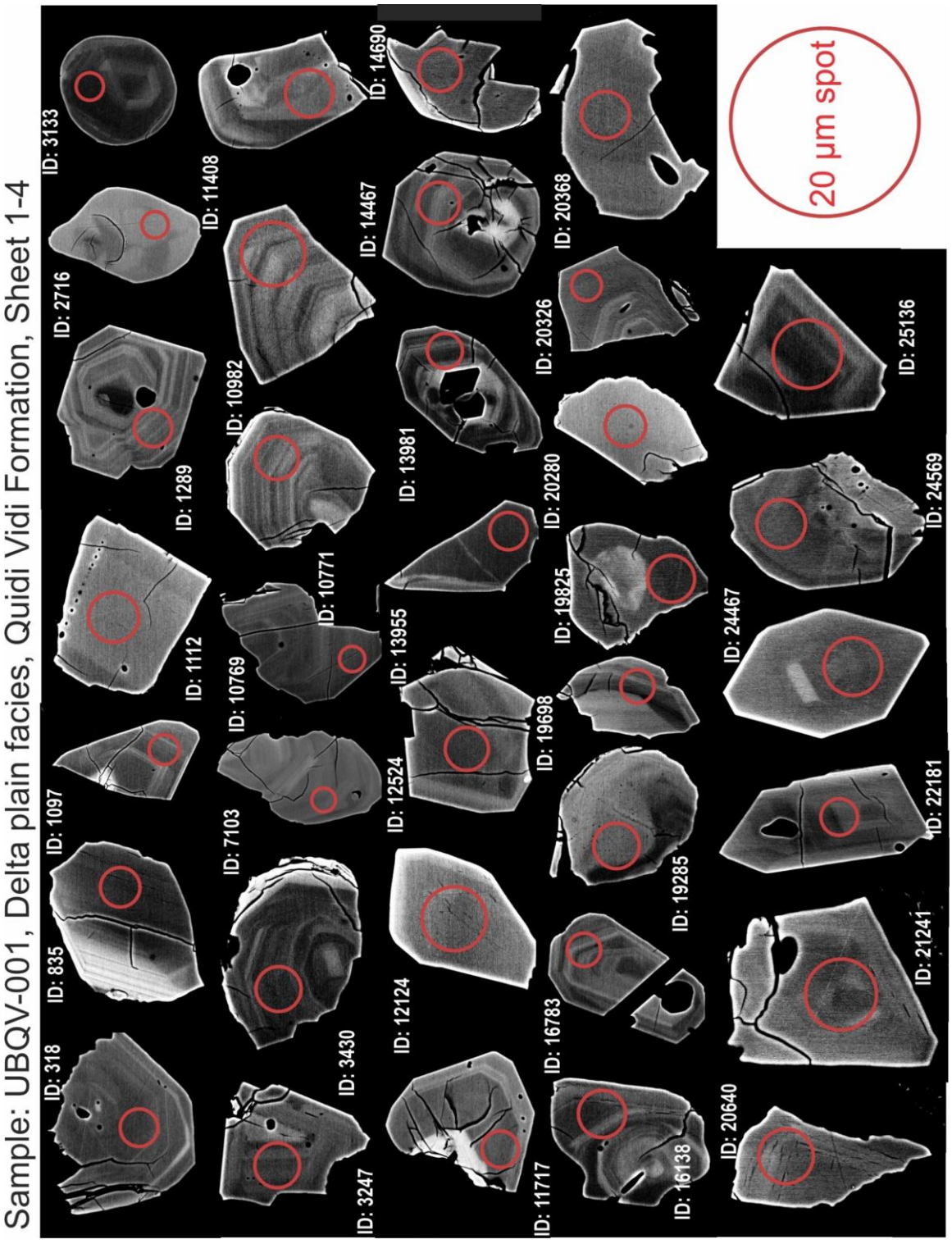

Appendix J: Backscatter images of concordant zircon grains (continued)

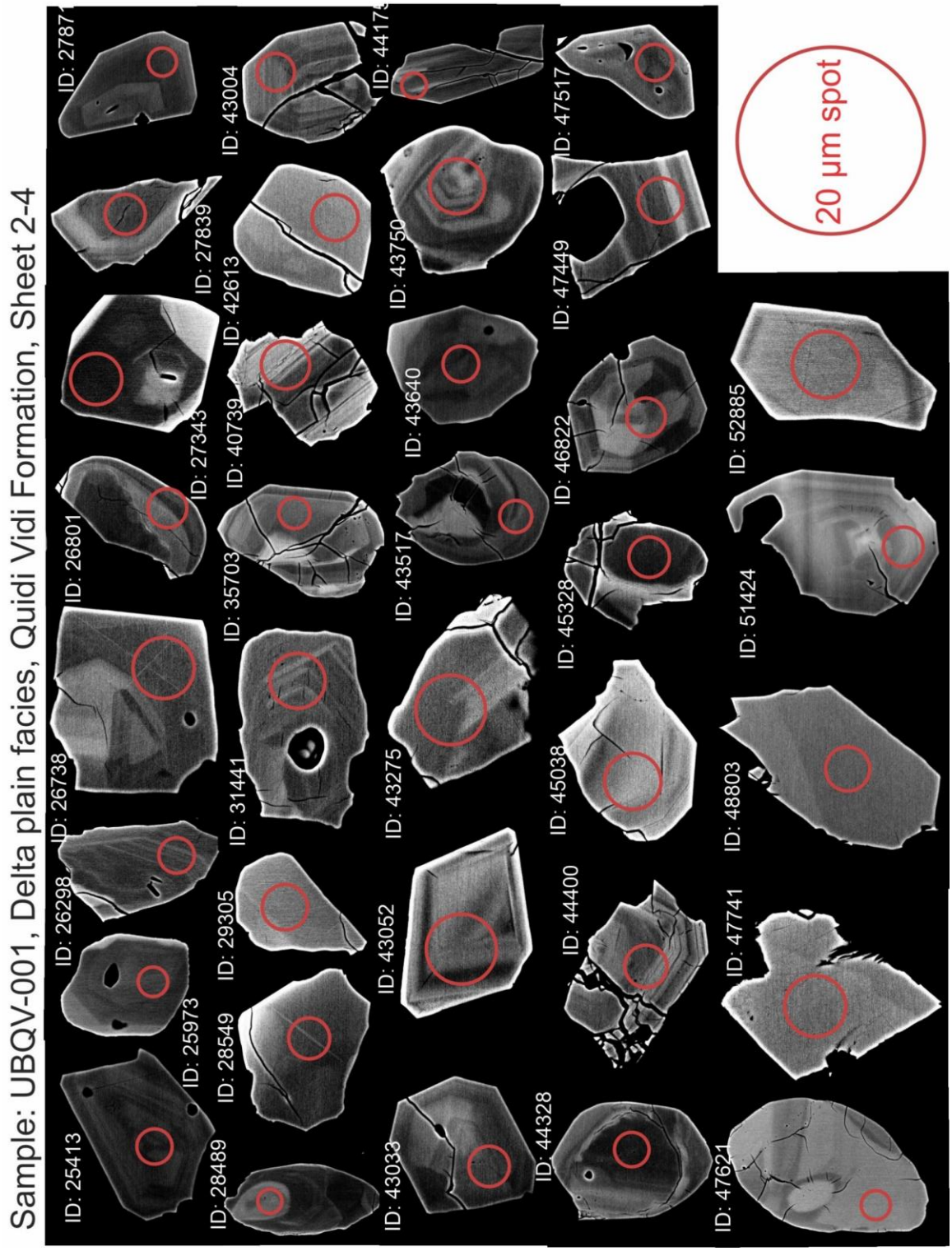

Appendix J: Backscatter images of concordant zircon grains (continued)

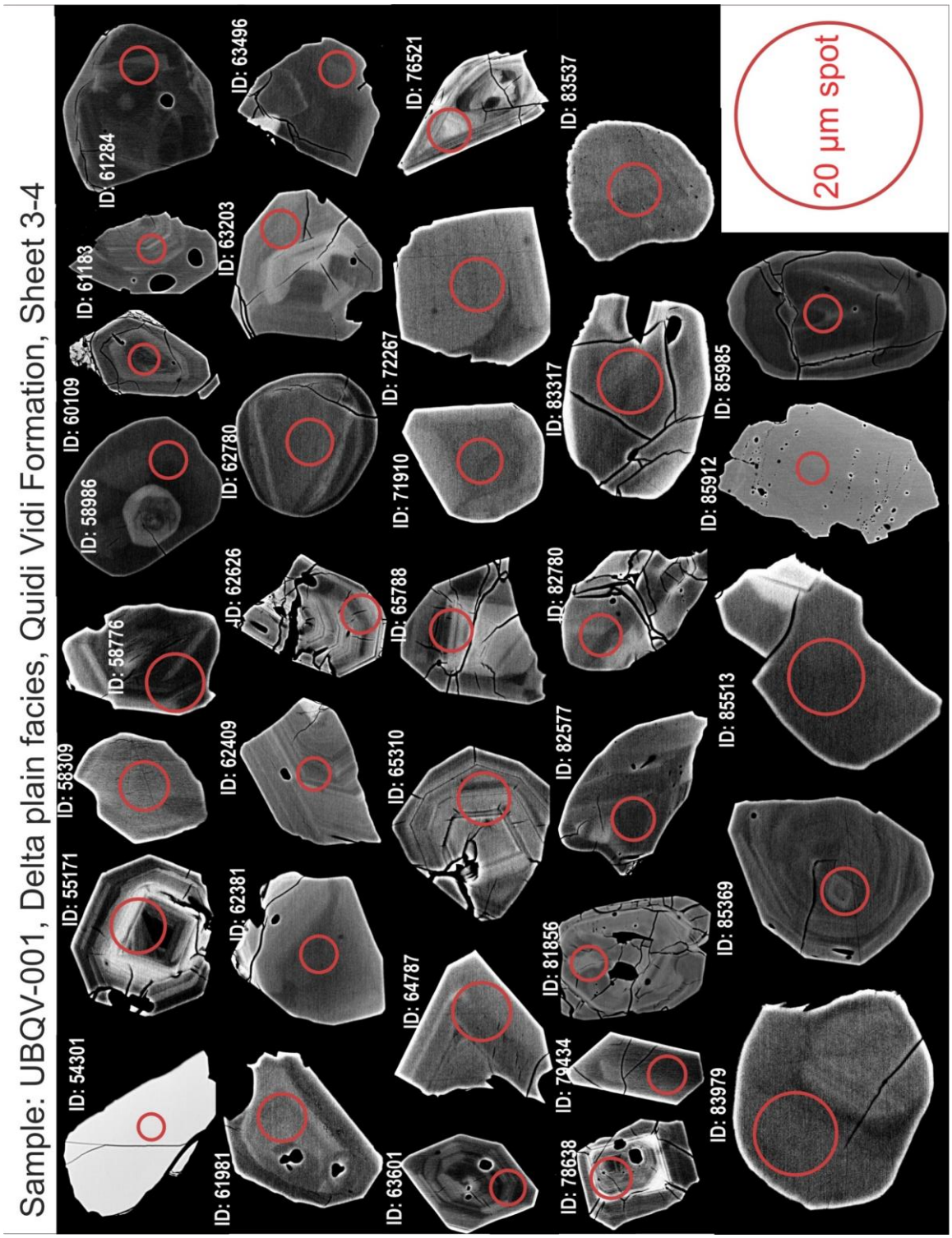

Appendix J: Backscatter images of concordant zircon grains (continued)